THE EFFECT OF HYDROTHERMAL AND ACID DEALUMINATION ON THE STRUCTURAL, ACIDIC AND CATALYTIC PROPERTIES OF MORDENITE

By

Anthony William O'Donovan (B.Sc. Chem. Eng.)

Thesis Presented for the Degree of

DOCTOR OF PHILOSOPHY

in the Department Chemical Engineering

UNIVERSITY OF CAPE TOWN

October 1995

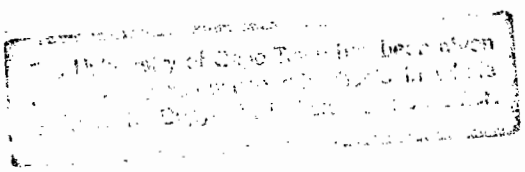

ACKNOWLEDGEMENTS

Thanks are definitely due to my supervisor Professor Cyril O'Connor who gave great support throughout the project. Also thanks to Doctor Jack Fletcher, who was involved at the start of the project, and to Professor Klaus Koch, whose help with the NMR studies was invaluable. A big thanks also to all the staff in the department, both in the workshops and offices, it has been a pleasure to work in such a great team.

Postgraduate studies would not have been the same without the rest of the Chem. Eng. postgrads. In particular I would like to thank the "old boys" of the Catalysis Unit, James, Miles and Klaus, who taught me a lot about research among other things. Thanks also to Gary, Jan, Suzi, Rob and Ashley all of whom have contributed greatly to both the social and academic aspects of postgrad life throughout my studies.

I am also very grateful to Dr. Helmut Karge for the supply of catalyst and the discussions during various stages of the project. Thanks for financial support must go to the Catalysis Research Unit, the FRD, AECI and SASOL.

I would also like to thank my family and friends outside the university, particularly Dave, Andrew and Stef, for their patience and understanding. Lastly to my wife, Sam, thanks for everything particularly your unceasing support of me throughout what could otherwise have been a very stressful time.

SYNOPSIS

Although there have been a number of studies of the effect of hydrothermal and acid dealumination on the properties of Mordenite, there is a lack of clarity on many issues related to the changes which these treatments cause to the structure, acidity and catalytic activity of Mordenite. Both methods remove aluminium from the framework thus creating extra-framework aluminium species. Although there are some reports that these species, particularly when created by mild steaming, increase the acidity and catalytic activity of the dealuminated sample, it has also been reported that these species have either a negative or no effect on the catalyst's acidity and activity [Mirodatos and Barthomeuf, 1981; Chen *et al.*, 1992; Meyers *et al.*, 1988; Bamwenda *et al.*, 1994; Brunner *et al.*, 1994]. These conflicting reports are understandable when one considers that the dealumination conditions in the various studies are usually not equivalent to each other and consequently the resultant catalysts may differ. The use of Mordenite from different sources to compare acidity in one case and structure in another may also lead to different and conflicting results. This has affected the interpretation of observed trends in the structure, acidity and catalytic behaviour of dealuminated Mordenite.

A systematic study of the effect of acid washing of sodium Mordenite and hydrogen exchanged Mordenite, both before and after steaming, has been carried out. The bulk removal of aluminium was monitored by elemental analysis of samples. The study investigated the effect of different conditions of acid washing, steaming and steaming followed by acid washing on the solid state properties of Mordenite by use of solid state ^{27}Al and ^{29}Si nuclear magnetic resonance, x-ray diffraction and infrared techniques. The effect of these changes on the number, type and strength of acid sites in Mordenite was then investigated by ammonia temperature programmed desorption, Fourier-Transform infrared analysis of pyridine adsorption and proton nuclear magnetic resonance studies. The changes caused by dealumination to the catalytic activity and shape selective properties of Mordenite as determined by studies of isobutane cracking, cyclohexanol dehydration and isopropylation of naphthalene, were then explained in terms of the acidic and structural properties of the dealuminated Mordenite samples.

Steaming of Mordenite led to the production of large amounts of tetrahedral extra-framework

aluminium. The presence of these species reduced Brönsted acidity, probably by charge balancing these framework Brönsted sites. Brönsted acidity was directly dependent on the amount of framework aluminium atoms which were not charge balanced by cations such as sodium ions or tetrahedral extra-framework aluminium species. The amount of weak Lewis acidity in the sample increased and was equivalent to the total number of octahedral and tetrahedral extra-framework species. Although tetrahedral extra-framework aluminium species appeared to be active sites for isobutane cracking, their presence reduced the selectivity to products formed over strong acid sites during isobutane cracking and indicated that they are weak sites. Steamed samples therefore showed increased catalyst lifetimes during the isobutane cracking reaction. There was no indication of the migration of these species to the external surface of the catalyst by the cyclohexanol dehydration reaction and the external surface of the sample was less active than in the case of unsteamed H-Mordenite. Their close association with framework aluminium as evidenced by their effect on Brönsted acidity would suggest that these tetrahedral extra-framework aluminium species are present within the catalyst.

Calcination of the catalyst, particularly in a "deep bed" configuration, resulted in the annealing of the structure, which increased the relative crystallinity of the sample despite the creation of octahedral extra-framework aluminium. "Deep bed" calcination also produced a highly active catalyst as determined by isobutane cracking and the presence of a large amount of strong acidity was observed. The total number of acid sites was slightly more than the total aluminium content and this observation together with a lack of hydroxyl groups suggested that these Lewis sites have the form AlO^{+} or Al^{3+}. The presence of these sites increased the catalytic activity for isobutane cracking by exhibiting strong Lewis acidity which enhanced the initiation of the cracking reaction. Increased activity of the deep bed calcined sample for cyclohexanol dehydration indicates that these species may be present on the external surface of the catalyst. This effect appeared to be similar to observations made for cracking reactions over mildly steamed ZSM-5 and Zeolite-Y. The strong acidity, however, led to increased coking during the isobutane cracking reaction and a shorter catalyst lifetime for this reaction. The extra-framework aluminium species produced by the deep bed calcination could be hydrated with a wash in deionised water and the strong acidity reduced.

Acid washing of Na-Mordenite with acids of concentrations above 0.01N resulted in proton exchange for sodium cations which caused a reduction in weak Lewis acidity and an increase in Brönsted acidity. Over ninety percent proton exchange was achieved by a 0.1N acid wash, the residual sodium ions probably being located in side pockets. The presence of hydrated octahedral extra-framework aluminium species was observed in all acid washed samples, a maximum occurring after a 0.001N acid wash of H-Mordenite. These octahedral species, which may occur within the side pockets of the catalyst, appeared to contribute to weak Lewis acidity, but were not seen to be catalytically active for any reaction and in fact had a negative effect on the initial isobutane cracking activity of the dealuminated catalysts probably due as a result of sterically blocking the active sites from the reactant molecules. Acid washing of the Sodium-Mordenite showed selective sodium removal and dealumination from the external surface as evidenced by the cyclohexanol dehydration probe reaction results. Although selective removal of aluminium from the surface of steamed H-Mordenite was also observed, this was not seen in the case of unsteamed H-Mordenite.

Although isobutane cracking activity was mainly dependent on the amount of framework aluminium sites present in the catalyst, both the activity and lifetime of the catalyst were observed to be a function of the strength of acid sites in the catalyst. No evidence was found to support the hypothesis that the activity of the catalyst was enhanced by a synergistic effect between extra-framework Lewis and framework Brönsted acid sites.

Shape selectivity, measured by selectivity to 2,6-diisopropyl naphthalene during the isopropylation of naphthalene, was enhanced by the removal of external sites. Samples steamed and then acid washed were found to have the highest selectivities to 2,6-diisopropyl naphthalene and the lowest external activities as determined by cyclohexanol dehydration.

TABLE OF CONTENTS

LIST OF FIGURES

LIST OF TABLES

NOMENCLATURE

η_Q	assymetry parameter
A	infrared absorbance in "cm^{-1}"
A_x	integrated absorbance over band x
Al-p	pentacoordinated aluminium
Al_f	framework aluminium
c	concentration of adsorbate expressed as $moles.dm^{-3}$
C	concentration of adsorbate expressed as $mmol/g_{cat}$
C_x	concentration of adsorbate identified by band x
D	thickness of wafer in infrared spectroscopy
DIPN	diisopropyl naphthalene
DME	dimethyl ether
DRIFTS	diffuse reflectance infrared spectroscopy
DSS	3-(trimethylsilyl) tetradeuterosodium propionate
ϵ	molar extinction coefficient
ϵ_x	integrated molar extinction coefficient for band x
EDTA	ethylenediamine tetra-acetic acid
EFAl	extraframework aluminium
EFAl-o	octahedral extraframework aluminium
EFAl-t	tetrahedral extraframework aluminium
EFAl-x	unknown extraframework aluminium species
e^2qQ/h	quadrupole coupling constant
eQ	nuclear quadrupole moment
eq	electric field gradient
FABMS	fast atom bombardment mass spectrometry
FID	flame ionisation detector
FTIR	fourier transform infrared
HTD	high temperature desorption peak
I(Si(*n*Al)	intensity of ^{29}Si MAS NMR peak associated with Si(*n*Al)
I^{iso}	intensity of isotropic line
I	intensity of sample beam

I_o	intensity of reference beam
LTD	low temperature desorption peak
MAS NMR	magic angle spinning nuclear magnetic resonance spectroscopy
MOR	Mordenite
P_{nap}	partial pressure of naphthalene
P_{prop}	partial pressure of propene
r_o	initial rate of conversion
S	selectivity
S_w	selectivity to products predicted to form over weaker acid sites in cracking reactions
SEM	scanning electron microscopy
Si/Al	silicon to aluminium ratio
Si/Al_f	framework silicon to aluminium ratio
Si(*n*Al)	silicon attached to *n* aluminium atoms via oxygen
TPD	temperature programmed desorption
T_{sat}	saturation temperature
$t_{1/2}$	time taken to reach half initial conversion
ν_o	spectrometer frequency
ν_Q	quadrupole frequency
ν_r	rotation frequency
ν_{RF}	radio frequency
W	weight of disk used in infrared spectroscopy
WHSV	weight hourly space velocity
X	conversion
XPS	x-ray photoelectron spectroscopy
XRD	x-ray diffraction
ϕ	amount of pyridine per cm^2 of disk
σ	wavenumber

LIST OF PUBLICATIONS

Posters:

Catalysis '92, Conference of the South African Catalysis Society, Kruger Park, South Africa, October, 1992.

International Conference on Catalysis and Catalytic Processing, Conference of the South African Catalysis Society, Cape Town, South Africa, 1993.

Environmental Catalysis, Conference of the South African Catalysis Society, Pretoria, South Africa, September, 1994.

Papers:

"The effect of acid and steam treatment of Na- and H-Mordenite on their structural, acidic and catalytic properties"
First International Convention of the South African Institute of Chemical Engineers, Johannesburg, South Africa, 1994.

"Steam and acid wash treatment of Mordenite: effect on catalyst characterisation and activity"
International Symposium on Catalysis and Zeolites, Hsinchu, Taiwan, 1994.

"The effect of hydrothermal and acid treatment on the structure, acidity and catalytic activity of Na- and H-MOR"
Microporous Materials (In press).

CHAPTER ONE

INTRODUCTION

1.1 ZEOLITES

Mordenite is a crystalline aluminosilicate belonging to the zeolite family of minerals. Zeolites were first recognized by Cronstedt in 1752, who derived the name from the Greek words "zeo" and "lithos" meaning "to boil" and "stone" due to the observed intumescence of the mineral when it was heated [Flanigen, 1991]. The uniform pore dimensions, ion-exchange properties, ability to possess acidity and high thermal stability make zeolites suitable for a wide range of industrial processes. They are therefore widely used in the industrialised countries of Western Europe, North America and Japan, which had a combined estimated usage of approximately 550 thousand metric tons in 1984 [Moscou 1991]. The application of zeolites can be divided into four main areas according to their main applications :

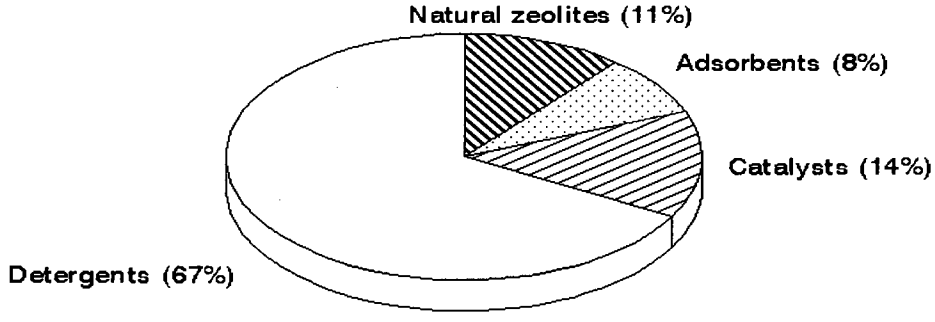

Figure 1.1. Estimated relative consumption of zeolite in 1988 for various applications in North America, Western Europe and Japan. (From Moscou, 1991)

Adsorbents and separation agents:
: Including applications as drying agents, in gas purification and in separation processes which utilize their shape selective properties.

Catalysts:
: Mainly in petroleum refining, synfuels production and petrochemicals production.

Detergents:
: As a substitute for phosphates (limited nearly exclusively to Zeolite A).

Miscellaneous:
: For waste water treatment, nuclear effluent treatment, animal feed supplements and soil improvement.

1.1.1 Structure of zeolites

The family of zeolites possess frameworks of various topologies, pore structures ranging from one dimensional (non-interconnecting parallel pores, e.g. Mordenite) to two dimensional (Ferrierite) and three dimensional pore systems (Faujasite, ZSM-5). Chemically, the zeolite framework consists of tetrahedrally coordinated aluminium and silicon atoms (and sometimes heteroatoms such as Ga, Be, Ti, B, Fe, V and P) linked by oxygen atoms. These silicon and aluminium atoms are also referred to as T atoms and zeolites are frequently characterized according to the number of T atoms in the rings that form the pore structure.

Table 1.1. Channel systems and pore sizes for selected zeolites taken from Breck [1974]

Zeolite Name	Channel System	Pore size T atoms/ring	Free aperture (Å)	Largest Molecule Adsorbed at 298 K
Large Pore				
Faujasite (X, Y)	3D	12	7.4	$(C_2F_5)_3N$
Gmelinite	3D	12	7.0	C_3H_8
L	1D	12	7.1	$(C_4H_9)_3$
Mordenite	1D	12	6.7 x 7.0	C_6H_6
Medium pore				
Dachiardite	2D	10	3.7 x 6.7	-
Epislitbite	2D	10	3.2 x 6.7	H_2O
Ferrierite	2D	10	4.3 x 5.5	C_2H_4
Heulandite	2D	10	4.4 x 7.2	NH_3
Stilbite	2D	10	4.1 x 6.2	H_2O
ZSM-5	3D	10	5.2 x 5.8	-
Small pore				
A	3D	8	4.2	C_2H_4
Bikitaite	1D	8	3.2 x 4.9	-
Brewsterite	2D	8	2.3 x 5.0	H_2O
Chabazite	3D	8	3.7 x 4.2	n-paraffins
Edingtonite	2D	8	3.5 x 3.9	H_2O
Gismondine	3D	8	3.1 x 4.4	H_2O
Levynite	2D	8	3.2 x 5.1	N_2, O_2
Very small pore				
Analcime	1D	6	2.6	NH_3
Sodalite	3D	6	2.6	H_2O

These may range from large (12-atoms : 7-8 Å pore diameter) to very small (6-atoms : 2-3

Å pore diameter) as shown in Table 1.1. Channel dimensions are important in that they determine which molecules may enter the zeolite. This property classifies zeolites as molecular sieves. This sieving property is a function of both temperature and the cation content of the zeolite. Higher temperatures increase the flexibility of the zeolite structure and guest molecule while cations of different size and locations offer different steric restraints.

1.1.2 Acidity of zeolites

The acid sites in zeolites can be divided into two categories, namely Lewis and Brönsted sites. These two categories are discussed separately as there are fundamental differences between them with regard to their location and structure.

1.1.2.1 Brönsted acidity

The incorporation of trivalent aluminium into the zeolite framework as a substitute for tetravalent silicon results in the formation of a net negative charge in the framework, which gives the zeolite its cation exchange properties. Usually, acidic forms of zeolites are made by exchanging cations with protons, either directly or by means of an ammonium ions which

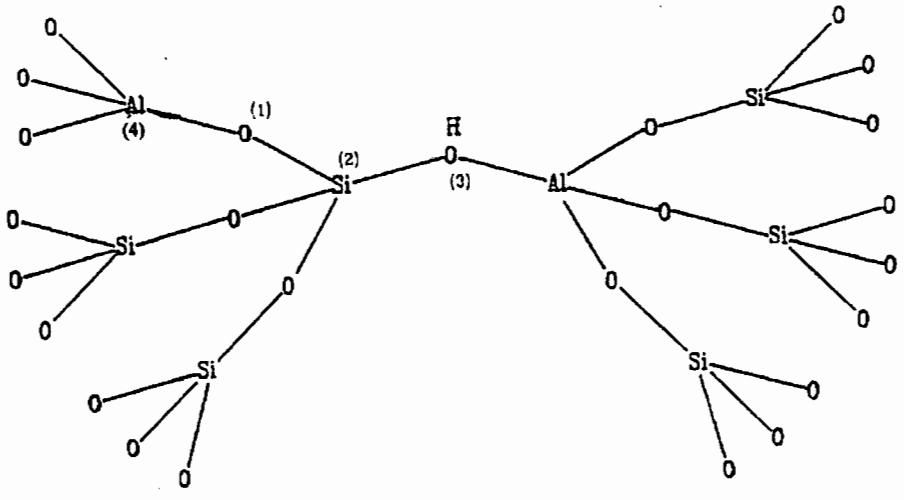

Figure 1.2 Model of Brönsted acid site [Nieuwenhuys *et al.*, 1993; Moulijn *et al.*, 1993]]

decompose at higher temperatures. This results in the formation of a hydroxyl group which acts as a Brönsted acid site (Fig. 1.2) [Niewenhuys *et al.*, 1993; Moulijn *et al.*, 1993; van Santen, 1994; Sauer, 1989]

Although it has been intuitively believed that these adsorbed protons are of an ionic nature, this has been disputed recently by strong evidence, primarily obtained by use of DRIFTS, in favour of the covalent nature of the bond [Kazansky, 1994].

While it has been widely accepted that the number of Brönsted sites is determined by the number of aluminium atoms in the framework [Stach *et al.*, 1992_b], an important factor which controls the Brönsted acidity of these catalysts is the lattice composition. As the silicon to aluminium ratio changes, the deprotonation energy, and thus the strength of Brönsted acid sites, is seen to vary.

Kazansky [1991] has found that the covalent hydroxyl interaction energy varies little with acidity and concluded that the factor contributing most to strong acidity is the stabilization of the negative charge left on the lattice after deprotonation. The existence of other negative centres, i.e. aluminium atoms in the lattice, in close proximity would hinder this stabilisation. In either scenario, aluminium atoms in the second coordination sphere (i.e. the twelve framework T-atoms which are linked to the acid site by an -O-Si-O- group) lead to a decrease in acid strength.

From cluster calculations, van Santen [1994] has shown that the addition of a second proton in a four ring cluster decreases the strength of the hydroxyl bond. This can be understood by considering the tetrahedra in the second coordination shell of the zeolite with respect to the acidic proton (e.g. atom labelled (4) in Fig. 1.2). Because of the lower charge on Al^{3+} its interaction with oxygen atoms such as O(1) is less than that of a Si^{4+} ion. The attached silicon atom (2) therefore becomes more strongly bound to this oxygen atom (1) and its bond strength with oxygen atom (3) decreases. This increases the strength of the hydroxyl bond

and hence the deprotonation energy and therefore decreases acidity [Nieuwenhuys *et al.*, 1993].

Since no aluminium in the zeolite lattice can be bonded via an oxygen atom to another aluminium atom (Löwenstein's Rule), between three and zero aluminium atoms may exist in the second coordination sphere. The strongest acid site is that associated with no aluminium atoms in its second coordination sphere (Next-Nearest-Neighbour Theory) [Nieuwenhuys *et al.*, 1993]. This condition is met for Mordenite with a Si/Al ratio of 9.4 (Figure 1.3) [Stach and Jänchen, 1992] and for Zeolite-Y with a Si/Al ratio of 5.6 [Stach *et al.*, 1992_a].

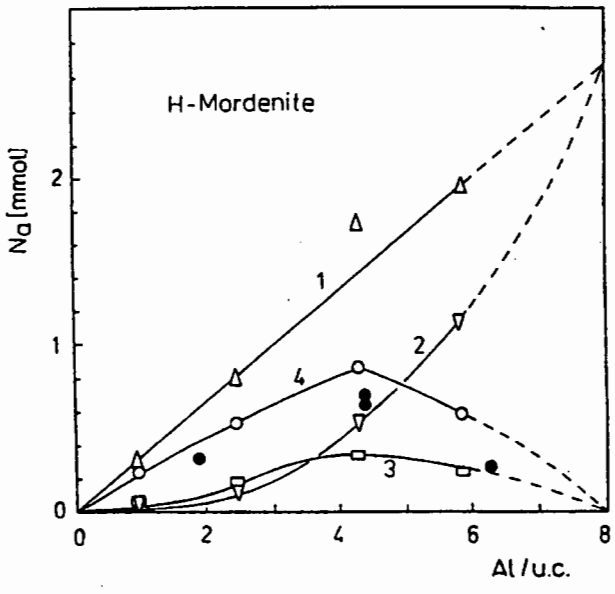

Figure 1.3 Distribution of acid strengths in dependence on the aluminium content of the framework in dealuminated H-Mordenites [Stach *et al.*, 1992]

Other factors may also influence the strength of Brönsted acidity. Zholobenko *et al.* [1993] investigated the Brönsted acid sites in H-Mordenite using FTIR spectroscopy of adsorbed molecules and discovered an inhomogeneity in Brönsted sites which was not explained by the next nearest neighbour theory. After investigating the adsorption and desorption of ammonia on Brönsted sites in H-Mordenite, they proposed the existence of two types of

adsorption sites. One of these types is proposed to be a hydroxyl group in the main channel. This type has a low effective acidity and readily allows desorption of ammonia, benzene and cyclohexane. The other type of site consists of hydroxyls in the smaller side-channels which have a higher effective acidity and do not allow desorption to occur as easily. The ratio of these two sites was established to be 2:1. This ratio is fairly close to that found between the aluminium located in the site pockets and that found in the main channels by Mortier *et al.* as long ago as 1975. They determined ratio to be ≈ 46:29 by x-ray diffraction. Similar differences in acidic strengths of Brönsted sites in crystalographically inequivalent sites were found in Zeolite-Y by van Santen [1994].

1.1.2.2 Lewis acidity

During early investigations from 1965, Lewis sites in zeolites were found in zeolites after high temperature treatment of the protonic form. It was assumed by Uytterhoeven *et al.* [1965] that Lewis sites were produced by dehydroxylation of zeolites and occurred as tricoordinated aluminium atoms and Si^+ sites in the anionic structure. The relative quantities of Lewis sites in the catalyst as identified by infrared spectroscopy of adsorbed pyridine were shown to increase with increasing temperature of calcination [Ward, 1967]. Later, in 1984, Kustov *et al.* used infrared spectroscopy of adsorbed hydrogen to investigate these sites. They reported the existence of three bands of adsorbed hydrogen (4010, 4030 and 4060 cm^{-1}) after dehydroxylation with which they identified three different kinds of Lewis sites: tricoordinated aluminium, tricoordinated silicon in the framework structure and aluminium on cationic sites.

These early theories have since been contested. Kühl [1973, 1977] proposed that if tricoordinated silicon and aluminium do occur in dehydroxylated zeolites they do this as intermediates. The tricoordinated aluminium would be removed from the crystal structure by the formation of oxyaluminium species (approximately AlO^+) which were called the "true Lewis sites." Later work of Jacobs and Beyer [1979] and Engelhardt *et al.* [1983], where hexacoordinated aluminium was observed by ^{27}Al MAS-NMR spectroscopy after

dealumination, supported Kühl's dehydroxylation scheme. Karge and Dondur [1990] investigating the acidic properties of acid washed Mordenites, reported that all dealuminated samples contain significant amount of extra-framework aluminium and that this generates Lewis acidity as measured by infrared spectroscopy of adsorbed pyridine. The association of Lewis acidity with extra-framework aluminium has become a feature of recent literature, although the possibility still exists for Lewis acidity to be created by tricoordinated aluminium occurring at defects sites in the catalyst [Karge, 1993].

The Lewis sites can be seen by infrared spectroscopy of pyridine adsorption where a typical band at 1450 cm^{-1} has been widely reported [Uytterhoeven *et al.*, 1965; Cannings, 1968; Ward, 1976; Karge, 1991]. A band at 1462 cm^{-1} has also been observed and ascribed to a second, stronger Lewis site, but there is no clarity as to its nature.

In principle the charge-compensating alkali metal ions can be seen as Lewis sites, as they are sites which can also act as an electron pair acceptor. These sites can be observed by adsorbed pyridine bands in the infrared region 1438 to 1452 cm^{-1}. However, these cations do not seem to play a role in the catalysis of hydrocarbon reactions [Rabo and Poutsma, 1971].

In summary the Lewis sites in zeolites are generally regarded as emanating from extra-framework cations. Weak Lewis acidity from charge compensating alkali metal ions (particularly sodium) do not appear to contribute to activity, while stronger Lewis acidity appears with extra-framework aluminium upon dealumination. The creation of these sites during dealumination and postulations as to their nature are discussed later as part of the effect of dealumination on the acidity of zeolites.

1.1.3 Zeolites in catalysis

The use of zeolites as catalysts was first announced in 1960 [Rabo et al., 1960; Weisz and Frilette, 1960]. They are used mainly in the area of petroleum refining, synfuels production

and petrochemicals production, although much work is being done in the synthesis of specialised fine chemicals [Holderich and van Bekkum, 1991].

Petroleum refining uses mainly Zeolite-Y for fluidized catalytic cracking (FCC) and hydrocracking, and ZSM-5 and Mordenite for catalytic dewaxing (i.e. the removal of long chain hydrocarbons from the linear paraffin products). Mordenite based catalysts are receiving more and more attention in the field of paraffin isomerisation due to their simplicity of operation and high tolerance of feed impurities. Paraffin isomerisation is an important reaction in the production of higher octane gasoline as it promotes the formation of highly branched paraffin isomers [Pujado *et al.*, 1992].

Synthetic fuels production includes processes such as the production of high quality gasoline and distillate fuels from natural gas via the methanol and the oligomerisation of olefins to form gasoline and distillate range products. The zeolite ZSM-5 is used primarily for these processes [Tabak and Yurchak, 1990].

Zeolites are also used in many important petrochemical processes, such as aromatic alkylation, xylene isomerisation and aromatic disproportionation, to produce valuable petrochemicals. An example of aromatic alkylation is the Mobil-Badger process which uses H-ZSM-5 as a catalyst for the alkylation of benzene to produce ethylbenzene [O'Connor *et al.*, 1995]. Cumene formed by the alkylation of benzene with propene can be produced in gas phase using dealuminated Mordenite or in the liquid phase over zeolites Beta and ZSM-12. Xylene isomerisation reactions often utilise the shape selectivity of zeolites such as ZSM-5 and Mordenite. The same catalysts are used for disproportionation and transalkylation reactions [Pujado *et al.*, 1992]. Dealuminated Mordenite has also been found to show potential for the shape selective alkylation of aromatics such as the isopropylation of naphthalene or biphenyl [Katayama, 1991; Sugi *et al.*, 1994].

1.2 MORDENITE

In 1864 How suggested the name Mordenite for the fibrous zeolite found in radial aggregates in Morden County, Nova Scotia, Canada [Passaglia, 1975]. Mordenite was first synthesised by Barrer in 1948 and its structure was determined by Meier [1961]. Since its discovery, Mordenite has received increasing attention as an acid catalyst in various industrially important reactions and also as a molecular sieve in gas-liquid and liquid-liquid separations [Bajpai, 1982].

1.2.1 Synthesis

Initial syntheses of Mordenite, using temperature of above 250°C, Si/Al ratios of 6 and water/Al_2O_3 ratios of several hundred, produced Mordenite with channel diameters of approximately 4 Å (small port Mordenite), similar to that found in natural Mordenites [Barrer, 1959]. Later, in 1961, Sand synthesized large port Mordenite, having channel diameters of approximately 8 Å [Meier, 1961]. The reduced channel diameter observed in small port Mordenites was ascribed to either crystal stacking faults or the blocking of pores with amorphous materials [Whittemore, 1972]. The observed conversion of small-port Mordenite to large-port Mordenite after 20% removal of aluminium supports the latter [Stach *et al.*, 1992_b]

Mordenite is generally synthesized in an alkaline medium of pH ≈ 12. Although gels with a high pH lead to the dissolution of Mordenite and its recrystallisation into different phases, reduction of the pH to 7 or 8, results in the retardation of crystallisation and the formation of smaller crystallites [Bodart *et al.*, 1986]. Bodart *et al.* also found that although both crystallinity and crystallite size increased with synthesis time, the pH of the synthesis gel remained constant - suggesting that the synthesis comprised of only one nucleation step.

Sand [1968] demonstrated the importance of gel water content. Crystallisation kinetics can

be altered by changing the starting materials used and, in addition to this, crystal size can be varied from less than one micron to over 100 microns. Sand also reported that low synthesis temperatures necessitated long crystallisation times (75°C, 168 hours) when compared to higher synthesis temperatures (260°C, 4 hours).

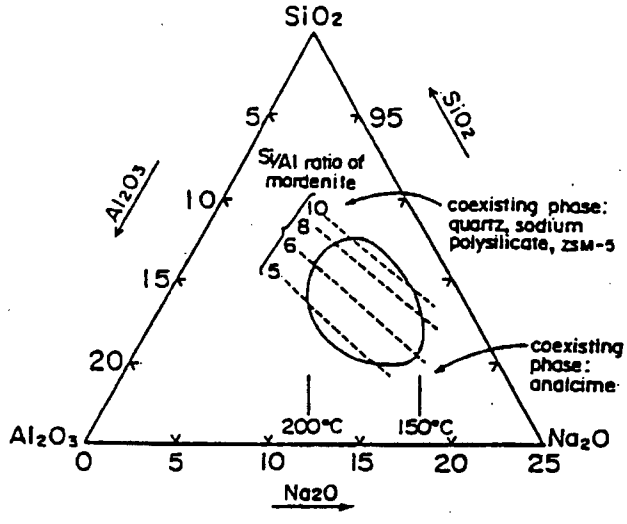

Figure 1.4. Composition diagram of synthesis gel composition and temperature required for the synthesis of siliceous mordenite [Inaoka *et al.*, 1990]

The composition of Mordenite can be modified by changing the composition of the synthesis gel (Figure 1.4). Early synthetic Mordenites were made with Si/Al ratios between 4.5 and 5.5, later, in 1972, Whittemore reported the synthesis of Mordenite with ratios ranging between 6 and 10. A more siliceous Mordenite can be synthesised by either ageing the synthesis gel or by the addition of benzyltrimethylammonium ions to the gel [Ueda, 1980].

1.2.2 Structure

Mordenite has an orthorhombic crystal structure with a unit cell of dimensions; a = 18.13 Å, b = 20.49 Å and c = 7.52 Å [Meier, 1961] and a general chemical structure of $Na_xAl_xSi_{(48-x)}O_{96}{\cdot}24H_2O$. Natural Mordenite has an almost uniform silicon to aluminium ratio

(Si/Al) of 5, i.e. x = 8 and their only variation in chemical composition is a change of extra-

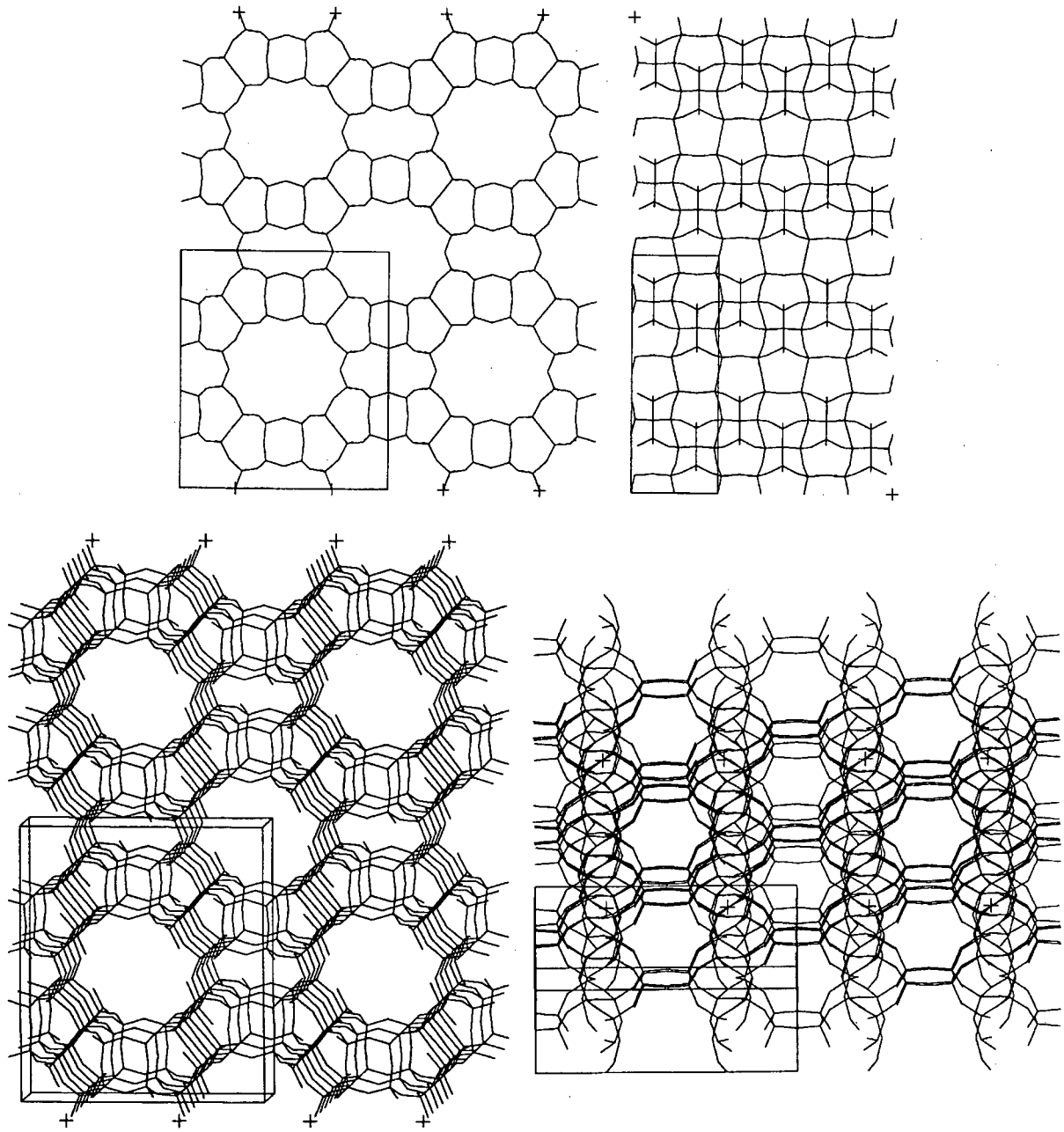

Figure 1.5. Structure of mordenite simulated using Biosym showing views along c-axis (top left), b-axis (top right), main channel (bottom left) and side channel (bottom right)

framework cations [Passaglia, 1975]. In its synthetic form Mordenite can have surface areas

as high as 600 m^2/g.

The structure of Mordenite is made up of building units that consist of four and five-member rings [Szostak, 1992]. The pores are made up of parallel elliptical channels with free apertures of 6.5 by 7.0 Å interlinked by smaller pores in the *b* direction [Meier, 1961]. Rather than interconnecting the main channels, the smaller channel branch through twisted 8-membered rings, which have an aperture of only 2.9 by 5.7 Å [Meier and Olson, 1978] and are too small to allow access to most molecules and therefore rendering the catalyst unidimensional. This structure is shown by the Biosym reproduction in Figure 1.5.

In the hydrated sodium form of the catalyst, four of the eight sodium atoms in each unit cell are believed to reside in the centre of the 8-membered ring, while the other four are located close to the entrance of this side pocket [Sefik, 1978]. Sanders [1985] has shown the existence of crystallographic faults, occurring particularly in natural Mordenite, which run parallel to the main channels, however these do not appear to block these channels.

1.3 DEALUMINATION METHODS

Early attempts at ion exchange by acids showed that not all zeolitic materials could be exchanged in this way due to a loss in crystallinity. However, some zeolites did not undergo structural degradation, but it was not realised at that time that these structural changes were due to framework aluminium removal and consequently this was not investigated.

Selective aluminium removal without structure collapse was first reported by Barrer and Makki in 1964 when they obtained the removal of framework aluminium from cliptonite through treatment with hydrochloric acid. Soon Mordenite, Erionite and Zeolite L were also shown to be dealuminated in the same manner. Of these Mordenite was of particular interest due to its availability and potential as a catalyst [Szostak, 1991] and because it differs from other zeolites in so far as large amounts of aluminium can be easily removed without a loss in crystallinity [Eberly and Kimberlin, 1970]. Aluminium removal may be achieved by hydrothermal treatment, treatment with mineral or organic acids, or treatment with a variety of metal halides, oxyhalides or metal alcoholates [Fejes *et al.*, 1988].

1.3.1 Acid leaching

This is the most common form of dealumination as acids are often used for proton exchange with cations in the zeolites and dealumination occurs in this process. It has been reported by Wang *et al.* [1991] that aluminium can be drawn completely out of the zeolite framework by acid washing and that a large part of extra-framework aluminium (EFAl) found in zeolites especially after steaming can be removed using a treatment with acid, without the removal of framework aluminium (Al_f). It has been found that mild acid washing will result in a more active catalyst and this is seen as a result of the removal of this EFAl as well as the generation of strong acid sites by aluminium removal. Van Niekerk *et al.* [1992], however, have reported that the extent of dealumination is strongly influenced by the properties of the catalyst such as crystal size.

1.3.2 Hydrothermal dealumination

This method of dealumination involves the calcination of the catalyst at relatively high temperatures in the presence of steam. Even in cases where steam is not fed to the catalyst, water vapour can be produced by dehydroxylation of the zeolite. McDaniel and Maher [1968] and Kerr [1969] reported the formation of ultra-stable Zeolite-Y by thermal treatment in a static environment. The resultant catalyst was seen to be strongly dependent on the bed conditions and Kerr [1969] proposed that "deep bed" calcination allowed the gases removed by the catalyst on calcination to act on the remainder of the catalyst bed and remove framework aluminium. Ward [1970] subsequently obtained samples of Zeolite-Y with similar characteristics by steaming at a low partial pressure of water (13.8 kPa). Scherzer [1984] reports that this treatment results in the expulsion of tetrahedral aluminium from the framework, but not from the zeolite, leading to the formation of neutral or cationic EFAl. Sites vacated by the aluminium can be filled with silica, which leads to a very stable, highly siliceous framework. Although considerable activity enhancements have been reported for some catalysts after hydrothermal treatment (e.g. Lago *et al.* [1986]), this method of dealumination has seldom been used on Mordenite.

1.3.3 Combinations of steam and acid treatments

The first use of a combination of acid and thermal treatment was reported by Sand and co-workers in 1970. The ease with which the aluminium was removed by acid leaching after steam treatment suggested that at least a portion of the aluminium was removed from the framework during thermal treatment. Mishin *et al.* [1973], using a similar procedure, studied the effect of preheating temperature on the degree of dealumination and from this concluded that preheating temperatures and acid concentration are the major factors influencing the degree of dealumination [Chen and Smith, 1976].

1.3.4 Washing with chelating agents

Washing with chelating agents has been primarily used for the selective removal of external aluminium from Zeolite-Y. EDTA, an acid and a chelating agent, is too large to fit into the pores of most zeolites and so extracts the aluminium from the surface. However, either the zeolite or the EDTA must be at least partially in the hydrogen form for dealumination to occur [Kerr, 1968]. Other chelating agents which have been used for aluminium removal are acetylacetone and several amino-acid-derived agents [Beaumont and Barthomeuf, 1972 and 1973].

1.3.5 Reactions with other compounds

Beyer and Belenykaia [1980] have been able to dealuminate Zeolite-Y by reaction with silicon tetrachloride vapours at high temperatures. Dealumination of Mordenite with $SiCl_4$ has been reported [Klinowski *et al.*, 1983] but this is more difficult to achieve because of steric hindrances. Dealumination has also been achieved by reaction with fluorine and ammonium hexafluorosilicate [Skeels and Breck, 1984]. Both methods result in the substitution of framework aluminium for silicon. To achieve high degrees of dealumination intermediate calcination between washes is requierd [Szostak, 1991]. Other methods for aluminium removal require its removal for the insertion of other metals (e.g. chrome in chrome chloride), but this is better categorised as impregnation or substitution.

1.4 CHARACTERISTICS OF DEALUMINATED ZEOLITES

The removal of aluminium from the framework results in changes to the structure, acidic nature and catalytic activity of the catalyst. This is a result of the reduction in framework aluminium content of the catalyst, the production or removal of extra-framework aluminium species and framework distortions and rearrangements to accommodate both of these.

1.4.1 Mechanisms of dealumination

Most studies on the mechanisms of zeolite dealumination have been performed on Zeolite-Y and, to a lesser extent, ZSM-5. These can be used for zeolites in general as they do not depend on crystal structure. Barrer and Peterson [1964] have proposed the following mechanism for acid dealumination of zeolites:

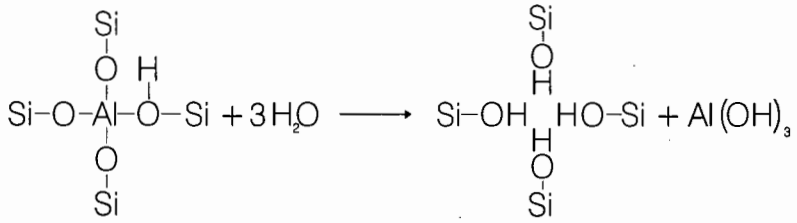

Hydrolysis of the framework oxygen takes place, leaving a hydroxyl nest and removing the aluminium. Goovaerts *et al.* [1989] reports that the first framework aluminium atoms to be leached by acid are those in the four membered rings and that these are deposited in the side pockets during mild dealumination.

More severe acid washes would extract more aluminium from these four membered rings, opening up the side pockets and moving the extracted aluminium into the twelve-membered rings as completely hydrated Al^{3+}. However, Sawa [1992] has reported that EFAl is preferentially removed by acid washing and therefore one would not expect a large amount of aluminium to remain in the zeolite pore after acid washing.

Wang *et al.* [1991$_a$] proposed a mechanism for the hydrothermal treatment of Zeolite-Y, which is essentially the same as the one shown for acid dealumination. They proposed that the product species above underwent silicon insertion to repair the defect site:

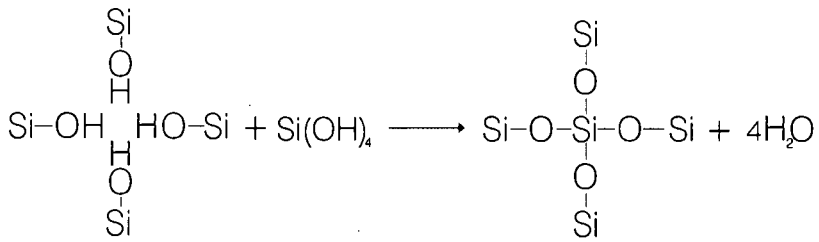

Under conditions of self steaming they proposed that, due to an absence of water to speed up the migration of silicic species and a shortage of these species after such mild dealumination, this last step could not occur. This results in an observed decrease in crystallinity. No aluminium was observed to migrate to the surface.

Wang *et al.* [1991$_a$] divide steaming into two periods: the first is a rapid step where the repair of defect sites is more rapid than aluminium removal and aluminium migrates to the surface as indicated by an increase in crystallinity and XPS data. The second period is much slower due to the limitations of diffusion on water entering the zeolite and the possibility of cationic EFAl exchanging in the zeolite.

It has been reported by Sano *et al.* [1987] that the rate of hydrothermal dealumination from ZSM-5 is second order with respect to the concentration of framework aluminium. This also predicts an initially fast dealumination followed by a progressively slower reaction, but does not take into account diffusive effects and the presence of EFAl.

Stabilization of the framework during steaming has been reported by many authors and various reasons have been given. Firstly, it has been postulated by Kerr that the cationic EFAl of unknown charge or form associates with framework aluminium, stabilising it and does not allow its removal by steaming. This was based on the fact that only those

framework aluminium atoms which are associated with protons are hydrolysable [Chen and Smith 1976]. Chen and Smith therefore calculated that since the hydroxyaluminium ion can have a charge from 1+ to 3+, the maximum degree of dealumination in one steaming step is between 16.7 and 50%.

Secondly, the elimination of water from "hydroxyl nests" to form Si-O-Si bonds has been postulated [Scherzer, 1984; Brunner *et al.*, 1988]. Fejes *et al.* [1985] studied the thermal stability of these hydroxyl nests in acid dealuminated Mordenite and found evidence from TG-DTA to show that they were stable up to about 500 K at which point dehydration occurred.

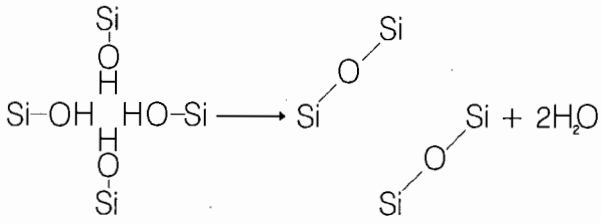

However, Beyer *et al.* [1984], have reported that at least partial dehydration occurs at 430 K and above. Various linkages with different ring structures which were postulated are shown in the schematic below. At low temperatures (430 K) partial dehydroxylation takes

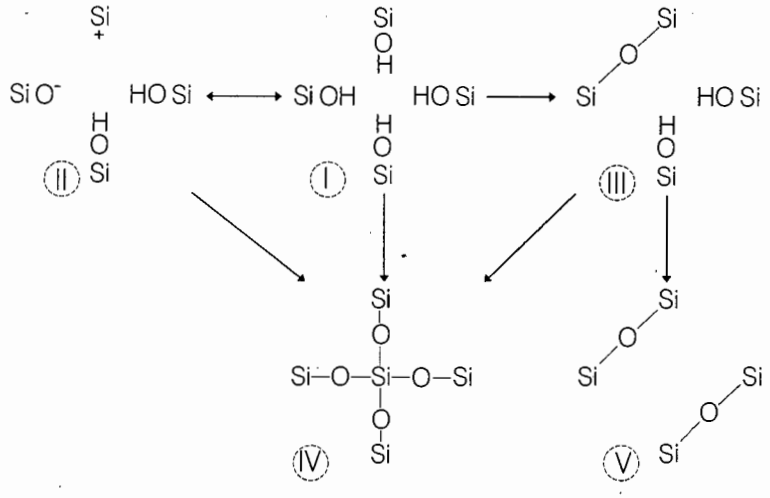

place - producing species II or III. However, these mechanisms imply a strong distortion of the lattice and would affect its stability. Therefore, based on the conception that the opened rings would increase the flexibility of the lattice, Beyer *et al.* [1984] suggested that scheme III existed in partially dehydroxylated Mordenites as well as possibly scheme II.

Thirdly, silica migration and insertion into the vacancies left by dealumination, which recent sorption studies tend to support, could also stabilise the structure. This mechanism is also supported by infra red studies [Scherzer, 1973] and was the conclusion of the mechanism of Wang *et al.* [1991$_a$]. Finally, von Ballmoos suggested what has become known as the "T-Jump" reaction. The reaction is based on the assumption that vacancies formed by dealumination migrate slowly to the catalyst surface, exchanging places with neighbouring T atoms [von Ballmoos, 1981].

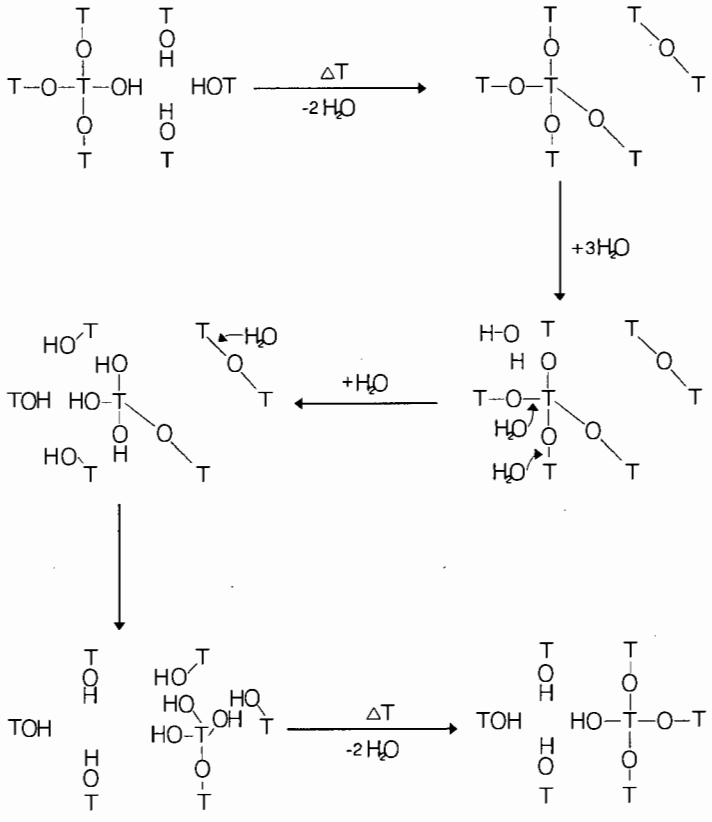

"T-jump" reaction (from Scherzer [1984])

1.4.2 Structure of dealuminated zeolites

1.4.2.1 Crystal Structure

Olsson and Rollmann [1977] have measured the unit cell dimensions of acid leached NH_4-Mordenite using X-ray diffraction. They found that lattice contractions occurring on dealumination are strongly anisotropic and non-linear. Initial aluminium removal (the first 25%) strongly reduces the *b* lattice parameter and to a lesser extent the *c* parameter, but leaves the *a* parameter unchanged. Thereafter, intermediate levels of dealumination reduce all three parameters by roughly the same amount. This they interpreted as evidence of aluminium occurring in four basic site types in the Mordenite structure. The differently sited aluminium atoms show different susceptibility for removal. Raatz *et al.* [1985] investigated the effect of thermal treatment on Mordenite and saw a decrease in unit cell size with increasing treatment temperature.

1.4.2.2 Creation of an aluminium gradient

Although is has been shown that synthesis conditions are largely responsible for the creation of aluminium gradients within zeolite crystals [Kokotailo *et al.*, 1995], dealumination treatments have also been determined to result in changes to these gradients. Mishin and Klyachko [1989] found dealuminated Mordenite to have an aluminium-lean surface compared to Mordenite synthesised with the same Si/Al ratio.

From adsorption studies it has been observed that acid dealumination occurs mainly at the pore mouths of Mordenite [Sawa, 1992]. This was reasoned to be the result of competition between the relative rates of diffusion of the acid and the dealumination reaction, i.e. a strong acid which dealuminates faster than it diffuses into the crystal will remove aluminium preferentially from the surface [Sawa, 1989]. However, no aluminium gradient was seen by XPS after thermal and acid treatment and a slight surface enrichment was seen for steam treatment by Meyers *et al.* [1988] as well as a blocking of 60% of the micropore volume.

In a similar investigation, however, Remy *et al.* [1993] showed that the surface of a Mordenite sample which has been steamed and then acid washed contained only tetrahedral aluminium in untreated mildly dealuminated samples. Tricoordinated, and hexacoordinated aluminium species were produced on the surface only after more severe dealumination.

Dwyer *et al.* [1982] has used Fast Atom Bombardment Mass Spectrometry to study the surface and bulk compositions of steamed and acid washed zeolites. In general, Mordenite was found to have less aluminium at the surface than in the bulk, particularly in its protonic form, and this effect was increased by acid washing. Aluminium migration to the surface was observed after steam treatment. Each of the researchers used different dealumination conditions and combinations of dealumination methods and therefore no consistent results were seen. However, in general, acid washing has the potential to remove aluminium preferentially from the surface, while steaming has been seen to produce an aluminium rich surface.

1.4.2.3 Changes in pore size

Chen [1976] reported an increase in sorption capacity for cyclohexane after acid leaching of H-Mordenite. This was ascribed to the removal of extra-framework material. Dealumination by acid leaching and by steaming followed by acid leaching has also been reported to lead to an increase in pore size or an enlargement of the side pockets [Beyer, 1984] and an increase in mass transfer through the channels [Musa *et al.*, 1987].

However, from analysis of H_2O adsorption on dealuminated Mordenites, Belenkaja *et al.* [1971] concluded that micropore volume actually decreases and the increase in pore volume is a result of mesopores formed by the unification of adjacent pores and by removal of framework aluminium or silicon.

Dashevskii *et al.* [1978] studied the structure of dealuminated Mordenite (Si/Al = 23.5) using

transmission electron microscopy and reported that a considerable number of channels had a diameter which was enlarged to 20 Å. Mesopores have also been observed using nitrogen adsorption isotherms after acid treatment of H-Mordenite [Ajot *et al.*, 1991]. These were thought to be a result of acid leaching of aluminium rich nodules providing that the initial Si/Al ratio is high enough to avoid framework collapse and crystallographic defects are present, thus their formation is primarily a function of Si/Al ratio and synthesis conditions.

Olken and Garces [1993] observed the hydroconversion of n-decane over Mordenite which has been thermally treated and acid washed. An increase in dimensionality was observed by a shift in selectivity towards a symmetrically cracked product (i.e. they concluded that the Mordenite structure change from one dimension to two or three dimensions). This could be indicative of the creation of mesopores, or the enlargement of the side pockets.

An increase in acid strength combined with a more constricted pore diameter has been reported in ZSM-5 after steaming by Vasques *et al.* [1989] as a result of experiments conducted using n-heptane cracking and m-xylene isomerisation. However, Lohse *et al.* [1984], using the adsorption of water, cyclohexane, benzene and n-hexane to show the effect of steaming on the diffusional properties of steamed ZSM-5, found that only the diffusion of water was greatly affected by steaming. These results suggest that although the hydrophobicity of the catalyst may have altered, the pore diameter has not decreased.

1.4.3 Extra-framework aluminium species

The existence of extra-framework aluminium is well known and has been discussed frequently in the literature [Scherzer, 1984; Karge and Weitkamp, 1986; Engelhardt, 1991, Hannus *et al.*, 1995]. However, although it is known that their nature and distribution is dependent on the initial composition and structure of the catalyst and the dealumination procedure, there is no comprehensive view that can be given concerning the chemical nature

of these species [Crocker *et al.*, 1993]. Although the production of extra-framework aluminium is interlinked with both acidic and catalytic changes within the catalyst, this section is described here separately in order to present the types of species thought to exist before looking at the effects these might have on the acidic or catalytic properties of zeolites.

In 1967, Kerr proposed that the $Al(OH)_3$, produced by hydrolysis of the Si-O-Al bond, goes on to dehydrate in combination with protons from Brönsted sites to form cationic extra-framework species of the type $Al(OH)^{2+}$ or $Al(OH)_2^+$. Kühl [1977] was in agreement with this proposal and thus suggested that the EFAl species in Zeolite-Y and dealuminated Mordenite were present, at least partly, in a cationic form (i.e. AlO^+) but he was not certain of its coordination.

Engelhardt *et al.* [1987] saw a greater number of extra-framework hydroxyaluminium species after steam treatment than after thermal treatment as evidenced by ^1H MAS NMR. However, the detected number of aluminium hydroxy species was not related to number of EFAl species as with increasing time of treatment (from 1.5 to 12 hours), dehydroxylation reactions were thought to occur.

Goovaerts *et al.* [1989], studied the hydroxyl group populations in acid washed and dried Mordenites to investigate this dehydroxylation. They suggested that, on the basis that EFAl in hydrated samples are octahedral $[Al(H_2O)_6]^{3+}$ species, the dehydrated EFAl species $Al(OH)_3$, AlOOH and AlO^+ are formed at increasing temperatures 473, 673 and 773 K respectively. The species $Al(OH)_2^+$ and AlOOH were speculated to exist in the side pockets of Mordenite in dehydrated, acid leached samples. The presence of extra-framework AlOOH was also reported [Brunner *et al.*, 1991]. The aluminium was proposed to be in tetrahedral coordination through its proximity to two framework oxygens.

In a review on the ultrastabilisation of zeolites, Fejes *et al.* [1988] proposed that, while the formation of the AlO^+ species was a possibility, the partial formation of a charged polymeric

aluminium-oxygen compound seemed to be more probable. It was subsequently reported by Sawa [1992] that most of the non-structural aluminium was occluded as clusters. This supported the work of Janin *et al.* [1988 and 1991] who suggested that the non-acidic hydroxy-aluminium species occur as highly dispersed alumina-rich silica-alumina phases, while the acidic hydroxy-aluminium species would be due to a more silica rich phase. However, Gruver and Fripiat [1994] have concluded from an infrared study of CO chemisorption that the Lewis sites generated from EFAl are highly dispersed throughout the zeolites. A similar conclusion was drawn by Hong and Fripiat [1995] after studies of nitrogen and pentane adsorption on calcined Mordenite.

The fact that exchange capacities of platinum on deep bed calcined Mordenite decreased with increasing temperature prompted Raatz *et al.* [1985] to concluded that the number of exchange site had been reduced by framework dealumination and the creation of unexchangeable cationic Al^{VI} species. The nature of these species were thought to depend on the calcination temperature, high temperatures favouring the formation of neutral hydroxyaluminium complexes.

Rhodes and Rudham [1993] studied the effect of steaming and EDTA washing on Zeolite-Y using a number of characterisation techniques. They concluded that the majority of EFAl species in the steamed sample were present as asymmetric species or polymeric oxides which were extensively removed by EDTA washing. They also found that there was possibly a charge balancing effect of EFAl species on the framework aluminium and calculated that such EFAl had a single positive charge, although other investigators have assigned other charges. For instance Fritz and Lunsford [1989] proposed that EFAl in Zeolite-Y exists in the form $AlOOAl^{2+}$ or $Al(OH)^{2+}$ on the basis of infra-red studies of the hydroxyl region.

Compensating effects of EFAl have also been observed in Mordenite. Miller *et al.* [1992] has recently reported that Mordenite dealuminated up to 20% possesses octahedral, non-structural and non-acidic aluminium groups but, after about a 50% dealumination, internal

pentacoordinated non-structural aluminium species were formed. These were proposed to be either non-acidic or weakly acidic and significantly reduced the strength of the remaining structural ions.

As shown here and in other reports [Jeanjean, 1991; Sun, 1991; Corma, 1989_a; Scherzer, 1984] EFAl has been described variously as species which could be neutral, located in cationic sites on the framework such as Al^{3+}, AlO^{+}, $Al(OH)^{2+}$ or $Al(OH)_2^{+}$ with octahedral or tetrahedral symmetry or in the zeolite cages in the form of a dimer or polymer.

1.4.4 Acidity of dealuminated zeolites

Lewis acidity, as has been mentioned, is usually associated with extra-framework aluminium, while Brönsted acidity is associated with framework aluminium. Both are however affected by dealumination and seem to be somewhat interlinked.

1.4.4.1 Increased acidity by framework aluminium removal

The number of Brönsted acid sites has been found to decrease with removal of framework aluminium, while the density of strong acid sites showed a maximum [Stach and Janchen, 1992]. This observed effect fits well with the Next Nearest Neighbour Theory discussed previously (Fig 1.3). This peak in strong acidity has been reported to possibly be shifted in some cases by diffusional effects from the calculated position of Si/Al = 9.5 to a higher ratio [Ribeiro *et al.*, 1991].

In 1978, Kiovsky *et al.* reported that Mordenite differed from Zeolite-Y in that the number of strong acid sites increased with acid dealumination. They ascribed this to the formation of a hydroxyl nest, by the removal of aluminium, which acts through the lattice to polarize the hydroxyl electron cloud away from the proton of a nearby Brönsted site.

This concept was supported by Ghosh and Curthoys [1984] who reported increased acidity to be due to both the formation of SiOH groups and easier access to Brönsted sites by the removal of amorphous material [Ghosh and Curthoys, 1983 and 1984]. However, more recently it has been reported that the silanol defect sites produced by strong acid dealumination, measured by infrared spectroscopy, were found to have no effect on acid strength as measured by ammonia temperature programmed desorption [Miller *et al.* 1992].

Zholobenko *et al.* [1993], who proposed the existence of high and low frequency Brönsted acid sites, found that with increased dealumination, the amount of low frequency acid sites decreased, while the amount of high frequency sites increased. The same trend was observed by Makarova *et al.* [1994] in ultrastable Zeolite-Y where increased catalytic activity was directly linked to an increase in high frequency and a decrease in low frequency hydroxyls.

1.4.4.2 The effect of EFAl on Lewis acidity

Lefrancois and Malbois [1971] have reported the existence of three types of acid sites on Mordenite distinguished by infrared spectroscopy of adsorbed pyridine. They found Brönsted acidity showing a band at 1545 cm^{-1}, Lewis centres, assumed at that time to be tricoordinated aluminium atoms with an electron free orbits, at 1455 cm^{-1} and a third site probably due to strong interactions between cation and pyridine atom at 1445 cm^{-1}. Lercher and Rumplmayr [1985] investigated acid dealuminated HZSM-5 and found similar sites.

Bosacek and Freude [1988] investigated Zeolite-Y using aluminium NMR and infrared spectroscopy of carbon monoxide. They proposed that after dehydroxylation of the zeolite by treatment above 450°C under vacuum, aluminium released from the lattice probably exists as a cation of simple composition i.e. Al^{3+} or AlO^{+}, exhibiting very strong lewis acidity. After hydration these could be transformed into various hydroxocations. Alternatively, Garralon *et al.* [1989] suggested that the super-acid sites are due to the presence of amorphous silica alumina in the pores formed during dealumination. Zholobenko *et al.*

[1993] and Witzel *et al.* [1995] also reported the existence of Lewis sites created by EFAl, although the exact nature of the Lewis acid site has not been explained.

1.4.4.3 The effect of EFAl on Brönsted acidity

In several zeolites, the existence of enhanced Brönsted acid sites has been reported to be associated with the presence of EFAl in addition to isolated framework aluminium ions [Mirodatos and Barthomeuf, 1981; Lago *et al.*, 1986; Beyerlein *et al.*, 1988; Vasques *et al.*, 1989; Garralon *et al.*, 1989; Goovaerts *et al.*, 1989].

The EFAl species was proposed to either give rise to Brönsted acidity directly according to $AlO^+ + H_2O \rightleftarrows AlO(OH) + H^+$ or enhance the Brönsted acidity of other acid sites in proximity to it, giving rise to "super acid sites" [Mirodatos and Barthomeuf, 1981]. The latter proposal, that a portion of the EFAl is located in the cages of some zeolites, which withdraws electrons from the framework hydroxyl groups, making them more acidic, has been proposed by a number of authors [Beyerlein *et al.*, 1988; Carvajal *et al.*, 1990; Chen *et al.* 1992]. This "synergistic effect" between the Lewis site and the nearby proton of a strong Brönsted site has also been investigated by Brunner *et al.* [1994] using ^1H MAS NMR, but the EFAl produced by steaming at "mild" conditions was not found to increase the strength of Brönsted acid sites.

Negative effects of EFAl on acidity have also been reported. After high temperature thermal dealumination Meyers *et al.* [1988] reported strong acidity to have been nearly completely destroyed or made inaccessible by amorphous material created during hydrothermal treatment. Subsequent treatment by acid was reported to remove this material and allow access to the strong acid sites. A similar result has been observed by Bamwenda *et al.* [1994] and they concluded that EFAl species reduced the acidity of steamed catalysts by blocking pores or covering individual acid sites indiscriminantly.

None of the nonstructural aluminium produced by acid and steam treatment by Miller *et al.* [1992] was seen to be acidic. When present in low concentrations, the octahedral EFAl had no effect on acid strength of the remaining framework aluminium. However, when large amounts of nonstructural, pentacoordinated aluminium are present in the pores of Mordenite, the acid strength of many of the framework sites decreased.

1.4.5 Catalytic activity of dealuminated zeolites

Mild acid washing has been shown to generally result in Mordenite becoming a more active catalyst [Bierenbaum *et al.*, 1971; Koriada *et al.*, 1980; Scherzer, 1984] which is superior to Mordenites synthesized with comparable Si/Al ratios and which show a slower decline in activity [Chumbale *et al.*, 1992]. This has been assigned to the removal of amorphous material created during synthesis from the channels and the generation of strong acid sites [Scherzer, 1984]. The increase in quantity of strong acid sites by the removal of aluminium, discussed in the previous section, results in a more active catalyst (as was shown by Miller *et al.* [1992]). Catalytic reactivity for n-hexane cracking was found to increase with the number of acid sites with an enthalpy of absorption for ammonia greater than 130 kJ/mole.

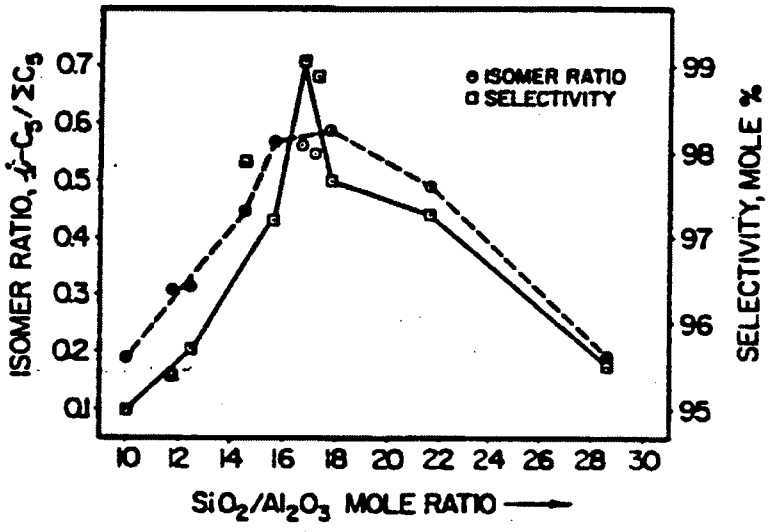

Figure 1.6. Isomer ratio and selectivity versus SiO_2/Al_2O_3 mole ratio of modified H-M in the isomerisation of n-pentane.
[Koriada et al., 1980]

There have been many studies of acid leached Mordenite using various probe reactions which have exhibited increases in catalytic activity up to a Si/Al ratio of between 8.5 to 9.5 followed by a subsequent decrease. These include n-pentane isomerisation [Koriada et al., 1980] (shown in Fig. 1.6.), cumene cracking [Bierenbaum *et al.*, 1971] o-dichlorobenzene isomerisation [Pardillos *et al.* 1989], and others. This corresponds to the maximum seen in strong acidity for dealuminated Mordenites.

It has been demonstrated that mild steaming of ZSM-5 and Zeolite-Y can result in an enhancement of the activity of these zeolites. Most investigators explain this enhancement by an interaction of the Brönsted acid sites of HZSM-5 and of Lewis sites of EFAl. The possibility of an inductive effect of Lewis sites on the protonic acidity of zeolites was mentioned a long time ago [Hopkins, 1968; Lunsford 1968]. According to Mirodatos and Barthomeuf [1981], this influence could explain why, during toluene disproportionation, steamed Mordenite samples could activate hydrogen and thus reduce coke formation [Gnep *et al.*, 1980].

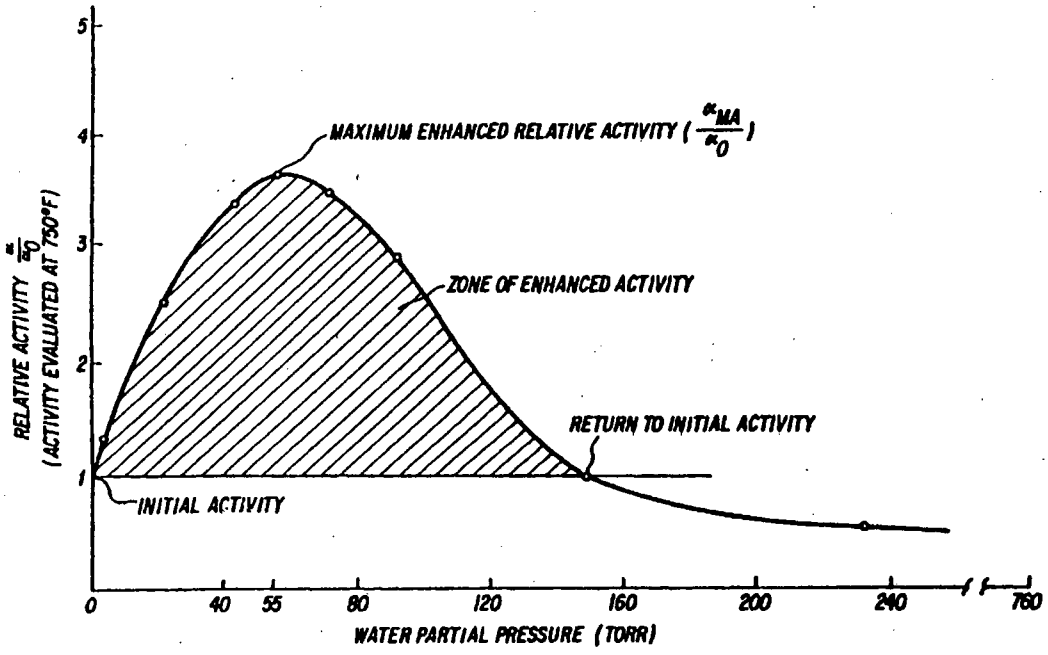

Figure 1.7. Dependence of relative activity for n-hexane cracking on amount of water present in calcination of HZSM-5/Al_2O_3. [Haag, 1983]

Many authors have reported activity enhancements over mildly steamed Zeolite-Y [Corma, 1989; Addison *et al.*, 1988; Pellet *et al.*, 1988; Kubelkova *et al.*, 1989] and ZSM-20 [Kosslick *et al.*, 1994]. However, prior to this, Haag [1983] and Lago *et al.* [1986] observed that the activity of HZSM-5 for hexane cracking increased about fourfold upon mild steaming of the catalyst (Figure 1.7). They postulated that the enhanced activity arises from aluminium atoms in close proximity to each other, such as paired Al centres.

One member of a paired Al region is then modified during hydrothermal treatment, possibly by being partially hydrolysed. This species then acts as a strong electron withdrawing centre for the remaining tetrahedral aluminium, creating a stronger Brönsted site. During steaming, a substantial portion of the aluminium is removed from the framework and much of this is extra-crystalline. The remaining strong sites exhibited a specific activity 45-75 times greater than that of a normal site of ZSM-5.

Brunner *et al.* [1989] and Sendota and Ono [1988] propose that the reacting n-hexane molecules simultaneously react with the Brönsted and Lewis centres. They proposed that the presence of bridging OH groups are necessary for activity enhancement and therefore a convenient spatial arrangement of the reacting molecule on a bridging OH group and an extra-framework aluminium species leads to enhanced activity. This model requires a balance of structural and extra-framework aluminium for optimum activity. More recently, Hong *et al.* [1994] found the rate of isomerisation of n-pentane and o-xylene to be proportional to the product of the amounts of Brönsted and Lewis sites present in steamed and calcined Mordenite. They concluded that this was proof of a synergistic effect between Brönsted and Lewis acid sites.

Investigating this area co-workers Zholobenko *et al.* [1990, 1991] and Löffler *et al.* [1991] concluded from studies of n-hexane and 1-hexene cracking and infrared spectroscopy on mildly steamed HZSM-5 that there was no inductive effect of an EFAL on the proton donor properties of the OH groups. The increase in activity was therefore not explained by

variations in Brönsted activity, but rather by a change in Lewis acidity.

In the proposed mechanism, the Lewis acids are responsible for the initiation of n-hexane cracking via dehydrogenation or demethanation of the substrate molecule, regarded as the limiting step. This leads to the formation of reactive olefins that react via a classical carbenium ion mechanism involving Brönsted acid sites. This is supported by the results in Figure 1.8 which show that the steaming has a minimal effect on the reaction of n-hexane/1-hexene mixture compared to the n-hexane alone.

In agreement with this, Luk'yanov [1991] found that steamed samples of ZSM-5 gave increased selectivity for propane and decreased selectivity for ethane and so concluded that the enhancement is due to the increased activity of the hydrogen transfer step of the reaction.

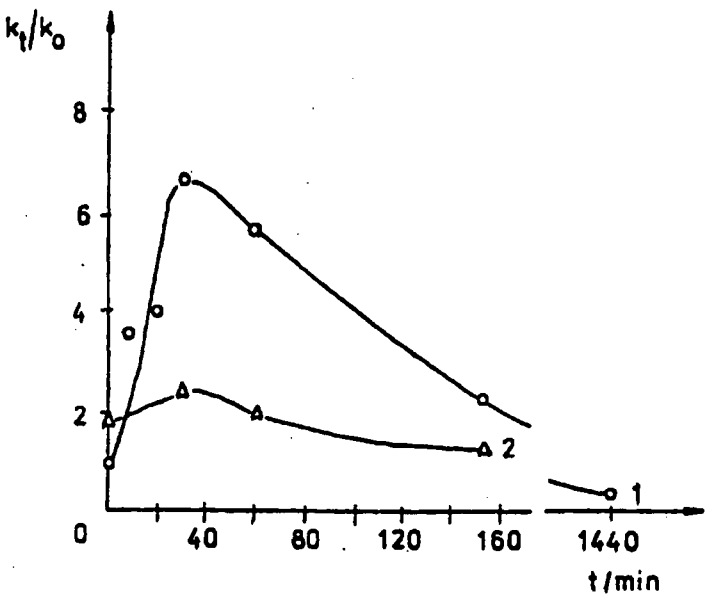

Figure 1.8. Dependence of k_t/k_0 on the time of steaming pretreatment of HZSM-5 zeolite: (1) for cracking of pure hexane; (2) for cracking of the mixture containing 99% n-hexane and 1% 1-hexene. [Zholobenko et al., 1991]

Wang *et al.* [1991$_b$], investigating the effect of steaming and acid washing on Zeolite-Y on the cracking of n-heptane, found activity to be dependent on both framework and extra-framework aluminium content. When large amounts of framework aluminium are present

the EFAl appeared to have a promoting effect on the activity for all reactions including coking. This was explained by an inductive effect of the Lewis acid sites of these species on the protonic sites of the zeolite. However, with reduced framework aluminium these EFAl species have practically no effect due to the large distances between them and the protonic site.

However, certain authors [Jacquinot *et al.*, 1989; van Broekhoven *et al.*, 1989; Mavrodina *et al.*, 1989] have claimed steaming has a negative effect on the activity of zeolites. In particular it was the residual monotonic cations which were reported to have a dramatic negative effect on activity for Zeolite-Y [Hansford, 1967; Ward and Hansford, 1969; Beaumont and Barthomeuf, 1973]. Although there was a small amount of sodium in the catalysts used (up to 10 wt%) and Beyerlin *et al.* [1988] has showed that residual sodium cations decrease isobutane cracking activity, the observed effect may not be fully explained by sodium poisoning.

Nock and Rudham [1987] found that the presence of EFAl, possibly located at the crystallite surface of the Zeolite-Y, was detrimental to the catalytic activity for cumene cracking due to an increase in the level of pore-mouth coking and thus their removal increased catalyst lifetimes. Öhlmann *et al.* [1991] found similar results for methanol to olefin reactions over ZSM-5.

Studies of the effect of EFAl on the catalytic activity of Mordenite have also shown mixed results. In a review on dealumination Scherzer reports that steaming of Mordenite results in a decrease in catalytic activity due to the elimination of acid sites and the creation of diffusional constraints [Scherzer, 1984]. Abbot and Guerzoni [1992] found that the formation of aromatics and coke during reactions of n-octane on H-Mordenite was enhanced by the presence of Lewis sites on the catalyst surface, leading to rapid deactivation.

Deactivation in Mordenite is pronounced due to the effect not only of acid site poisoning and

the consumption of the active hydroxyl groups, but also that of pore blocking [Karge and Boldingh, 1988]. Therefore small increases in coke formation would have severe negative effects on the catalytic activity. Mishin and Klyachko [1989], on the other hand, speculated from work on dealuminated Mordenite and Zeolite-Y that the significance of EFAl as an active site is negligible.

A maximum in activity for hexane cracking was observed for Mordenite dealuminated with dilute acid [Goovaerts *et al.*, 1989]. Alternatively, very strong acid sites were observed by temperature programmed desorption on mildly steamed Mordenite [Mirodatos and Barthomeuf, 1981]. In both studies the enhanced acid strength or catalytic activity was accompanied by the formation of extra-framework Lewis acid sites. Goovearts *et al.* [1989] proposed that the function of the Lewis acid was to dehydrogenate paraffins to olefins, while Mirodatos and Barthomeuf [1981] suggested that the Lewis acid bridged the structural hydroxyl acid site, withdrawing electron density and increasing the acid strength of the structural Brönsted hydroxyl group.

Ratnasamy *et al.* [1981] investigated the isomerisation and disproportionation of o-xylene over Na-Mordenite protonated to various levels. Comparing their results to the creation of EFAl proposed by Kühl [1977], they concluded that a Brönsted site associated with a extra-framework AlO^+ species was responsible for the observed enhanced activity at high levels of Na exchange.

1.5 THE USE OF PROBE REACTIONS

One of the best methods for catalyst characterisation is the use of probe reactions. This method probes the catalytic properties of the sample directly. However, care must be taken in choosing a probe reaction. The reaction should be well understood and thus be able to probe a particular aspect of the catalyst's behaviour. Other reaction effects such as mass and heat transfer limitations also need to be eliminated as these obscure the true catalytic nature of the catalyst that one wants to observe. The probe reactions discussed here were chosen on these criteria and are used to probe the number and strength of acid sites (isobutane cracking), the external activity (cyclohexanol dehydration) and shape selective effects (isopropylation of naphthalene) of the dealuminated Mordenite samples.

1.5.1 Isobutane cracking

Isobutane cracking has been proposed as a sensitive probe reaction over solid acid catalysts [McVicker *et al.*, 1983; Lombardo and Hall, 1988]. When subjected to high temperature cracking, the isobutane molecule provides a sizeable number of products with which to investigate reaction selectivity, but these are limited in number and so do not become unmanageable. The reaction has also been shown not to be dominated by mass transfer limitations [McVicker *et al.*, 1983].

The mechanism of paraffin cracking has been extensively reviewed. As a result of the fact that small product molecules were typical of gas phase radical reactions McVicker *et al.* [1983] suggested that feed paraffin molecules combine with Lewis sites on solid acid catalysts to form radical ions which then decompose to small alkanes or hydrogen and alkenes. The latter may then form carbonium ions which isomerise, oligomerise and crack. The radical mechanism produces hydrogen, methane, propene and isobutene, while the products from the carbonium ions would be propane, n-butane and pentanes.

Later, however, Haag and Dessau [1984] and Corma *et al.* [1985] proposed an alternative

mechanism. The initial step of this mechanism is the direct protonation of a paraffin to form a non-classical pentacoordinated carbonium ion. This then decomposes to form a small alkane or hydrogen and a carbenium ion which deprotonates to form an olefin.

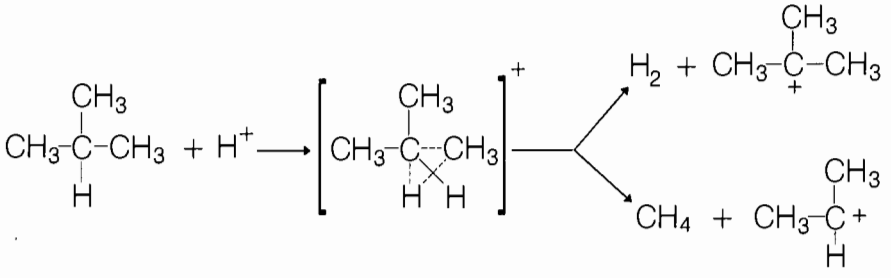

More recently, Lombardo and Hall [1988] have proposed a single mechanism to account for the observed product distribution of neopentane and isobutane over solid acid catalysts. The initial step is the same as that described by Haag and Dessau [1984] and shown above. The tertiary butyl cation (t-$C_4H_9^+$) equilibrates with its isomerised linear form and an equilibrium is established between all the carbenium ions and their corresponding alkenes.

$$
\begin{array}{lcl}
C_3H_7^+ + A^- & \rightleftarrows & C_3H_6 + HA \\
t\text{-}C_4H_9^+ + A^- & \rightleftarrows & i\text{-}C_4H_8 + HA \\
\downarrow\uparrow & & \\
n\text{-}C_4H_9^+ + A^- & \rightleftarrows & n\text{-}C_4H_8 + HA
\end{array}
$$

The lifetimes of these carbenium ions play a vital role in this mechanism. For a weak acid catalyst the lifetimes of these ions is short and thus the equilibrium would lie to the right. The only products expected would be the olefins formed by the above reactions and the hydrogen and methane formed in the initial step. For stronger acid catalysts under favourable reaction conditions the equilibrium lies to the left as the carbenium ion lifetime is long. These ions may then undergo reactions such as oligomerisation, isomerisation, β-scission and hydride transfer. This would produce propane, n-butane, pentanes and higher products from isobutane.

This mechanism encompasses the two separate mechanisms proposed by Haag and Dessau

[1984] and differs from the mechanism of McVicker *et al.* [1983] only in the mechanism for the formation of the carbenium ion. All mechanisms predict the same distribution of products. Shigeishi *et al.* [1991] have noted that there is an increase in the production of hydrogen, methane, propene and butenes at high temperatures. This can be explained by a shift in the equilibrium equations towards the right due to the endothermic nature of the reaction, which results in a decrease in lifetime of the carbenium ion and its participation in further reactions. The same result is seen when contact time is reduced as well as with increasing unit cell size of zeolite [Corma *et al.*, 1994], indicating that it is necessary for the reaction to be carried under identical conditions when comparing catalysts..

Dumisic *et al.* [1993] have studied the kinetics of this reaction and shown that all olefin desorptions and carbenium ion isomerisations are equilibrated reactions. The kinetically significant, and essentially irreversible, reactions were established to be the initiation steps; the oligomerisation and hydride transfer reactions and the ethylene production step. With weaker acid sites the rates of hydride transfer relative to initiation reactions was reduced as was the production of ethylene. The hydride transfer reactions may, however, be sterically hindered on Zeolite-Y, particularly for the production of isopentane.

1.5.2 Cyclohexanol dehydration

The dehydration of cyclohexanol has been proposed by Karge *et al.* [1983] as a suitable reaction to probe the activity of the external crystallite sites of Mordenite. The dehydration reaction has been found to occur on both strong and weak Brönsted acid sites and produces water and cyclohexene as products [Datka *et al.*, 1995]. Polymerisation of cyclohexene should not be able to occur if the ring structure remains intact. Datka *et al.* [1995] found secondary reaction to occur only at temperatures above 450°C on HZSM-5, therefore irreversible deactivation due to coking is not expected.

Although rapid deactivation of the catalyst was observed to occur in this reaction, this was reversible and the catalyst could be completely regenerated. The initial drop in activity was

therefore ascribed to the adsorption of cyclohexanol and a retarding effect of product water by competitive adsorption [Karge *et al.*, 1983]. The conversion then reaches a steady state. The cyclohexanol and product cyclohexene molecules were reported not to be able to enter the Mordenite pores, even though their dimensions are of the same magnitude. This behaviour was attributed to the strongly adsorbed cyclohexene blocking these pores at the pore mouth [Karge, 1983].

1.5.3 Isopropylation of naphthalene

2,6-dialkylnaphthalenes are useful in industry as monomers for the production of liquid crystal polymers. However, it is difficult to obtain high selectivity towards 2,6-dialkylnaphthalene in conventional industrial methods such as Friedel-Crafts Alkylation and gas phase reaction over silica-alumina catalysts [Katayama, 1991]. During the diisopropylation of naphthalene several diisopropylnaphthalene (DIPN) isomers are formed, particularly the 2,7 isomer which is difficult to separate from the linear 2,6 isomer [Horsely, 1994], a process which is usually done by azeotropic distillation. The highest equilibrium percentage of the 2,6 isomer among other DIPN isomers is about 39% with a 2,6/2,7 isomer ratio of 1 [Horsely, 1994, Fellman, 1991].

The use of Mordenite, particularly with a high Si/Al ratio, as a shape selective catalyst for the production of the 2,6-DIPN isomer has been reported by several authors. Improved selectivity to 2,6-DIPN were noted up to 63% for dealuminated H-Mordenite and up to 73% for a cerium modified dealuminated Mordenite [Sugi, 1994_b].

The formation of the two isomers (2,6- and 2,7-DIPN) in the pores of Mordenite can be seen in Figure 1.9. It can be seen from this representation that the structure of Mordenite would favour the formation of the 2,6-DIPN isomer. Therefore increase selectivity to this product can be expected due to shape selective effects.

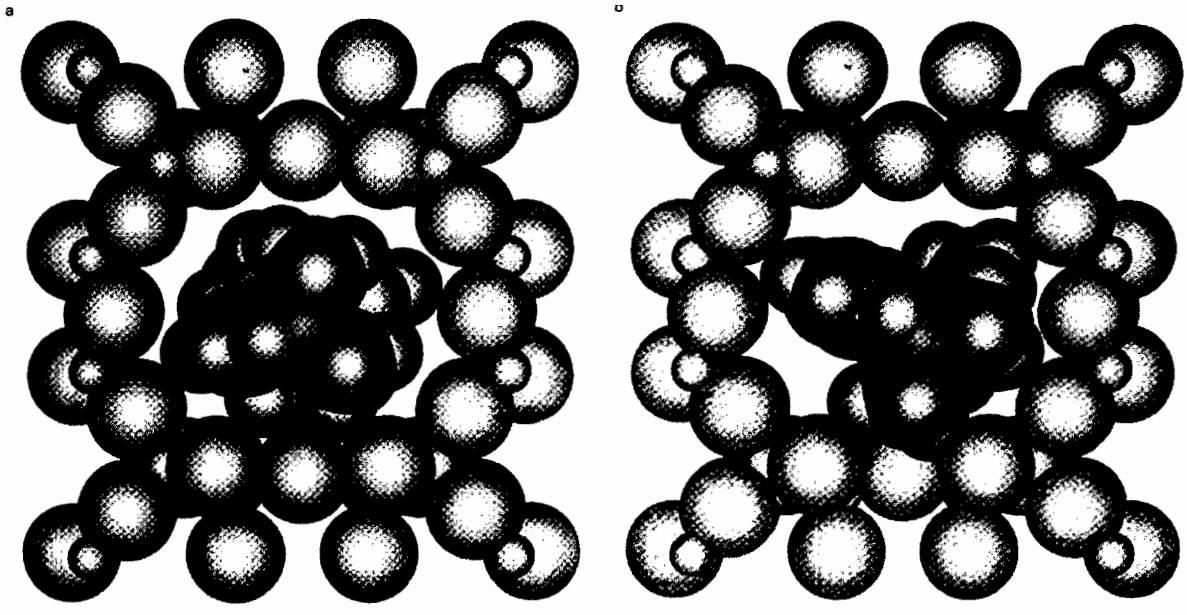

Figure 1.9. Space filling models of (a) 2,6-DIPN and (b) 2,7-DIPN in mordenite. [Horsely *et al.*, 1994]

Shape selectivity towards a particular product can be a result of three general types of phenomenon. Firstly, size exclusion can occur when reactants are prohibited from reacting because their size restricts them from access to the catalyst surface or the size of their products prohibits their return from the catalyst surface to the bulk.

Secondly, when the reactant and product molecules are both able to diffuse through the zeolite channel, the reaction intermediates can be spatially constrained by the zeolite structure, this is referred to as spatiospecific or transition state shape selectivity. Thirdly, diffusive selectivity can occur when reactant or product molecules are in the configurational diffusion regime, described by Weisz [1973]. A small change in a molecule's dimensions can result in a large change in diffusivity as shown in Figure 1.10.

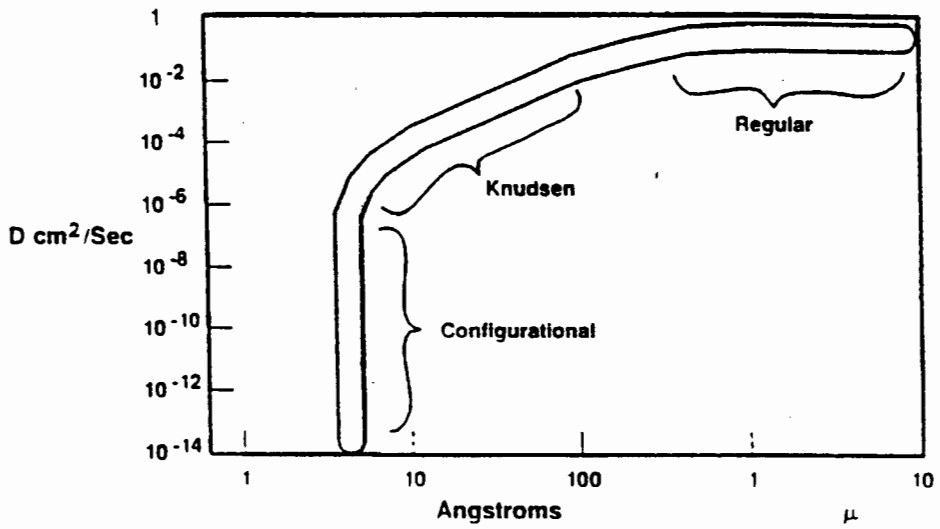

Figure 1.10. Diffusivity and size of aperture (pore): regimes of diffusion. [Weisz, 1973]

This effect is observed in DIPN synthesis due to the steric differences in the 2,6 and 2,7 isomers where diffusive selectivity is seen to limit the production of the less linear 2,7 isomer. Horsely *et al.* [1994] showed, using a simulation on Biosym, that the 2,6 isomer had a lower energy associated to its diffusion through the Mordenite channel than the 2,7 isomer (Figure 1.11).

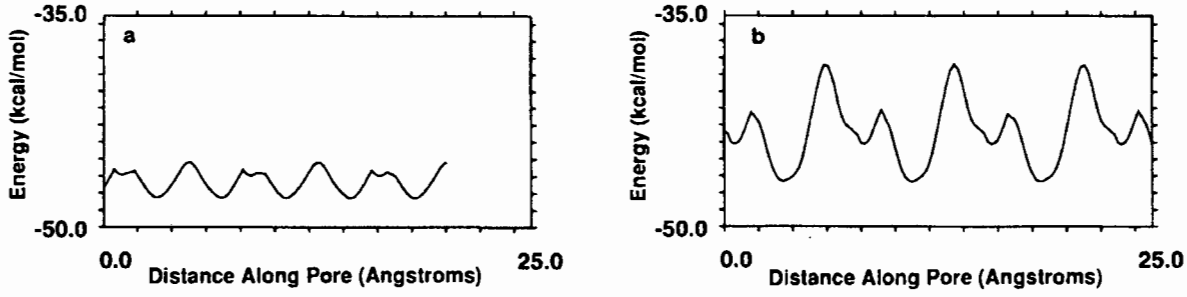

Figure 1.11. Minimum energy profiles for diffusion of (a) 2,6-DIPN and (b) 2,7-DIPN in mordenite. [Horsely *et al.*, 1994]

Since small changes in the catalyst structure, particularly in its pore size, will result in a marked effect on the catalyst's selectivity in this reaction, it has been chosen as a suitable reaction to probe changes in the shape selectivity of dealuminated Mordenite. However, it must be noted that as shape selectivity only occurs in the catalyst's pore structure any external acidity would result in a reduction in the shape selectivity of the catalyst.

Sugi *et al.* [1994] have investigated the effect of acid site density and strength on the activity of Mordenite for the alkylation of biphenyl. They observed an increase in coke formation with dealumination whish was thought to be due to increased acid site density and acid strength. A reduction in coke led to increased selectivity and yield to alkylated biphenyls.

Therefore the most shape selective catalyst is likely to be one with low external acidity, minimal pore restrictions and low acid site density and strength.

1.6 OBJECTIVES OF THIS RESEARCH

As has been outlined in the previous section, despite the attention this topic has received, there is a significant lack of clarity on many issues related to the changes in the structure, acidity and catalytic activity of Mordenite caused by dealumination. There are several reasons for this. Firstly, the dealumination conditions used in various studies are usually not equivalent to each other particularly in the case of steaming. Secondly, the use of Mordenite from different sources could easily lead to different and conflicting results.

The objectives of this research were:

1. To conduct a systematic study of the effect of acid washing, steaming and steaming followed by acid washing on a single batch of well characterised Mordenite;

2. To characterise the solid state properties of the samples thus modified with respect to:
   - 2.1 Aluminium removal from the framework (AA, ^{29}Si MAS NMR, ^{27}Al MAS NMR);
   - 2.2 The creation of extra-framework species (^{29}Si MAS NMR, ^{27}Al MAS NMR);
   - 2.3 Changes to catalyst morphology and structure (XRD, SEM, FTIR);

3. To characterise the acidity of the samples, with respect to:
   - 3.1 Number of acid sites (TPD of ammonia, ^{1}H MAS NMR);
   - 3.2 Type of acid site (FTIR of adsorbed pyridine, ^{1}H MAS NMR);
   - 3.3 Strength of acid site (TPD of ammonia, FTIR of adsorbed pyridine);

4. To characterise the catalytic properties of the dealuminated catalysts with respect to the:
   4.1 Number and strength of active sites (Isobutane cracking);
   4.2 Presence of active sites on the external surface of the catalyst crystallites (Cyclohexanol dehydration);
   4.3 Relative activity of the internal and external surface sites of the catalyst and its shape selective catalytic properties (Isopropylation of naphthalene);

5. To determine the method of treatment, viz. acid washing and steaming and combinations thereof, which are conducive to the promotion of particular acid sites and of particular catalytic properties.

CHAPTER TWO

EXPERIMENTAL METHODS

2.1 CATALYST MODIFICATIONS

The catalyst used in this study was from a single batch of sodium-mordenite sample, Lot 299 (DEGUSSA KM 440), obtained from the Fritz-Haber Institute in Berlin.

2.1.1 Ion exchange

Sodium was exchanged using an excess of 2N ammonium nitrate solution stirred at 25°C for 12 hours. The catalyst was filtered out of the solution by vacuum filtration and washed with deionized water before being dried at 80°C overnight.

2.1.2 Calcination

Samples were calcined by heating at 3°C/min to 550°C in a stainless steel reactor (shown in Figure 2.1.) under a nitrogen atmosphere, at which stage air was passed over the catalyst for 18 hours at 240 ml/min (superficial velocity of 200 $cm.s^{-1}$). The catalyst was then cooled under nitrogen. "Deep bed" calcination took place using a catalyst bed depth of 150 mm (19 g_{cat}) as opposed to the normal bed depth of 25 mm (3.25 g_{cat}).

2.1.3 Steaming

The experimental rig used for steaming is shown in Figure 2.1. For hydrothermal treatment the reactor was heated to 550°C at 5°C/min. Mild steaming was carried out using 190 ml/min of 230 torr steam in a nitrogen carrier gas (total pressure = 760 torr) passed over the catalyst for 5 hours. Severe steaming was carried out using 190 ml/min of 1520 torr pure steam (T_{sat}= 120°C) for 30 hours. The catalyst was then cooled under nitrogen. This resulted in six "parent" catalysts subsequently used in the acid washing studies, viz, fresh sodium mordenite, mildly steamed sodium mordenite, deep and shallow bed calcined hydrogen mordenite and mildly and severely steamed hydrogen mordenite.

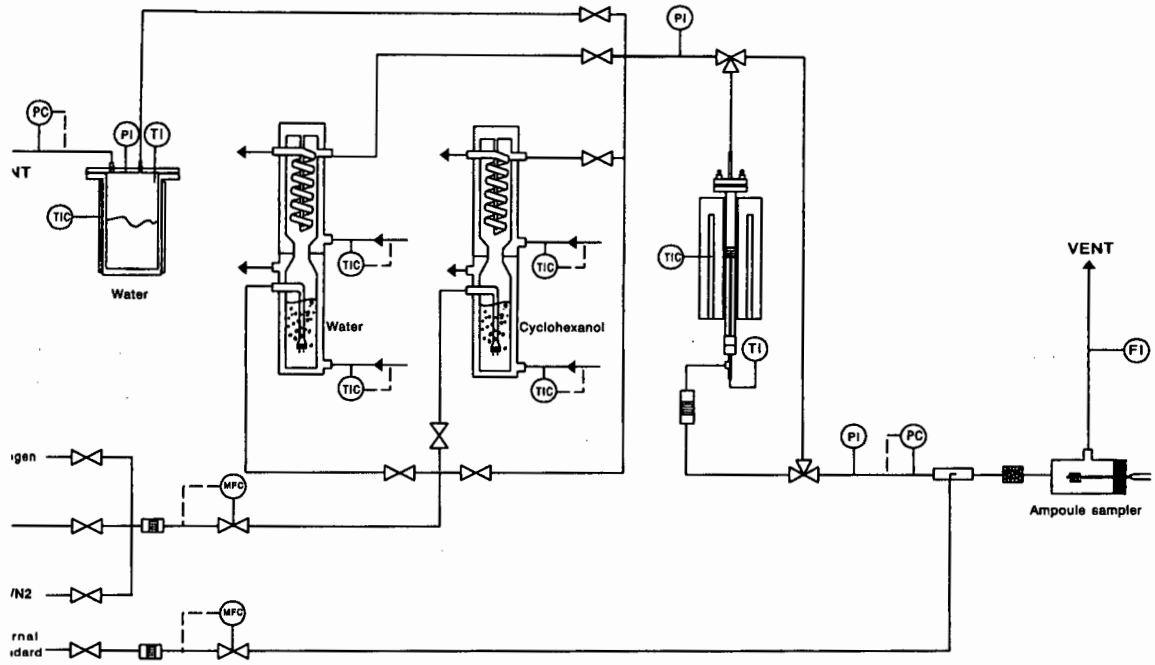

Figure 2.1. Diagram of experimental rig used for hydrothermal treatments, isobutane cracking and cyclohexanol dehydration.

2.1.4 Acid washing

Each acid wash was carried out using 3.5 g of catalyst in 100 ml nitric acid with the following concentrations: 0.001N, 0.01N, 0.1N, 1N, 2N, 5N and 10N. A wash with deionized water was also carried out. The temperature was held constant at 70°C and the slurry was stirred for four hours. Acid was removed by vacuum filtration and the catalyst subsequently washed with 1 litre of deionised water before drying at 80°C for 12 hours.

2.1.5 Washing with ethylenediamine tetra-acetic acid (EDTA)

An EDTA wash was performed at 80°C for 7 hours on 5 g catalyst with 2 g EDTA in 200 ml deionized water. The EDTA was removed by vacuum filtration and washed with 5 litres of deionised water before drying at 80°C for 12 hours.

2.1.6 Referencing of catalyst samples

When referencing the catalysts in this thesis, the terminology NaS#.## or HSS#.## was used (#.## being a number between 0 and 10). S stands for mild steaming and SS for severe steaming and #.## represents the concentration of nitric acid used for washing. A complete table of all the samples used in this study and their reference codes is given in Table 2.1.

Table 2.1 Catalyst coding

Sample	Treatment
Na	Untreated Na-MOR
Na0	Na-MOR washed with deionized water
Na#.##	Na-MOR washed with #.##N nitric acid
NaS	Na-MOR steamed
NaS0	NaS washed with deionized water
NaS#.##	NaS washed with #.##N nitric acid
H	Na-MOR ion exchanged and calcined
H0	H washed with deionized water
H#.##	H washed with #.##N nitric acid
CH	Na-MOR ion exchanged and "deep bed" calcined
CH0	CH washed with deionized water
CH#.##	CH washed with #.##N nitric acid
HE	H-MOR washed with EDTA
HS	H-MOR mildly steamed
HS0	HS washed with deionized water
HS#.##	HS washed with #.##N nitric acid
HSS	H-MOR severely steamed
HSS0	HSS washed with deionized water
HSS#.##	HSS washed with #.##N nitric acid

2.2 CATALYST CHARACTERISATION

2.2.1 Structural composition

2.2.1.1 Elemental analysis

Bulk chemical analyses were performed using a Varian SpectrAA-30 spectrometer with a DS 15 data station. 0.2 ± 0.05 g of each sample was digested in 5 ml of 40% concentration hydrofluoric acid at 100°C for 2 hours in teflon Parr bombs. 50 ml of boric acid was then added and the solution made up to 500 ml with deionized water. Standard 100 ml solutions of sodium, silicon and aluminium were made in the ranges 5 to 50 ppm, 50 to 275 ppm and 5 to 50 ppm respectively using the base matrix of 1 ml hydrofluoric acid and 10 ml boric acid.

2.2.1.2 ^{27}Al and ^{29}Si MAS NMR

^{27}Al and ^{29}Si MAS NMR spectroscopy was used to determine the coordination state of the aluminium and the local environment of the silicon. Results were recorded using a Varian Unity 400 spectrometer operating at 104 MHz and 79.5 MHz respectively. Spectra were acquired using a 7 mm ZrO_2 rotor at ambient temperature. Typically flip angles of ≈50° were used, with a 1 s pulse delay.

Spinning speeds of between 3-5 kHz and between 128 and 256 scans gave good results. In all cases measurements were carried out at at least two spinning speeds to allow for the identification of spinning sidebands. Where necessary a linebroadening factor of 25 - 100 Hz was applied. ^{27}Al and ^{29}Si chemical shifts are quoted relative to external 1000 ppm $Al(NO_3)_3$ solution or an aqueous solution of DSS (3-(trimethylsilyl)tetradeuterosodium propionate), set to 0 ppm.

2.2.1.3 X-ray diffraction

Percentage crystallinity and unit cell size was determined by X-ray diffraction (XRD). The XRD spectra were obtained using a Phillips X-ray diffractometer with Cu-Kα radiation of wavelength 1.54 Å. The scan range used was $6° < 2\theta < 37°$ at a step size of 0.1°. A sample washed with EDTA was found to have the most crystalline structure as measured by the summed intensities of the (330), (150), (202), (350) and (511) reflections and was assigned a crystallinity of 100%. Other samples were assigned percentage crystallinities relative to this. Lattice constants *a*, *b* and *c* were derived from the (200), (020) and (002) reflections, respectively.

2.2.1.4 Infra-red spectroscopy

Infrared spectra of the samples were obtained on a Nicolet 5ZDX FTIR spectrometer using KBr wafers that contained 10 wt% mordenite. The scanning range was 4000-400 cm^{-1}.

2.2.1.5 BET Micropore analysis

Micropore volume and catalyst surface area were determined using a Micromeritics ASAP 2000. The sample was dried *in situ* at 350°C under vacuum. Nitrogen was then adsorbed at liquid nitrogen temperatures at a rate of 3 ml per step until ambient pressure was reached.

2.2.1.6 Scanning electron microscopy

A Leica S440 scanning electron microscope was used to produce photographs of the catalyst samples. Magnifications between 1 400 and 50 000 times were achieved operating at 15 kV with a probe current of 10 pA.

2.2.2 Catalyst acidity

2.2.2.1 Temperature programmed desorption of ammonia

Number and strength of acid sites was measured by ammonia temperature programmed desorption under flowing helium. 0.5 g of sample was loaded into a quartz cell and dried at 500°C.

Ammonia (2.5% in He) was adsorbed for 1 hour at 100°C and purged at the same temperature for 24 hours to remove physisorbed material before starting the temperature ramp. A heating rate of 5°C/min was used from 100°C to 800°C. Desorbed ammonia was measured by a TCD and checked by titration.

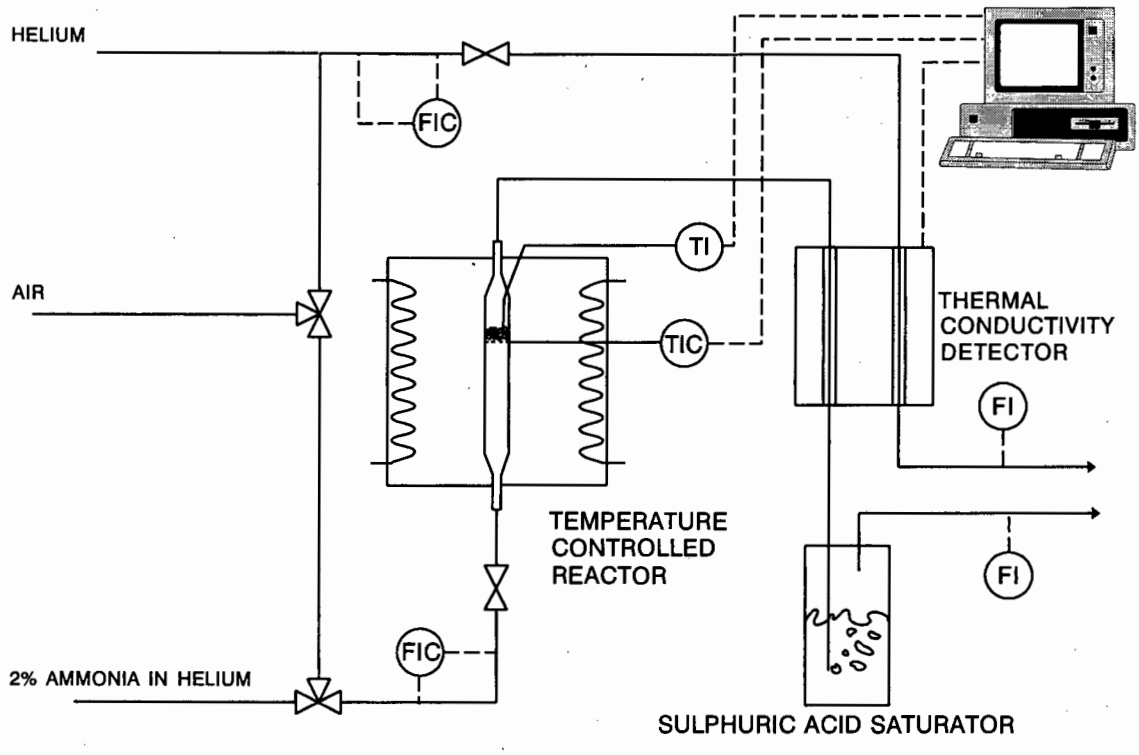

Figure 2.2. Diagram of temperature programmed desorption rig

2.2.2.2 FTIR spectroscopy of pyridine desorption

Infrared spectra of the samples were obtained on a Nicolet 5ZDX FTIR spectrometer. A 15 mg sample was pressed into self supporting wafer of 13 mm diameter at 17 tons pressure. This was cut to the required 10 mm diameter and loaded into the cell shown in Fig 2.3.

The cell was evacuated to between 10^{-4} and 10^{-5} bar using a rotary pump and an oil diffusion pump. The sample was then dried at 400°C. Pyridine adsorption took place at 100°C for 30 min. The cell was evacuated for a further 45 minutes before spectra were taken. Spectra were taken after desorption at 100, 200, 300, 400, 500, 600 and 700°C. The spectral range was limited to 4000 - 1300 cm^{-1} by the CaF_2 windows.

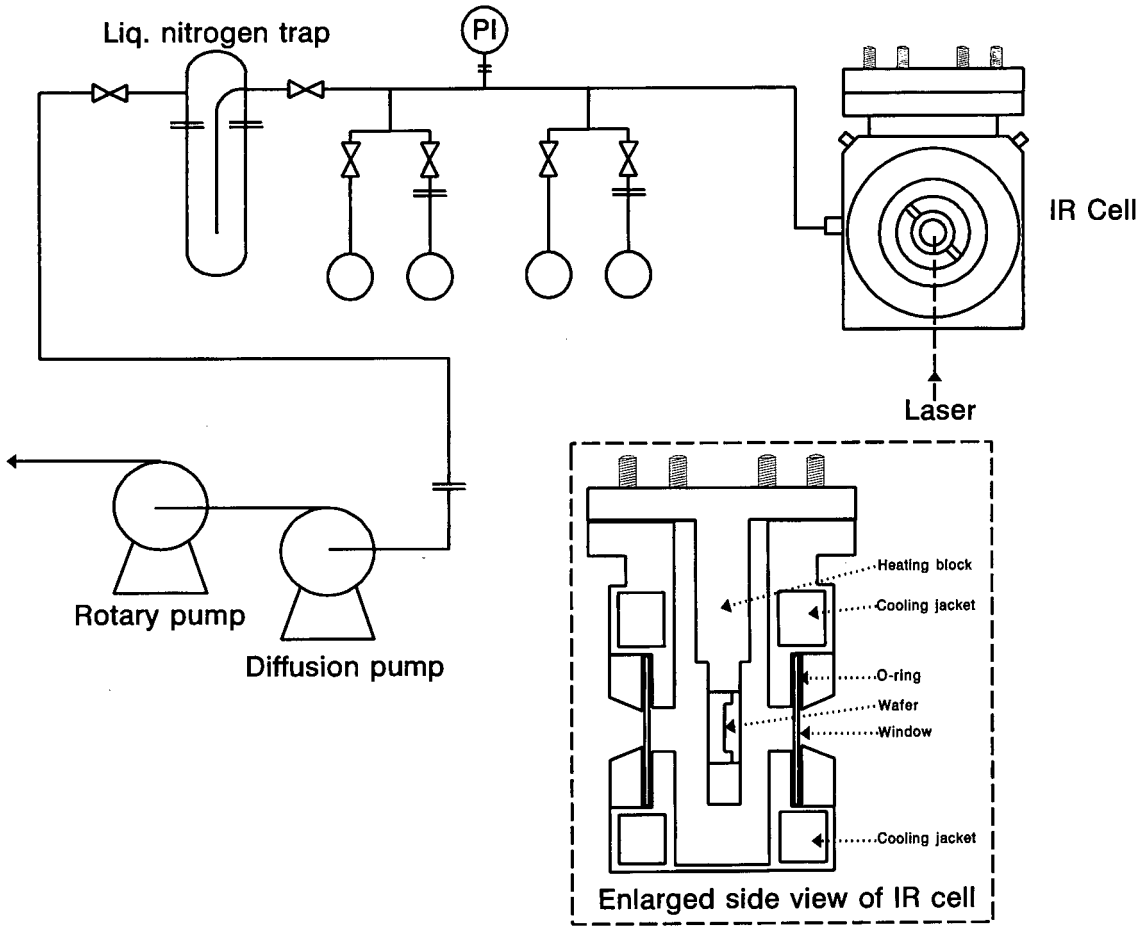

Figure 2.3. Diagram of vacuum line and infra-red cell used for spectroscopy of pyridine adsorption.

2.2.2.3 ^1H MAS NMR

Samples were dried at 400°C at a pressure below 0.01 Pa for 24 hours, cooled to room temperature and sealed in fused glass ampoules. ^1H MAS NMR measurements were made on a Bruker MSL 300 spectrometer at the Unstitut für Technische Chemie I at the University of Stuttgart. Home-made MAS equipment was used to spin the glass ampoules. This was carefully cleaned to prevent spurious proton signals. A Larmor frequency of 300 MHz, a pulse length of 4 μs for a $\pi/2$ pulse, a recycle delay of 10 s and a rotational frequency of 2500 ±5 Hz were used.

2.2.3 Determination of catalytic properties

2.2.3.1 Isobutane cracking

After the catalyst sample had been dried at 500°C for 16 hours under flowing nitrogen, isobutane cracking was carried out at 200 kPa and 450°C in the tubular plug flow reactor shown in Figure 2.1. Diluted isobutane (5% in nitrogen) was fed via a mass flow controller to the reactor at a WHSV of 1.8 h^{-1}. n-Hexane was used as an internal standard for mass balance purposes. In all experiments reported, a carbon balance of greater than 95% was obtained. Inline sampling for analysis was performed using the ampoule sampling technique of Schulz *et al.* [1986].

Samples of product gas were taken by breaking the tip of a heated, evacuated glass ampoule in the ampoule sampler (shown in Figure 2.1). Once the sample had entered the ampoule the tip of the ampoule was the resealed using a spot flame. Analysis of the sample was then performed in a gas chromatograph using a flame ionisation detector (FID). A Supelco Polar 4343 column was used to separate the gases. An example of the calculation of conversion and selectivity from the raw data is shown in Appendix VII.

2.2.3.2 Cyclohexanol dehydration

Samples were dried at 400°C for 16 hours under flowing nitrogen before cyclohexanol dehydration was performed at atmospheric pressure and 120°C in the reactor described in Figure 2.1. Nitrogen, fed via a mass flow controller, was saturated with cyclohexanol at 80°C before being introduced to the reactor (WHSV = 1.5 h^{-1}). Dimethylether (DME) was used as an internal standard and the ampoule sampling method was used in the analysis. The sample was analysed in a gas chromatograph with FID and a 50 m Durabond capillary column. The three detected peaks were the reactant cylcohexanol, product cyclohexene and internal standard DME. Calculations of conversion were based on carbon content as water cannot be detected by the FID.

2.2.3.3 Naphthalene isopropylation

The propylation of naphthalene was carried out in both a batch reactor and a plug flow reactor. The batch reaction was carried out in a 500 ml autoclave at 160°C. 5 g of naphthalene was diluted in 50 ml undecane and then propene was introduced to the autoclave until the total pressure reached 10 bar. The reaction took place over 1 g of catalyst. Liquid samples were taken with a syringe and injected into to a gas chromatograph. The compounds were separated in a 50 m Durabond capillary column and analysed by an FID, the solvent undecane was used as an internal standard.

The plug flow reaction was performed at 500 kPa and temperatures between 190°C and 300°C in the tubular reactor shown in Figure 2.4. Nitrogen introduced by a mass flow controller was saturated with naphthalene at temperatures between 85°C and 120°C before being introduced to the reactor. A propene gas feed was introduced via a mass flow controller at a WHSV between 2.6 and 6.0 h^{-1}. Inline sampling was performed by the ampoule sampling technique. The compounds were again separated in a 50 m Durabond capillary column and analysed by an FID attached to the gas chromatograph.

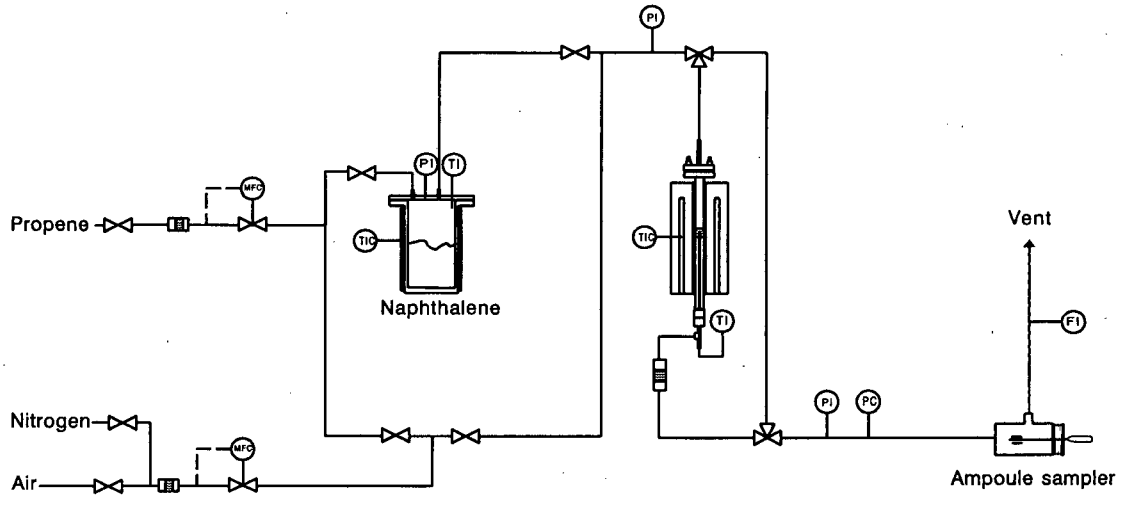

Figure 2.4. Diagram of experimental rig used to perform propylation of naphthalene

CHAPTER THREE

RESULTS

3.1 PHYSICAL AND CHEMICAL CATALYST CHARACTERISATION

3.1.1 Comparison of characterisation with that of the Fritz-Haber Institute

The parent sample of Na-Mordenite was supplied by the Fritz-Haber Institute in Berlin from synthesis batch Lot 299 (DEGUSSA KM 440). The sample was characterised at that institute after synthesis. The results of that charactersiation are presented in Appendix XI. These results compare well to the results of analysis methods used in this research. This supports the validity of the results presented in the following sections.

3.1.2 Elemental analysis of samples

The chemical compositions of all samples were determined by atomic absorption and are presented in Tables 3.1 to 3.3. Readings of the absorbance of each digested sample were repeated three times as part of the experimental method and the repeatability of the experiment was found to be within 0.5 ppm for silicon, 0.1 ppm for aluminium and 0.05 ppm for sodium. The reproducibility of the digestion method was tested with a sample Na-Mordenite. Although differences in concentration of each constituent element were found, these were within the repeatability of the experiment and corresponded well with the values provided by the Fritz-Haber Institute, i.e. Si/Al = 6.42, Na/Al = 1.03.

The parent catalyst, Na-Mordenite (called Na) was found to have a bulk Si/Al of 6.4 and every aluminium atom was balanced by a sodium atom. Washing this catalyst with deionised water and acid of concentration less than 0.1N had no significant effect upon the bulk chemical composition. However, most of the sodium was removed with a 0.1N wash together with a small amount of aluminium (Fig. 3.1). Aluminium and sodium were removed in increasing quantities with increasing concentrations of nitric acid washes. After a 10N acid wash 52% of the aluminium and 97% of the sodium had been removed.

Table 3.1 Bulk chemical compositions of dealuminated Na-Mordenite samples as determined by atomic absorption

Sample	Si/Al	Na/Al	Sample	Si/Al	Na/Al
Na	6.40	1.02	Na10	14.5	0.07
Na0	6.45	1.02	NaS	6.40	1.04
Na0.001	6.50	1.03	NaS0	6.40	1.03
Na0.01	6.54	0.90	NaS0.01	6.47	0.94
Na0.1	6.81	0.30	NaS0.1	6.51	0.30
Na1	7.12	0.15	NaS1	6.65	0.14
Na2	7.55	0.12	NaS2	6.96	0.12
Na5	8.16	0.08	NaS5	8.26	0.02

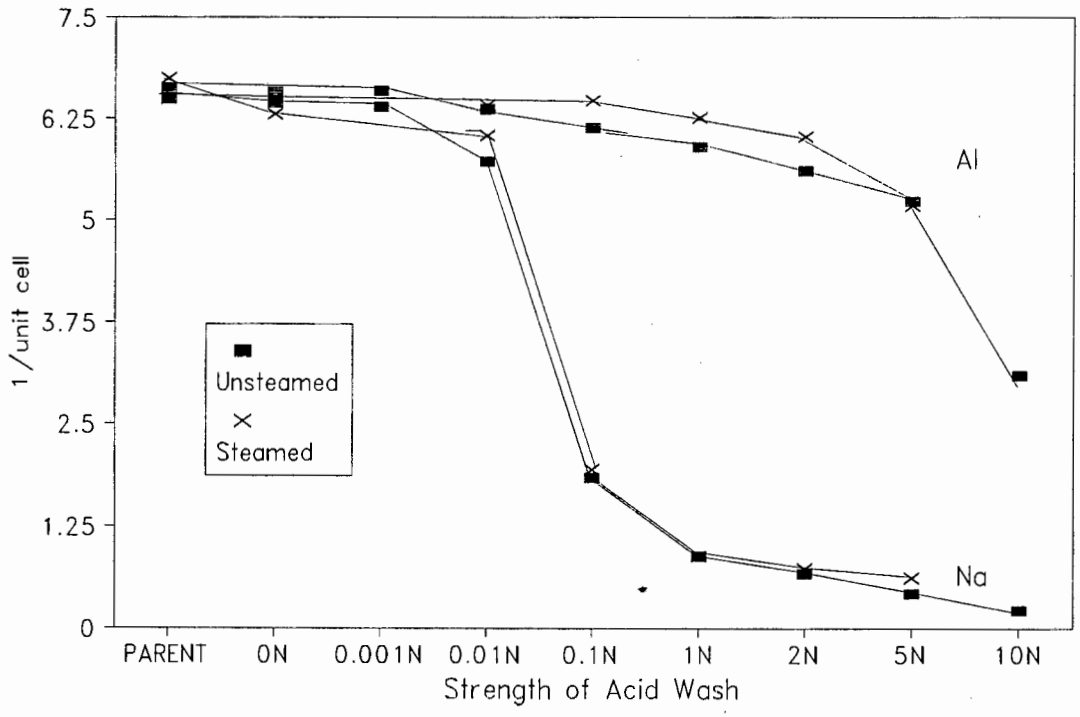

Figure 3.1 Bulk aluminium and sodium content for steamed and unsteamed Na-Mordenite as a function of strength of acid wash

Steaming of Na-Mordenite (NaS) resulted in no change to the bulk chemical composition

of the catalyst. Generally aluminium and sodium removal from NaS by acid washing followed the same trend as their removal from the unsteamed Na (Fig. 3.1).

Table 3.2 Bulk chemical compositions of calcined and acid washed H-Mordenite samples as determined by atomic absorption

Sample	Si/Al	Na/Al	Sample	Si/Al	Na/Al
NH_4	6.40	0.02	H5	8.13	0.01
H(400)	6.50	0.02	CH	6.40	0.02
H(550)	6.40	0.02	CH0	6.40	0.02
H0	6.40	0.02	CH0.001	6.52	0.02
H0.001	6.52	0.02	CH0.01	6.52	0.02
H0.01	6.64	0.02	CH0.1	6.72	0.02
H0.1	6.74	0.02	CH1	7.14	0.01
H1	7.13	0.01	CH2	7.24	0.01
H2	7.24	0.01	HE	8.76	0.06

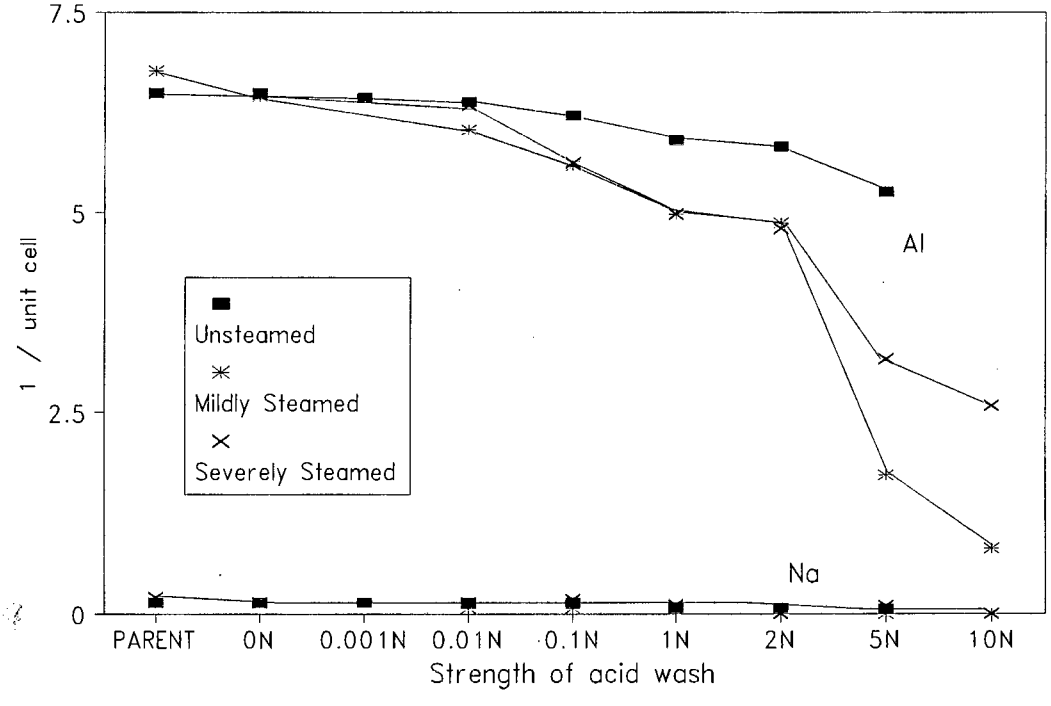

Figure 3.2 Bulk aluminium and sodium content of steamed and acid washed H-Mordenite compared to strength of acid wash.

Ion exchange procedures with ammonium nitrate removed 98% of the sodium without affecting the Si/Al ratio and there was no significant loss of bulk aluminium during subsequent calcination at 400 and 550°C. Washing of the H-Mordénite sample calcined at 550°C (H(550)) with deionised water did not change its bulk chemical composition. Increasing acid wash concentrations showed a gradual removal of aluminium, 22% of the bulk aluminium being removed with a 5N wash (Fig.3.2).

Table 3.3 Bulk chemical compositions of steamed and acid washed H-Mordenite samples as determined by atomic absorption

Sample	Si/Al	Na/Al	Sample	Si/Al	Na/Al
HS	6.41	0.02	HSS	6.40	0.03
HS0	6.41	0.02	HSS0	6.41	0.02
HS0.01	6.95	0.01	HSS0.01	6.57	0.02
HS0.1	7.59	0.01	HSS0.1	7.55	0.03
HS1	8.64	0.00	HSS1	8.63	0.00
HS2	8.85	0.00	HSS2	8.82	0.00
HS5	26.87	0.00	HSS5	14.14	0.03
HS10	58.78	0.00	HSS10	17.60	0.00

Steaming of sample H(550) did not remove aluminium from the bulk (samples HS and HSS). However, acid washing with 10N nitric acid removed up to 87% of the bulk aluminium from mildly steamed H-Mordenite. Aluminium was removed in greater quantities by acid washing from the bulk of steamed H-Mordenite than from unsteamed H-Mordenite as shown in Figure 3.2.

3.1.3 X-ray diffraction

Figures 3.3 and 3.4 show the XRD patterns of H-Mordenite together with its simulated pattern [van Ballmoos, 1984]. Although the two patterns show the same characteristic peaks

and the same relative intensities of these peaks above 2θ=10°, a slight decrease in intensity of the peaks below 2θ = 10° compared to the simulated pattern was noted in all the XRD patterns.

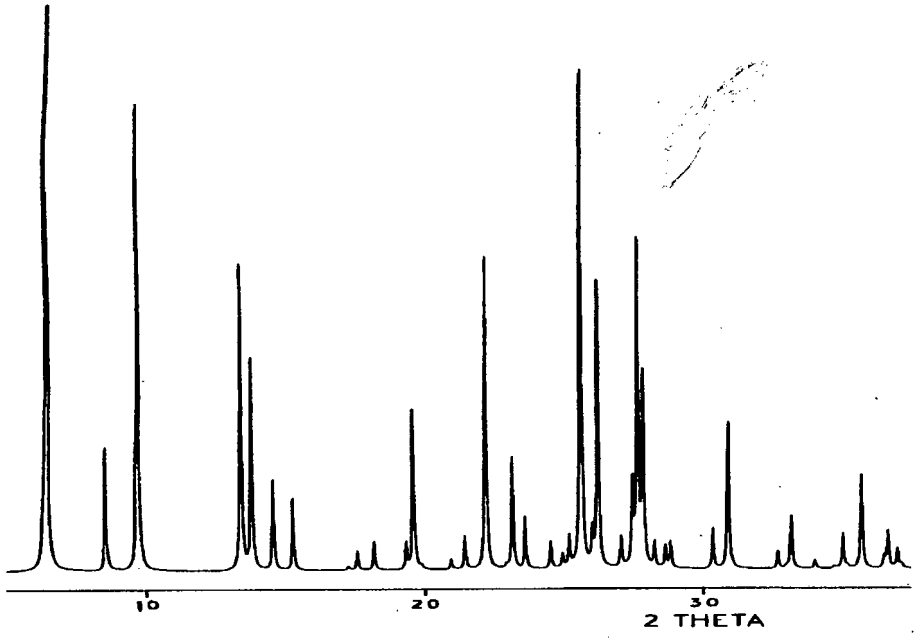

Figure 3.3 Simulated x-ray diffraction pattern of Mordenite [von Ballmoos, 1984]

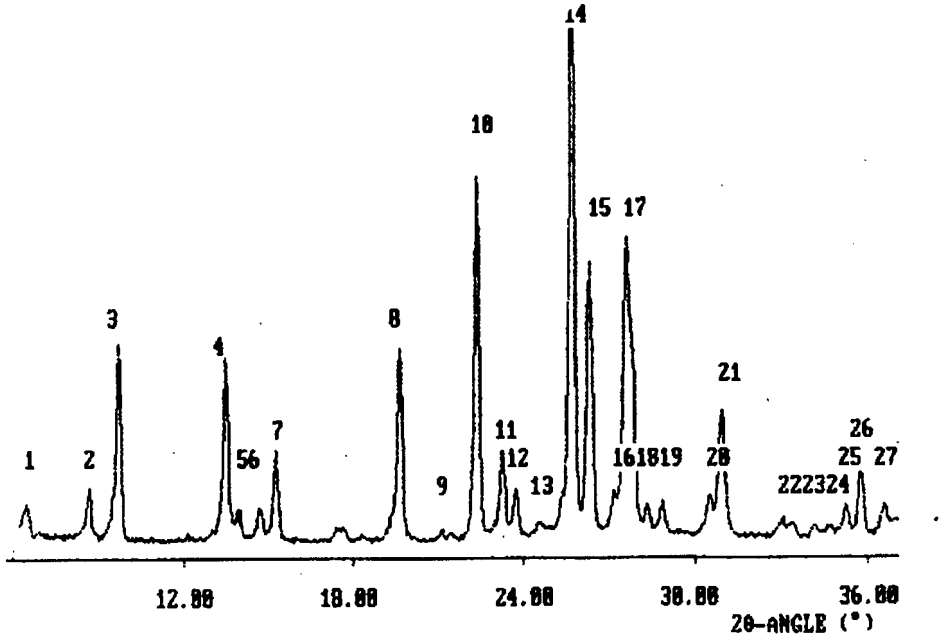

Figure 3.4 X-ray diffraction pattern of sample H(550)

Decreased intensities of peaks in this region have been ascribed due to adsorbed water on the crystal [Hardenberg *et al.*, 1992]. As the experimental system was open to the atmosphere and an adsorption of water up to 15-17 wt% can be expected, this seems to be a likely cause. Line broadening seen in Figure 3.4. is probably due to the small crystallite size of the H-Mordenite sample [Klug and Alexander, 1974] and the step size of the diffractometer (0.1°), which is broader than some of the peaks in the simulated pattern. The pattern, however, appears almost identical to that of a standard sample of Mordenite [Szostak, 1992].

Percentage crystallinity was assigned relative to a sample washed with EDTA (HE), which was found to have the most crystalline structure of all the samples used, as measured by the sum of the intensities of the (330), (150), (202), (350) and (511) reflections [van Hooff and Roelofsen, 1991; van Niekerk, 1992, Hardenberg *et al.*, 1992].

The intensities and d-spacings of all major peaks of all samples are presented in Appendix I. Calculated unit cell constants and percentage crystallinities of dealuminated sodium Mordenite samples are presented in Table 3.4. Samples Na_1, Na_2 and Na_3 refer to repeated experiments on Na-Mordenite to establish if errors created during sample loading were significant. The similarity in the calculated unit cell constants and percentage crystallinities indicates that these errors are small and that the experiment is reproducible.

The parent catalyst Na-Mordenite (Fig 3.5) was not fully crystalline and was assigned a percentage crystallinity of 75%. The unit cell constants compared well with literature values of $a = 18.13$, $b = 20.49$ and $c = 7.52$ [Meier, 1961; Karge and Weitkamp, 1986]. Percentage crystallinity of the sodium form increased from 78 % after the 0.1N wash to a maximum of 96% after a 2N acid wash. A 5N wash resulted in a catalyst with a greatly reduced crystallinity of 60%. As expected all unit cell constants decreased with acid washing.

Table 3.4 Percentage crystallinities and unit cell constants, determined by XRD, of Na-Mordenite samples dealuminted by acid washing, steaming and steaming followed by acid washing

Sample	Crystallinity %	a Å	b Å	c Å
Na_1	75.0	18.12	20.51	7.525
Na_2	75.2	18.14	20.52	7.524
Na_3	75.3	18.13	20.53	7.524
Na0	75.8	18.22	20.60	7.550
Na0.001	76.1	18.19	20.56	7.537
Na0.01	81.7	18.22	20.52	7.537
Na0.1	77.6	18.28	20.56	7.544
Na1	86.5	18.18	20.45	7.522
Na2	95.7	18.19	20.42	7.508
Na5	60.3	19.28	20.51	7.528
NaS	68.1	18.07	20.37	7.506
NaS0	65.2	18.16	20.56	7.537
NaS0.01	69.1	18.13	20.54	7.528
NaS0.1	75.8	18.15	20.49	7.515
NaS1	74.8	18.16	20.44	7.512
NaS2	83.0	18.33	20.53	7.557

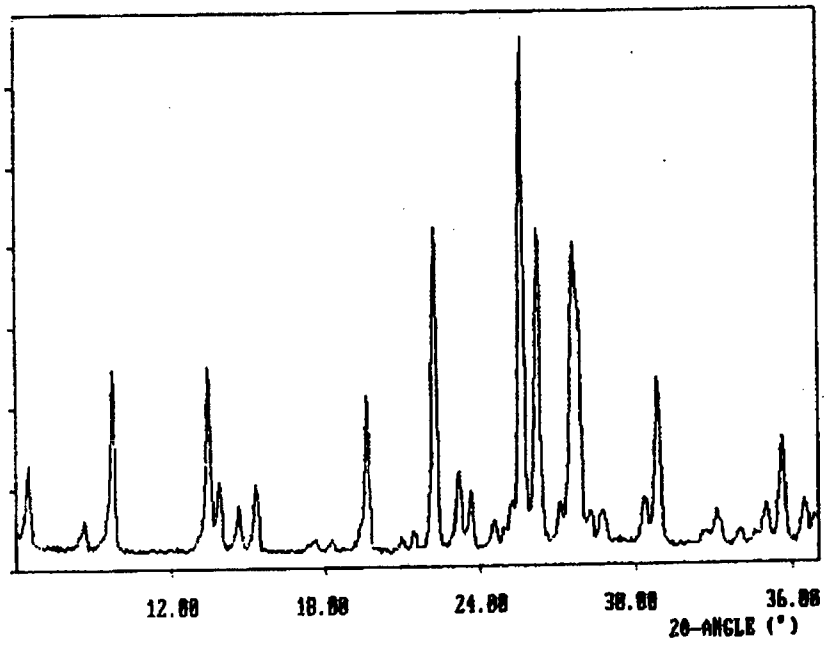

Figure 3.5 X-ray diffraction pattern of sample Na

Steaming of Na-Mordenite (NaS) resulted in decreased crystallinity (68%) and unit cell size. Washing NaS in deionized water virtually restored the unit cell to its former dimensions. 2N acid washing of NaS (NaS2) increased the crystallinity of the material to 83%.
Table 3.5 shows that ion exchange led to an increase in percentage crystallinity from 77% to 84%. This was ascribed to the removal of amorphous material. The unit cell was reduced in the *a* and *c* directions, while it remained constant in the *b* direction.

The deep bed calcined catalyst (CH) had a smaller unit cell size and increased percentage crystallinity compared to that calcined under standard conditions, viz. H(550) (Table 3.5). The XRD patterns of deep and shallow bed calcined Mordenite samples are shown in Figure 3.6 and 3.4 respectively. Washing of the H-Mordenite sample deep bed calcined at 550°C (CH) with deionised water increased its relative crystallinity to 99% without changing bulk chemical composition or unit cell size.

Table 3.5 Percentage crystallinities and unit cell constants of acid washed H-Mordenite samples as determined by XRD

Sample	Crystallinity %	a Å	b Å	c Å
NH_4	83.6	18.21	20.53	7.524
H(550)	84.3	18.20	20.52	7.528
H0	84.6	18.19	20.47	7.512
H0.001	98.4	18.19	20.42	7.508
H0.01	90.1	18.19	20.44	7.493
H0.1	88.3	18.19	20.44	7.493
H1	76.6	18.17	2.044	7.493
H2	75.6	18.17	20.42	7.493
H5	71.4	18.19	20.42	7.508
H10	70.4	18.19	20.44	7.508
HE	100.0	18.19	20.42	7.508
CH	85.7	18.03	20.37	7.493
CH0	98.8	18.12	20.42	7.493
CH0.001	97.6	18.19	20.40	7.493
CH0.01	96.4	18.19	20.41	7.508
CH0.1	82.3	18.19	20.43	7.493
CH1	82.2	18.17	20.43	7.493

Acid washing of all H-Mordenite samples with 0.01N led to increased percentage crystallinities, indicative of the removal of amorphous material. Unit cell constants decreased slightly in the case of shallow bed calcined H(550) but increased in the *a* and *b* directions in the case of deep bed calcined CH.

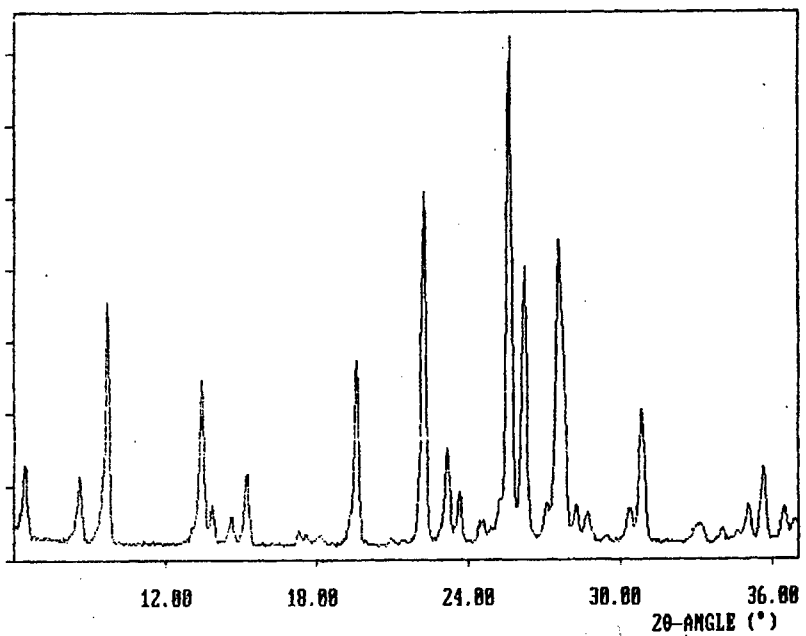

Figure 3.6 X-ray diffraction pattern of sample CH

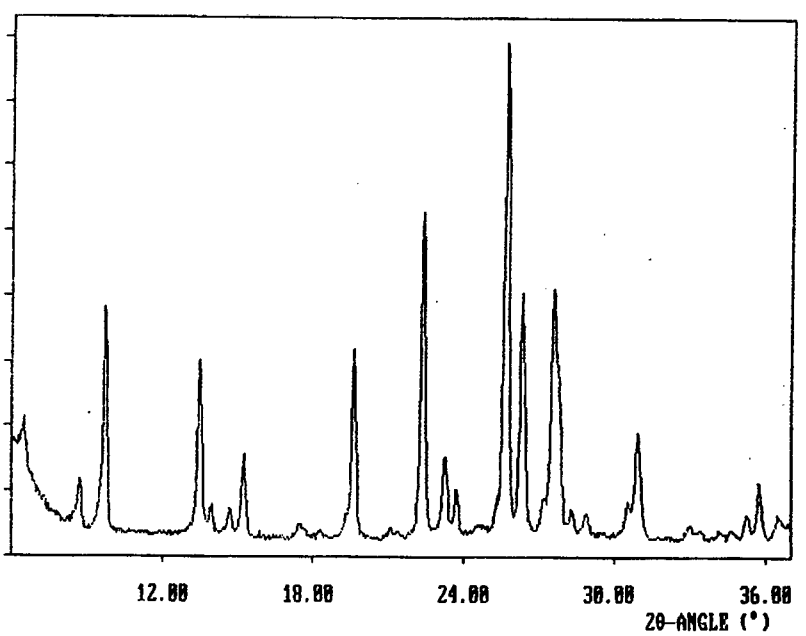

Figure 3.7 X-ray diffraction pattern of sample H5

After 0.1N acid wash the structure of both calcined samples were equivalent in terms of unit cell dimensions. Percentage crystallinity decreased with stronger acid washing as did the unit cell size slightly in the *a* and *b* directions..

Table 3.6 Percentage crystallinities and unit cell constants of acid washed steamed H-Mordenite samples as determined by XRD

Sample	Crystallinity %	a Å	b Å	c Å
HS	84.9	18.19	20.52	7.524
HS0	84.6	18.19	20.50	7.508
HS0.01	77.2	18.19	20.50	7.508
HS0.1	79.3	18.19	20.49	7.508
HS1	74.4	18.19	20.48	7.508
HS2	88.8	18.12	20.42	7.493
HSS	70.3	18.17	20.42	7.493
HSS0	76.6	18.10	20.42	7.477
HSS0.1	75.7	18.10	20.33	7.477
HSS1	74.3	18.10	20.33	7.477
HSS2	70.4	18.10	20.33	7.477
HSS5	78.7	18.10	20.33	7.477

The percentage crystallinity decreased with severe steaming, while unit cell constants remained unchanged. Subsequent acid washing of both mildly and severely steamed samples (HS and HSS in Figures 3.8 and 3.9 respectively) showed gradual decreases in percentage crystallinity for mild acid washing (64% and 70% for HS1 and HSS2) followed by an increase for stronger acid washes (89% and 79% for HS2 and HSS5). Unit cell dimensions of mildly steamed Mordenite decreased in the *b* and *c* directions with acid washing, but there was no change in the case of severely steamed Mordenite.

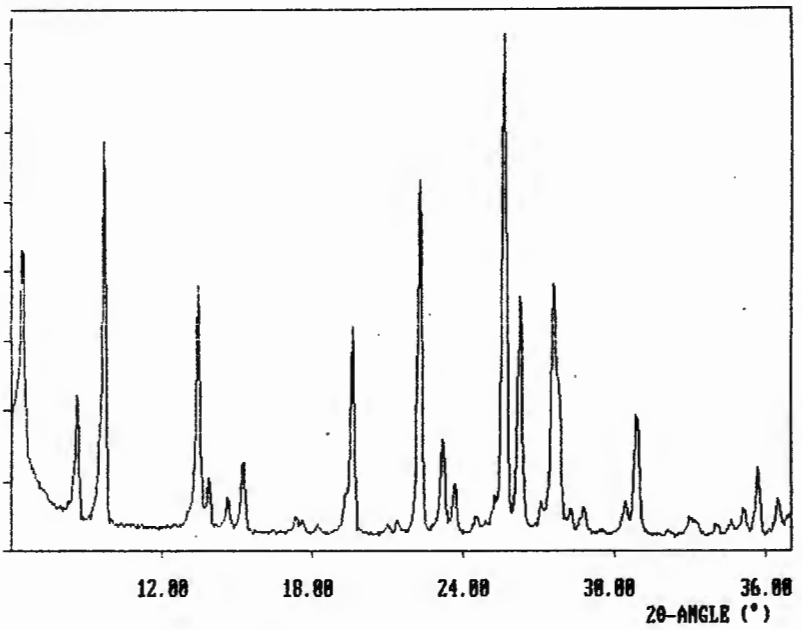

Figure 3.8 X-ray diffraction pattern of sample HS

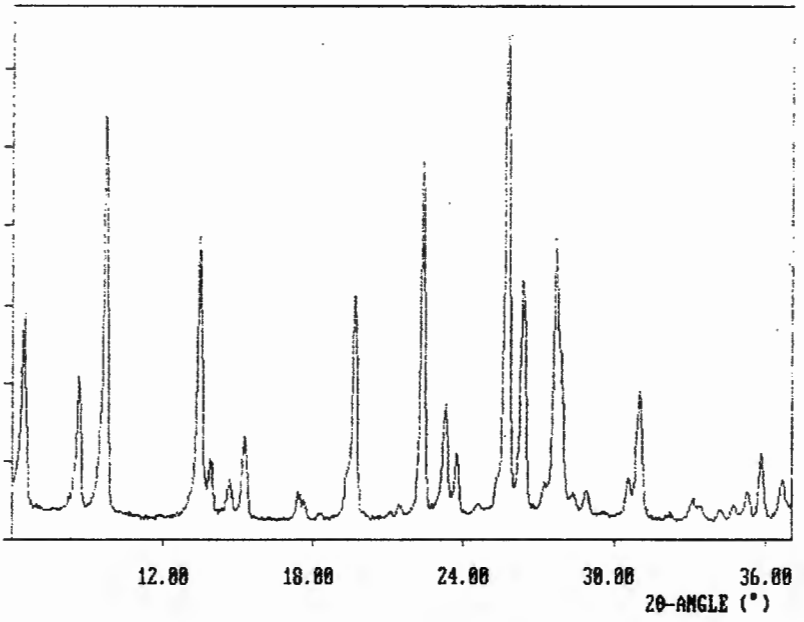

Figure 3.9 X-ray diffraction pattern of HSS

3.1.5 Scanning Electron Microscopy

The electron micrographs of the samples show the Mordenite samples to be a fine powder with the largest crystals being ≈ 2.5 x 1.5 μm and appearing as large agglomerates (Fig. 3.10). No significant structural changes were seen on acid dealumination (Fig. 3.12), although there were signs of pitting in the surface of HS10 (Fig. 3.14) which could be indicative of the creation of mesopores. Steamed samples had less well defined crystal borders and both samples HS and HSS (Figs. 3.13 and 3.15) showed interlinked crystals.

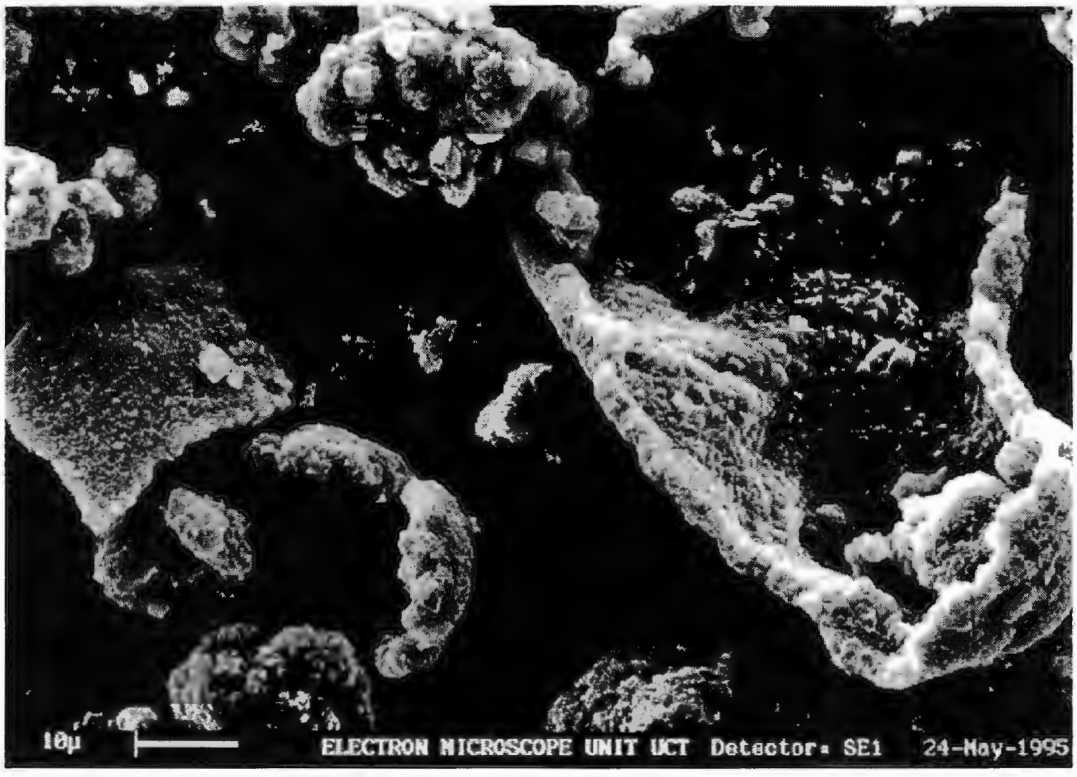

Figure 3.10 Scanning electron micrograph of sample H-MOR

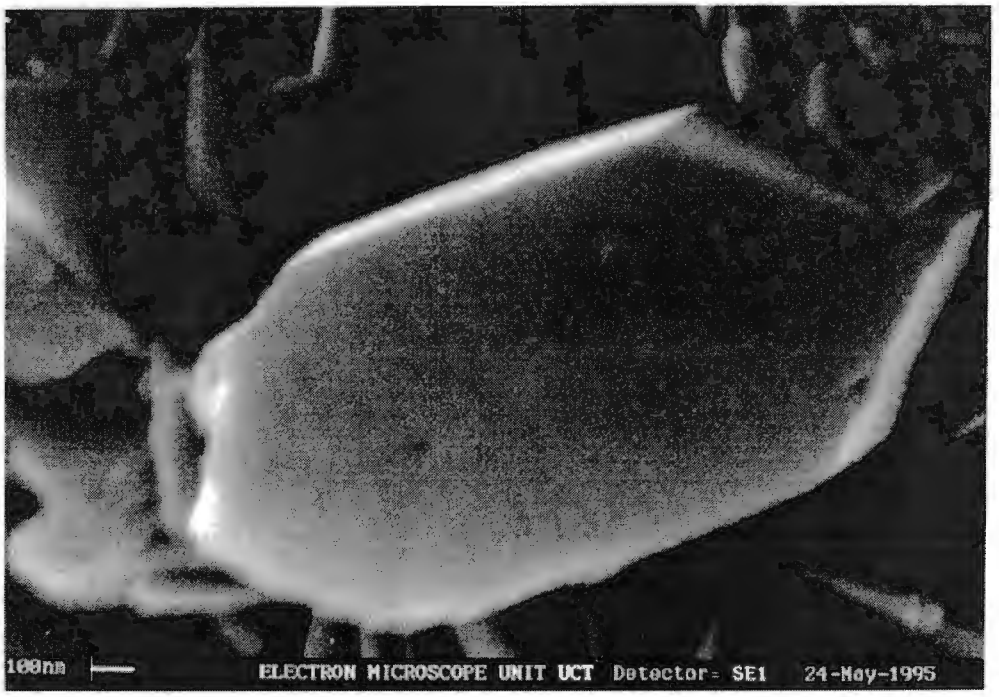

Figure 3.11 Scanning electron micrograph of sample CH

Figure 3.12 Scanning electron micrograph of sample H10

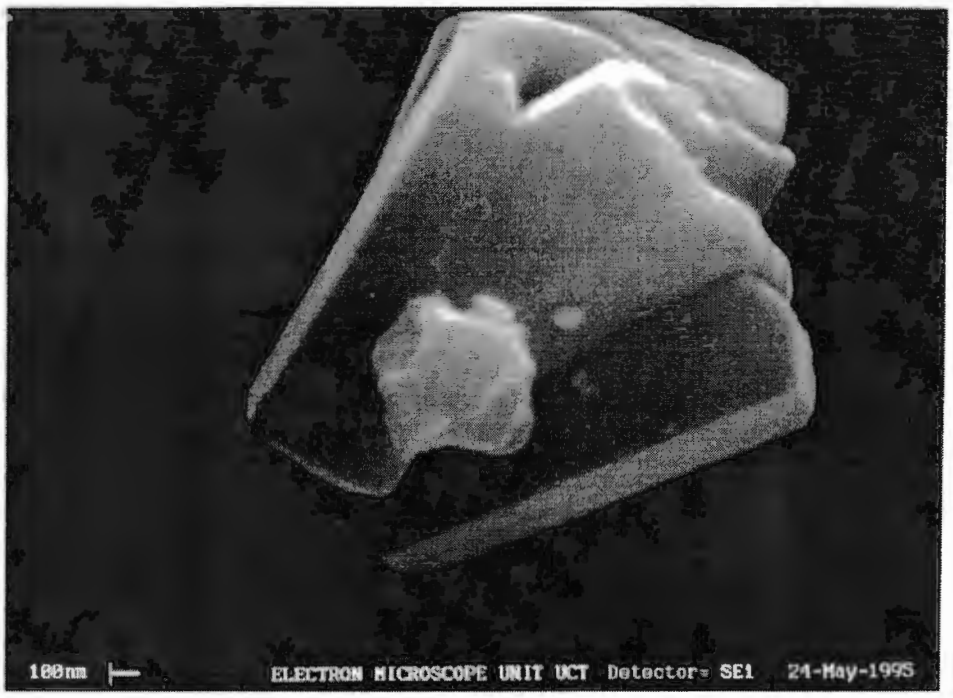

Figure 3.13 Scanning electron micrograph of sample HS

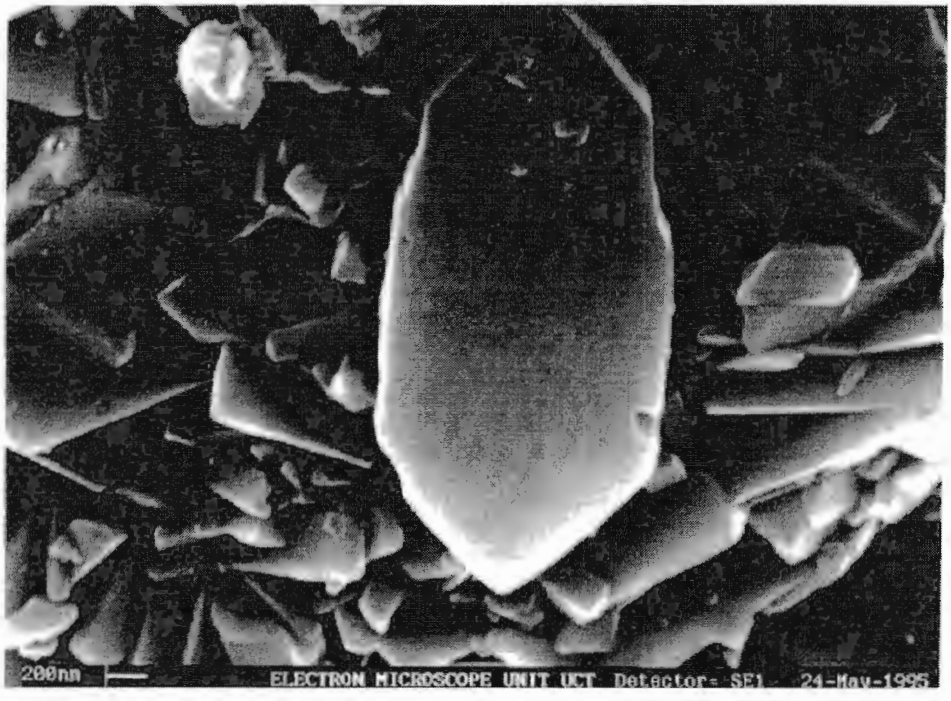

Figure 3.14 Scanning electron micrograph of sample HS10

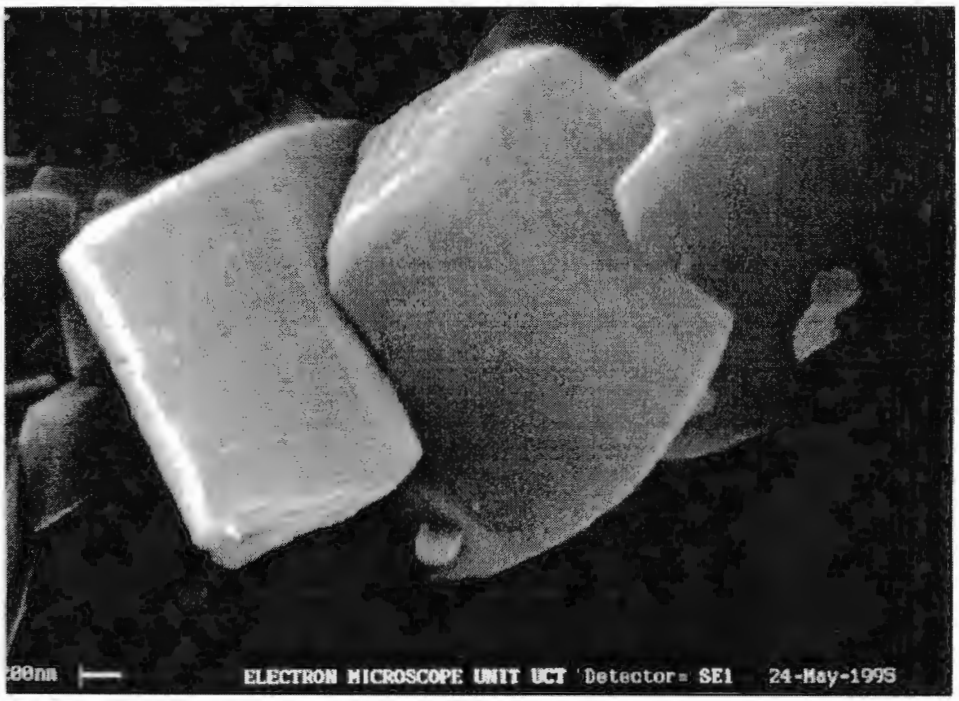

Figure 3.15 Scanning electron micrograph of sample HSS

3.1.5 ^{29}Si MAS NMR

^{29}Si MAS NMR was used to determine the framework silicon to aluminium ratio in selected samples chosen to cover a range of these ratios. These ratios were then used for comparison with results from elemental analysis combined with ^{27}Al MAS NMR to determine the reliability of the latter method. ^{29}Si MAS NMR analysis of the parent sample (Na) performed by the Fritz Haber Institute in Berlin showed a framework silicon to aluminium ratio (Si/Al_f) of 6.46 which correlated well with the elemental analysis of the sample (Si/Al = 6.42), assuming all aluminium present in this sample formed part of its framework.

Peak assignments for ^{29}Si NMR have been well established previously [Hays *et al.*, 1984; Engelhardt and Michel, 1987] and are presented in Table 3.7.

Table 3.7 Peak assignments for ^{29}Si MAS NMR

-85 ppm	Si(4Al)
-90 ppm	Si(3Al)
-100 ppm	Si(2Al)
-106 ppm	Si(1Al)
-112 ppm	Si(0Al) T_1
-113 ppm	Si(0Al) T_4
-115 ppm	Si(0Al) $T_2 + T_3$

In this Table Si(*n*Al) indicates a silicon atom linked to *n* aluminium atoms via an oxygen bridge and T_1 to T_4 indicate the four crystallographically inequivalent silicon sites in the structure of Mordenite as shown in Fig 3.16 [Kolodziejski *et al.*, 1991].

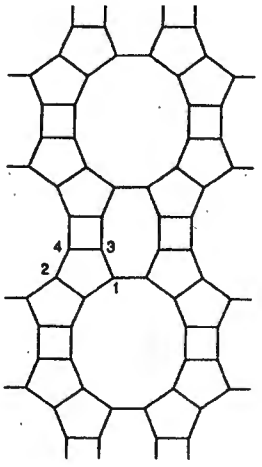

Figure 3.16 Crystallographically inequivalent T-atom sites in MOR [Kolodziejski *et al.*, 1991]

Since both ^{27}Al and ^{29}Si MAS NMR techniques were used to characterize the catalysts, comparison can be made between framework Si/Al ratio obtained from the ^{29}Si NMR spectra by the equation $Si/Al_f = \Sigma\ I(Si(nAl)) / \Sigma\ 0.25\ n\ I(Si(nAl))$ and the same ratio obtained from

a combination of chemical analysis and ^{27}Al NMR as shown in Table 3.8.

Table 3.8 Comparison of framework aluminium content determined by ^{29}Si MAS NMR and by chemical analysis with ^{27}Al MAS NMR.

	Chemical analysis with ^{27}Al NMR		^{29}Si NMR				
			Si(0Al)	Si(1Al)	Si(2Al)		
	Si/Al_f	Al_f/uc	-114	-107	-97	Si/Al_f	Al_f/uc
Na	6.4	6.5	46	46	9	6.3	6.5
Na2	9.4	4.6	57	43	0	9.4	4.6
NaS	15.5	2.9	70	30	0	13.4	3.3
H0	8.2	5.2	57	36	7	8.1	5.3
H0.001	8.7	4.9	60	33	6	8.6	5.0
CH	7.7	5.5	56	38	5	8.2	5.2
CH0.01	8.9	4.9	60	35	5	8.8	4.9
HE	9.2	4.7	88	74	0	8.8	4.9
HS0	10.8	4.1	72	19	9	10.9	4.0
HS0.01	10.8	4.1	72	22	7	11.3	3.9
HS0.1	11.6	3.8	70	26	4	11.6	3.8
HS10	79.0	0.6	164	12	0	58.7	0.8
HSS	42.6	1.1	93	7	1	47.1	1.0

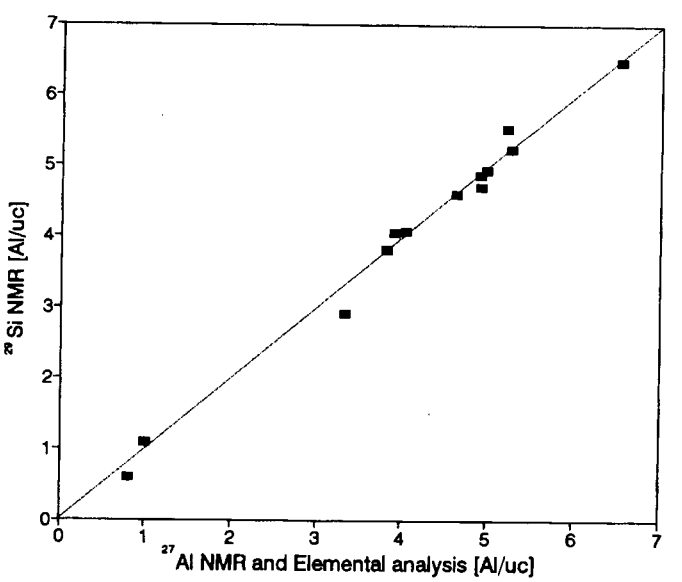

Figure 3.17 Framework aluminium content determined by ^{29}Si MAS NMR as a function of framework aluminium content determined by ^{27}Al MAS NMR and elemental analysis

Figure 3.17 shows these have a good correlation ($R^2 = 0.987$) and suggests that negligible or no "NMR invisible" aluminium exists and that ^{27}Al NMR results can be used to estimate the amounts of the different aluminium species relative to each other.

The ^{29}Si MAS NMR spectra of the parent sample Na-Mordenite and the severely dealuminated samples HSS and HS10 are shown in Fig 3.18. All other ^{29}Si MAS NMR spectra are shown in Appendix II.

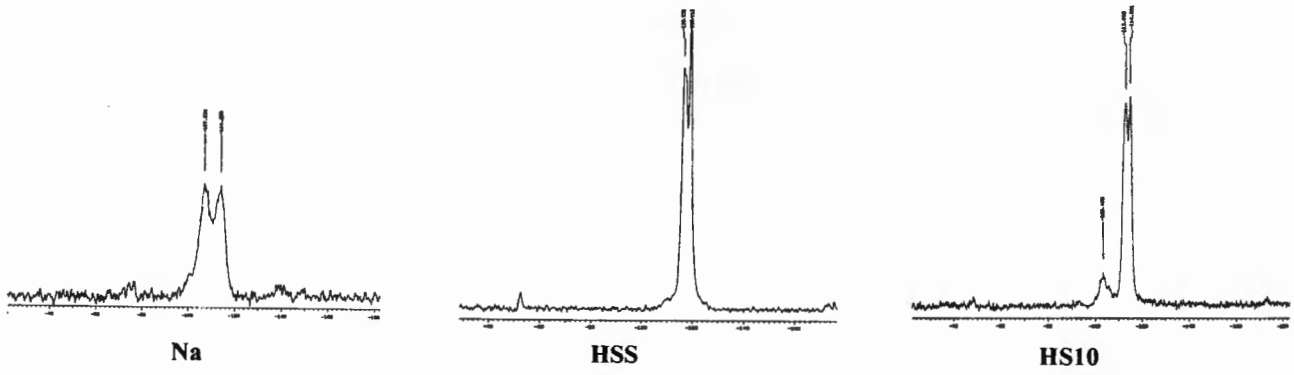

Figure 3.18 ^{29}Si MAS NMR spectra of samples Na, HSS, HS10

The spectra of the parent sodium form clearly showed the peaks at -114 and -107 ppm, assigned to Si(0Al) and Si(1Al) respectively, and a small peak at -97 ppm indicating Si(2Al).

The spectra of HSS and HS10 show that while the majority of the aluminium was removed from the framework during severe dealumination, the silicon framework remained intact. No species other than framework silicon was detected in sample HSS despite the low crystallinity (70%). Since no amorphous silicon phase was present the low crystallinity was probably caused by amorphous aluminium. HS10 shows a broad peak at -103 ppm which could be due to an amorphous silicon and aluminium phase.

3.1.6 ^{27}Al MAS NMR

3.1.6.1 Peak assignments

Selected ^{27}Al NMR spectra representing a range of dealumination techniques are shown in Figure 3.19. All other spectra obtained in this study are shown in Appendix III.

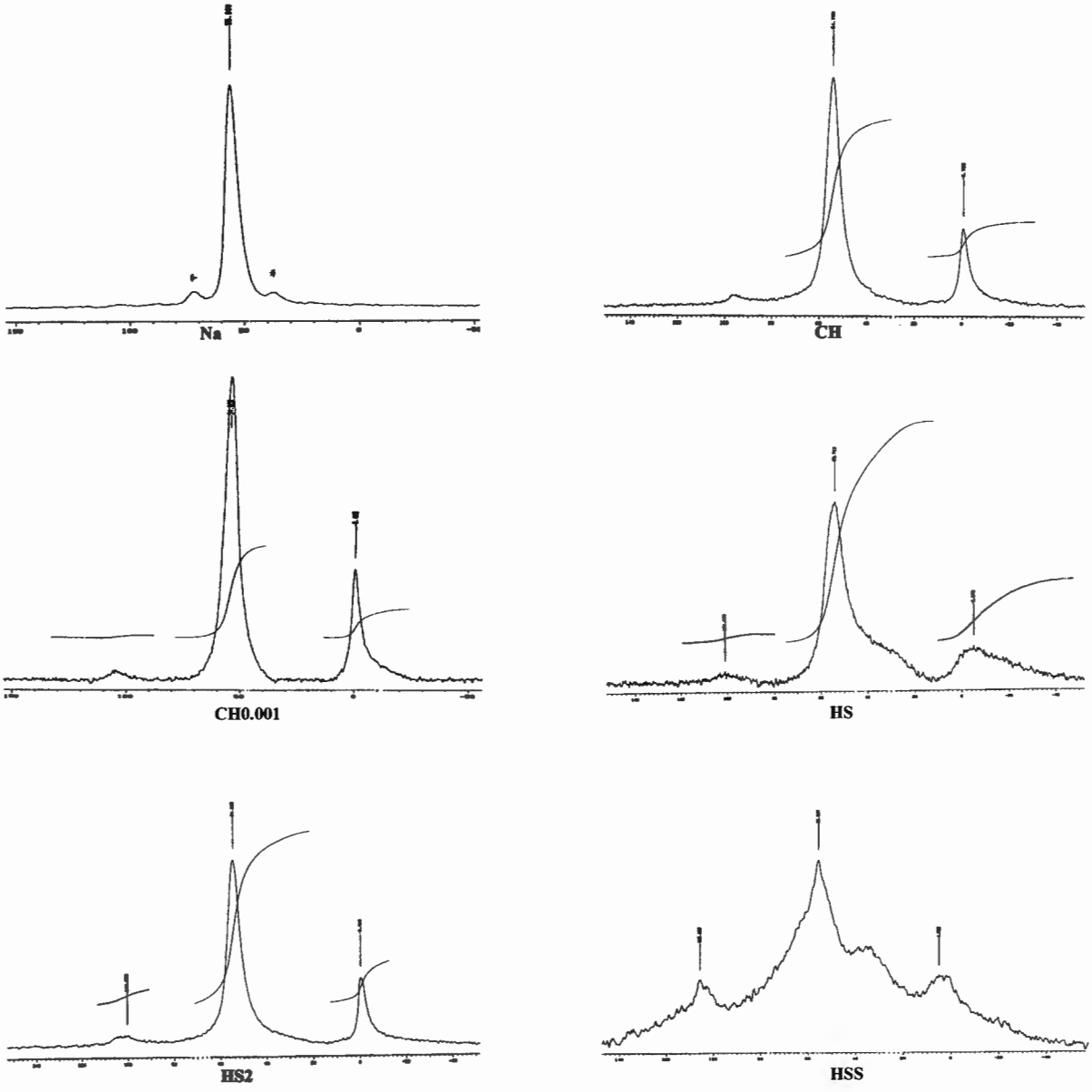

Figure 3.19 ^{27}Al MAS NMR spectra of samples Na, CH, CH0.001, HS, HS2 and HSS

Figure 3.19 shows all the peaks observed in dealuminated Mordenite. A major peak at 55

ppm, which is the only peak in the spectra of Na-Mordenite, is assigned to framework tetrahedral aluminium (FAl) [Geurts *et al.*, 1985; Samoson *et al.*, 1987; van Geem *et al.*, 1988]. In all other samples a peak at 0 ppm represents extra-framework octahedral aluminium (EFAl-o) species [Geurts *et al.*, 1985; Samoson *et al.*, 1987; van Geem *et al.*, 1988].

In samples HS and HSS, a shoulder to the 55 ppm peak is distinctly apparent. This has previously been assigned to contributions from both extra-framework or partially extracted tetrahedral aluminium with some possible contribution by a penta-coordinated species [Samoson *et al.*, 1987; Miller *et al.*, 1992; Stach *et al.*, 1992_b]. In all dealuminated samples, particularly HSS, a peak at 100 ppm is observed. This does not appear to be a spinning side band as decreasing the rotation frequency (ν_r) to 2.5 and then 1 kHz did not change its chemical shift (Fig. 3.20) in sample HS10.

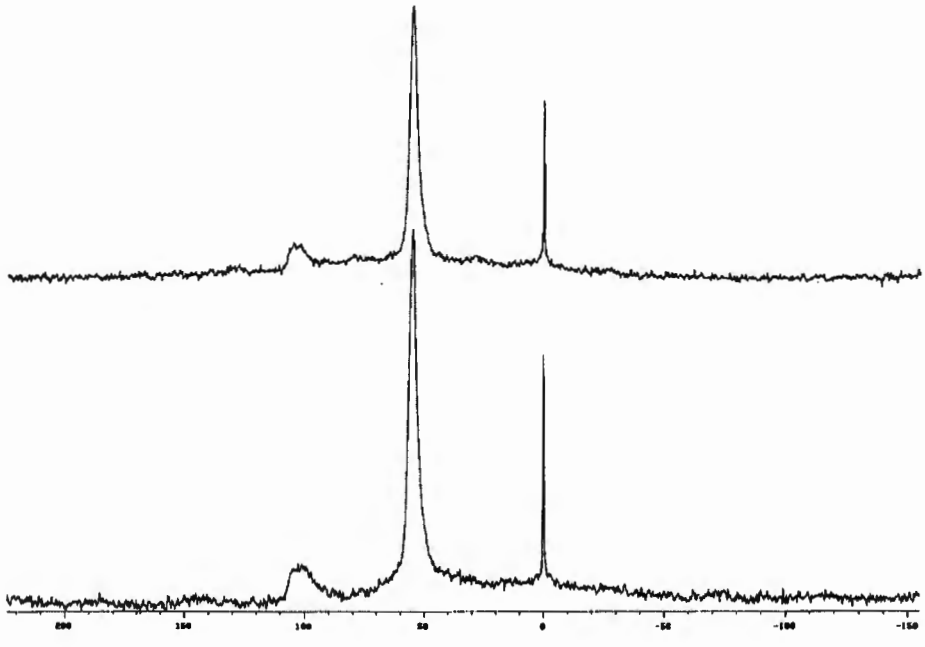

Figure 3.20 Comparison of ^{27}Al MAS NMR spectra of sample HS10 at different rotation frequencies (1000 Hz - top and 2500 Hz - bottom)

The chemical shift of this peak suggests that it could possibly be due either to a $Al(OH)_4^-$ anion [Freude *et al.*, 1985] or a tetrahedral aluminium species linked to another aluminium via an oxygen atom [Akitt, 1989]. However, since the exact species of this extra-framework species has not been identified, it is referred to as EFAl-x.

3.1.6.2 Correction for quadrupole moment

The ^{27}Al nucleus has a spin of $^5/_2$ and as this is greater than $^1/_2$ its MAS NMR spectra is affected by the nuclear quadrupole moment of the aluminium atom. This raises complications due to electrical interactions between the nuclear quadrupole moment of the aluminium nucleus (eQ) and the electric field gradient (eq) at the site of the nucleus.

The quadrupole interaction is described in terms of the asymmetry parameter η and the quadrupole coupling constant e^2qQ/h (or the related quadrupole frequency ν_Q = $(3/20)(e^2qQ/h)$), which can be large in many cases, even in the MHz range, and may exceed any chemical shift or dipolar interaction of the ^{27}Al nucleus. All transitions except for the central $+^1/_2 \leftrightarrow -^1/_2$ transition are subject to first order quadrupole interactions which are proportional to e^2qQ/h and depend on the orientation of the electric field gradient tensor with respect to the magnetic field. However, in randomly packed powder samples, these transitions are spread over the whole range of possible frequencies and are therefore normally too broad to be observed.

In contrast, the central $+^1/_2 \leftrightarrow -^1/_2$ transition is not affected by these first order interactions and is usually the only transition observed in powder spectroscopy. It is however affected by much smaller second order interactions, which cause frequency shifts and line broadening. The second order quadrupole linewidth can be strongly reduced by high magnetic fields and by spinning the sample at the magic angle (≈54.74°). Also, to ensure quantitative excitation of the spin system the radio frequency (RF) pulse should be less than $\pi/6$ for the 5/2 spin of ^{27}Al.

To quantify the population ratios of aluminium species one must make comparison of the areas over the whole transition system. However, it is not always possible to excite the whole transition system depending on the comparative sizes of ν_Q and ν_{RF}. The spectrum will therefore be distorted by the excitation function which must be calculated. Massiot *et al.* [1990] compared the relative areas of the isotropic rotation line of different sites to calculate quantifiable ratios of different aluminium species.

The proportion of magnetization under the isotropic line was first calculated. This is dependent of the quadrupolar interaction, the magnetic field and the spinning speed. For small ν_Q, the amount of magnetisation in the isotropic band is bigger than that for the $+^1/_2 \leftrightarrow -^1/_2$ transition alone, while for large ν_Q, it is only a fraction. Massiot *et al.* [1990] defined the intensity of the isotropic line as the fraction of the magnetisation contained in this line and described this intensity by the following equation:

$$I^{iso} = I^{iso}_{1/2} + \sum_{m \neq 1/2} I^{iso}_{m}$$

Here I^{iso}_m depends only on $|1-2m| \nu_Q/\nu_r$ and η_Q, and $I^{iso}_{1/2}$ depends on $\nu^2_Q/\nu_r\nu_o$ and η_Q. In this way I^{iso} can be calculated and the experimentally measured area corrected by $1/I^{iso}$. Quadrupole coupling constants for trigonal and tetragonal sites (0.632 Mc/s and 6.017 Mc/s respectively) were obtained from Brog *et al.* [1966] and the quadrupole frequency of 6 MHz from Samoson *et al.* [1987]. These produced calculated correction factors of 1.02, 0.98 and 0.97 respectively.

3.1.6.3 Effect of dealumination on ^{27}Al MAS NMR spectra

Washing of Na-Mordenite with acid resulted in the formation of octahedral EFAl (EFAl-o) as is evident from the data presented in Table 3.9.

Table 3.9 Amount of each aluminium species per unit cell in acid washed Na and NaS samples

Sample	Al_f	EFAl-o	EFAl-x	EFAl-t or Al-p	Total Al
Na	6.5	-	-	-	6.5
Na0	6.4	-	-	-	6.4
Na0.001	6.4	-	-	-	6.4
Na0.01	6.2	0.1	0.1	-	6.4
Na0.1	5.4	0.6	0.1	-	6.1
Na1	5.0	0.8	0.2	-	5.9
Na2	4.5	0.9	0.2	-	5.6
Na5	4.1	1.0	0.2	-	5.2
Na10	2.4	0.6	0.1	-	3.1
NaS	4.7	1.0	0.0	0.8	6.5
NaS2	4.9	1.1	0.0	-	6.0

The shape of the peak corresponding to this species appeared to possess a shoulder at -5 ppm in all cases. This indicates that more than one form of the octahedral species was present. Also a small amount of EFAl-x shown by a peak at 100 ppm was formed in all samples which showed framework dealumination.

Table 3.10 Amount of each aluminium species per unit cell in acid washed H-Mordenite samples

Sample	Al_f	EFAl-o	EFAl-x	EFAl-t or Al-p	Total Al
NH_4	6.5	-	-	-	6.5
H(400)	5.5	0.7	0.2	-	6.4
H(550)	5.4	0.8	0.2	-	6.5
H0	5.1	1.2	0.2	-	6.5
H0.01	4.7	1.3	0.3	-	6.3
H0.1	4.8	1.0	0.4	-	6.2
H1	4.8	0.9	0.2	-	5.9
H2	4.6	1.1	0.2	-	5.8
H5	4.3	0.8	0.1	-	5.3
HE	4.7	0.2	-	-	4.9

As shown in Table 3.10, calcination of the ion-exchanged NH_4-Mordenite resulted in the

production of EFAl, which increased slightly with increasing temperature. Washing with deionised water increased the amount of octahedral EFAl relative to calcined H-Mordenite, but no aluminium was removed from the bulk.

A maximum number of extra-framework aluminium species was attained after a 0.01 N wash. As the acid strength of the washes increased from 0.01N to 1N acid, the framework aluminium content remained constant while extra-framework species were removed. Thereafter framework aluminium was once more removed.

Deep bed calcination produced a catalyst which is identical to the shallow bed calcined sample with respect to the ^{27}Al MAS NMR spectra. The production of EFAl-o and removal of Al_f corresponded well with that observed in acid washing of shallow bed calcined Mordenite washed with the same concentrations of nitric acid.. A wash in deionized water increased EFAl-o content and reduced the amount of tetrahedral aluminium. Samples washed with acid concentrations varying between 0.001 and 1N acid all possessed the same amount of framework aluminium. The amount of EFAl-o produced was at a maximum after a 0.001 N acid wash.

Table 3.11 Amount of each aluminium species per unit cell in deep bed calcined and acid washed H-Mordenite samples

Sample	Al_f	EFAl-o	EFAl-x	EFAl-t or Al-p	Total Al
CH	5.4	0.8	0.2	-	6.5
CH0	5.1	1.2	0.2	-	6.5
CH0.001	4.8	1.5	0.1	-	6.4
CH0.01	4.8	1.3	0.3	-	6.4
CH1	4.8	0.9	0.2	-	5.9

Steaming of Mordenite had three major influences on the ^{27}Al NMR spectra. Firstly the spectra generally showed broader resonances with decreased signal to noise ratios for spectra acquired for the same time. This phenomenon is reproducible and does not feature in other

spectra. Secondly, the shoulder to the 55 ppm peak, assigned to extra-framework tetrahedral aluminium (EFAl-t) with some possible contribution by penta-coordinated aluminium (Al-p), became distinctly apparent. The peak previously described at 0 ppm was present, but is broader than that seen in acid washed samples. This could be as a result of a change in the species attached to the central aluminium atom producing variations in peak positions.

Table 3.12 Amount of each aluminium species per unit cell in steamed and acid washed H-Mordenite samples

Sample	Al_f	EFAl-o	EFAl-x	EFAl-t or Al-p	Total Al
HS	3.6	1.4	0.2	1.3	6.5
HS0	3.9	1.3	0.4	0.8	6.5
HS0.01	3.9	1.1	0.1	1.0	6.0
HS0.1	3.7	1.1	0.3	0.6	5.6
HS1	3.3	1.1	0.0	0.5	5.0
HS2	3.3	0.9	0.3	0.4	4.9
HS10	0.6	0.1	0.1	-	0.8
HSS	1.0	1.1	1.9	2.4	6.5
HSS0	1.0	1.4	1.9	2.1	6.5
HSS10	0.9	1.5	1.0	1.5	4.9

Washing the steamed samples with deionised water had the effect of removing tetrahedral aluminium from the framework and producing octahedral aluminium species (Table 3.12). Thereafter, with subsequent increases in the strength of the acid wash, tetrahedral EFAl was consistently removed from the bulk while the octahedral aluminium content remained relatively constant. There were changes to the shape of the octahedral peak with acid washing, the peak becoming more defined and assuming a shape similar to that appearing in acid washed Mordenite (H0.01 compared to HS0.1). Framework aluminium was removed to a greater extent than the octahedral species.

A more severe steaming of H-Mordenite showed an increase in the occurrence of EFAl peaks already observed after mild steaming, in particular the peak at 30 ppm. Also of note

is the reproducible peak shift of the octahedral species to 5 ppm thus indicating the presence of a different octahedral species to those noted in unsteamed samples. Also significant in this spectrum was the small peak at a chemical shift of 95-105 ppm (Al-x).

3.1.7 Infra-red spectroscopy

3.1.7.1 Peak assignments

Figures 3.21 and 3.22 show spectra representing a range of dealumination techniques. The dominant feature of the 1300 - 400 cm^{-1} region is the asymmetric T-O stretching band (ν_{as}) at 1040 cm^{-1} (identified as peak "a"). This has been reported to shift to higher wavenumbers with increasing dealumination [Ha *et al.*, 1978; Musa *et al.*, 1987; Loeffler *et al.*, 1988; Chumbale *et al.*, 1992]. The same trend was noted for the 620 - 630 cm^{-1} band (e), which has been assigned to vibrations in single 4-rings [Flanigen, 1976], alternating SiO_4 and AlO_4 tetrahedra [Ha *et al.*, 1978] and, more recently, to isolated AlO_4 tetrahedra in single 4-rings [van Geem *et al.*, 1988; van Niekerk *et al.*, 1992_a]. The decreasing intensity of the broad 700 - 730 cm^{-1} band (d) has also been reported to be due to the removal of aluminium and it has been assigned to framework AlO_4 tetrahedra [Chumbale *et al.*, 1992].

A shoulder to the ν_{as} band, at 920 - 950 cm^{-1} (b), has been observed to form in some acid washed samples [Dunken and Stephanowitz, 1983; Beyer *et al.*, 1984; Fejes *et al.*, 1985; Musa *et al.*, 1987; van Niekerk *et al.*, 1992]. This band has been attributed to a hydroxyl nest which is formed during aluminium removal by hydrolysis or to opened rings [Beyer *et al.*, 1984]. It has also been attributed to new Si-O lattice bonds, characterised by irregular bond lengths and angles, formed during dealumination, but is still characteristic of the empty nests in the zeolite structure [Fejes *et al.*, 1985]. Musa *et al.* [1987] agree with the assignation of Fejes *et al.* and noted that disappearance of this shoulder after steam treatment indicating ring closure. This is consistent with the results of van Niekerk *et al.* [1992_a] where a relationship was seen between the area of this band and the amount of aluminium

removed from the Mordenite framework during dealumination.

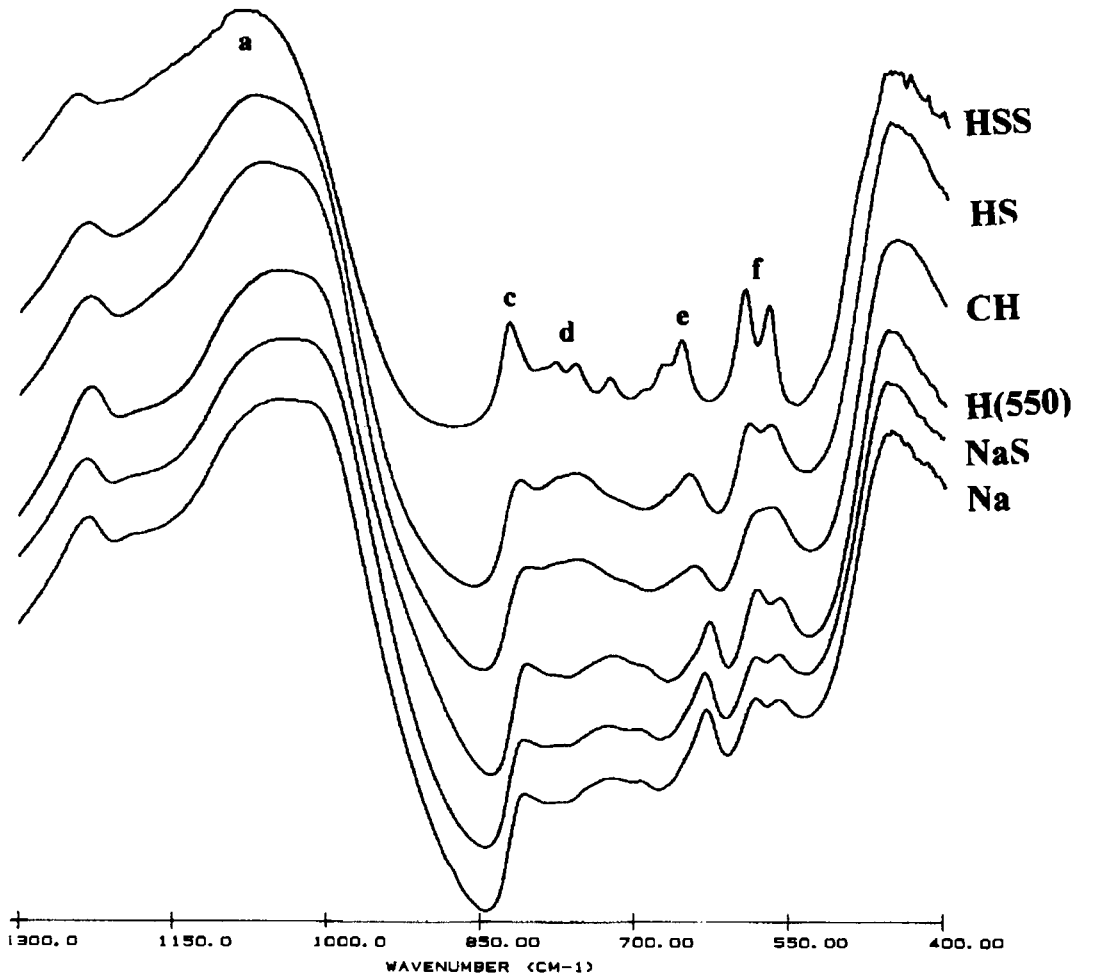

Figure 3.21 Infrared spectra of hydrothermally treated samples: Na, NaS, H(550), CH, HS, HSS

The band at 820 cm^{-1}(c) has been assigned to the O_3Si-O-SiO_3 bond which is formed after dehydroxylation of the hydroxyl nest [Ha *et al.*, 1978; Chumbale *et al.*, 1992]. Two bands at 560 and 580 cm^{-1} have been attributed to the two different types of pentasil building blocks present in Mordenite [Jansen *et al.*, 1984].

3.1.7.2 The effect of dealumination on the infrared spectra of Mordenite

The series of infrared spectra of all samples in the range from 1350 to 400 cm^{-1} is presented in Appendix IV. Spectra selected to represent hydrothermal treatment and acid washing are

shown in Figures 3.21 and 3.22 respectively. Figure 3.21 shows the effects of calcination and steaming of the sodium and hydrogen forms of the catalysts. Although steaming of the sodium form of the catalyst did not appear to have a significant effect on the spectra, the same cannot be said of the hydrogen form. A shift of the 1040 cm^{-1} (a) and 620 - 630 cm^{-1} (e) bands to higher wavenumbers was seen after steam treatments and is consistent with framework dealumination [Jacobs *et al.*, 1993].

The band at 700 - 730 cm^{-1} (d) was not seen to decrease, as expected with framework dealumination[Chunbale *et al.*, 1992], but rather increased as the spectra became more defined. The increased definition is consistent, however, with a more structured framework as a result of rearrangements made possible during steaming [Chumbale *et al.*, 1992]. The separation of the 560 and 580 cm^{-1} bands (f) is seen as added evidence of this.

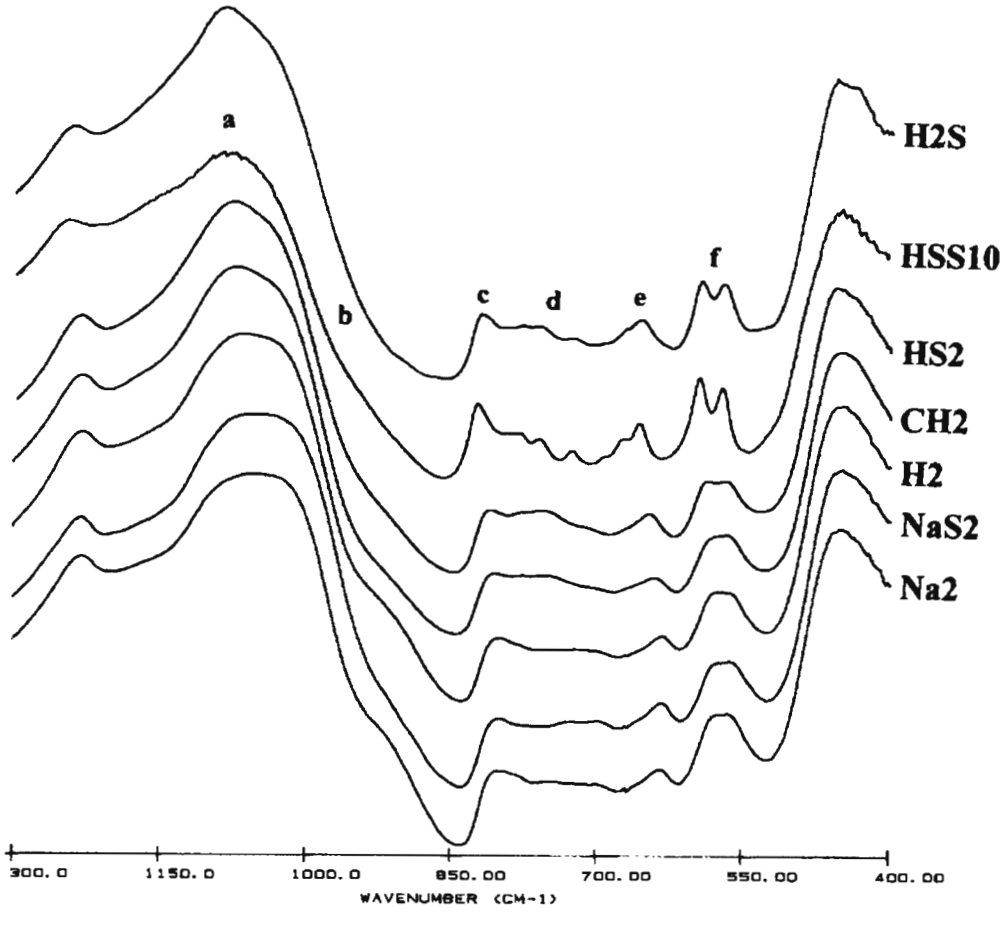

Figure 3.22 Infrared spectra of acid washed samples: Na2, NaS2, H2, CH2, HS2, HSS10

No shoulder to the ν_{as} band was observed indicating that any nests created by dealumination were removed by thermal treatments [Musa *et al.*, 1987]. This is supported by the increase in the band at 820 cm^{-1} (c). Although a broad band was observed after both deep bed calcination and steaming in the 760 - 790 cm^{-1} region, this could not be assigned to a particular vibration.

Acid washing of all samples produced spectra with similar features as seen in Figure 3.22. The ν_{as} moved to higher wavelengths (e.g. from 1047 cm^{-1} for Na to 1059 cm^{-1} for Na2 and from 1049 cm^{-1} for H(550) to 1066 cm^{-1} for H2) as did the bands at $\approx$ 630 cm^{-1} (629 to 633 cm^{-1} and 627 to 632 cm^{-1} for the same samples) once again indicating framework dealumination. This effect was however less pronounced in the case of steamed samples (e.g. 1071 to 1074 cm^{-1} and 644 to 645 cm^{-1} for HS and HS2).

A decrease in the intensity of the band at 720 cm^{-1} was also seen. A shoulder to the ν_{as} band (b) was formed in all cases, but to a lesser extent in the steamed samples. This shoulder was removed and the band at 820 cm^{-1} increased upon steaming (e.g. steaming of H2 to produce H2S) as expected [Musa *et al.*, 1987] due to the dehydration of the hydroxyl nest. In general the spectra lost definition, particularly with respect to the 580 and 560 cm^{-1} bands which is consistent with a loss in framework symmetry. The broad band formed during hydrothermal treatment at 760 - 790 cm^{-1} was removed by acid washing.

3.2 CHARACTERISATION OF CATALYST ACIDITY

3.2.1 Temperature programmed desorption of ammonia

The total number of acid sites and their relative strengths were measured using ammonia temperature programmed desorption (TPD). Readsorption has been shown to seriously affect the shape and position of the TPD peaks [Gorte, 1982; Jones and Griffin, 1983]. Demmin and Gorte [1984] have proposed a set of design parameters in the form of dimensionless groups which can be used to investigate whether the TPD experiments are in an area where sound data interpretations can be made. However, since first order kinetics were assumed and the bed modelled as a CSTR, these parameters cannot be predict the effect of the design parameters on each of the observed effects with great accuracy but do provide guide as to their influences. The dimensionless groups are shown in Table 3.13.

Table 3.13 Dimensionless groups characterising the TPD experiment

	Parameter	Definition	Observed Effect	Ideal Requirement	Calculated Value
1.	$\frac{\epsilon_B V\beta}{Q(T_f-T_o)}$	Residence time of carrier gas	Convective lag	Must be < 0.01 for negligible lag	(3.7×10^{-5})
2.	$\frac{\epsilon_p r^2\beta}{D_p(T_f-T_o)}$	Time constant for diffusion out of an individual particle	Diffusive lag	Must be < 0.01 for negligible lag	(7.4×10^{-8})
3.	$\frac{Qr}{4\pi r^2 N D_p}$	Ratio of carrier gas flowrate to rate of diffusion	Particle concentration gradients	Must be < 0.05 for negligible gradients	(3.6×10^{-4})
4.	$\frac{QL^2}{VD_B}$	Ratio of carrier gas flowrate to axial mixing	Bed concentration gradients	Must be < 0.1 for CSTR	(6×10^{-2})
5.	$\frac{\alpha\rho sFr^2}{\pi^2 D_p}$	Ratio of adsorption rate to diffusion rate	Readsorption at infinite flowrate	Must be < 1 for negligible readsorption	(3×10^{4})
6.	$\frac{\alpha\rho sFV(1-\epsilon_B)}{Q}$	Ratio of adsorption rate to carrier gas flowrate	Readsorption at low flowrates	Must be < 1 for negligible readsorption	(9×10^{7})

where, α = particle surface area (3.6×10^6 cm^2/g)

β = heating rate (0.083 K/s)

D_B = bed dispersion coefficient (3.8 cm^2/s at 750 K and 0.73 at 298 K)

D_P = particle diffusion coefficient ($\approx 1 \times 10^{-5}$ cm^2/s)

ϵ_B = bed porosity (0.3)

ϵ_P = particle porosity (0.28)

F = $(RT/2\pi M)^{1/2}$ (23722 cm/s)

L = bed length (0.5 cm)

M = molar mass (17.03 g/mol)

N = number of particles in the bed ($\approx 2 \times 10^{11}$ assuming spherical particles)

ρ = particle density (1.52 g/cm^3 from He picnometry and BET)

Q = carrier gas flowrate (1.35 cm^3/s)

r = radius of particles (max. 1.5×10^{-4} cm)

R = ideal gas constant (83140 g $cm^2/mol\ s^2$ K)

s = sticking coefficient (1×10^{-3})

T = temperature (373 to 1073 K)

T_f = final temperature (1073 K)

T_o = initial temperature (373 K)

V = bed volume (1.4 cm^3)

Bed porosities or voidages have been calculated using data from BET analysis and helium pycnometry. Particle diffusion coefficients at 200-293 K for water in ZK4, 5A and 4A, methane in NaX and HZSM-5 (4×10^{-6}, 3×10^{-6}, 1×10^{-6}, 3×10^{-4} and 2×10^{-5} cm^2/s respectively) [Karger and Ruthven, 1992] were used to approximate an order of magnitude of the actual diffusion coefficient.

The sticking coefficient has been determined using the equation $s = A \exp(-E_a/RT)$, where A has been taken as 0.15×10^8 [Karge and Dondur, 1990] and heats of desorption in the range of 130 to 160 kJ/mol [Sawa *et al.*, 1990]. Using these values, s was then calculated to be

$1x10^{-3}$.

All the dimensionless groups apart from group numbers five and six are within the suggested constraints as can be seen from comparison of the calculated value and the reqirements list in Table 3.13. This suggests that the lag times resulting from pore diffusion (group two) and the sample cell (group one) were negligible and concentration gradients in the pores (group three) and bed (group four) were not significant.

Readsorption will influence the TPD results (groups four and five), but this is due to the nature of the zeolite rather than the experimental setup. Since $N_{Re} = 6$ and $D_{eff}/ul = 5x10^{-4}$ plug flow is indicated and therefore peak broadening and distortion resulting from flow dispersion between the cell and the thermal conductivity detector are negligible.

The response curves, shown in Appendix V, consisted of two main features similar to those seen by other researchers [Mirodatos and Barthomeuf, 1981; Hidalgo *et al.*, 1984; Karge and Dondur, 1990; Stach *et al.*, 1992]. There was a sharp peak at ≈250°C referred to as the low temperature desorption (LTD) peak followed by a broader peak in the 500-550°C range referred to as the high temperature desorption (HTD) peak. The low temperature desorption peak (LTD) has not been ascribed to physisorbed ammonia as it did not decrease even after a 60 hour desorption in flowing helium as shown in Figure 3.23.

This Figure also shows the reproducibility of the experiment. Two different samples of steamed H-Mordenite were used to generate these two response curves. The difference in measured acidity was 0.02 $mmol.g^{-1}$. The number of acid sites determined by the response curves of each TPD experiment was checked by dissolving the desorbed ammonia in sulphuric acid and titrating with sodium hydroxide. The difference between the two results was below 0.02 mmol of ammonia in all experiments.

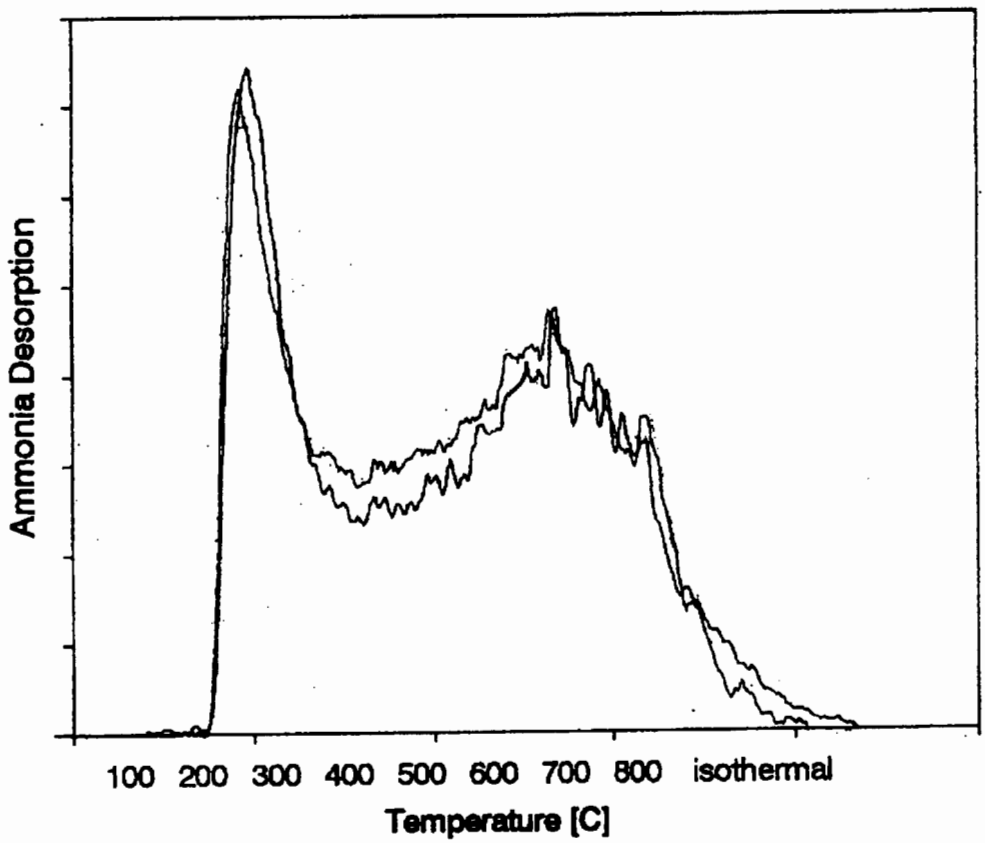

Figure 3.23 Effect of increase desorption time on the temperature programmed desorption response curve of sample HS.

3.2.1.1 Deconvolution of response curve

As the HTD peak was seen to contain up to three types of acid sites , the response curves were deconvoluted into four peaks and assigned to weak Lewis, weak and strong Brönsted and strong Lewis in increasing temperature of desorption [Karge and Dondur, 1990]. A typical example of this deconvolution is shown in Figure 3.24.

Assuming parallel and independent desorption processes, a first order rate of desorption and using a distribution of desorption energies described by $P(E)$, the rate of desorption from a particular site, S_n, is given by the following equation [Karge and Dondur, 1990]:

$$-(\frac{d\theta}{dt})_n = \theta_n \int_{E_{max}}^{E_{min}} P(E_n) A_n \exp(-\frac{E_n}{RT}) dE_n$$

A gaussian function was found to define $P(E_n)$ adequately by Karge and Dondur [1990]. This distribution function was therefore used to deconvolute the response curves. In order to simplify the solution so that it could be found using available software, it was reasoned that if each desorption energy was related singularly to a desorption temperature, the gaussian function could be written in terms of temperature.

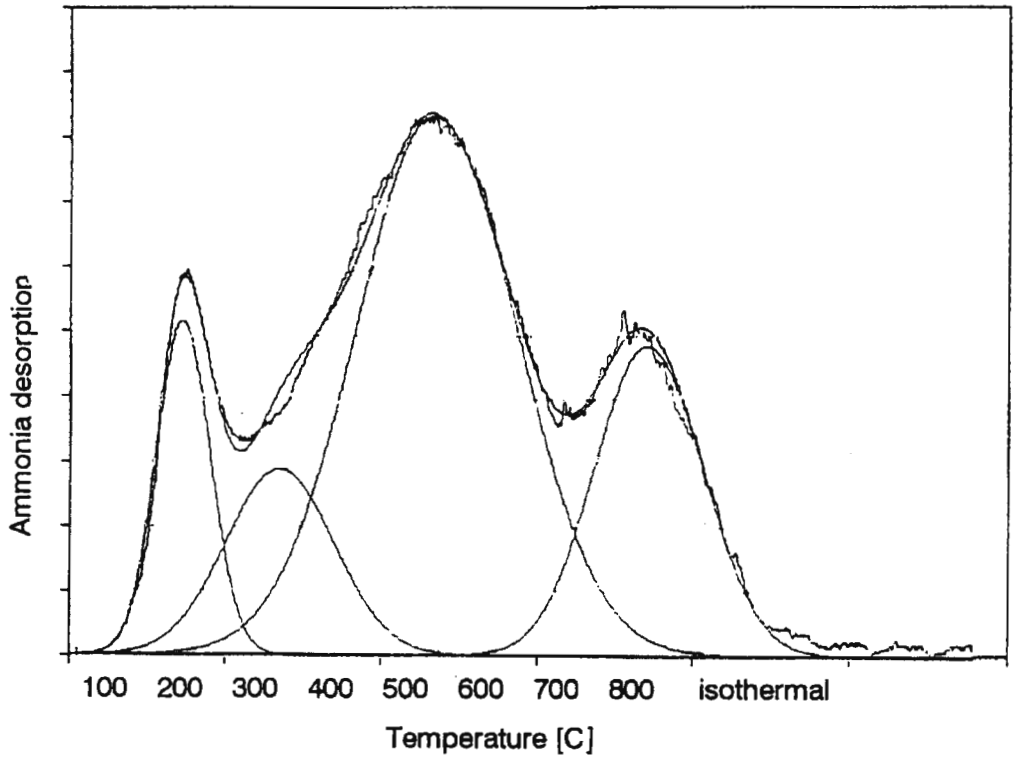

Figure 3.24 TPD response curve of shallow bed calcined H-MOR (sample H(550)) showing deconvolution results.

This new function was tested on the TPD results as shown in Figures 3.24 and 3.25 where the fit can be seen to be very good. Deviations from experimental data were mainly at high temperatures where it is possible that dehydroxylation has led to water molecules in the TPD

cell outlet, resulting in increased TCD readings.

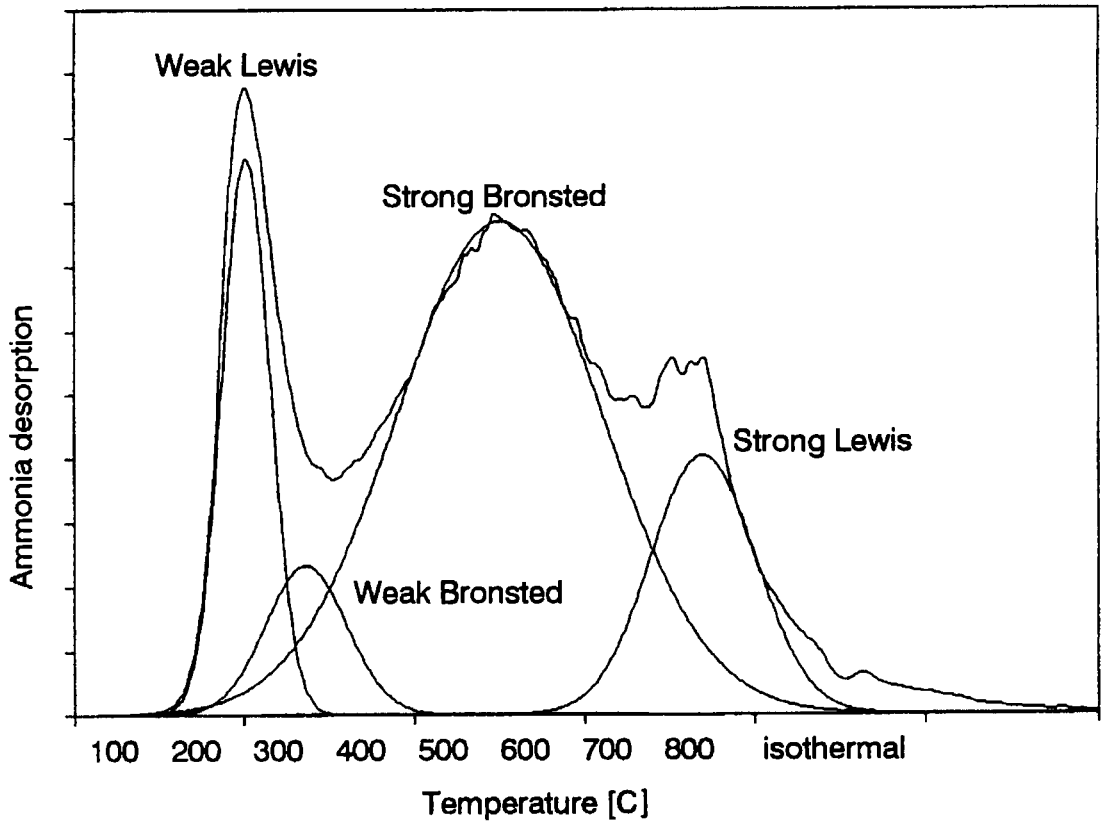

Figure 3.25 TPD response curve of deep bed calcined H-MOR (sample CH) showing deconvolution results.

3.2.1.2 Effect of dealumination of the TPD response curve of Mordenite

The acid amounts (mmol NH_3/g_{cat}) determined from the deconvolution procedure and the desorption peak temperatures are shown in Tables 3.14 to 3.17. Some response curves typical of different dealumination techniques are shown in Figures 3.26 to 3.29 and the full set of response curves are presented in Appendix V.

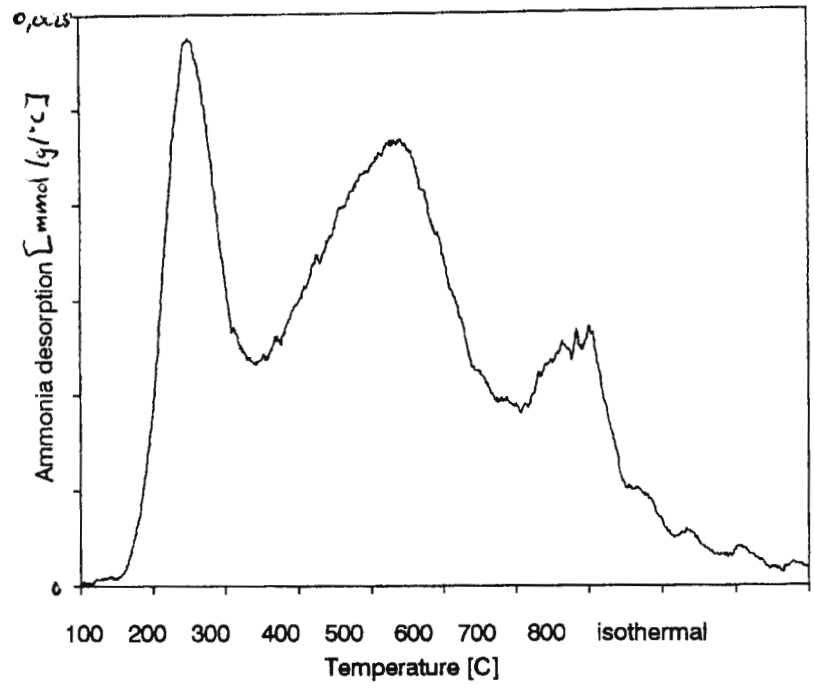

Figure 3.26 TPD response curve of sample Na1

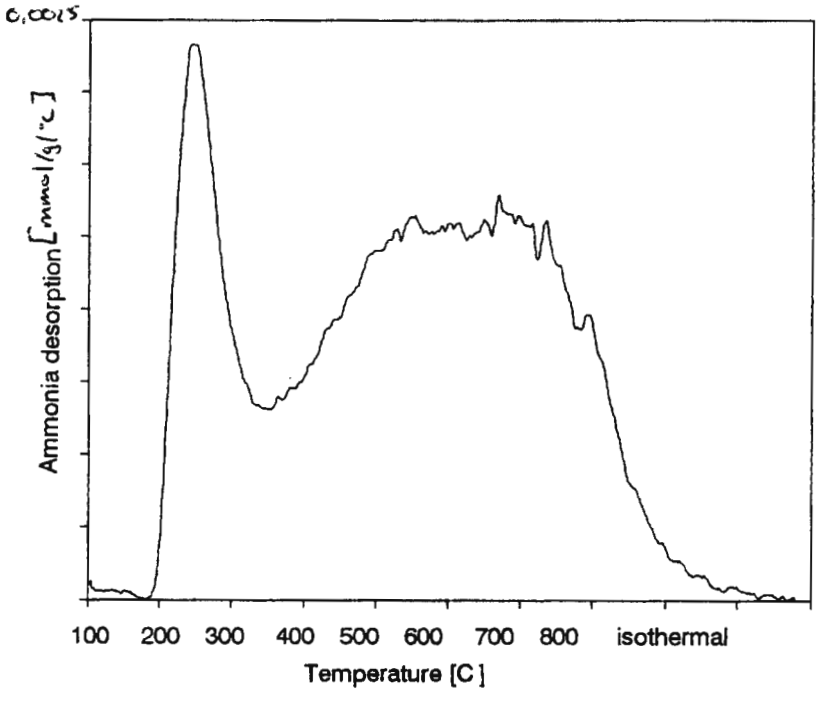

Figure 3.27 TPD response curve of sample H5

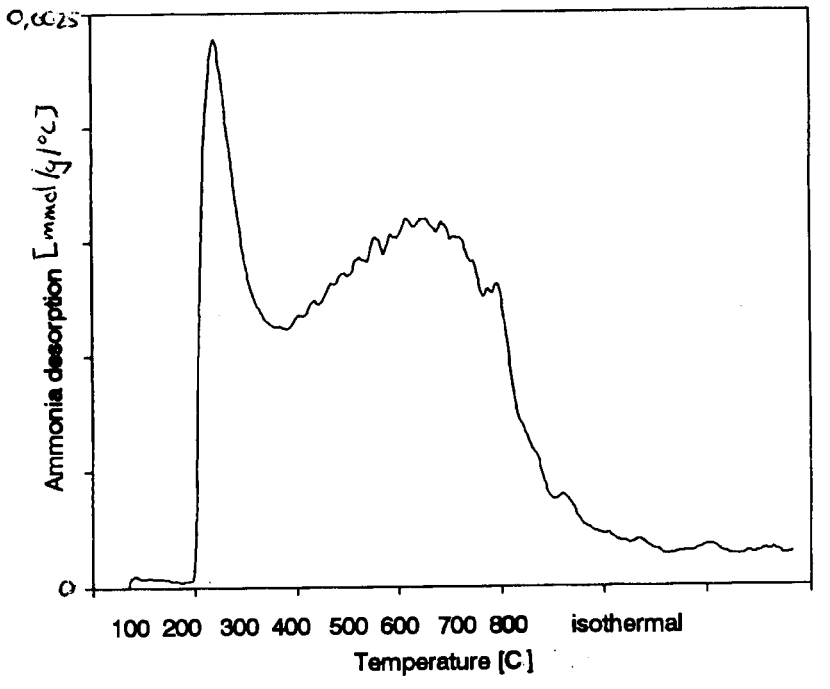

Figure 3.28 TPD response curve of sample HS1

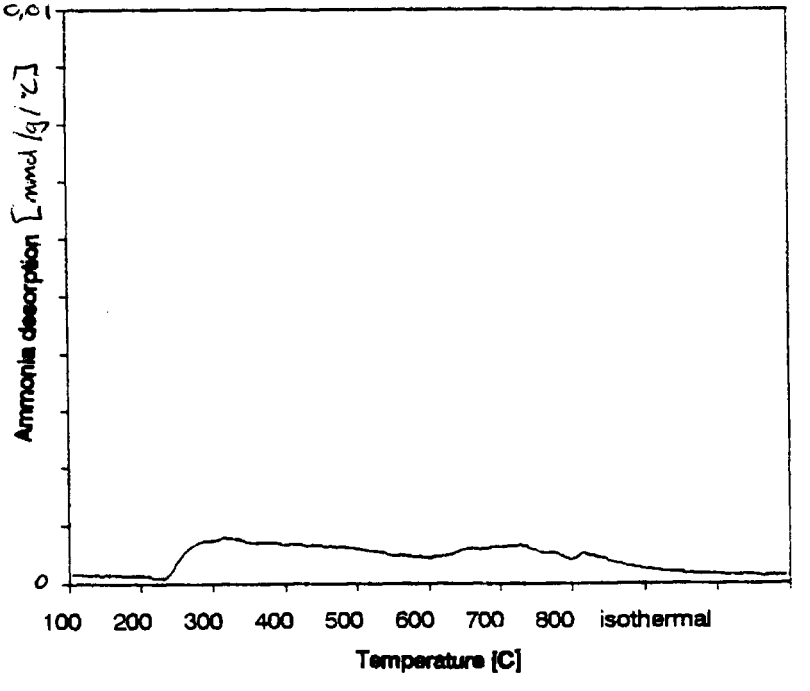

Figure 3.29 TPD response curve of sample HSS

Table 3.14 Acid amounts (mmol.g^{-1}) and desorption temperatures determined by deconvolution of TPD spectra for dealuminated Na-Mordenite samples (Peaks assigned according to Karge and Dondur [1990])

	Weak Lewis		Weak Brönsted		Strong Brönsted		Strong Lewis	
Sample	Amount	Tmax	Amount	Tmax	Amount	Tmax	Amount	Tmax
	mmol/g	°C	mmol/g	°C	mmol/g	°C	mmol/g	°C
Na	0.87	275	-	-	0.04	625	-	-
Na0.01	0.70	270	-	-	0.47	560	-	-
Na0.1	0.65	260	-	-	0.90	550	-	-
Na1	0.35	270	0.28	390	0.90	545	0.05	770
Na2	0.22	276	0.32	400	1.06	555	0.15	750
Na5	0.32	245	0.15	355	1.06	555	0.21	750
Na10	0.16	235	0.56	435	0.54	540	0.32	730
NaS	1.02	315	-	-	-	-	-	-
NaS0.01	0.91	295	-	-	-	-	-	-
NaS0.1	0.77	280	-	-	1.39	560	-	-
NaS1	0.32	275	0.06	400	1.37	555	0.13	785
NaS2	0.38	255	0.23	405	1.14	550	0.09	775
NaS5	0.21	230	0.51	400	0.92	540	0.14	760

The starting material, Na-Mordenite, showed essentially no Brönsted or strong Lewis acidity. With acid washing, however, the number Brönsted acid sites and then strong Lewis acid sites increased as the amount of weak Lewis acid sites decreased. Steaming of Na-Mordenite increased the amount of weak Lewis acid sites slightly. Subsequent acid washing of this sample reduced the number weak Lewis acid sites to below the level of the corresponding unsteamed samples. Brönsted acidity as determined by the deconvolution of the TPD response curve was only observed after a 0.1N acid wash.

H-Mordenite showed a large number of strong acid sites. Subsequent acid washing did not affect weak Lewis acidity, but decreased the number of strong acid sites (Table 3.15). The peak temperature for the peak assigned to strong Brönsted acidity increased with increased concentration of acid washing.

Table 3.15 Acid amounts (mmol.g^{-1}) and desorption temperatures determined by deconvolution of TPD spectra for acid washed H(550) samples (Peaks assigned according to Karge and Dondur [1990])

	Weak Lewis		Weak Brönsted		Strong Brönsted		Strong Lewis	
Sample	Amount	Tmax	Amount	Tmax	Amount	Tmax	Amount	Tmax
	mmol/g	°C	mmol/g	°C	mmol/g	°C	mmol/g	°C
H(550)	0.20	240	0.22	350	1.15	530	0.17	760
H0	0.35	240	0.18	360	1.19	540	0.20	750
H0.01	0.41	240	0.16	355	1.08	540	0.23	755
H0.1	0.33	240	0.49	450	0.95	540	0.08	760
H1	0.27	240	0.29	455	1.11	575	0.06	760
H2	0.25	240	0.26	430	1.02	575	0.09	760
H5	0.22	235	0.21	355	0.85	575	0.12	750
HE	0.11	225	0.17	300	1.18	540	0.33	750

Increased strong acidity was found in deep bed calcined H-Mordenite (CH) as evidenced by increased desorption of ammonia (Fig. 3.29 and Table 3.16). Comparison between the response curves of deep and shallow bed calcined Mordenite CH and H(550) shows that the increased desorption occurs at temperatures around 600°C. Although there was no decrease in Brönsted acidity this effect is similar to that seen by Mirodatos and Barthomeuf [1981] for mildly steamed H-Mordenite.

Table 3.16 Acid amounts (mmol.g^{-1}) and desorption temperatures determined by deconvolution of TPD spectra for acid washed CH samples (Peaks assigned according to Karge and Dondur [1990])

	Weak Lewis		Weak Brönsted		Strong Brönsted		Strong Lewis	
Sample	Amount	Tmax	Amount	Tmax	Amount	Tmax	Amount	Tmax
	mmol/g	°C	mmol/g	°C	mmol/g	°C	mmol/g	°C
CH	0.36	255	0.16	325	1.37	550	0.36	770
CH0	0.39	240	0.16	360	1.19	540	0.20	750
CH0.001	0.40	240	0.17	360	1.18	540	0.19	750
CH0.01	0.40	240	0.21	360	1.13	540	0.13	755
CH0.1	0.34	220	0.26	450	1.17	590	0.09	780
CH1	0.27	240	0.31	460	1.09	575	0.07	760

Mild steaming caused a large drop in the amount of both Lewis and Brönsted acid sites (see, for example, H(550) and HS), although an increase in Brönsted acid strength as determined by the peak temperature was observed. Although an apparent modulation, which was reproducible, can be seen in the response curves of all steamed samples washed with acid below 0.1N strength (for example sample HS in Figure 3.23), no explanation for this phenomenon can be offered at this time. Increasing the acid wash concentration to 0.1N resulted in an increase in the amount of Brönsted acid sites. Thereafter the amount of Brönsted acid sites decreased with increasing concentration of acid wash, the weak Lewis acidity remaining largely unaffected.

Table 3.17 Acid amounts (mmol.g^{-1}) and desorption temperatures determined by deconvolution of TPD spectra for acid washed steamed H-Mordenite samples (Peaks assigned according to Karge and Dondur [1990])

	Weak Lewis		Weak Brönsted		Strong Brönsted		Strong Lewis	
Sample	Amount	Tmax	Amount	Tmax	Amount	Tmax	Amount	Tmax
	mmol/g	°C	mmol/g	°C	mmol/g	°C	mmol/g	°C
HS	0.33	245	0.24	380	0.57	645	0.09	765
HS0	0.26	240	0.23	355	0.69	635	0.01	765
HS0.01	0.28	245	0.21	365	0.75	640	0.01	770
HS0.1	0.29	250	0.20	370	0.80	655	0.04	770
HS1	0.17	265	0.21	370	0.75	645	0.02	770
HS2	0.15	265	0.21	370	0.59	640	0.01	765
HS5	0.02	265	0.08	390	0.31	555	0.23	760
HS10	0.09	430	-	-	0.18	620	-	-
HSS	0.07	300	0.16	430	0.10	675	0.07	755
HSS0	0.04	310	0.26	390	0.01	640	0.07	720
HSS10	0.01	300	0.36	400	0.01	690	0.00	720

Severe steaming of H-Mordenite resulted in a decrease in number of acid sites that was not restored by subsequent acid washing.

3.2.2 Infra-red spectroscopy of adsorbed pyridine

The infrared results are presented in this section in two ways. One representation shows the actual spectra, the other shows plots of the concentration of the adsorbed species versus temperature. All spectra were recorded in the absorbance mode and thus the parameter indicating band intensities in the plots is a measure of the concentration of the molecular group absorbing energy at that particular frequency.

These concentrations can be reported in two ways. Firstly, as absorbance per gram which represents the true optical density of the absorption bands in absorbance units divided by the mass of catalyst. Secondly, as millimoles of pyridine adsorbed per gram of catalyst. The second method takes into account the difference in extinction coefficients of the different adsorbed species. This method uses the Beer-Lambert Law:

$$A = \log\left(\frac{I_o}{I}\right)_\sigma = \epsilon c D$$

Where A = absorbance in cm^{-1}

$(I_o/T)_\sigma$ = ratio of reference beam to sample beam transmittance as measured with a spectrometer set at wavenumber σ.

c = concentration of adsorbate expressed as moles/dm^3

ϵ = molar extinction coefficient

D = thickness of wafer

to evaluate the data. Although this method has limitations with relatively aluminous zeolites (Si/Al < 4) [Makarova *et al.*, 1995] it is applicable in the case of Mordenite [Emeis, 1993]. Values for the integrated molecular extinction coefficients have been reported by a number of authors [Hughes and White, 1967; Stock et al., 1984; Datka *et al.*, 1992; Emeis, 1993] and are shown in Table 3.18. A factor of 0.4343 used by Hughes and White to convert the apparent integrated absorption intensity to the intensity used in their calculations. The adjustment of the coefficients (from 3.03, 3.26 and 3.88 to 1.31, 1.41 and 1.68) has been

made in the table.

Table 3.18 Molecular extinction coefficients for pyridine on Lewis and Brönsted sites

Source	Catalyst	Brönsted	Lewis	Ratio
Hughes and White [1967]	Zeolite-Y	1.31	1.41,1.68	0.77
Stock *et al.* [1984]	NaX, NaY	1.2-1.5		
Datka *et al.* [1992]	Supported Nobium oxide	0.73	1.11	0.66
Emeis [1993]	MOR, Y, Silica-alumina	1.67	2.22	0.75
Makarova *et al.* [1995]	H-Y, H-EMT	1.1-1.6		

As the coefficients of Emeis [1993] were determined using Mordenite, it was decided to use these values to determine the pyridine concentrations. The discrepancy in extinction coefficients (a difference of ≈20%) leads one to question the reliability of the calculated concentrations. They may however be used at the very least as the relative quantities of pyridine adsorbed on the different types of acid sites. This is supported by the fact that the ratios of the extinction coefficients of Brönsted and Lewis sites are fairly similar in the three cases given and to the ratio of 0.75 used by Miller *et al.* [1992].

Although the choice of method to determine site density varies between use of the band height [Karge, 1980; Makarova *et al.*, 1995] to the band area [Hughes and White, 1967; Emeis, 1993], latter is regarded by some as a better measure of concentration when the half-width of an adsorption band is not large compared to the spectral slit width [Hughes and White, 1967] and was used in the present work.

The integration of the Beer-Lambert Law over absorption band X gives:

$$A_x = \epsilon_x \, c \, D$$

The amount of pyridine per cm^2 of catalyst disk is:

$$\phi = c \, D \quad [mmol/cm^2]$$

therefore $\phi = A_x/\epsilon_x$

and $C_X = A_X \pi r^2 / \epsilon_X W$

where C = concentration [mmol/g_{cat}]

W = weight of disk [mg]

For Brönsted sites: $C_B = 0.0188\ A_B/W$

and Lewis sites $C_L = 0.0142\ A_L/W$

3.2.2.1 Peak assignments

Bands of adsorption have been assigned to physisorbed pyridine (Py), hydrogen bonded pyridine (HPy), pyridinium ion (BPy) and co-ordinately bonded pyridine (LPy) species, as well as to structural hydroxyl groups according to Table 3.19.

Table 3.19 Peak assignments for pyridine adsorbed on Mordenite

Wavenumber	Assignment	Reference
1440	Py	[Parrillo *et al.*, 1990]
1445	HPy	[Parry, 1963]
1450	LPy	[Parry, 1963]
1462	LPy	[Cannings, 1968]
1485	BPy,LPy,HPy	[Parry, 1963]
1540-1550	BPy	[Parry, 1963; Lefrancois and Malbois, 1971]
1580	LPy	[Miller et al., 1992]
1590	HPy,BPy	[Parry, 1963, Lefrancois and Malbois, 1971]
1620	BPy,LPy	[Lefrancois and Malbois, 1971]
1635	BPy	[Parry, 1963]

HPy has been predominantly seen in highly cationated samples and has thus been assigned to pyridine associated with a cation [Lefrancois and Malbois, 1971]. The peaks which were used in this work are those at 1545 cm^{-1}, 1462 cm^{-1}, 1450 cm^{-1} and 1445 cm^{-1}. They were chosen as they are bands which are easily identifiable and do not overlap with other adsorption bands in the region. They represent pyridine associated with Brönsted acid sites,

strong Lewis acid sites, Lewis acid sites and cations respectively [Ghosh and Curthoys, 1983_b]

3.2.2.2 Analysis of the acidity of dealuminated Mordenite

Spectra recorded after pyridine was adsorbed onto samples at 100 °C are shown in Figure 3.30. All samples showed Brönsted acidity except for Na-Mordenite, which showed a large amount of pyridine adsorbed on cations at 1445 cm^{-1}. The peak at 1445 cm^{-1} does not appear in sample Na0.1 and the 0.1N nitric acid wash appears to have removed these cations. A small amount of Lewis acidity also appears at 1450 cm^{-1} after acid washing of Na-Mordenite (Na0.1).

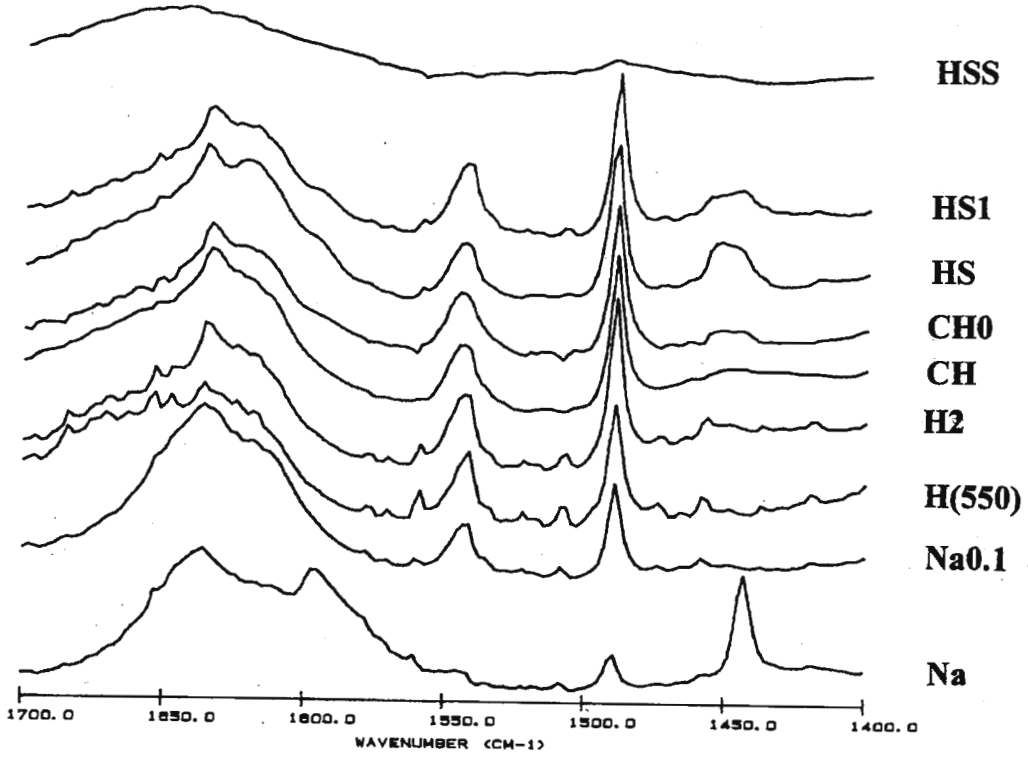

Figure 3.30 Infrared spectra of samples Na, Na0.1, H(550), CH, CH0, H2, HS, HS1 and HSS with pyridine adsorbed at 373 K

The calcination both shallow and deep beds to produce H-Mordenite, namely H(550) and

CH, resulted peaks at both 1450 and 1462 cm^{-1} indicative of Lewis acidity. It was interesting to note the broadening of this band on washing with deionised water (CH0) and 2N acid (H2). A large broad band between 1465 cm^{-1} and 1435 cm^{-1} was observed in mildly steamed H-Mordenite (HS). This peak is in the region which is indicative of pyridine associated with both Lewis acid sites and cations and was reduced upon acid washing (HS1). Severely steamed H-Mordenite (HSS) showed essentially no adsorbed pyridine.

The spectra of adsorbed pyridine on the samples at increasing temperatures are shown in Appendix VI. Figures 3.31 to 3.38 show the relative amounts of Lewis and Brönsted acidity represented by pyridine concentrations on each site as a function of increasing temperature. Pyridine is removed from the cations of Na-Mordenite as the temperature increased from 100°C. This indicates that the low temperature peak in ammonia TPD has been correctly assigned to weak Lewis or cationic sites. This sample does seem to possess a small amount of Brönsted acidity (indicated by the peak at 1550 cm^{-1}).The pyridine does not desorb from this site even at elevated temperatures (600°C) therefore indicating that although low in concentration, these sites are relatively strong.

Washing this sample with 0.1N acid (Fig. 3.32) increased the amount of Brönsted acidity substantially. There is an increase in amount of pyridine adsorbed on Brönsted sites with increasing temperature from 100 to 300°C, a phenomenon noted previously [Karge, 1971; Rautenbach, 1985]. This is probably as a result of the pyridine being able to access a larger area of the catalyst due to its increased movement at high temperatures. Although, pyridine desorbs from Brönsted acid sites in the catalyst at temperatures between 400 and 600°C, there is still residual pyridine at 600°C. This would appear to confirm the assignment of desorption at these temperatures in ammonia TPD studies to be from Brönsted sites. A small amount of Lewis acidity is also observed.

Shallow bed calcined H-Mordenite (Fig. 3.33) shows the same increase in adsorbed pyridine as Na0.1 for the same reasons. The increase is more severe indicating that a larger number

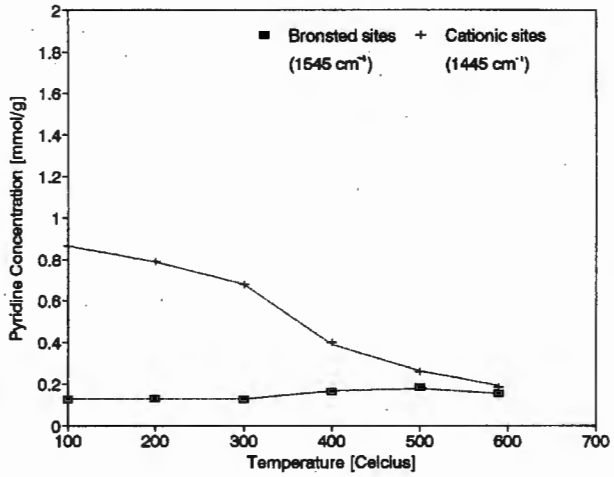

Figure 3.31 Concentration of pyridine adsorbed on Brönsted acid and cationic sites in sample Na measured by infrared spectroscopy as a function of temperature

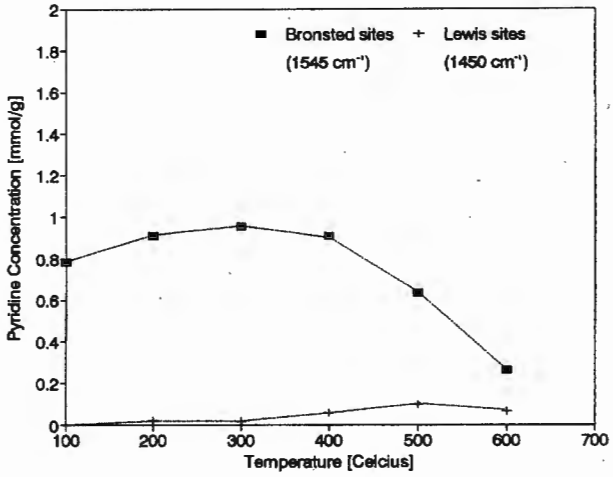

Figure 3.32 Concentration of pyridine adsorbed on Brönsted and Lewis acid sites in sample Na0.1 measured by infrared spectroscopy as a function of temperature

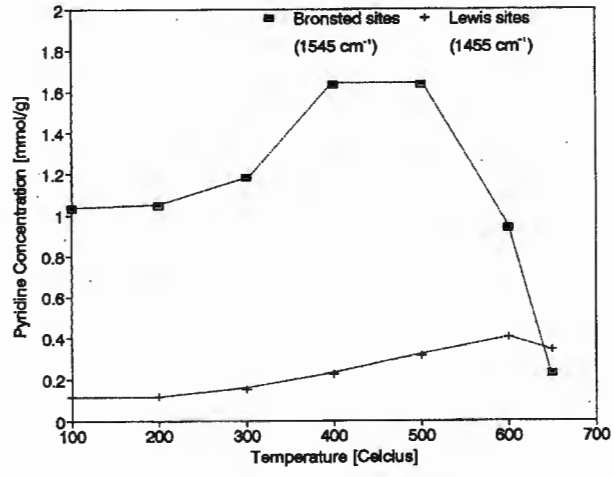

Figure 3.33 Concentration of pyridine adsorbed on Brönsted and Lewis acid sites in sampleH (550) measured by infrared spectroscopy as a function of temperature

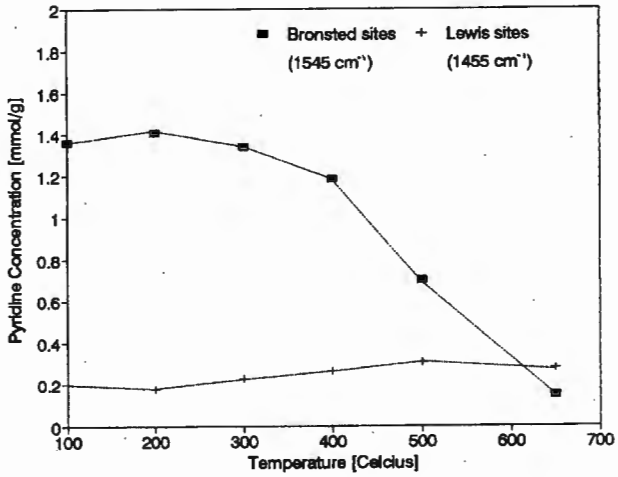

Figure 3.34 Concentration of pyridine adsorbed on Brönsted and Lewis acid sites in sample H2 measured by infrared spectroscopy as a function of temperature

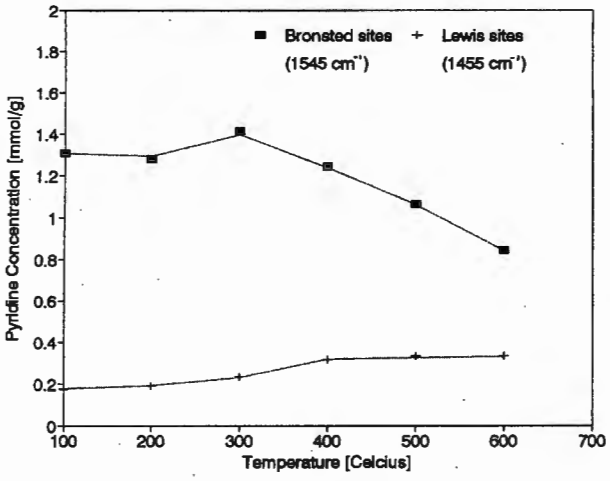

Figure 3.35 Concentration of pyridine adsorbed on Brönsted and Lewis acid sites in sample CH measured by infrared spectroscopy as a function of temperature

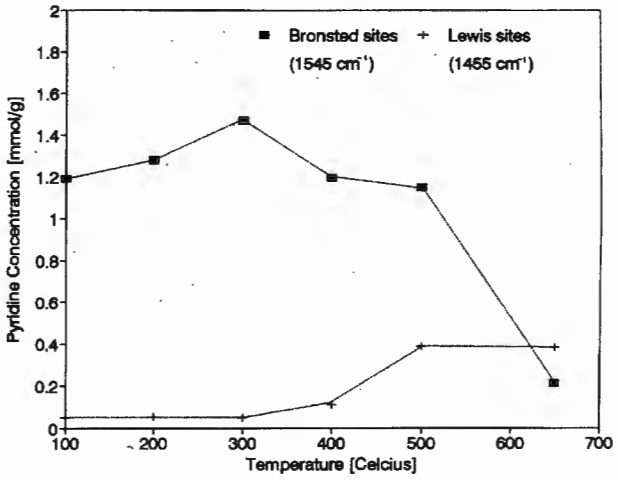

Figure 3.36 Concentration of pyridine adsorbed on Brönsted and Lewis acid sites in sample CH0 measured by infrared spectroscopy as a function of temperature

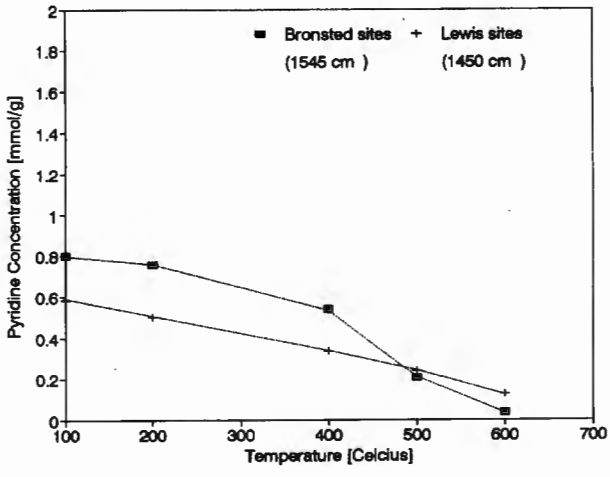

Figure 3.37 Concentration of pyridine adsorbed on Brönsted and Lewis acid sites in sample HS measured by infrared spectroscopy as a function of temperature

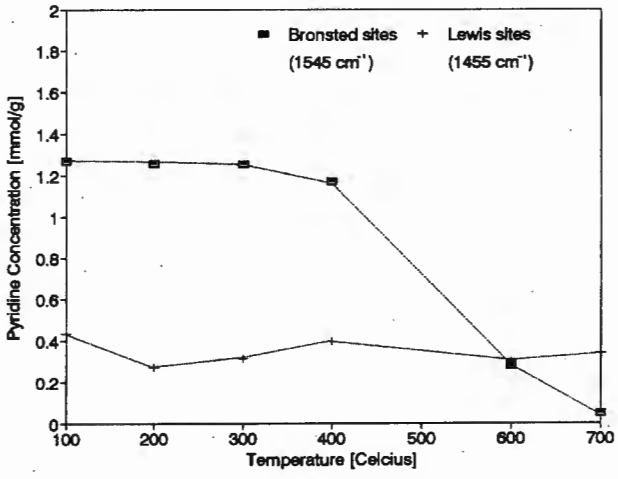

Figure 3.38 Concentration of pyridine adsorbed on Brönsted and Lewis acid sites in sample HS1 measured by infrared spectroscopy as a function of temperature

of Brönsted acid sites were not accessed by pyridine at 100°C. This is probably due to greater diffusional or steric constraints restricting the access of pyridine to acid sites until sufficient energy had been supplied to overcome these via a temperature increase.

Deep bed calcined H-Mordenite (Fig. 3.35) does not show this increase in adsorption on Brönsted acid sites, but maintains a constant amount of adsorption on these sites until desorption begins at 400°C. A larger amount of Lewis acidity is present in this catalyst, the amount increasing slightly with increasing temperature up to 600°C.

Washing the deep bed calcined H-Mordenite with deionised water had the effect of decreasing the adsorption on Brönsted sites slightly, although at 300°C both sample CH and sample CH0 showed the same amount of Brönsted acidity. Lewis acidity was dramatically reduced (Fig. 3.36).

Steaming of H-Mordenite reduced Brönsted acidity dramatically, but increased the measured amount of Lewis acidity (Fig. 3.37). Both quantities decreased continually with increasing temperatures. A wash with 1N acid increased the level of Brönsted acidity seen in steamed H-Mordenite (Fig. 3.38) and this level was maintained until the onset of desorption at 300°C. Although Lewis acidity was seen to decrease, a constant level was maintained throughout the experiment. Severe steaming of H-Mordenite virtually eliminated all acidity.

The desorption of pyridine seems to initially be from cationic or weak Lewis sites and then from Brönsted sites with increased temperature between 400 and 650°C. The remaining pyridine is adsorbed to mainly Lewis sites, although there is a significant number of Brönsted sites present particularly in sample CH. This would indicate that the peak assignments made in the TPD deconvolution were essentially correct although the peak seen at the highest temperatures could have made significant contributions to Brönsted acidity.

3.2.2.3 Investigation of the 3000 to 4000 cm^{-1} region

The region of the infrared spectrum between 3000 and 4000 cm^{-1} can be used to provide information on the nature of hydroxyls present in Mordenite. The spectrometer used, however, showed low emittance in this region thus leading to a low signal to noise ratio. Therefore ^{1}H MAS NMR was used in preference to infrared spectroscopy to investigate hydroxyls in dealuminated Mordenite. The spectra of the 4000 to 2500 cm^{-1} region of samples Na, H2, CH, CH0 and HS1 are, however, presented in Figure 3.39 for completeness.

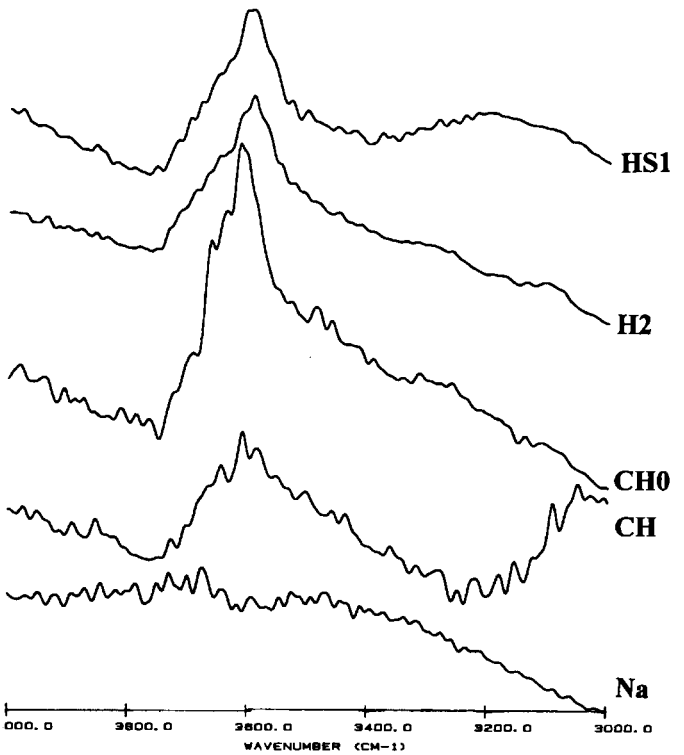

Figure 3.39 Region from 4000 to 2500 cm^{-1} of the infrared spectra of samples Na, H(550), H2, CH, CH0 and HS1

Qualitatively one can see the presence of hydroxyl groups in H-Mordenite samples and the lack of them in Na-Mordenite. Interestingly the deep bed calcined sample CH seemed to possess less hydroxyl groups than the same sample washed with water.

3.2.3 ^{1}H MAS NMR

Proton MAS NMR was performed on selected samples which are shown in Table 3.20. Samples Na0.1 and Na10 were chosen to investigate the effect of sodium and aluminium removal by acid washing on the ^{1}H MAS NMR spectra. Hydrothermal treatments were also investigated using samples CH, HS and HSS. The effect of deionised water on deep bed calcined mordenite and acid washing on steamed mordenite were investigated using samples CH0 and HS1. The spectra exhibited peaks at 1.5-2.5 ppm and 4 ppm. A small peak at 6.6 ppm was also detected in samples Na10 and HS1.

Assignments of the peak at 4 ppm has been made to acidic bridging hydroxyl groups by Freude *et al.* [1986]. The peak at 1.5-2.5 ppm is probably made up of two peaks, the major one at 1.8 ppm which is assigned to terminal hydroxyl groups attached to silicon (SiOH) [Freude *et al.* 1986] and a peak at 2.5 ppm which has been assigned by Lohse *et al.* [1987] to extra-framework hydroxoaluminium species (EFAlOH). The peak at 6.6 ppm is probably caused by the protons of ammonia [Jacobs *et al.*, 1993] and indicates that ammonium exchange may have occurred during treatment with nitric acid. Table 3.20 shows the relative amounts of each type of hydroxyl as determined at the Institut für Technische Chemie at the University of Stuttgart.

Table 3.20 Concentration of hydroxyl groups in selected samples

Sample	SiOH and EFAlOH	Acidic SiOHAl	Total
	mmol.g^{-1}	mmol.g^{-1}	mmol.g^{-1}
Na0.01	0.15	0.45	0.6
Na10	0.35	1.3	1.65
CH	0.15	0.45	0.6
CH0	0.4	1.65	2.05
HS	0.25	0.15	0.4
HS1	0.4	0.95	1.35
HSS	0.25	0.2	0.45

Samples Na0.1, Na10, CH0, HS1 and HSS all show acidic hydroxyl groups equal to the amount of ammonia represented by the high temperature desorption peak of ammonia TPD, suggesting that all sites in this peak are due to Brönsted acid sites. Samples CH and HS present contradictions. A large number of Brönsted acid sites were found by infrared spectroscopy of pyridine adsorption and large amount of acidity seen by ammonia TPD, but the values found by ^{1}H MAS NMR was less than half of that seen by other techniques for both thermally treated samples.

The number of silanol groups and extra-framework hydroxyl groups increase with increased concentration of acid washing as expected (Na0.1 to Na10 and HS to HS1). The amounts of these were low in the case of hydrothermally treated samples, probably due to framework repair during the high temperature treatment. Sample CH, which had been deep bed calcined, exhibited the same number of these hydroxyls as sample Na0.1 despite undergoing the same level of framework dealumination (17% from Na-Mordenite) and having more EFAl present. Sample CH0 showed a large number of these hydroxyls despite the relatively low degree of framework dealumination (21%) suggesting a hydration effect not seen in other samples.

3.3 CATALYTIC PROPERTIES

3.3.1 Isobutane cracking

All the detailed results in the study of isobutane cracking over mordenite samples as well as a sample calculation showing the derivation of selectivity and conversion is presented in Appendix VII. A detailed explanation of the reason for using isobutane cracking as a probe reaction and an analysis of the significance of selectivity changes has been given in Section 1.5.1. Initial conversion rates were calculated by extrapolating the experimental data back to time zero using the empirical equation $r = r_o/(1+bt^n)$ to model the catalyst life-time. This equation was found to fit the experimental data very well as shown by the example in Figure 3.39.

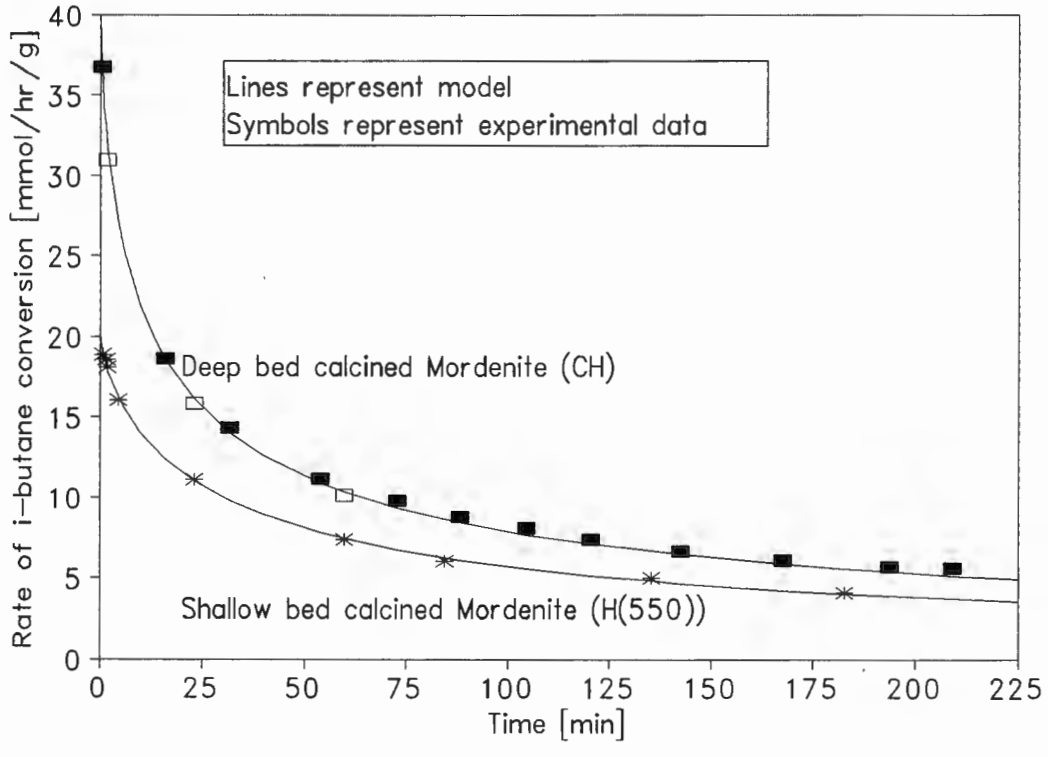

Figure 3.39 Rate of isobutane conversion as a function of time on stream over deep and shallow bed calcined H-Mordenite.

The data points shown as empty squares indicate samples taken during a reproducibility study on deep bed calcined H-Mordenite (CH). Isobutane cracking was carried out on a fresh batch of CH made from the original Na-Mordenite. As both sets of data fit the empirical model well the calcination method and the reaction itself were regarded as reproducible. A similar test was carried out on sample HS0.1.

The time taken before the catalyst deactivated to give half the initial conversion was used to quantify catalyst life-time. This is termed the half-life of the reaction ($t_{½}$) in the reaction results listed in Tables 3.21 to 3.23. The half-life is related to the variable of the empirical equation modelling deactivation by the formula $t_{1/2} = (1/b)^{1/n}$.

Table 3.21 Initial isobutane cracking conversion (r_o), selectivity to products predicted by the model for reaction over weaker acid sites (Sw) and time to reach half the initial conversion ($t_{1/2}$) for dealuminated Na-Mordenite samples

	Isobutane cracking		
Sample	r_o mol.g^{-1}.hr^{-1}	S_w %	$t_{1/2}$ min
Na	< 0.1	-	-
Na0.001	< 0.1	-	-
Na0.01	0.2	63.0	288
Na0.1	9.7	12.7	292
Na1	15.1	11.0	282
Na2	18.2	9.3	178
Na5	16.4	9.5	257
Na10	3.9	11.0	734
NaS	< 0.1	-	-
NaS0.01	< 0.1	-	-
NaS0.1	0.1	(73.0)	-
NaS1	6.8	15.0	506
NaS2	10.9	12.0	341
NaS5	2.4	9.1	80

As shown in Table 3.21, the sodium form of the catalyst had essentially no activity for isobutane cracking. When the catalyst was washed with increasing strengths of nitric acid, the catalyst became more active (cf. Na0.01: r_o = 0.2 mol.g^{-1}.h^{-1}, Na/Al$_f$ = 0.92 and Na0.1: r_o = 9.7 mol.g^{-1}.h^{-1}, Na/Al$_f$ = 0.34). In the case of the Na-Mordenite samples, with increasing strength of acid wash the selectivity changed from those products predicted by the model to form on weak acid sites (S_w) to those predicted to form over strong sites (S_s) (Table 3.20). A decrease in initial cracking rate was seen after 5N and 10N acid washes.

When Na-Mordenite samples were steamed prior to acid washing, the catalysts were less active than in the absence of steaming. This is possibly due to the removal of framework aluminium during steaming. The selectivity towards the products predicted by the model for a weaker acid site was slightly higher in the case of steamed samples thus inferring that the steaming eliminated the stronger acid sites.

Table 3.22 Initial isobutane cracking conversion (r_o), selectivity to products predicted by the model for reaction over weaker acid sites (Sw) and time to reach half the initial conversion ($t_{1/2}$) for H-Mordenite samples which have been acid washed

	Isobutane cracking		
Sample	r_o mol.g^{-1}.hr^{-1}	S_w %	$t_{1/2}$ min
H(550)	20.2	8.4	30
H0	22.0	7.4	19
H0.01	21.2	7.5	29
H0.1	33.3	7.3	34
H1	35.3	7.4	32
H2	31.4	7.5	39
H5	17.8	7.9	95
H10	14.9	6.6	50
CH	41.0	5.8	12
CH0	25.7	7.1	28
CH0.001	24.4	7.3	41
CH0.01	22.2	7.5	26
CH1	34.9	7.3	32
HE	18.9	17.0	495

The hydrogen form of the catalyst showed increased activity compared to acid washed sodium form, but deactivated more rapidly (seen by comparison of r_o and $t_{1/2}$ in Tables 3.21 and 3.22). Although the initial activities of the acid washed hydrogen form of the catalyst are higher than the acid washed sodium form catalysts, all of these samples (apart from HE, HS, HS5 and HS10) also showed greatly reduced half-lives (30-40 minutes compared to > 200 minutes). The selectivity of these catalysts to products predicted by the model to form over strong acid sites (see Section 1.5.1) is consistently greater than 90%.

Deep bed calcination of H-Mordenite (sample CH) produced a catalyst which was highly active, viz. r_o = 41.0 mol.g^{-1}.h^{-1} (Table 3.22), however, the half-life of 12 minutes for this sample was notably short. Comparison of the TG-DTA curves of two samples (H0.001 and H1S1) showing different deactivation behaviour ($t_{½}$ = 29 and 166 min respectively) showed marked difference in the amount of coke formed during reaction (3.5 and 1 wt% respectively after 3 hours of reaction).

Washing the deep bed calcined sample with deionised water resulted in a less active catalyst (r_o = 25.7 mol.g^{-1}.h^{-1}) with a longer half-life (30 minutes) and a small increase in selectivity to the products predicted for reaction over weak acid sites. After a 0.01N wash the deep bed calcined catalyst shows almost identical isobutane cracking characteristics to the shallow bed calcined sample washed with the same concentration of nitric acid ($r_o \approx$ 22 mol.g^{-1}.h^{-1}, Sw = 7.5 %, $t_{1/2} \approx$ 27 min). A peak in activity can be seen after a 1N acid wash (r_o = 35.3 mol.g^{-1}.h^{-1}), followed by a decrease after stronger acid washes. All acid washed samples showed essentially the same selectivities.

EDTA washing of the catalyst decreased the initial activity marginally, but gave the highest catalyst lifetime. Since EDTA is too large to enter the pores of the catalyst, its dealumination effect is restricted to the external layers of the catalyst [Kerr, 1968]. This removal of external acid sites would reduce initial activity, but may increase the lifetime of the catalyst by reducing the probability of formation of coke precursors at the pore mouth

[Schultz *et al.*, 1991].

Table 3.23 Initial isobutane cracking conversion (r_o), selectivity to products predicted by the model for reaction over weaker acid sites (Sw) and time to reach half the initial conversion ($t_{1/2}$) for steamed H-Mordenite samples which have been acid washed.

	Isobutane cracking		
	r_o	S_w	$t_{1/2}$
Sample	mol.g^{-1}.hr^{-1}	%	min
HS	19.4	13.8	279
HS0	20.6	8.7	73
HS0.01	20.2	9.3	40
HS0.1	20.3	7.3	58
HS1	27.9	8.2	72
HS2	29.0	7.8	89
HS5	12.7	10.7	204
HS10	1.3	26.5	-
HSS	0.04	-	-
HSS2	0.04	-	-

Mild steaming of the hydrogen form of the catalyst resulted in a small decrease in activity (r_o = 19.4 mol.g^{-1}.h^{-1}) shown in Table 3.23. The most significant observation, however, is the increase in catalyst lifetime and decrease in the selectivity to the products predicted for reaction over strong acid sites of the sample HS.

Severe steaming of the catalyst (sample HSS) resulted in an almost complete loss in activity due to the removal of framework aluminium. Acid washing of the mildly steamed H-Mordenite resulted in an optimum in activity after a 2N acid wash. Thereafter the activity decreased rapidly viz. HS5, HS10. Severely steamed H-Mordenite, however, showed no increase in cracking activity after acid washing.

In summary three different effects on cracking activity were seen by different methods of dealumination. In the case of deep bed calcined Mordenite there was an enhancement of activity. Steaming, however, had a negative effect on activity but resulted in an increase in catalyst lifetime. The mild acid washing increased cracking activity in all cases, but washing with increased nitric acid concentration resulted in lower cracking activities.

3.3.2 Cyclohexanol dehydration

Cyclohexanol dehydration was carried out over a number samples chosen to represent a range of dealumination techniques. The reason for using this reaction as a probe of external activity has been explained in Section 1.5.2. The steady state conversion of cyclohexanol over these samples, as calculated by the method shown in Appendix VIII, is shown in Table 3.24. Silica-alumina was used to test the reaction over an amorphous catalyst. As 99% conversion was found for this test, the low conversions over the Mordenite samples indicate that the reaction is occurring on the external sites as discussed in Section 1.5.2. The reproducibility of this reaction was tested on sample H2 and it was found to reproducible to within 0.2% conversion. Mass balances were within 5% at steady state for all runs reported.

Table 3.24 Cyclohexanol conversion at steady state

Sample	Conversion [%]	Sample	Conversion [%]
SiO_2/Al_2O_3	99.0	CH	12.9
Na	0.0	CH0	1.1
Na0.001	0.8	CH0.1	5.4
Na0.01	1.0	CH1	5.2
Na0.1	5.9	HE	7.3
Na1	9.4	HS	2.8
Na2	3.4	HS0.1	1.5
Na10	1.8	HS1	2.5
H(550)	4.1	HS2	14.9
H0.1	5.5	HS5	16.5
H1	5.2	HS10	2.2
H2	4.9 (5.1)	HSS	3.3
H5	3.6	HSS5	3.6
H10	3.6		

As in the case of isobutane cracking, the sodium form (Na-Mordenite) showed no activity. Mild acid washing increased conversion as sodium was proton exchanged. A conversion of 0.8% (shown in Table 3.24) indicating the first significant surface activity was seen after a 0.001N nitric acid wash. Cyclohexanol dehydration activity increases to a maximum of

9.4% conversion after a 1N acid wash before decreasing after washes with higher concentration acids.

The shallow bed calcined H-Mordenite showed a steady state conversion of 4% which is comparable to that seen by Karge *et al.* [1983] for acid dealuminated Na-Mordenite (Si/Al = 19.9 conversion = 3%). Deep bed calcination on the other hand showed much increased activity with a steady state conversion of 13%. This is consistent with the high activity seen for this sample during isobutane cracking and would suggest that the highly active sites created during calcination are formed at the surface of the catalyst.

Although washing of both shallow and deep bed calcined H-Mordenite with 0.1N acid results in a catalysts with almost the same activity for this reaction, washing the deep bed calcined sample with deionized water reduces cyclohexanol dehydration activity significantly. This reduction could be as a result of strongly adsorbed water (reported to be a poison in this reaction [Karge et al., 1983]) which was not removed during the catalyst pretreatment (400°C).

Further acid washing of H-Mordenite showed a gradual decrease in cyclohexanol conversion, with still 3.6% conversion remaining after a 10N acid wash. This would suggest that preference for surface dealumination by acid washing is not significant in the case of H-Mordenite. The low conversion rates of the H-Mordenite acid washed series compared to Na-Mordenite washed with 0.1 and 1N acid suggests that, apart from the case of deep bed calcined H-Mordenite, there was an acid site deficiency at the surface of ion exchanged samples.

Steaming the hydrogen form of the catalyst decreased the activity slightly, probably as a result of framework dealumination. The low surface activity was observed in spite of an expected increase in surface aluminium after steaming. A further decrease in cyclohexanol conversion is seen after washing the steamed catalyst with mild acid.

An increase in cyclohexanol conversion was seen after 2N and 5N acid washes despite the extensive dealumination of these samples. A similar result was also seen in the case of EDTA washing of the catalyst. Washing with EDTA is thought to be especially able to remove external aluminium [Kerr, 1968] and would thus reduce the number of surface acid sites. It is possible that the increased activity is due to the widening of pore mouth [Sawa et al., 1988] and the creation of mesopores near the surface during dealumination. These larger pore mouths would allow access to more surface area of the catalyst thus resulting in higher activity.

3.3.3 Isopropylation of naphthalene

3.3.3.1 The effect of dealumination of Mordenite on the reaction

The results from a series of autoclave reactions using a selection of modified Mordenite catalysts chosen to represent each dealumination technique is presented in Table 3.25. The low conversions allowed the selectivities and activities of the different samples to be compared without significant influences of a change in reactant composition. The selectivity to 2,6-DIPN over the non shape selective catalyst aluminium chloride is 33% which is close to the reported equilibrium value of 39%, although the 2,6/2,7 ratio of 0.67 is lower than that seen over silica alumina [Horsely *et al.*, 1994; Fellman *et al.*, 1991]. The high conversion seen over this catalyst is probably due to the large number of exposed acid sites present as all catalysts were added on a mass basis.

Table 3.25 Diisopropylnaphthalene production and selectivity data for autoclave reactions

Sample	$AlCl_3$	Na	Nal	H(550)	H2	HE
Time [min]	480	480	480	480	480	480
Conversion	14.8	0.1	0.7	2.6	1.5	1.0
DIPN selectivity	82.7	33.2	7.2	65.0	32.5	30.2
2,6-DIPN Selectivity	32.9	16.0	3.2	40.0	4.0	12.9
2,6/2,7 ratio	0.67	1.99	6.19	1.88	2.44	6.28
2,6-DIPN Yield	4.9	0.0	0.0	1.0	0.1	0.1

Sample	CH	HS	HS0.1	HS1	HS5	HSS
Time [min]	480	480	480	480	480	480
Conversion	4.3	3.9	5.1	3.2	3.9	1.5
DIPN selectivity	82.3	81.7	85.8	77.6	69.6	25.17
2,6-DIPN Selectivity	64.0	60.0	73.8	64.0	59.1	7.79
2,6/2,7 ratio	4.28	4.00	7.26	7.75	7.56	0.78
2,6-DIPN Yield	2.8	2.3	3.8	2.0	2.3	0.1

An interesting observation was made that selectivity to DIPN increased with increasing conversion in most cases. This is not surprising as isopropylation is a series reaction and

increased reaction would drive the reaction from isopropylnaphthalene to diisopropylnaphthalene. For this reason only the ratios of DIPN isomers were used to compare the shape selective effects of catalyst samples.

The low conversion seen over sample Na was expected due to the lack of acidity in this catalyst. Although washing this catalyst with 1N nitric acid resulted in a slight increase in conversion and the ratio between 2,6-DIPN and 2,7-DIPN, the selectivity to DIPN decreased as a large amount of isopropyl naphthalene was produced.

The hydrogen form of the catalyst (shallow bed calcined) showed increased conversion and selectivity to DIPN, but the 2,6/2,7 ratio remained low. Although acid washing of this sample again led to decreased selectivity to DIPN and increased 2,6/27 ratio, there was a significant drop in conversion. This same trend was noted after a wash with EDTA, although the 2,6/2,7 ratio was more than double that of the sample washed in nitric acid. The product spectrum also changed slightly and a five percent selectivity to heavy products (carbon number greater than 16) was seen.

Deep bed calcination produced a much more active catalyst with a high selectivity to 2,6-DIPN and therefore a high yield. Mild steaming produced very similar catalytic results, although conversion and 2,6-DIPN selectivity were both slightly reduced. Severe steaming produced an inactive catalyst with low selectivity to DIPN.

Acid washing the mildly steamed catalyst with 0.1N nitric acid increased both conversion and 2,6-DIPN selectivity. Although these were reduced upon washing with increased strength of acid, the 2,6/2,7 ratio remained unusually high (>7).

3.3.3.2 Study of the isopropylation reaction

The sample HS0.1, having shown the best results from the batch tests with respect to 2,6-DIPN yield, was used in a flow system. To calculate a power law rate equation, the reaction was performed with feeds of different partial pressures as shown in Table 3.26. The conversion (X) was calculated with respect to naphthalene and selectivity (S) refers to selectivity towards 2,6-diisopropyl naphthalene.

Table 3.26 Conversion (X) and selectivity (S) data used to investigate the kinetics of DIPN synthesis over HS0.1

Temp [°C]	P_{nap} [kPa]	P_{prop} [kPa]	X [%]	S [%]	2,6/2,7 Ratio	Yield [%]	k [$mol.kPa^{-1}.s^{-1}.g^{-1}$]
300	1.57	12.85	12.7	59	12.5	7.5	0.77
275	1.57	12.85	11.4	78	12.3	8.9	0.69
250	1.57	12.85	8.7	69	8.6	6.0	0.52
250	1.54	19.50	10.6	55	6.1	5.8	0.52
250	1.54	21.25	11.5	62	7.5	7.1	0.54
250	1.53	23.28	12.0	61	8.4	7.3	0.54
250	2.49	12.90	7.4	74	7.9	5.5	0.53
250	3.22	29.23	9.9	70	7.1	6.9	0.54
235	1.57	12.85	6.0	82	7.4	4.9	0.36
225	1.57	12.85	4.6	71	6.2	3.3	0.27

CHAPTER FOUR

DISCUSSION

The discussion of the results of this research is divided into three sections. In this first section, the effects of dealumination on the Mordenite structure and on the number and type of acid sites are discussed. This is followed in Section 4.2 by a discussion of the catalytic properties of the dealuminated samples, including the activity of both strong acid sites and those sites located on the surface of the catalyst. The shape selective properties of the modified samples are also discussed. Finally in Section 4.3 these catalytic properties are then discussed with reference to the structural and acidic properties of the dealuminated samples.

4.1 EFFECT OF DEALUMINATION TREATMENTS ON THE STRUCTURE AND ACIDITY OF MORDENITE

4.1.1 Sodium Mordenite

In this section the effects of acid washing and steam treatment on a sample of sodium Mordenite on its structural and acidic properties are discussed. The sample used was acquired from the Fritz-Haber Institute in Berlin and was characterised in that Institute. Characterisation results from both the Fritz-Haber institute and our own laboratories are shown in Appendix XI and compare very favourably. The results referred to in this part of the discussion can be found in Tables 3.1, 3.4, 3.9, 3.14 and 3.20 of Sections 3.1 and 3.2.

The parent sodium form (Na) showed weak Lewis acidity, which was identified by both a peak of low desorption temperature in the response curve of ammonia TPD [Karge and Dondur, 1990] and by a band at 1445 cm^{-1} in the infrared spectrum of adsorbed pyridine [Lefrancios and Malbios, 1971]. The desorption of ammonia and pyridine from these sites at low temperatures suggests that they are weak. These weak Lewis sites are likely to be ascribed to sodium ions [Meyers *et al.*, 1988].

Brönsted acidity was determined from the infra-red spectra of adsorbed pyridine and from ammonia TPD. A band at 1545 cm^{-1} identified these Brönsted sites, while deconvolution procedures were used to identify four peaks in the ammonia TPD response curve. These have previously been assigned to weak Lewis, weak Brönsted, strong Brönsted and strong Lewis sites with increasing temperatures of desorption [Karge and Dondur, 1990].

Both sites of intermediate acid strength (viz. those identified as Brönsted sites by Karge and Dondur [1990]) and strong acid sites (viz. both Brönsted and strong Lewis acid sites identified by Karge and Dondur [1990]) as determined by ammonia TPD are shown in Figure 4.1 as a function of Brönsted acidity as determined by an infra-red spectroscopic investigation of pyridine adsorption.

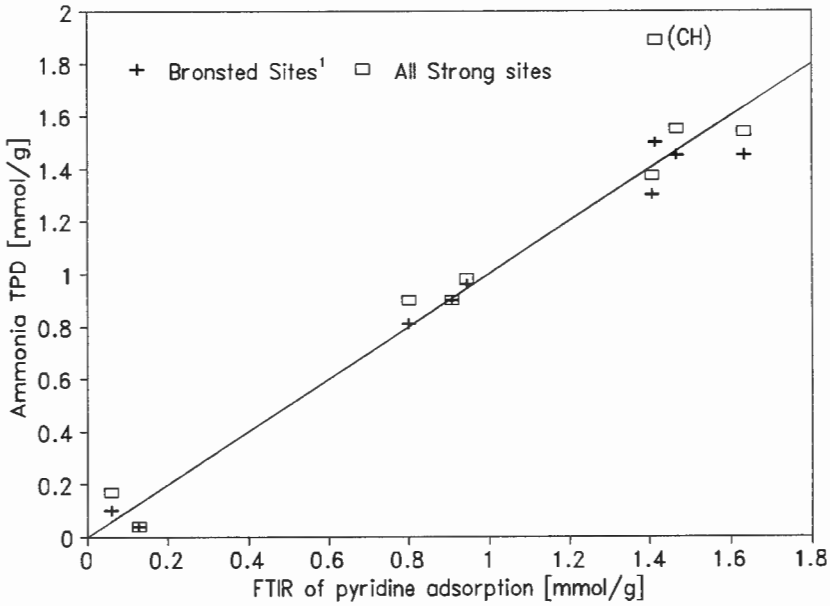

Figure 4.1 Brönsted and strong acidity determined by deconvolution of ammonia TPD response curve as a function of Brönsted acidity determined by infra-red spectroscopy of adsorbed pyridine

[1] **Determined by deconvolution of ammonia TPD response curve**

A very good correlation is seen between the two sets of values determined for number of

Brönsted acid sites. It is only the sample that has been deep bed calcined (CH) which showed a large number of strong acid sites that were not Brönsted sites (i.e. Lewis sites). In all other samples, the amount of strong Lewis acidity is small and essentially all strong acid sites seen by ammonia TPD were assigned to Brönsted acidity.

Essentially no strong Brönsted acidity was observed in the parent Na-Mordenite sample. The low percentage crystallinity of 77% (relative to a sample washed with EDTA which had the highest crystallinity and was therefore assigned a value of 100%) indicates the existence of crystal defects or the presence of amorphous material. Any amorphous material present in the sample would not appear to include aluminium as no EFAl was observed by ^{27}Al MAS NMR. It is more likely therefore that any amorphous phase present would contain contributions from sodium and possibly silicon species.

The first indication of sodium removal from the sample occurred after a 0.01N acid wash. This wash also resulted in a decrease in the amount of weak Lewis acidity in the sample and the production of the first significant amounts of Brönsted acidity. This would indicate the onset of proton exchange for sodium during the 0.01N acid wash. An increase in both unit cell size and percentage crystallinity was seen despite the creation of small amounts of EFAl-o. Olsson and Rollmann [1977] and Raatz *et al.* [1985] have made similar observations which they ascribed to a release of strain on the framework by the removal of minor structural defects during the acid wash.

A 0.1N acid wash removed 90% of the sodium with minimal loss of bulk aluminium, but production of significant amounts of EFAl-o (0.2 mmol/g). The observed increase in Brönsted acidity and decrease in weak Lewis acidity is consistent with proton exchange for sodium during acid washing since the weak Lewis sites are probably sodium cations. The number of Brönsted sites is slightly less than the number of framework aluminium atoms not

charge balanced by sodium (0.90 mmol/g compared to 1.15 mmol/g) suggesting that not all the acid sites could be accessed by the probe molecules as some may be located in the side pockets.

No weak Lewis acid sites were identified on sample Na0.1 by infra-red spectroscopy of adsorbed pyridine. These sites were therefore probably not accesible to the pyridine molecule and the residual sodium ions may be located in the side pockets of the crystal.

Increasing the strength of the acid used for washing the Mordenite up to 2N continued to remove sodium and also increased the number of strong Brönsted acid sites. This increase in acid wash concentration also resulted in a maximum in percentage crystallinity seen in all the acid washed Na-Mordenite samples. Higher concentrations of acid increased the extent of removal of both sodium and aluminium from 6.6 Na/uc and 6.5 Al_f/uc in the parent Na-Mordenite sample to 0.2 Na/uc and 2.4 Al_f/uc after a 10N acid wash. As sodium was removed from the catalyst, the amount of weak Lewis acidity was reduced but not eliminated. EFAl-o species were created and remained in the catalyst as sodium was removed and therefore it is likely that these residual EFAl-o species are responsible for weak Lewis acidity referred to above.

Increasing the strength of acid wash led to a decrease in the amount of Brönsted acidity and increased the extent of framework dealumination. This coincided with a sharp drop in crystallinity. The large number of silanol groups, as seen in ^{1}H MAS NMR spectra (Section 3.2.3), of sample Na10 compared to Na0.01 and the formation of a shoulder at 950 cm^{-1} in the infra-red spectra (Fig 3.22) is consistent with the formation of a hydroxyl nest [Musa *et al.*, 1987]. This appears to be stable after drying at 80°C, but is removed by hydrothermal treatment at 550°C. This is consistent with observations made by Beyer *et al.*, [1984] and Fejes *et al.* [1985].

Although steaming of the Na-Mordenite sample did not affect its bulk chemical composition, nearly a third of its framework aluminium was removed to create both EFAl-o and EFAl-t. The observed decrease in percentage crystallinity is consistent with the production of these extra-framework species. No strong acidity was created and in fact the small amount of strong acidity seen in the unsteamed sample (Na) was removed. As will be shown in Section 4.2.1, both these samples were catalytically inactive. As mentioned above, the shrinking of the unit cell has been previously reported by Raatz *et al.* [1985]. The unit cell size was restored after a wash with deionised water, although the percentage crystallinity decreased further.

Steam pretreatment of the Na-Mordenite sample before acid washing did not appear to affect the removal of sodium from the sample during acid washing. This was not surprising. The removal of aluminium from the bulk by acid washing was significantly retarded in the sample pretreated with steam. It was expected that the EFAl created in the catalyst during steaming would be more easily removed than the framework aluminium in the unsteamed sample. It is likely that the presence of sodium was the cause of this result as the same feature was not seen in the case of H-Mordenite. The possibility exists of the formation of a sodium aluminate extra-framework species which may be stable in the catalyst or there may be steric restrictions to dealumination by the presence of both sodium and EFAl in the pores of the catalyst.

4.1.2 Calcined H-Mordenite

In the following section, the methods of shallow and deep bed calcination and the acid washing of H-Mordenite are discussed. The deep bed calcined sample was of particular interest due to the high number of strong acid sites and high catalytic activity seen in the sample. The data referred to in the discussion can be found in Tables 3.2, 3.5, 3.10, 3.11, 3.15, 3.16 and 3.20 of Sections 3.1 and 3.2.

A 98% removal of sodium was achieved by ion exchange with ammonium nitrate. No change to framework composition was observed after ion exchange, although an increase in crystallinity was seen. This may be due to the removal of amorphous material present in the Na-Mordenite sample. Although it did not seem likely that the crystallinity of the sample could be related to sodium content, crystallinity generally increased with the removal of sodium from the samples. The presence of water may have aided the removal of amorphous material by dissolution in the liquid phase.

Calcination of the ammonium form of the catalyst did not result in the removal of any aluminium from the bulk. Both deep and shallow bed calcined samples did show roughly 17% framework dealumination to produce EFAl-o which is similar to the amount seen by Miller *et al.* [1992] in a similarly treated sample. The crystallinity of the catalyst increased after calcination despite the creation of EFAl, with deep bed calcined CH being more crystalline than shallow bed calcined H(550). This suggests that annealing of the catalyst structure may be taking place during calcination and this annealing is aided by the high temperature and presence of water vapour created by dehydroxylation within the deep bed [Bosacek and Freude, 1988; Medin *et al.*, 1990]. The unit cell size decreased after calcination particularly in the *a* and *b* directions as has been observed by Raatz *et al.* [1985].

Amounts of weak and strong acid sites and framework and extra-framework aluminium are

shown as a function of strength of acid wash in Figure 4.2. All mildly acid washed H-Mordenite samples showed a number of strong acid sites roughly equal to the number of framework aluminium atoms and weak acidity slightly less than the amount of EFAl.

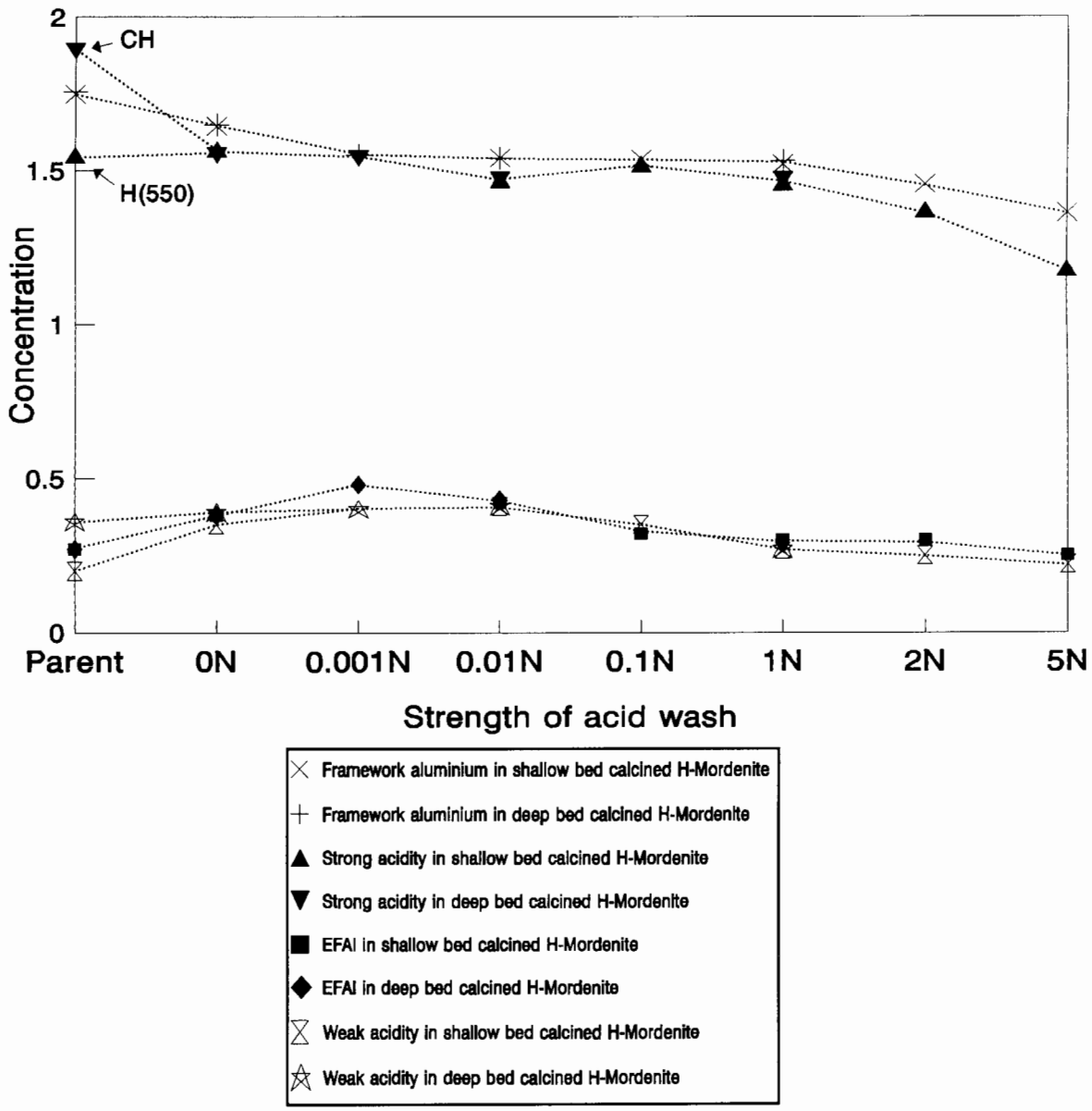

Figure 4.2 Acidity of calcined and acid washed H-Mordenite as determined by deconvolution of ammonia TPD response curve and framework and extra-framework aluminium content as a function of strength of acid wash

This would indicate that the strong acid sites are associated with framework Brönsted sites

(as was shown in Figure 4.1), while the weak acidity can be ascribed to EFAl species which act as weak Lewis sites. Although a small amount of Lewis acidity is shown by the presence of a peak at 1455 cm^{-1} in the infra-red spectra of adsorbed pyridine on acid washed H-Mordenite, no desorption takes place from these sites at all and they are therefore probably very strong although few in number. The weak acidity is not detected by pyridine and therefore the EFAL-o species responsible for these sites are probably located in the side pockets [van Niekerk *et al.*, 1992].

Sample H(550) showed slightly less Brönsted acidity than number of framework aluminium atoms in that sample. This was expected as ammonia has limited access to sites associated with framework aluminum in the side pockets. It would be expected that a larger probe such as pyridine would have even more limited access to these framework sites. Pyridine adsorption on sample H(550) is seen in Figure 3.33. The increasing amount of pyridine adsorbed on Brönsted sites with increasing temperature indicates that there are steric restrictions blocking access to Brönsted sites which can only be overcome by an increase in temperature increasing the diffusivity.

A sample of H-Mordenite which was deep bed calcined showed unusual properties, in particular a large increase in catalytic activity as will be shown in Section 4.2. The calcination method was found to be reproducible as was shown by a repeat synthesis of the sample from the starting material (Na-Mordenite) and its testing using the isobutane cracking probe reaction (Figure 3.38).

In contrast to shallow bed calcined H(550), deep bed calcined CH showed a greater amount of strong acidity than the number of framework aluminium atoms predicted. Deep bed calcined Mordenite appeared to possess a significant amount of strong Lewis acidity not seen in its shallow bed calcined counterpart (Figure 4.1). The extra Lewis sites were not all seen

by pyridine adsorption and could therefore be located in positions which are sterically shielded from pyridine such as in the side pockets.

The adsorption of pyridine did not increase with increased temperature as in the case of H(550) and so it appears that some steric hindrances have been removed, despite the reduced unit cell volume. Annealing of crystal defects in this sample may have allowed greater access to acid sites.

To investigate the repair of framework defects and the removal of hydroxyls during this treatment, a ^{1}H MAS NMR study was performed on this sample. However, an unusually low number of hydroxyls was seen in this sample despite the expected dehydroxylation during calcination above 500°C [Medin *et al.*, 1990]. Although a reduced number of hydroxyls was also seen in the infra-red spectra of the hydroxyl region of the sample, the amount of Brönsted acidity determined by pyridine adsorption remained high. The NMR was performed at a reputable institution and the discrepancy seems too large to be accounted for by line broadening effects of the NMR spectra by hydroxyls in close proximity [Fenske *et al.*, 1991] and therefore this result is difficult to explain [Liu, 1995].

Washing the deep bed calcined sample with deionised water increased the crystallinity of the sample to a relative percentage of 99% and increased the unit cell in the *a* and *b* directions (a feature also noted with steamed Na-Mordenite). This is consistent with the relaxation of the framework from strain induced during calcination. After washing with deionised water the number of strong acid sites of the deep bed calcined sample decreased to just below the number of framework aluminium atoms. The amount of weak acidity increased slightly as did the amount of EFAl-o.

The increase in the amount of pyridine adsorbed on Brönsted sites in sample H(550) with

increasing temperature was ascribed to the overcoming of steric constraints. This effect was not seen in deep bed calcined H-Mordenite, but appears to return after washing with deionised water. The increase in steric constraints together with a high hydroxyl content observed in proton MAS NMR indicates that it is possible that the EFAl species in the sample have become hydrated [Bosacek and Freude, 1988]. This would also account for the reduction in number of acid sites seen in this sample.

Washing shallow bed calcined H(550) with deionised water increased the crystallinity of the sample. This indicated a cleaning of the pores due to the removal of amorphous material. The slight decrease in unit cell size is indicative of the observed removal of aluminium from the framework.

Washing of both deep and shallow bed calcined samples with acid up to 0.01N led to the removal of framework aluminium and the formation of EFAl-o, with little removal of aluminium from the bulk. Despite the creation of EFAl, the crystallinity of the samples remained high (above 90%). The decrease in size of the unit cell in the *b* and *c* directions compares well in magnitude to literature values [Meyers *et al.*, 1988] and is consistent with aluminium removal from the framework.

Samples of both deep and shallow bed calcined H-Mordenite washed with 0.1N and 1N nitric acid showed essentially the same characteristics respectively. Framework aluminium content remained relatively constant for acid washes between 0.001 and 1N, with only EFAl being removed from the bulk as shown in Figure 4.2. Weak acidity and the amount of EFAl decreased simultaneously, while the number of strong sites was almost identical to the number of framework aluminium atoms.

Greater concentrations of acid used in the washing led to framework dealumination and a

corresponding decrease in crystallinity. Although the number of strong sites decreased with decreasing framework aluminium, the acid strength, indicated by T_{max} (at constant heating rates), increased until a framework Si/Al ratio of nine was reached, whereafter a constant strength was maintained. This is consistent with literature reports [Stach and Jansen; 1992].

The amount of pyridine adsorbed onto Brönsted sites in H-Mordenite washed with 2N acid did not increase with increasing temperature, as in the case of sample H(550). It would appear that the steric restrictions, to which this observation was ascribed, have been removed by acid washing. This could be a result of dealumination in the side pockets leading to their enlargement, but this is not conclusively shown by this result.

Washing H-Mordenite with EDTA after calcination removed a further 14% of aluminium from the framework and reduced the EFAl content dramatically. A correspondingly low amount of weak acidity was seen. The observed high relative percentage crystallinity is probably due to the removal of amorphous material and a sharp reduction in EFAl.

4.1.3 Steamed H-Mordenite

The effects of dealumination by steaming and by acid washing of steamed H-Mordenite samples on the structure and acidity of Mordenite are discussed in this section. The deep bed calcined sample was of particular interest due to the large number of strong acid sites and high activity seen in the sample. The data which is referred to in the discussion can be found in Tables 3.3, 3.6, 3.12, 3.17 and 3.20 of Sections 3.1 and 3.2.

Mild steaming of H-Mordenite did not remove aluminium from the bulk but led to the production of substantial quantities of extra-framework aluminium species. EFAl-o and EFAl-t were present in large quantities possibly together with some pentacoordinated

aluminium. All three increased in quantity with severity of steaming.

Percentage crystallinity and unit cell constants remained unaltered, however, despite the production of a large amount of EFAl. In fact no relationship was seen between crystallinity and the amount of EFAl present in the samples. The maintenance of the crystal structure indicates that a degree of framework stabilisation or annealing has taken place despite the large extent of framework dealumination.

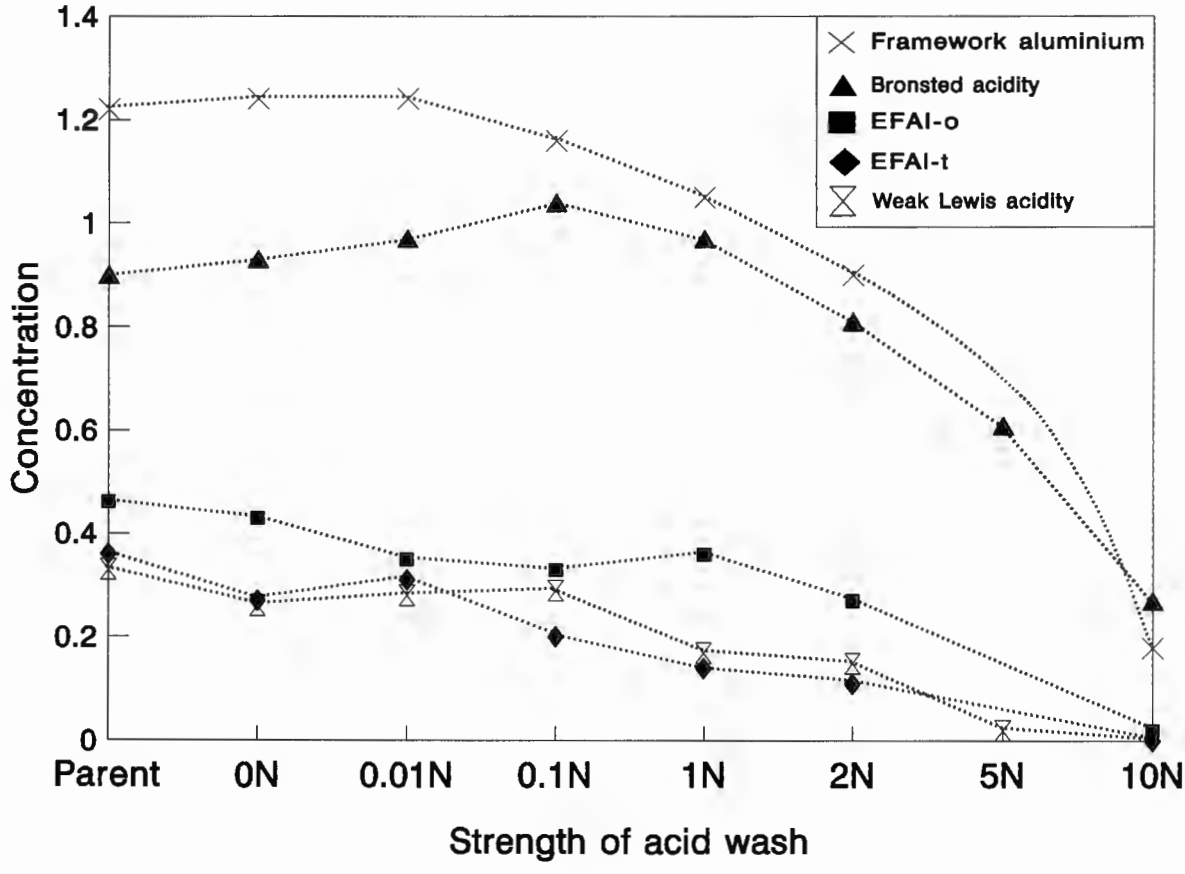

Figure 4.3 Acidity of steamed and then acid washed H-Mordenite as determined by deconvolution of ammonia TPD response curve and framework and extra-framework aluminium content as a function of strength of acid wash

As shown in Figure 4.3, the number of Brönsted sites decreased to below the number of

framework aluminium atoms after steaming and was approximately equal to the number of framework aluminium atoms less the amount of EFAl-t (≈ 0.9 mmol/g). A large increase in weak Lewis acidity as evidenced by both infra-red spectroscopy of adsorbed pyridine and ammonia TPD was seen.

The infrared band ascribed to pyridine adsorbed on Lewis acid sites was broad and appeared to include contributions from pyridine adsorbed on cationic sites. It is possible that the pyridine-EFAl interaction represented by this peak, is similar in nature to that of pyridine interactions with cations such as sodium. This indicates the probability that EFAl-t species are cationic and can associate with framework anionic sites to reduce Brönsted acidity in a similar manner to sodium ions.

The same amounts of Brönsted and Lewis acidity determined by the deconvolution of the response curve of ammonia TPD were shown to be present by infra-red spectroscopy of pyridine adsorption indicating that all sites which were equally accessible to ammonia are also accessible to pyridine. The amount of Lewis acidity seen in the infrared spectra of adsorbed pyridine is equivalent to the total amount of EFAl (including both EFAl-o and EFAl-t), but considerably less is evidenced by the desorption of ammonia. It has been shown by Sharma *et al.* [1993] that pyridine has a higher energy required for desorption than ammonia ($\Delta H_{ads}(NH_3)$ = 157 kJ.mol^{-1} and ΔH_{ads}(Pyridine) = 200 kJ.mol^{-1}) and therfore desorbs at higher temperatures. It is possible therefore that some of the Lewis sites present in steamed H-Mordenite are weak and are not detected by ammonia TPD.

Washing the mildly steamed catalyst did not change the bulk aluminium content, but there was an increase in EFAl-o as well as a decrease in the amount of EFAl-t. The positively charged extra-framework species created by steaming appears to remain localised in the catalyst structure associated with negatively charged framework aluminium.

The high temperatures used during steaming do not appear to permit the full hydration of these species. The broad peak at 0 ppm in ^{27}Al MAS NMR also indicates that the EFAl-o species are not all uniform and may possibly be in different hydration states. A subsequent wash with excess water at relatively low temperatures (70°C) probably hydrated these species to form octahedral extra-framework species of the type shown below which could then be removed [Wang *et al.*, 1991].

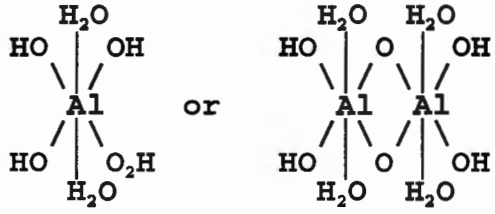

If it is assumed that the tetrahedral extra-framework aluminium is strongly bonded to a framework aluminium anionic site, then it can be predicted from the above observation that acid washing weakens this bond, resulting in the removal or proton exchange of the EFAl-t species and the creation of a Brönsted acid site. This is also substantiated by the observation that an increase in the amount of EFAl-t is accompanied by a decrease in the amount of Brönsted acidity.

Figure 4.4 shows the relationship between total number of Brönsted acid sites as determined from ammonia TPD and the number of framework aluminium sites which are not charge balanced by cationic EFAl-t as determined from elemental analysis and ^{27}Al MAS NMR. If it is assumed that the EFAL-t species has a single positive charge, then there is a remarkably good correlation ($R^2 = 0.98$) This species could therefore possibly have the form $Al(OH)_2^+$ or AlO^+ [Goovearts, 1989], but these results do not conclusively show this.

Washing with highly concentrated nitric acid (10N) removed most of the EFAl and over

90% of the framework aluminium from the original Na-Mordenite. It is possible that extra-framework species containing both silicon and aluminium [Janin *et al.*, 1991] were produced by acid washing of this sample, as evidenced by ^{29}Si MAS NMR, but the concentration of these is low.

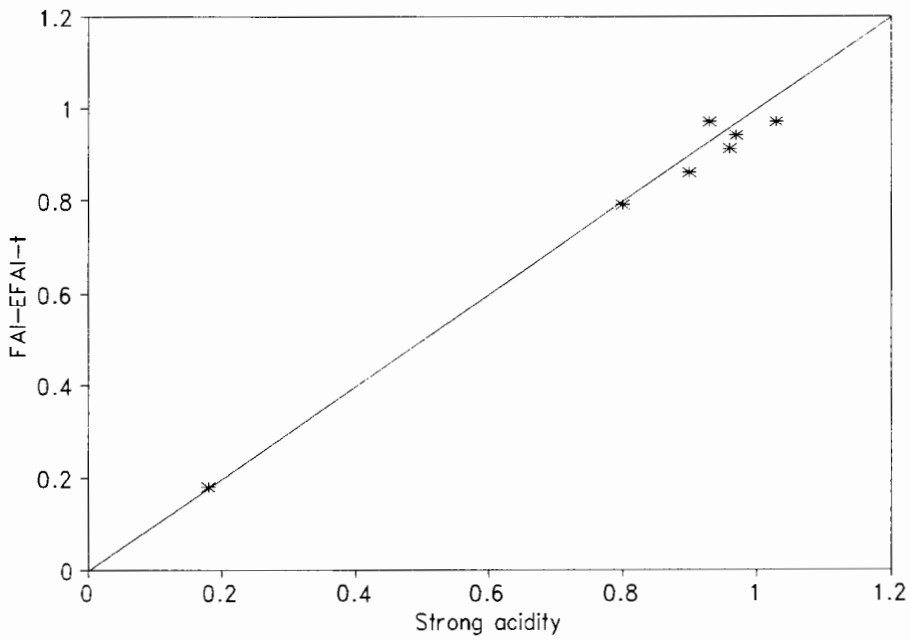

Figure 4.4 Strong acidity as determined by deconvolution of the ammonia TPD response curve as a function of framework aluminium less tetrahedral extra-framework aluminium

Severe steaming of H(550) produced large amounts of EFAl with over 50% framework dealumination and no loss of aluminium from the bulk. A distinct peak indicating a large amount of pentacoordinated aluminium was observed by ^{27}Al MAS NMR in all severely steamed samples. The reduction of acidity in these samples is consistent with the large amount of framework dealumination.

Although crystallinity was reduced, the Mordenite structure remained intact after this treatment producing a Si/Al_f greater than 40. The ^{29}Si MAS NMR shows predominantly silicon not attached to any aluminium (Si(0Al)). Although two peaks are shown (Fig. 3.18),

their chemical shifts indicate that they originate from two crystallographically non-equivalent Si(0Al) sites, the first peak being a composite of T_1 and T_4 and the second a composite of T_2 and T_3 [Hays *et al.*, 1984; Engelhardt and Michel, 1987].

In all subsequent acid washes there was no increase in acidity and the amount of EFAl-t was always greater than the amount of framework aluminium. The aluminium species represented by the 40 ppm shoulder in ^{27}Al MAS NMR are most likely to be associated with framework aluminium and are therefore probably located in the pores.

The presence of the peak at 100 ppm together with the broadening of the peak ascribed to octahedral species suggests the presence of a small amount of aluminium clusters formed by calcination and steaming. These are likely to be amorphous as seen by TEM micrographs of steamed samples [Meyers *et al.*, 1988], but whether they are located on the surface has not been conclusively shown [Scherzer, 1984; Meyers *et al.*, 1988]. No evidence of extra-framework silicon was seen and it is likely that the reduced crystallinity is due to amorphous EFAl. The unit cell size and crystallinity of the severely steamed sample does not vary greatly with acid washing.

4.2 EFFECT OF DEALUMINATION TREATMENTS ON THE CATALYTIC PROPERTIES OF MORDENITE

4.2.1 Strong acidity probed by isobutane cracking

Isobutane cracking was used to probe the strong acidity of the dealuminated Mordenite samples. A review of the use of isobutane cracking as a probe reaction for strong acid sites was given in Section 1.5.1 and the results of the cracking experiments over dealuminated samples were given in Section 3.3.1.

The isobutane cracking reaction was carried out at a fixed temperature of 450°C and a space velocity of 1.8 hr^{-1}. Both were held constant throughout the experiments as changes to either were expected to result in changes in selectivity and reaction mechanism. The initial rate of isobutane conversion was used as a measure of each sample's activity.

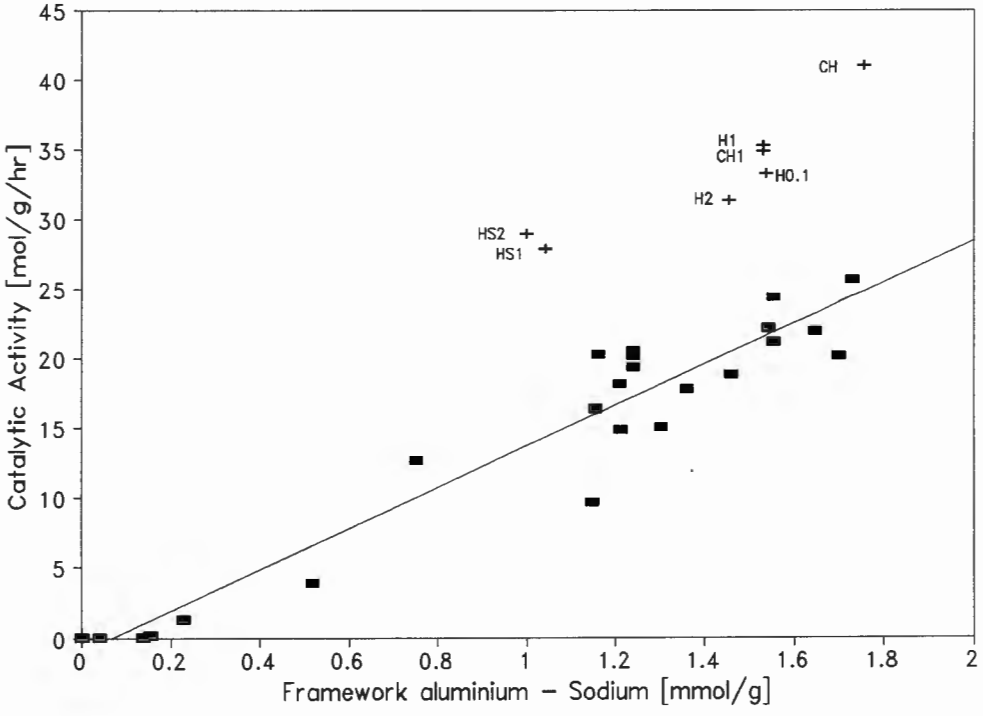

Figure 4.5 Initial rate of conversion of isobutane over Mordenite sample as a function of number of strong acid sites (Framework aluminium - sodium cations)

Isobutane cracking activity was found to increase with increasing number of Brönsted and strong Lewis acid sites as is expected for a cracking reaction [Kim and Ihm, 1992; Miller *et al.*, 1992]. This is shown in Figure 4.5 where the activity generally can be seen to increase linearly with number of framework aluminium sites not charge balanced by sodium.

The slope of the line drawn represents the number of isobutane atoms converted per framework site per second and is called the turn over number (TON). Most samples showed a good fit to this line ($R^2 = 0.94$) which represents a TON of 4 s^{-1}. Some samples increased activity above this line and these are labelled in Figure 4.5. The ensuing discussion will focus mainly on those samples showing increased activity.

Table 4.1 Isobutane activity and selectivity, aluminium content and acidity of dealuminated Mordenite samples

	Isobutane cracking		Aluminium content[3]			Number of strong
	r_o[1]	S_s[2]	Al_f	EFAl-o	EFAl-t	acid sites[4]
Sample	$mol.g^{-1}.hr^{-1}$	%	$mmol.g^{-1}$	$mmol.g^{-1}$	$mmol.g^{-1}$	$mmol.g^{-1}$
H(550)	20	92	1.75	0.27	0.00	1.54
H0.01	21	92	1.54	0.42	0.00	1.47
H0.1	33	92	1.54	0.32	0.00	1.52
H1	35	93	1.52	0.30	0.00	1.46
CH	41	94	1.76	0.27	0.00	1.89
CH0.01	22	92	1.54	0.43	0.00	1.47
CH1	35	93	1.53	0.29	0.00	1.47
HS	19	86	1.22	0.43	0.36	0.90
HS2	29	92	1.02	0.27	0.11	0.81

(1) Initial rate of conversion of isobutane
(2) Selectivity to products formed over strong sites
(3) Concentrations of different aluminium species as determined by ^{27}Al NMR and elemental analysis
(4) Number of strong acid sites as determined by deconvolution of ammonia TPD response curves

Summarised results of the cracking experiments over some dealuminated H-Mordenite samples are given in Table 4.1 together with acidic and structural data for these samples.

In the following discussion, the characteristics of each samples are referred to with reference to sample H(550).

Deep bed calcination of H-Mordenite (sample CH) produced a catalyst which was highly active, viz. $r_o = 41$ mol.g^{-1}.h^{-1}. The observation of enhanced activity for a cracking reaction is similar to n-hexane cracking results seen over mildly steamed ZSM-5 and zeolite-Y [Lago *et al.*, 1986; Zholobenko *et al.*, 1990 and 1991; Löffler *et al.* 1991]. The deep bed calcination procedure used to modify the Mordenite catalyst can be compared to a very mild form of steaming [Kerr, 1969; Szostak, 1991]. It is likely therefore that the same mechanism responsible for enhanced activity in mildly steamed ZSM-5 and Zeolite-Y is applicable to the deep bed calcined Mordenite.

This sample was observed to possess an increased amount of strong Lewis acidity as discussed in Section 4.1. Some authors have explained the activity enhancement of mildly steamed ZSM-5 and Zeolite-Y by an interaction of the Brönsted acid sites of the framework and Lewis sites of EFAl species [Lago *et al.*, 1986; Hopkins, 1968; Lunsford, 1968]. Very strong acid sites as determined by the temperature of the peak maximum in temperature programmed desorption of ammonia have been observed previously on mildly steamed Mordenite [Mirodatos and Barthomeuf, 1981]. However, it was suggested that they were a result of a synergistic effect between Lewis and Brönsted acid sites.

More recently, Zholobenko *et al.* [1990,1991] and Löffler *et al.* [1991] have attributed the increased activity of mildly steamed ZSM-5 samples for n-hexane cracking rather to an increased concentration of Lewis acid sites which act separately to Brönsted sites. They propose that the Lewis acid sites enhance the initial dehydrogenation or demethanation steps, which are the rate limiting steps and produce the primary products of reaction [Dumisic *et al.*, 1993]. This proposal is supported by the high observed selectivity to products formed

over strong acid sites and thus low selectivity to products formed over weak sites (S_w = 6%).

The half-life (viz. the time taken for the sample reach half its initial activity) for the deep bed calcined sample was 12 minutes, which is notably short and suggests that the acid sites responsible for enhanced activity also promote rapid coke formation which would lead to a short catalyst lifetime. Figure 4.6 shows the relationship between the time taken for the catalyst to be reduced to half its original activity and selectivity to products formed over strong acid sites. This clearly shows that there is a relationship between the amount of strong acid sites and the lifetime of the catalyst. No dierect relationship was found between catalyst lifetime and initial activity.

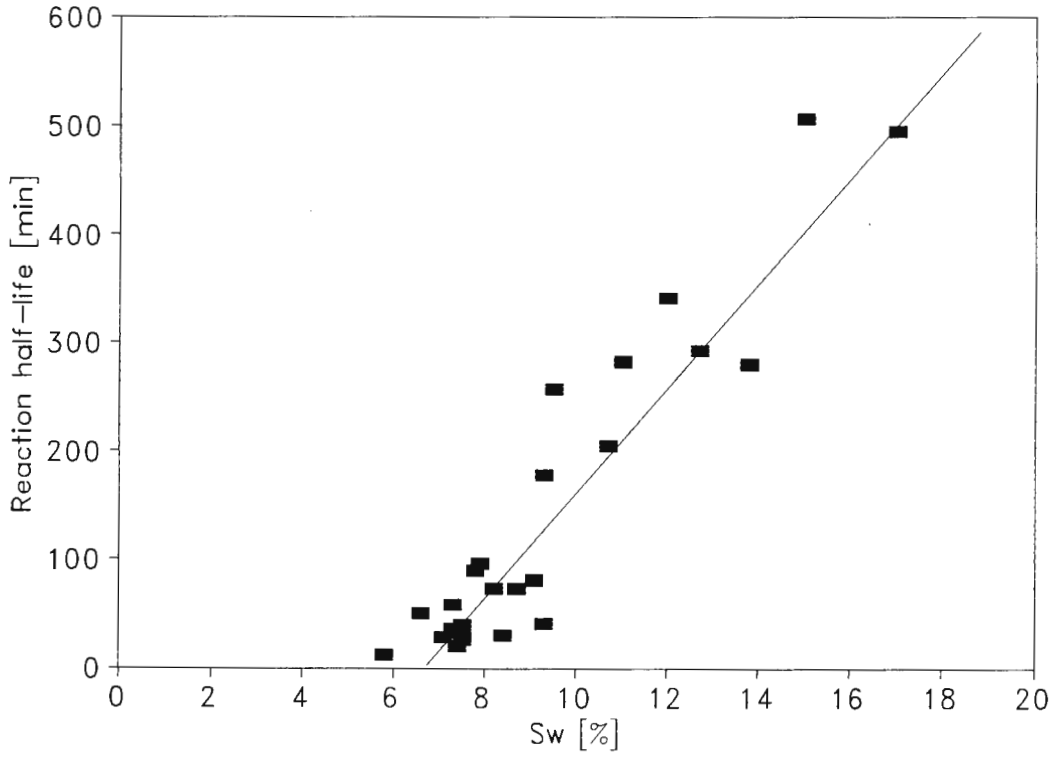

Figure 4.6 Isobutane cracking half-life ($t_{1/2}$) as a function of selectivity to products formed over weaker acid sites (S_w)

Deactivation is most probably caused by the strong sites driving selectivity towards secondary reactions and coke formation, which was predicted by the reaction model. Comparison of the TG-DTA curves of two samples (CH0.001 and H1S1) showing different deactivation behaviour ($t_{½}$ = 29 and 166 min respectively) showed marked difference in the amount of coke formed during reaction (3.5 and 1 wt% respectively after 3 hours of reaction).

Increased coke formation has been observed in the presence of Lewis sites in other cracking reactions [Abbot and Geurzoni, 1992]. The model of synergistic interactions between Lewis and Brönsted sites has been used to account for reduced coke formation in some steamed samples [Mirodatos and Barthomeuf, 1981; Gnep *et al.*, 1980]. This effect is not seen and in fact the rapid deactivation supports the model of the strong Lewis site enhancing the initiation steps of the reaction and leading to increased formation of secondary products and coke.

Washing the deep bed calcined sample with deionised water resulted in a less active catalyst (r_0 = 25.7 mol.g^{-1}.h^{-1}) with a longer lifetime ($t_{1/2}$ = 30 minutes). Although no aluminium was removed from the framework or bulk, it appears that the species responsible for Lewis sites have changed in nature and no longer provide enhanced activity. Possibly the extra-framework sites have been hydrated to become an inactive or even neutral species. After a 0.01N wash the deep bed calcined catalyst shows almost identical structural and acidic characteristics and catalytic behaviour to the shallow bed calcined samples washed with comparable strengths of acid.

Steaming of the hydrogen form of the catalyst at low partial pressures of water (230 torr) resulted in a small decrease in activity (r_0 = 19.4 mol.g^{-1}.h^{-1}). Clearly the mild steaming described by Mirodatos and Barthomeuf [1981], Lago *et al.* [1986], Zholobenko *et al.*

[1990,1991] and others is much more akin to deep bed calcination than the steaming performed on this sample. It is a feature of much of the published literature on mild steaming that the specific conditions of steaming are seldom reported (i.e. temperature, water partial pressure, flowrate and catalyst loading). This makes the comparison of different "mildly" steamed samples reported in literature difficult.

A significant observation made during isobutane cracking over steamed H-Mordenite is the increase in catalyst lifetime ($t_{1/2}$ = 279 min). This can be ascribed to the removal of strong acid sites which have been shown to lead to deactivation and thus changing the selectivity of the reaction. This is consistent with the investigation into the samples' acidic properties. A reduction of Brönsted acidity was seen, which was attributed to an interaction of EFAl-t with framework aluminium atoms. These sites were also seen to be weaker than those in unsteamed samples as pyridine desorbed from them at lower temperatures (this was shown in Figure 3.37). They would therefore be expected to show selectivity towards products formed over weaker acid sites.

A peak in activity in H-Mordenite samples can be seen after a 1N acid wash (r_o = 35.3 $mol.g^{-1}.h^{-1}$). Samples H0.01, H0.1 and H1 all possess similar framework aluminium concentrations equivalent to a Si/Al_f of 9, which is close to the theoretical point of maximum activity as described by the next-nearest-neighbour theory. The steady increase in initial activity from H0.01 (r_o = 22.2 $mol.g^{-1}.h^{-1}$) to H1 (r_o = 35.3 $mol.g^{-1}.h^{-1}$) coincides with a decrease in amounts of EFAl present in the catalyst. A similar trend is seen for deep bed calcined samples washed with the same concentrations of acid.

These results indicate that these EFAl species do not increase the activity of the catalyst as they did in the case of the deep bed calcined sample, but have the opposite effect. Miller *et al.* [1992] have also observed that, when present in low concentrations, octahedral EFAl

had no effect on acid strength of the framework aluminium and was not seen to be strongly acidic. It is therefore possible that the negative effect is due to their presence in the Mordenite channels blocking the hydrocarbons from access to the acid sites.

Acid washing of the steamed H-Mordenite also resulted in an optimum in activity. This was observed after a 2N acid wash (HS2). Thereafter the activity decreased rapidly viz. HS5, HS10. These last two cases are associated with a dramatic decrease in the aluminium content and the concentration of strong acid sites.

EDTA washing of the catalyst decreased the initial activity marginally, but gave the highest catalyst lifetime. Since EDTA is too large to enter the pores of the catalyst, its dealumination effect is restricted to the external layers of the catalyst [Kerr, 1968]. This removal of external acid sites would reduce initial activity, but may increase the lifetime of the catalyst by reducing the probability of formation of coke precursors at the pore mouth [Schulz *et al.*, 1991].

In summary, it has been shown that while isobutane activity generally increased with number of framework aluminium sites, the presence of EFAl and sodium had a great effect on the activity of the catalyst. Sodium acted as a charge balancing cation to the aluminium and thus reduced the number of Brönsted acid sites and consequently catalytic activity.

Deep bed calcined Mordenite showed an enhancement of activity, which is thought to be a result of the presence of an increased number of strong, extra-framework Lewis sites. Steaming at 230 torr probably produced cationic EFAl species which could have a negative effect on the amount of strong acidity due to their neutralisation of the strong framework sites. This resulted in a slight loss in activity, but an increase in catalyst lifetime. The EFAl-o produced by acid washing did not appear to affect the number or strength of

catalytically active acid sites. They did seem, however, to have a slight negative effect on the catalyst's activity, possibly due to steric hindrances due to their location in the Mordenite channels. The presence of strong acid sites was seen to increase the rate of deactivation.

Finally, these results did not show any evidence to support the hypothesis that the activity of mildly steamed zeolites is enhanced by synergy between framework Brönsted sites and extra-framework Lewis acid sites.

4.2.2 External activity and shape selectivity

The effect of the different methods of dealumination on the external activity and shape selectivity of Mordenite are discussed in this section. To assist this discussion, selected data has been extracted from Tables 3.23, 3.24 and 3.25 and is presented in Tables 4.2 and 4.3. The data in Table 4.2 shows the catalytic performance of a range of dealuminated H-Mordenite samples. In the ensuing discussion all conversions, yields and selectivities are referred to with reference to sample H(550).

Table 4.2 Cyclohexanol dehydration, 2,6-DIPN synthesis, isobutane cracking activity and acidity of dealuminated Mordenite samples

	Cyclohexanol	2,6-DIPN			Isobutane cracking		Strong acid sites[4]
	Conv.	Select.	Yield	2,6/2,7[1]	r_0[2]	S_s[3]	
Sample	%	%	%		$mol.g^{-1}.hr^{-1}$	%	$mmol.g^{-1}$
H(550)	4.1	40	1.0	1.9	20	92	1.54
H2	4.9	4	0.1	2.4	31	93	1.37
HE	7.3	13	0.1	6.3	19	83	1.41
CH	12.9	64	2.8	4.3	41	94	1.89
HS	2.8	60	2.3	4.0	19	86	0.90
HS0.1	1.5	74	3.8	7.3	20	93	1.04
HS1	2.5	64	2.0	7.8	28	92	0.98
HS5	16.5	59	2.3	7.6	13	89	0.62

(1) Ratio of 2,6-DIPN to 2,7-DIPN
(2) Initial rate of conversion of isobutane
(3) Selectivity to products formed over strong sites
(4) Number of strong acid sites as measured by the HTD peak of ammonia TPD

The shallow bed calcined H-Mordenite (H(550)) showed a steady state conversion of 4% for cylohexanol dehydration, which is comparable to that seen by Karge *et al.* [1983] for acid dealuminated Na-Mordenite (Si/Al = 19.9; conversion = 3%). Deep bed calcined H-Mordenite on the other hand, shows a much greater amount of external acidity (13% cyclohexanol conversion). Although this sample had identical structural characteristics to

H(550), with respect to aluminium content, ammonia TPD has shown that the deep bed calcined samples possessed a greater number of acid sites than its shallow bed calcined counterpart. The cyclohexanol results are consistent with the high activity seen for this sample during isobutane cracking and would suggest that the highly active sites created during calcination were in much greater concentration at the external surface. The presence of these active sites at the external surface of the catalyst suggests a migration to the surface of the EFAl responsible for enhanced activity.

A high naphthalene conversion and 2,6-DIPN/2,6-DIPN ratio was observed in the deep bed calcined sample. This indicated a large amount of reaction within the pores of the catalyst. This was surprising considering the high external activity. The removal of crystal defects during the calcination procedure was evidenced by the higher crystallinity shown by XRD. The removal of these defects may have allowed increased reactivity in the catalyst's pores due to the removal of diffusional constraints.

Washing the deep bed calcined sample reduced the cyclohexanol dehydration activity significantly. This is possibly caused by the removal of acid sites on the external surface. Moreover, another effect of water is to strongly adsorb on the external acid sites and thus decrease the activity of the catalyst for this reaction [Karge *et al.*, 1983].

Acid washing of shallow bed calcined H-Mordenite with acid concentrations up to 2N (sample H2) increased the cyclohexanol dehydration activity slightly, but led to a large decrease in naphthalene conversion and 2,6-DIPN yield. This treatment was also seen to reduce percentage crystallinity and the unit cell constants. The constriction of the unit cell as well as a slightly increased amount of EFAl-o may explain the reduced DIPN yields since both would lead to diffusional or steric constraints and reduce the rate of reaction in the pores. It is also possible that increased external acidity, shown by increased cyclohexanol

conversion, leads to reaction of naphthalene on the external sites and hence to external, non-shape selective reactions and coking. Both factors would explain the sharp reduction in total conversion and 2,6-DIPN yield.

Further acid washing of H-Mordenite showed a gradual decrease in cyclohexanol conversion (Table 3.24), with a 3.6% conversion remaining after a 10 N acid wash. This would suggest that a preference for surface dealumination by acid washing is not significant in the case of H-Mordenite. Preferential removal of aluminium from the surface of zeolites during acid washing has been reported to be a result of competition between the relative rates of diffusion of the acid and the dealumination reaction [Sawa *et al.*, 1989]. The lack of evidence for the preferential surface dealumination is consistent with the large pore size of Mordenite and the low concentration of acid allowing dealumination to occur freely throughout the catalyst as has been reported by Meyers *et al.* [1988].

The low cyclohexanol conversion over the H-Mordenite acid washed series compared to Na-Mordenite washed with 0.1 and 1N acid suggests that, apart from the case of deep bed calcined H-Mordenite, there was an acid site deficiency at the surface of ion-exchanged samples.

It has been proposed that after steaming there is an increase in surface aluminium [Scherzer, 1984; Dwyer *et al.*, 1982]. However in this present work, steaming the hydrogen form of the catalyst resulted in a decrease in the activity for cyclohexanol dehydration, which would indicate that the removal of framework aluminium from the external surface had occurred. This may indicate that the EFAl produced by steaming, are either not active for this reaction or did not migrate to the external surface. Since the EFAl-t produced by steaming are expected to possess acidity it is likely that they are not present on the external surface. Consistent with the cyclohexanol results, an increase in 2,6-DIPN/2,7-DIPN ratio was seen

in this catalyst. This is expected with a catalyst with a low external activity since all the reaction occurring would take place within the pore structure.

A mild acid wash (0.1N) of the steamed sample appeared to remove more external acid sites as shown by a decrease in cyclohexanol conversion. This suggests preferential removal of acid sites from the surface of the catalyst during dealumination. Consistent with the minimal external acidity of sample HS0.1 a very high 2,6-DIPN/2,7-DIPN ratio was observed. This indicated that the reaction took place mainly within the pores of the catalyst since there were very few external sites on which to react.

A relatively high yield of 2,6-DIPN was seen in this sample as a result of the activity of the catalyst. This high activity was also shown by shown by isobutane cracking. Ammonia TPD results also showed a large number of acid sites. Most of the samples showed 2,6-DIPN selectivity inversely related to their external activity probed by cyclohexanol dehydration. The low external and high internal acidity would appear to provide this sample with properties which are favourable for shape selective reactions.

Stronger acid washing of the steamed sample (sample HS5) led to increased amount of external acid sites as shown by cyclohexanol dehydration, but a significant loss of crystallinity and aluminium from the framework and bulk. This may be due to the creation of mesopores, the possibility of which were evidenced also by observed pitting of the catalysts by SEM. The selectivity to 2,6-DIPN in the isopropylation of naphthalene decreased slightly, possibly as a result of the presence of mesopores which would provide a non shape selective surface for reaction.

In the case of EDTA washing of the catalyst there was an increase in the cyclohexanol conversion from 4.1% to 7.3%. Most of the dealumination during EDTA washing [Kerr,

1968] and acid washing of steamed samples reportedly occurs at the pore mouths [Scherzer, 1984] and it is therefore quite possible that the increased activity was due to the widening of pore mouth following dealumination [Sawa *et al.*, 1988] and the creation of mesopores [Dashevskii *et al.*, 1978; Ajot *et al.*, 1991]. Increased external surface area would be expected to result from these structural changes and is consistent with the observed increase in external acidity as well as the relatively high 2,6-DIPN yield despite a large decrease in acidity. Both sample HE and sample HS5 showed increased selectivities to triisopropyl naphthalenes supporting the evidence for the presence of mesopores.

Acid washing of Na-Mordenite showed interesting trend with respect to the external activity of the samples. Cyclohexanol conversion and isobutane reaction rates for these samples are shown in Table 4.3.

Table 4.3 Cyclohexanol conversion and isobutane cracking activity of dealuminated Na-Mordenite samples

	Cyclohexanol dehydration Conversion	Isobutane cracking Initial reaction rate
Sample	%	$mol.g^{-1}.hr^{-1}$
Na	0.0	0.0
Na0.001	0.8	0.0
Na0.01	1.0	0.2
Na0.1	5.9	9.7
Na1	9.4	15.1
Na2	3.4	18.2
Na10	1.8	3.9

As in the case of isobutane cracking, the sodium form (Na) showed no activity for cylohexanol dehydration. Mild acid washing increased conversion as sodium was proton exchanged. A conversion of 0.8% indicating the first significant surface activity was seen after a 0.001N nitric acid wash. The same catalyst showed almost no activity for isobutane cracking. This suggests that, assuming that cyclohexanol dehydration only takes place on

the surface, sodium was removed preferentially from the surface of the catalyst, i.e. from sites at the entrances to the pores.

Cyclohexanol dehydration activity increases to a maximum of 9.4 % conversion after a 1N acid wash before decreasing after washes with higher concentration acids. The decrease in activity is ascribed to the removal of framework aluminium from the surface of the catalyst as ratio as the total framework aluminium content decreases. The decrease in surface activity occurs after a 2N concentration acid wash although the decrease in overall activity measured by isobutane cracking occurs after a 5N wash. This difference is probably indicative of the preferential removal of aluminium from the surface of the catalyst.

DIPN synthesis reactions performed over samples Na, Na1 and NaS resulted in negligible yields of 2,6-DIPN. The samples which had not been acid washed possessed very little acidity strong enough to catalyze the reaction and so minimal conversion of naphthalene was observed. Although acid washed Na-Mordenite (Na1) had a large number of acid sites, the high external acidity probably led to the observed low selectivity to DIPN.

4.3 STUDY OF THE NAPHTHALENE ISOPROPYLATION REACTION

A kinetic study of the isopropylation of naphthalene in a differential reactor was performed. The sample HS0.1, which showed the greatest selectivity to 2,6-DIPN in autoclave tests, was used is this study. The results of reactions performed under a range of temperatures and feed conditions are given in Table 3.26. The equation $r = k\ p_n^{0.6}\ p_p^{0.5}$, where p_n and p_p are the partial pressures of naphthalene and propene respectively and r the rate of naphthalene conversion, was found to fit these results closely. This equation was then used to determine the reaction rate constant over a range of temperatures.

An Arrhenius plot of the natural log of the rate of naphthalene conversion [$mol.s^{-1}.g^{-1}$] against inverse temperature [1/K] is shown in Figure 4.7.

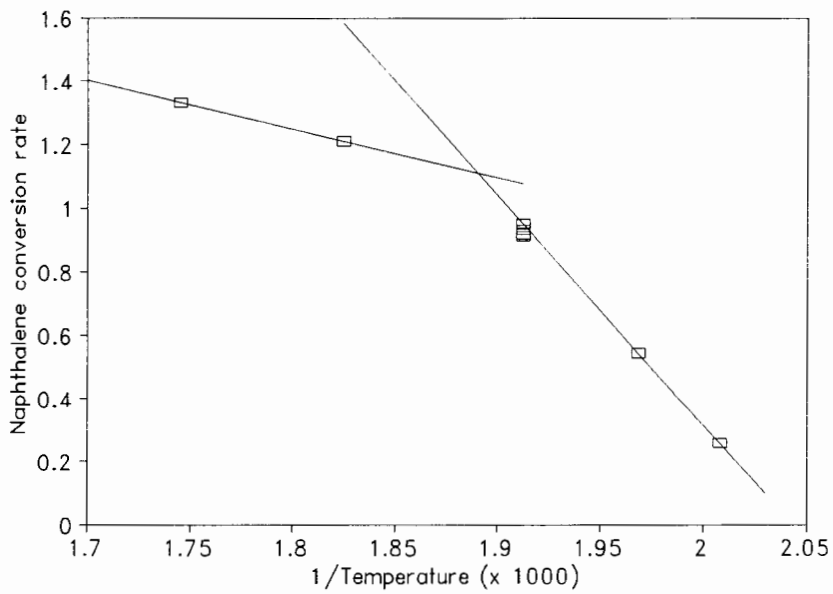

Figure 4.7 Plot of naphthalene conversion rate [$mmol.hr^{-1}.g^{-1}$] against inverse temperature [1/K] for isopropylation of naphthalene over HS0.1

The reaction deviates from a straight line by deviating to lower rates at higher temperatures and so appears to be diffusionally controlled. The slopes of the line fitted to the rates at low temperatures is double that of the line fitted to the rates at higher temperatures, indicating that the reaction is mass transfer controlled at higher temperatures [Smith, 1981]. Tha

calculated activation energy for the reaction was therefore 25.2 $kJ.mol^{-1}$ with an apparent activation energy of 12.6 $kJ.mol^{-1}$ at temperatures above 250°C.

This is also indicated by the increase in ratio of 2,6-DIPN to 2,7-DIPN from 3.3 at 225°C to 12.5 at 300°C showing that the diffusion controlled shape selectivity becomes more significant at high temperatures.

CHAPTER FIVE

CONCLUSIONS

5. CONCLUSIONS

As was outlined in Section 1.6, the objectives of this research were:

1. To conduct a systematic study of the effect of acid washing, steaming and steaming followed by acid washing on a single batch of well characterised Mordenite;
2. To characterise the solid state nature of the samples thus modified;
3. To characterise the acidity of these modified samples;
4. To characterise the catalytic properties of the samples;
5. To determine the method of treatment, acid washing and steaming and combinations thereof, and the conditions these which are conducive to the promotion of paticular acid sites and of particular catalytic properties.

The conclusions drawn from this study with respect to these objectives are presented in this section.

Steaming

Steaming of Mordenite at 230 and 1520 torr led to the production of large amounts of EFAl-t. No relationship was found, however, between the crystallinity of the sample and the amount of EFAl present and the maintenance of the sample's crystallinity despite the large extent of framework dealumination suggests that a degree of framework stabilisation or annealing has taken place. The presence of EFAl-t reduced Brönsted acidity probably by charge balancing with a single positive charge, but increased Lewis acidity.

Brönsted acidity was directly dependent on the framework aluminium content although the effects of charge balancing cations such as Na^+ and EFAl-t^+ had to be taken into account.

Figure 5.1 shows the number of Brönsted acid sites as a function of available framework aluminium atoms, viz. those sites not charge balanced by either a sodium ion or a cationic EFAl-t species. The amount of weak Lewis acidity in the sample was equivalent to the total number of octahedral and tetrahedral extra-framework species.

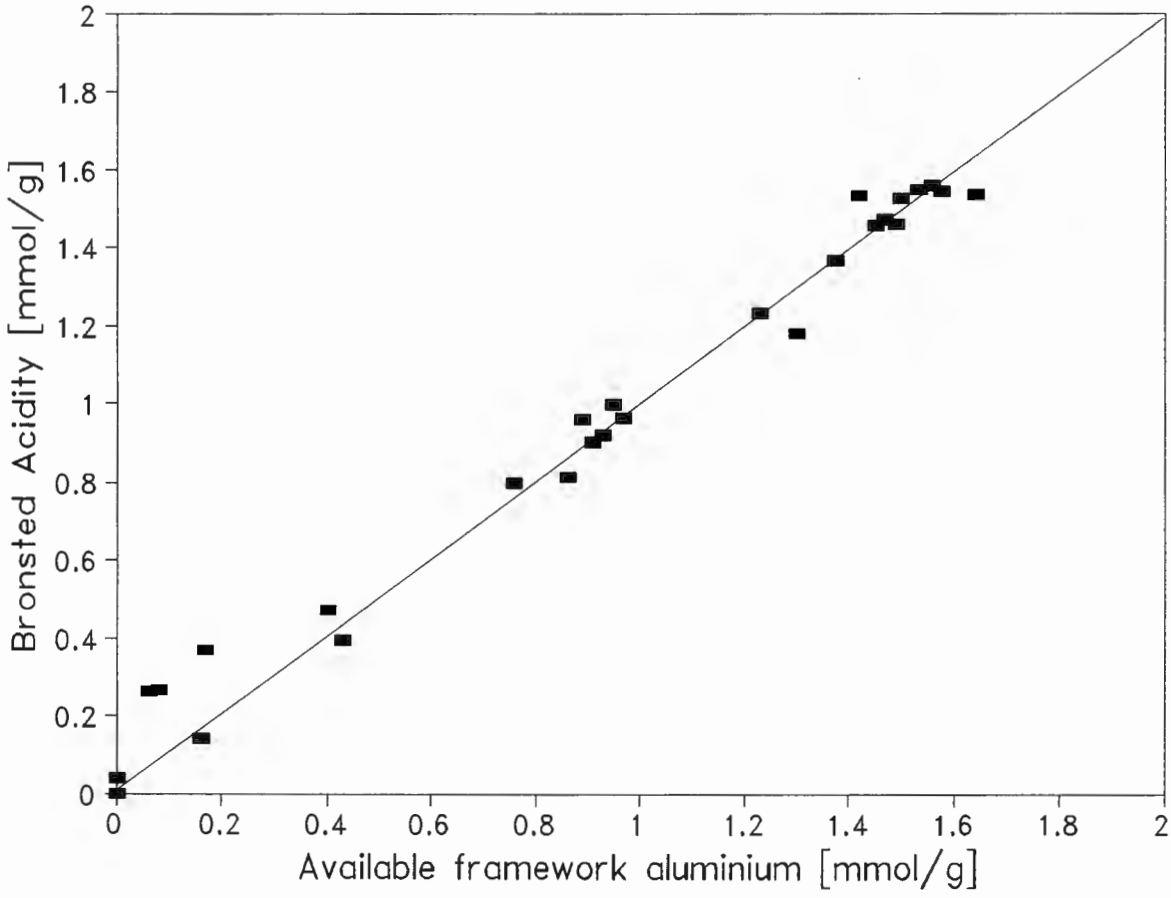

Figure 5.1 Brönsted acidity as measured by the deconvolution of ammonia TPD response curves as a function of the concentration of available framework aluminium

Although EFAl-t species appeared to be active sites for isobutane cracking, their presence reduced the selectivity to products formed over strong acid sites during isobutane cracking and indicated that they are weak sites. Steamed samples therefore showed increased catalyst lifetimes during the isobutane cracking reaction. There was no indication of the migration of these species to the external surface of the catalyst by the cyclohexanol

dehydration reaction and their close association with framework aluminium as evidenced by their effect on Brönsted acidity would suggest that these EFAl-t species are present within the catalyst pores.

The EFAl-t species were easily removed by acid washing as acid washing removed more aluminium from steamed samples than from their unsteamed counterparts. Low external acidity was seen in steamed H-Mordenite and the EFAl-t are therefore probably localised in the pores of the catalyst as is suggested by their probable association with framework aluminium sites.

"Deep bed" calcination

Calcination of the catalyst, particularly in a "deep-bed" configuration, resulted in the annealing of its crystalline structure, despite the creation of EFAl-o. "Deep bed" calcination produced a highly active catalyst as determined by isobutane cracking and the presence of a large amount of strong Lewis acidity was observed. The total number of acid sites was slightly more than to the total aluminium content and this observation together with a lack of hydroxyl groups observed in the catalyst suggested that these Lewis sites have the form AlO^{+} or Al^{3+}.

The presence of these EFAl type sites increased catalytic activity for isobutane cracking by exhibiting strong Lewis acidity which enhanced the initiation of the cracking reaction. Increased activity of the "deep bed" calcined sample for cyclohexanol dehydration indicates that these species may be present on the external surface of the catalyst. This effect appeared to be similar to observations made for cracking reaction over mildly steamed ZSM-5 and Zeolite-Y. The strong acidity, however, led to increased coking during the isobutane cracking reaction and shorter catalyst lifetime for this reaction. The EFAl species produced by the "deep bed" calcination could be hydrated with a wash in deionised water

to form the EFAl-o species seen in acid washed samples and the strong acidity reduced.

Acid washing

Acid washing of Na-Mordenite with acids of concentrations above 0.01N resulted in proton exchange for sodium cations which caused a reduction in weak Lewis acidity and an increase in Brönsted acidity. This exchange occurred preferrentially on the external surface of the catalyst. Over ninety percent proton exchange was achieved by a 0.1N acid wash, the residual sodium ions probably being located in side pockets.

The presence of hydrated octahedral EFAl species was observed in all acid washed samples. These appeared to contribute to the weak Lewis acidity observed in the catalyst as shown in Figure 4.2. Weak Lewis acidity was not probed by pyridine suggesting that these species occur within the side-pockets. The EFAl-o species were not seen to be catalytically active for any reaction despite their weak Lewis acidity and in fact had a negative effect on the initial isobutane cracking activity of the dealuminated catalysts probably due as a result of sterically blocking the active sites from the reactant molecules. The formation of hydroxyl nests during dealumination by acid washing was seen by a shoulder at 950 cm^{-1} in infra-red spectroscopy. These seemed to be stable at temperatures up to 80°C, but were removed at higher temperatures.

Acid washing of steamed H-Mordenite showed selective sodium removal and dealumination from the external surface as evidenced by the cyclohexanol dehydration probe reaction results. Selective removal of aluminium from the surface of unsteamed H-Mordenite was not observed.

General trends in catalytic properties

Although isobutane cracking activity was mainly dependent on the amount of framework aluminium sites present in the catalyst, both the activity and lifetime of the catalyst were observed to be a function of the strength of acid sites in the catalyst. No evidence was found to support the hypothesis that the activity of the catalyst was enhanced by a synergistic effect between extra-framework Lewis and Framework Brönsted acid sites.

Shape selectivity, measured by selectivity to 2,6-DIPN during the isopropylation of naphthalene, was enhanced by the removal of external sites. Samples steamed and then acid washed were found to have the highest selectivities to 2,6-DIPN and the lowest external activities as determined by cyclohexanol dehydration.

In conclusion, the three methods of dealumination investigated in this work, viz. acid washing, steaming and "deep-bed" calcination, each resulted in the formation of extra-framework aluminium species with different characteristics with respect to their acid strength. These have a strong influence on the different catalytic properties of Mordenite. Thus when preparing a sample of Mordenite for a particular catalytic process by dealumination, great care needs to be taken in deciding which dealumination method to use and at what conditions to use the chosen method.

APPENDIX I

X-ray diffraction data

Sample Na_1

h	k	l	d-spacing	2θ	Intensity
0	2	0	10.26	8.60	689
2	0	0	9.07	9.75	2603
3	3	0	4.530	19.60	2136
1	5	0	4.005	22.20	4174
0	0	2	3.762	23.65	932
2	0	2	3.480	25.60	6727
3	5	0	3.395	26.25	4391
5	1	1	3.227	27.65	4242

Sample Na_2

h	k	l	d-spacing	2θ	Intensity
0	2	0	10.27	8.60	632
2	0	0	9.07	9.75	2557
3	3	0	4.529	19.60	2186
1	5	0	3.995	22.30	4330
0	0	2	3.762	23.65	1491
2	0	2	3.463	25.75	6787
3	5	0	3.395	26.25	4300
5	1	1	3.232	27.65	4136

Sample Na_3

h	k	l	d-spacing	2θ	Intensity
0	2	0	10.28	8.60	622
2	0	0	9.07	9.75	2564
3	3	0	4.541	19.55	2183
1	5	0	4.004	22.25	4395
0	0	2	3.762	23.65	1008
2	0	2	3.480	25.60	6798
3	5	0	3.410	26.15	4346
5	1	1	3.232	27.60	4222

Sample Na0

h	k	l	d-spacing	2θ	Intensity
0	2	0	10.28	8.60	656
2	0	0	9.11	9.70	2594
3	3	0	4.541	19.55	2216
1	5	0	4.014	22.15	4419
0	0	2	3.775	23.55	827
2	0	2	3.487	25.55	6835
3	5	0	3.402	26.20	4213
5	1	1	3.232	27.60	4224

Sample Na0.001

h	k	l	d-spacing	2θ	Intensity
0	2	0	10.28	8.60	649
2	0	0	9.10	9.70	2536
3	3	0	4.541	19.55	2121
1	5	0	4.004	22.20	4431
0	0	2	3.769	23.60	836
2	0	2	3.480	25.60	6909
3	5	0	3.395	26.25	4259
5	1	1	3.232	27.60	4261

Sample Na0.01

h	k	l	d-spacing	2θ	Intensity
0	2	0	10.26	8.60	680
2	0	0	9.11	9.70	2809
3	3	0	4.541	19.55	2402
1	5	0	4.004	22.20	4943
0	0	2	3.769	23.60	892
2	0	2	3.480	25.60	7372
3	5	0	3.395	26.25	4495
5	1	1	3.232	27.60	4394

Sample Na0.1

h	k	l	d-spacing	2θ	Intensity
0	2	0	10.28	8.60	612
2	0	0	9.14	9.70	2607
3	3	0	4.553	19.50	2402
1	5	0	4.004	22.20	4944
0	0	2	3.772	23.60	977
2	0	2	3.480	25.60	6782
3	5	0	3.402	26.20	4030
5	1	1	3.244	27.50	4273

Sample Na1

h	k	l	d-spacing	2θ	Intensity
0	2	0	10.23	8.65	864
2	0	0	9.09	9.75	3450
3	3	0	4.530	19.60	2938
1	5	0	3.987	22.30	5443
0	0	2	3.761	23.65	1155
2	0	2	3.473	25.65	8011
3	5	0	3.389	26.30	4259
5	1	1	3.238	27.55	4332

Sample Na2

h	k	l	d-spacing	2θ	Intensity
0	2	0	10.21	8.65	932
2	0	0	9.09	9.75	4143
3	3	0	4.529	19.60	3502
1	5	0	3.978	22.35	6339
0	0	2	3.754	23.75	1243
2	0	2	3.473	25.70	8622
3	5	0	3.389	26.30	4541
5	1	1	3.238	27.55	4640

Sample Na5

h	k	l	d-spacing	2θ	Intensity
0	2	0	10.25	8.60	560
2	0	0	9.64	9.15	1539
3	3	0	4.553	19.55	1935
1	5	0	3.996	22.25	3489
0	0	2	3.764	23.65	777
2	0	2	3.480	25.60	5391
3	5	0	3.395	26.25	3139
5	1	1	3.238	27.55	3482

Sample NaS

h	k	l	d-spacing	2θ	Intensity
0	2	0	10.18	8.70	626
2	0	0	9.04	9.80	2316
3	3	0	4.518	19.65	2015
1	5	0	3.987	22.30	3988
0	0	2	3.753	23.75	850
2	0	2	3.467	25.70	5894
3	5	0	3.389	26.30	3742
5	1	1	3.221	27.70	4043

Sample NaS0

h	k	l	d-spacing	2θ	Intensity
0	2	0	10.28	8.60	606
2	0	0	9.08	9.75	2099
3	3	0	4.530	19.60	1963
1	5	0	3.996	22.25	3703
0	0	2	3.769	23.60	832
2	0	2	3.487	25.60	5773
3	5	0	3.395	26.25	3588
5	1	1	3.227	27.65	3826

Sample NaS0.01

h	k	l	d-spacing	2θ	Intensity
0	2	0	10.26	8.60	607
2	0	0	9.07	9.75	2447
3	3	0	4.530	19.60	2163
1	5	0	3.996	22.25	4070
0	0	2	3.764	23.65	870
2	0	2	3.487	25.60	6036
3	5	0	3.395	26.25	3805
5	1	1	3.227	27.65	3888

Sample NaS0.1

h	k	l	d-spacing	2θ	Intensity
0	2	0	10.25	8.60	604
2	0	0	9.07	9.75	2728
3	3	0	4.530	19.60	2429
1	5	0	3.987	22.30	4685
0	0	2	3.758	23.65	976
2	0	2	3.480	25.65	6771
3	5	0	3.39	26.30	3986
5	1	1	3.232	27.60	4046

Sample NaS1

h	k	l	d-spacing	2θ	Intensity
0	2	0	10.22	8.65	699
2	0	0	9.08	9.75	2773
3	3	0	4.530	19.60	2564
1	5	0	3.987	22.30	4650
0	0	2	3.756	23.70	951
2	0	2	3.480	25.65	6595
3	5	0	3.39	26.30	3613
5	1	1	3.232	27.60	4189

Sample NaS2

h	k	l	d-spacing	2θ	Intensity
0	2	0	10.27	8.60	861
2	0	0	9.16	9.65	3384
3	3	0	4.552	19.50	2875
1	5	0	3.987	22.30	5585
0	0	2	3.779	23.55	848
2	0	2	3.480	25.60	7058
3	5	0	3.389	26.30	4114
5	1	1	3.232	27.60	4339

Sample NH_4

h	k	l	d-spacing	2θ	Intensity
0	2	0	10.27	8.60	1182
2	0	0	9.11	9.70	3662
3	3	0	4.541	19.55	2822
1	5	0	3.995	22.25	5233
0	0	2	3.762	23.65	891
2	0	2	3.473	25.70	7419
3	5	0	3.395	26.25	4169
5	1	1	3.232	27.60	4528

Sample H(550)

h	k	l	d-spacing	2θ	Intensity
0	2	0	10.27	8.60	1241
2	0	0	9.11	9.70	3360
3	3	0	4.541	19.55	2662
1	5	0	4.005	22.20	4664
0	0	2	3.764	23.65	831
2	0	2	3.480	25.60	6914
3	5	0	3.402	26.20	3801
5	1	1	3.232	27.60	4331

Sample H0

h	k	l	d-spacing	2θ	Intensity
0	2	0	10.24	8.65	1190
2	0	0	9.10	9.70	3487
3	3	0	4.530	19.60	2771
1	5	0	3.987	22.30	4939
0	0	2	3.756	23.65	896
2	0	2	3.467	25.70	7150
3	5	0	3.389	26.30	3851
5	1	1	3.232	27.60	4139

Sample H0.001

h	k	l	d-spacing	2θ	Intensity
0	2	0	10.21	8.65	2019
2	0	0	9.10	9.70	5246
3	3	0	4.530	19.60	3751
1	5	0	3.987	22.30	6336
0	0	2	3.758	23.65	1205
2	0	2	3.473	25.65	8929
3	5	0	3.389	26.30	4635
5	1	1	3.232	27.60	4798

Sample H0.01

h	k	l	d-spacing	2θ	Intensity
0	2	0	10.22	8.65	1387
2	0	0	9.10	9.70	3959
3	3	0	4.530	19.60	3060
1	5	0	3.987	22.30	5306
0	0	2	3.756	23.65	996
2	0	2	3.467	25.70	7120
3	5	0	3.389	26.30	3875
5	1	1	3.232	27.60	4212

Sample H0.1

h	k	l	d-spacing	2θ	Intensity
0	2	0	10.22	8.65	1149
2	0	0	9.09	9.70	3382
3	3	0	4.518	19.65	3112
1	5	0	3.978	22.35	5519
0	0	2	3.751	23.70	997
2	0	2	3.467	25.70	7828
3	5	0	3.383	26.35	4368
5	1	1	3.227	27.65	4703

Sample H1

h	k	l	d-spacing	2θ	Intensity
0	2	0	10.22	8.65	1018
2	0	0	9.09	9.70	3452
3	3	0	4.529	19.60	3025
1	5	0	3.978	22.35	5423
0	0	2	3.754	23.70	1109
2	0	2	3.473	25.70	7788
3	5	0	3.389	26.30	4115
5	1	1	3.238	27.65	4311

Sample H2

h	k	l	d-spacing	2θ	Intensity
0	2	0	10.21	8.65	1169
2	0	0	9.09	9.70	3792
3	3	0	4.518	19.65	3152
1	5	0	3.969	22.40	5241
0	0	2	3.749	23.75	1019
2	0	2	3.467	25.70	7859
3	5	0	3.383	26.35	4010
5	1	1	3.232	27.60	4078

Sample H5

h	k	l	d-spacing	2θ	Intensity
0	2	0	10.22	8.65	897
2	0	0	9.10	9.70	3148
3	3	0	4.541	19.55	2812
1	5	0	3.978	22.35	4908
0	0	2	3.754	23.70	1063
2	0	2	3.473	25.70	7200
3	5	0	3.389	26.25	3933
5	1	1	3.238	27.65	4103

Sample H10

h	k	l	d-spacing	2θ	Intensity
0	2	0	10.22	8.65	592
2	0	0	9.11	9.70	1923
3	3	0	4.529	19.60	1790
1	5	0	3.978	22.35	3296
0	0	2	3.754	23.70	712
2	0	2	3.466	25.75	4819
3	5	0	3.382	26.25	2612
5	1	1	3.284	27.20	2736

Sample HE

h	k	l	d-spacing	2θ	Intensity
0	2	0	10.22	8.65	1686
2	0	0	9.19	9.65	5634
3	3	0	4.529	19.60	3923
1	5	0	3.978	22.35	6520
0	0	2	3.754	23.70	1294
2	0	2	3.466	25.75	9109
3	5	0	3.382	26.25	4486
5	1	1	3.232	27.60	4858

Sample CH

h	k	l	d-spacing	2θ	Intensity
0	2	0	10.19	8.70	1016
2	0	0	9.02	9.80	3060
3	3	0	4.518	19.65	2960
1	5	0	3.978	22.35	5437
0	0	2	3.746	23.75	1009
2	0	2	3.466	25.75	7573
3	5	0	3.382	26.25	4225
5	1	1	3.226	27.65	4564

Sample CH0

h	k	l	d-spacing	2θ	Intensity
0	2	0	10.21	8.65	1093
2	0	0	9.06	9.75	3364
3	3	0	4.529	19.60	3337
1	5	0	3.978	22.35	6362
0	0	2	3.746	23.75	863
2	0	2	3.466	25.75	8856
3	5	0	3.382	26.25	4893
5	1	1	3.232	27.60	5091

Sample CH0.001

h	k	l	d-spacing	2θ	Intensity
0	2	0	10.20	8.65	1101
2	0	0	9.10	9.70	3517
3	3	0	4.529	19.60	3429
1	5	0	3.978	22.35	6291
0	0	2	3.745	23.75	1114
2	0	2	3.466	25.75	8583
3	5	0	3.382	26.25	4717
5	1	1	3.232	27.60	5171

Sample CH0.01

h	k	l	d-spacing	2θ	Intensity
0	2	0	10.22	8.65	1042
2	0	0	9.10	9.70	3382
3	3	0	4.529	19.60	3324
1	5	0	3.978	22.35	6281
0	0	2	3.746	23.75	1048
2	0	2	3.466	25.75	8640
3	5	0	3.382	26.25	4618
5	1	1	3.232	27.60	4980

Sample CH0.1

h	k	l	d-spacing	2θ	Intensity
0	2	0	10.22	8.65	993
2	0	0	9.10	9.70	3089
3	3	0	4.529	19.60	2793
1	5	0	3.978	22.35	5237
0	0	2	3.746	23.75	944
2	0	2	3.466	25.75	7446
3	5	0	3.382	26.25	4033
5	1	1	3.226	27.65	4259

Sample CH1

h	k	l	d-spacing	2θ	Intensity
0	2	0	10.22	8.65	1119
2	0	0	9.09	9.70	3325
3	3	0	4.518	19.65	2909
1	5	0	3.978	22.35	5077
0	0	2	3.746	23.75	993
2	0	2	3.466	25.75	7447
3	5	0	3.382	26.25	4068
5	1	1	3.232	27.60	4244

Sample HS

h	k	l	d-spacing	2θ	Intensity
0	2	0	10.26	8.60	2058
2	0	0	9.10	9.70	6156
3	3	0	4.529	19.60	3379
1	5	0	3.995	22.25	5571
0	0	2	3.762	23.65	1012
2	0	2	3.473	25.70	7781
3	5	0	3.389	26.25	3801
5	1	1	3.232	27.60	4009

Sample HS0

h	k	l	d-spacing	2θ	Intensity
0	2	0	10.25	8.60	1258
2	0	0	9.10	9.70	4182
3	3	0	4.529	19.60	3153
1	5	0	3.987	22.30	5417
0	0	2	3.754	23.70	927
2	0	2	3.466	25.75	7493
3	5	0	3.389	26.25	4034
5	1	1	3.226	27.65	4345

Sample HS0.01

h	k	l	d-spacing	2θ	Intensity
0	2	0	10.25	8.60	1322
2	0	0	9.10	9.70	4177
3	3	0	4.529	19.60	2932
1	5	0	3.987	22.30	5084
0	0	2	3.754	23.70	958
2	0	2	3.466	25.75	6833
3	5	0	3.389	26.25	3506
5	1	1	3.226	27.65	3947

Sample HS0.1

h	k	l	d-spacing	2θ	Intensity
0	2	0	10.25	8.60	1564
2	0	0	9.10	9.70	4729
3	3	0	4.529	19.60	3005
1	5	0	3.978	22.35	5265
0	0	2	3.754	23.70	1002
2	0	2	3.466	25.75	6967
3	5	0	3.389	26.25	3668
5	1	1	3.266	27.65	3996

Sample HS1

h	k	l	d-spacing	2θ	Intensity
0	2	0	10.24	8.65	1611
2	0	0	9.10	9.70	4693
3	3	0	4.529	19.60	2889
1	5	0	3.987	22.35	4822
0	0	2	3.754	23.70	992
2	0	2	3.466	25.75	6566
3	5	0	3.382	26.35	3411
5	1	1	3.232	27.60	3798

Sample HS2

h	k	l	d-spacing	2θ	Intensity
0	2	0	10.21	8.65	1457
2	0	0	9.07	9.75	4475
3	3	0	4.518	19.65	3304
1	5	0	3.978	22.35	5722
0	0	2	3.747	23.75	1061
2	0	2	3.466	25.75	7925
3	5	0	3.382	26.35	4209
5	1	1	3.226	27.65	4488

Sample HSS

h	k	l	d-spacing	2θ	Intensity
0	2	0	10.21	8.65	1974
2	0	0	9.09	9.75	5093
3	3	0	4.518	19.65	2996
1	5	0	3.969	22.40	4538
0	0	2	3.746	23.70	1044
2	0	2	3.460	25.75	6119
3	5	0	3.376	26.40	3145
5	1	1	3.220	27.70	3525

Sample HSS0

h	k	l	d-spacing	2θ	Intensity
0	2	0	10.21	8.65	2036
2	0	0	9.05	9.80	5559
3	3	0	4.506	19.70	3222
1	5	0	3.969	22.40	5073
0	0	2	3.739	23.80	1132
2	0	2	3.460	25.75	6596
3	5	0	3.376	26.40	3444
5	1	1	3.220	27.70	3789

Sample HSS0.1

h	k	l	d-spacing	2θ	Intensity
0	2	0	10.16	8.70	1995
2	0	0	9.05	9.80	5313
3	3	0	4.506	19.70	3290
1	5	0	3.969	22.40	4849
0	0	2	3.739	23.80	1129
2	0	2	3.453	25.80	6503
3	5	0	3.370	26.45	3402
5	1	1	3.220	27.70	3820

Sample HSS1

h	k	l	d-spacing	2θ	Intensity
0	2	0	10.16	8.70	1884
2	0	0	9.05	9.80	4855
3	3	0	4.506	19.70	3131
1	5	0	3.969	22.40	4791
0	0	2	3.739	23.80	1092
2	0	2	3.453	25.80	6497
3	5	0	3.370	26.45	3362
5	1	1	3.220	27.70	3684

Sample HSS2

h	k	l	d-spacing	2θ	Intensity
0	2	0	10.16	8.70	1740
2	0	0	9.05	9.80	4909
3	3	0	4.506	19.70	3076
1	5	0	3.969	22.40	4535
0	0	2	3.739	23.80	994
2	0	2	3.453	25.80	6147
3	5	0	3.370	26.45	3110
5	1	1	3.220	27.70	3488

Sample HSS5

h	k	l	d-spacing	2θ	Intensity
0	2	0	10.16	8.70	2137
2	0	0	9.05	9.80	5427
3	3	0	4.506	19.70	3426
1	5	0	3.969	22.40	5049
0	0	2	3.739	23.80	1107
2	0	2	3.453	25.80	6728
3	5	0	3.370	26.45	3655
5	1	1	3.220	27.70	3885

APPENDIX II

^{29}Si MAS NMR Spectra

All figures show 29Si MAS NMR spectra with intensity plotted against chemical shift from -20 to -180 ppm

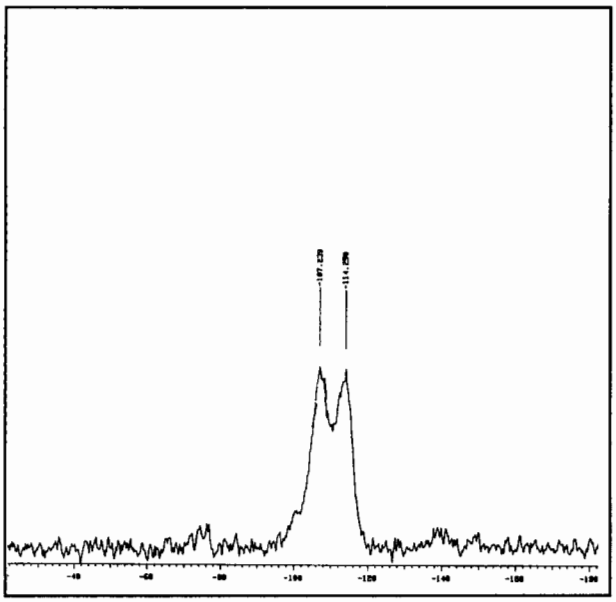

Na-MOR

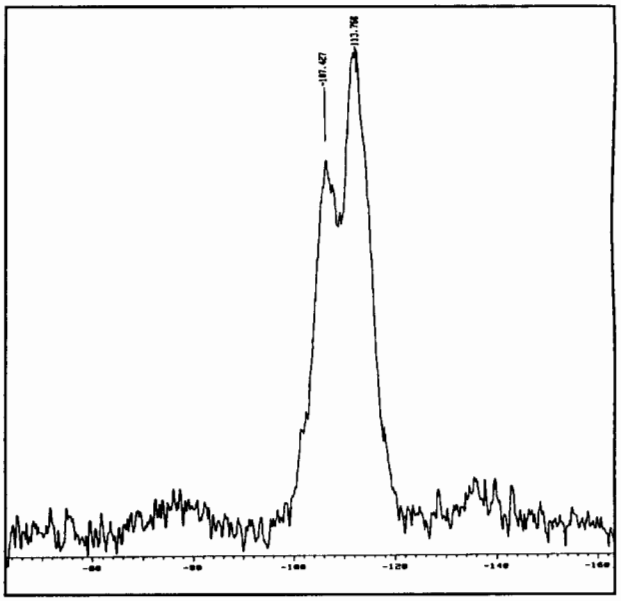

Na2

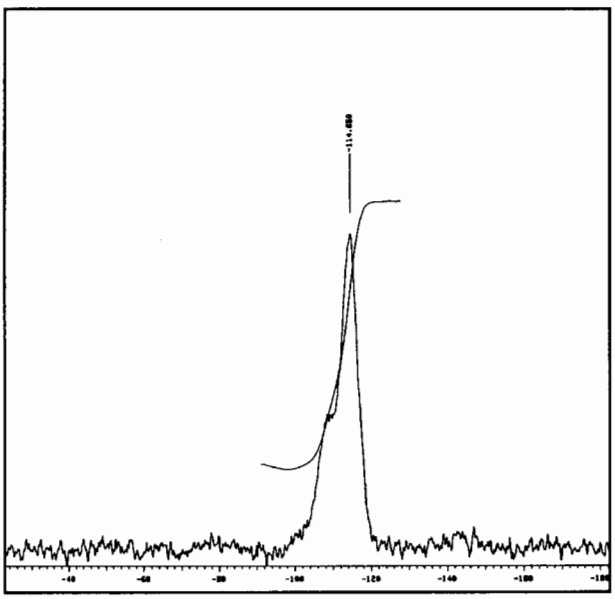

NaS

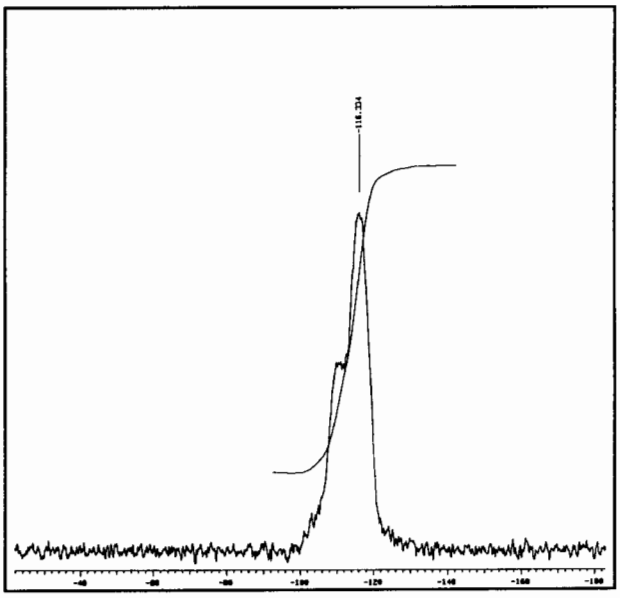

H0.001

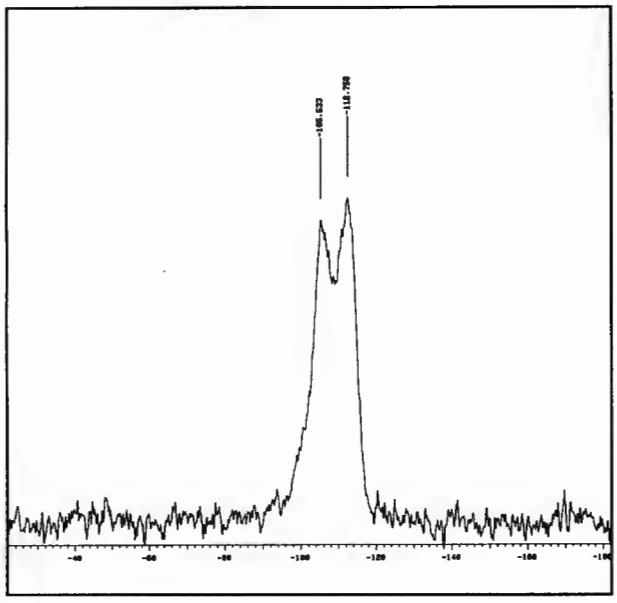

HE

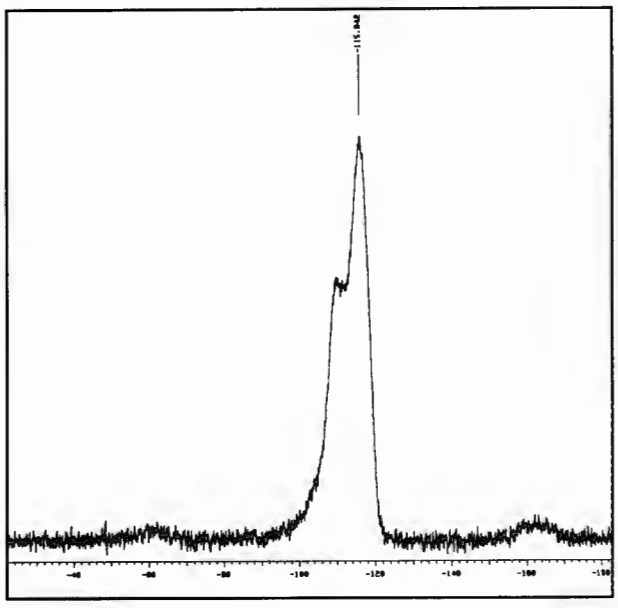

CH

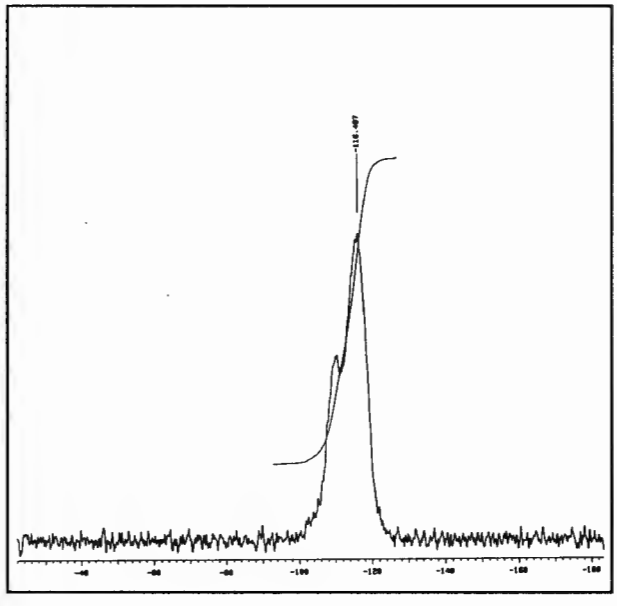

CH0

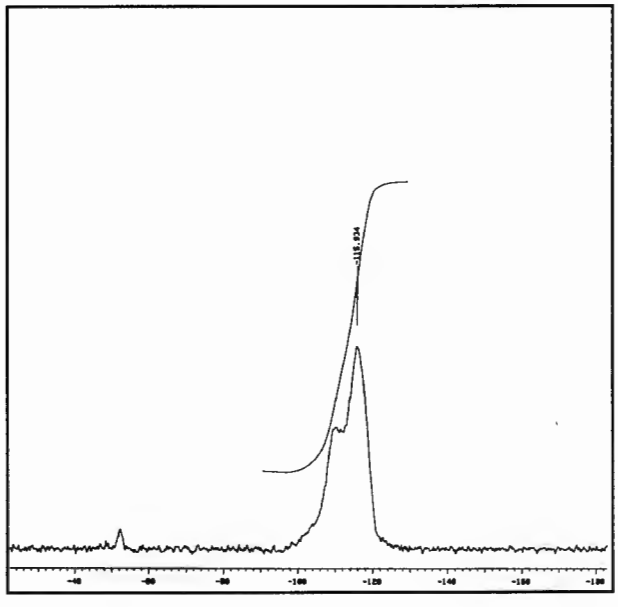

CH0.01

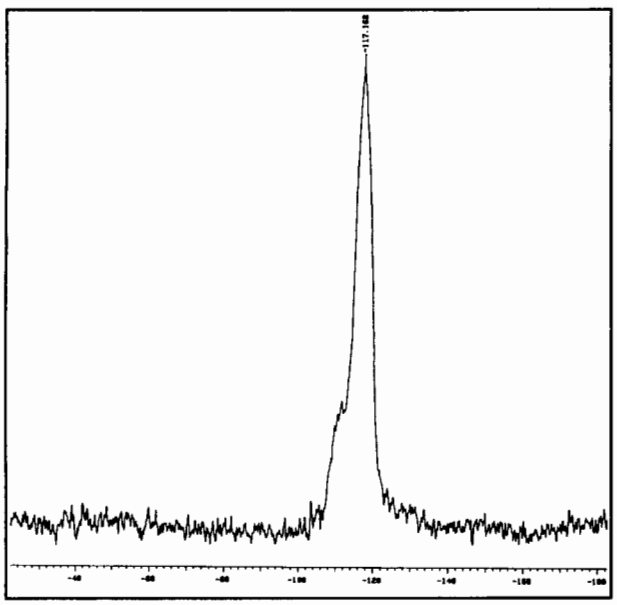

HS0

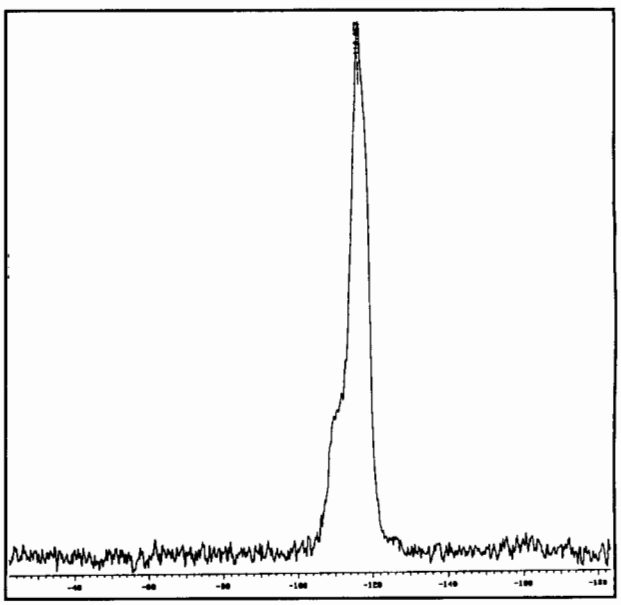

HS0.01

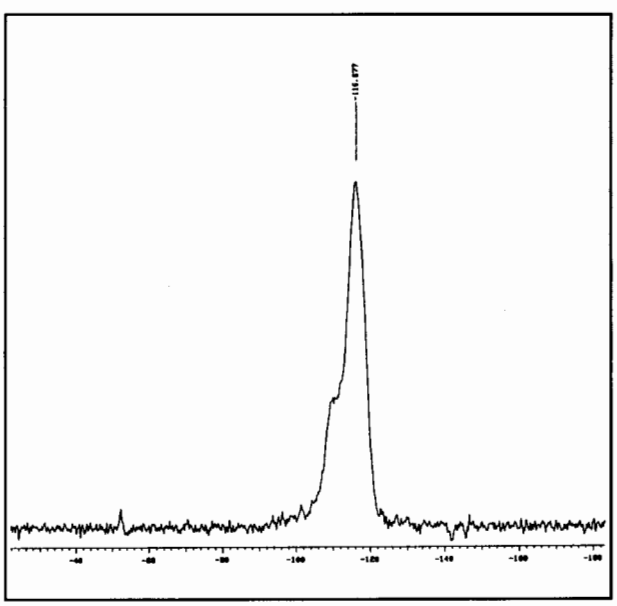

HS0.1

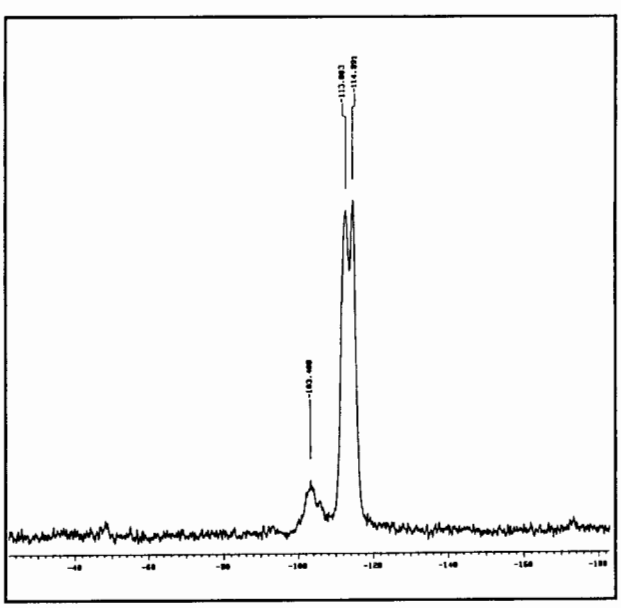

HS10

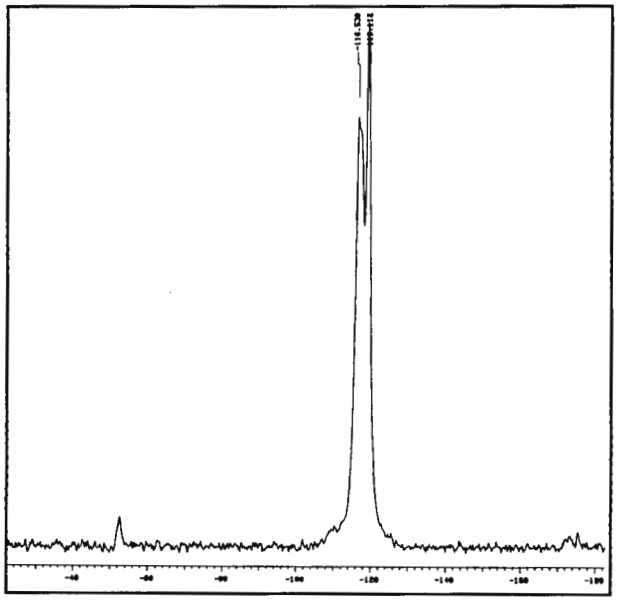

HSS

APPENDIX III

^{27}Al MAS NMR Spectra

All figures show ^{27}Al MAS NMR spectra with intensity plotted against chemical shift from 150 to -50 ppm.

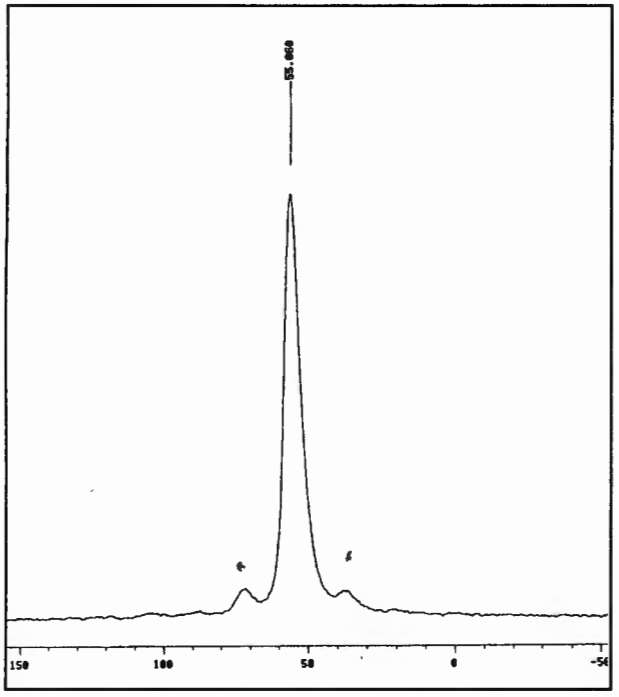

Na-MOR

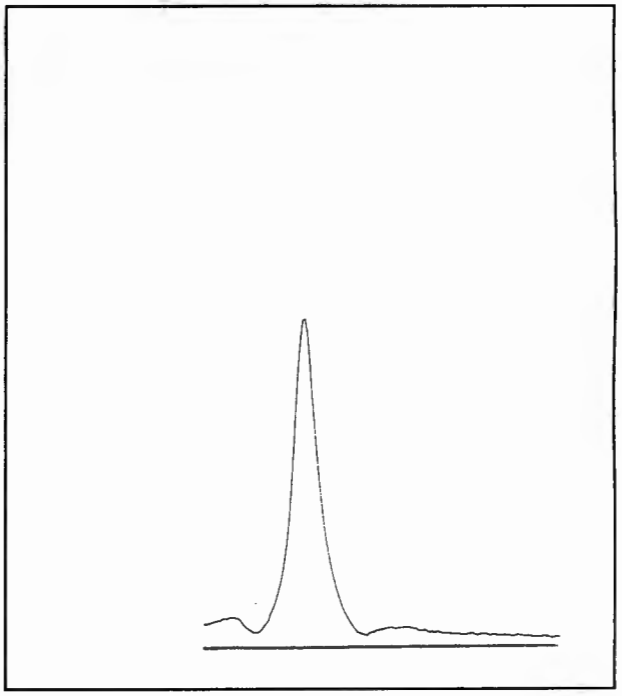

Na0

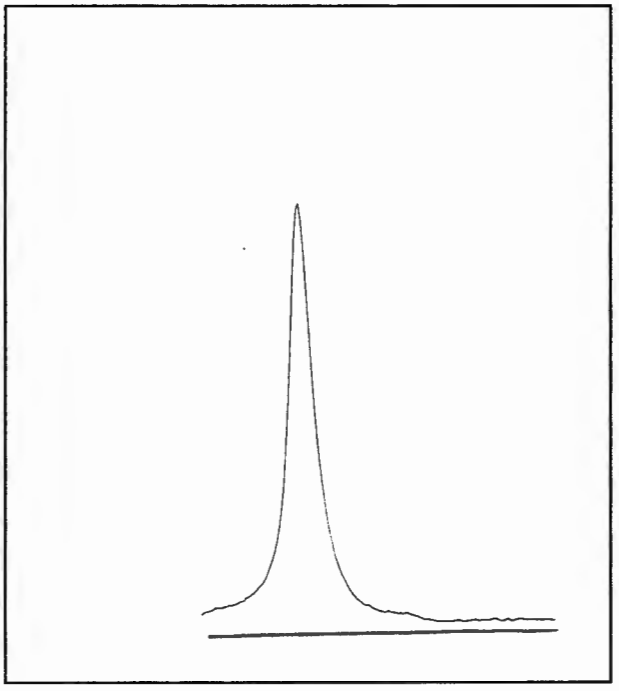

Na0.001

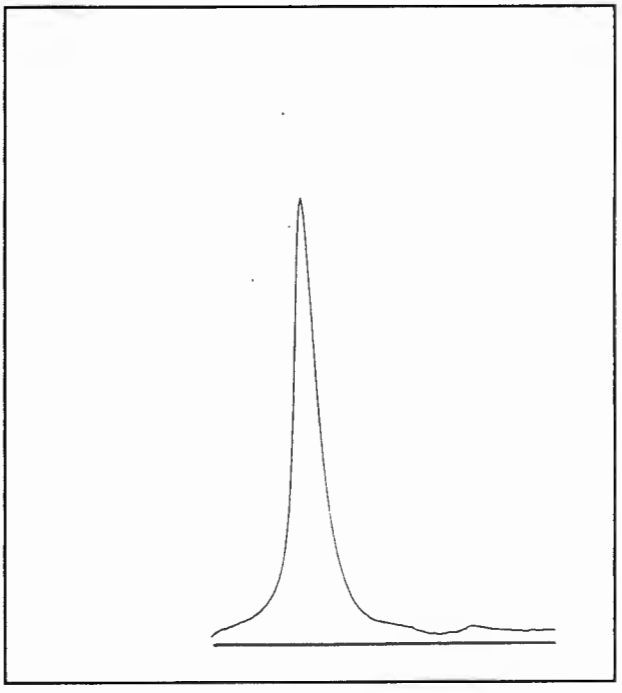

Na0.01

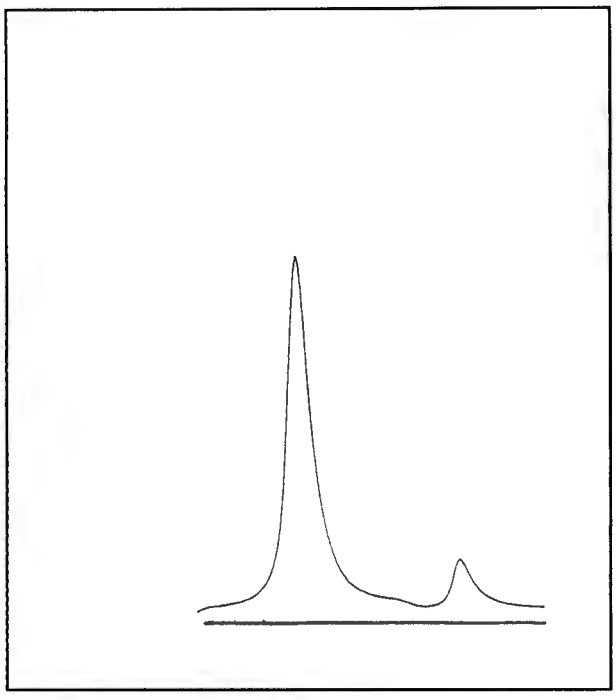

Na0.1

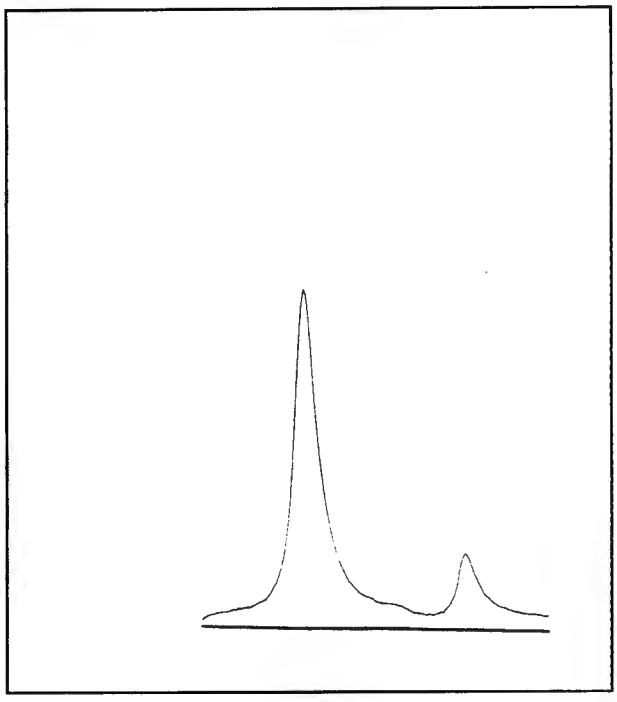

Na1

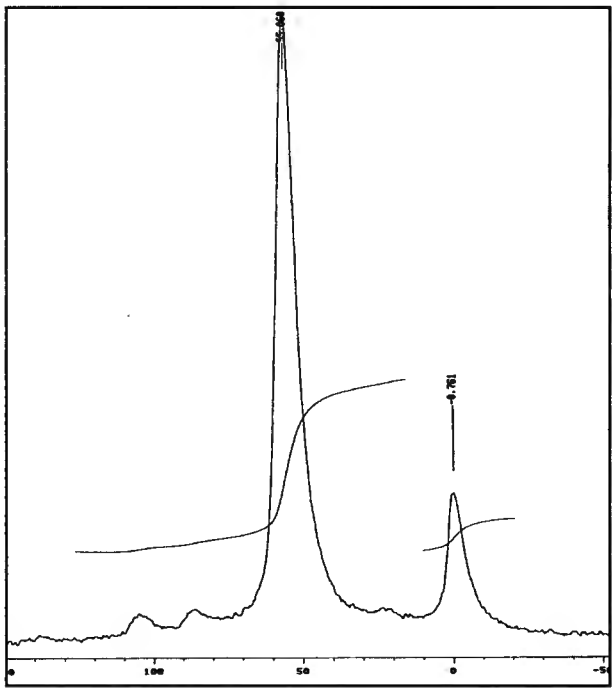

Na2

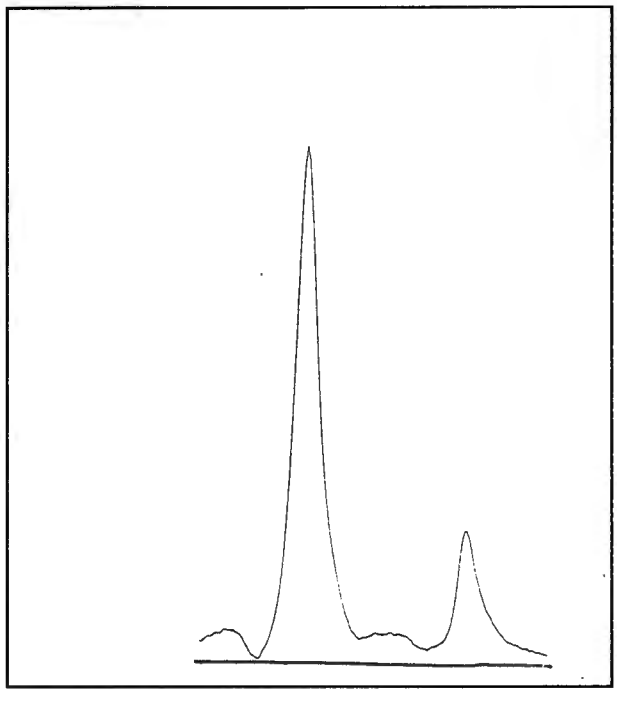

Na5

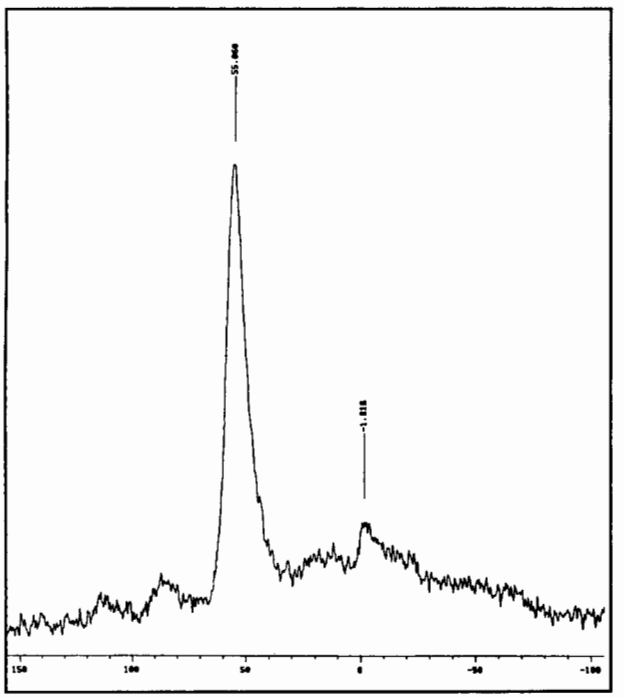

NaS

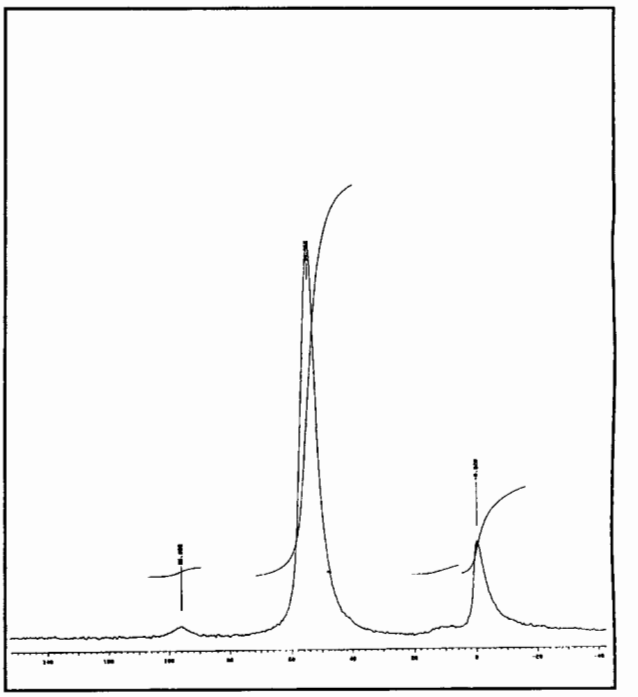

NaS2

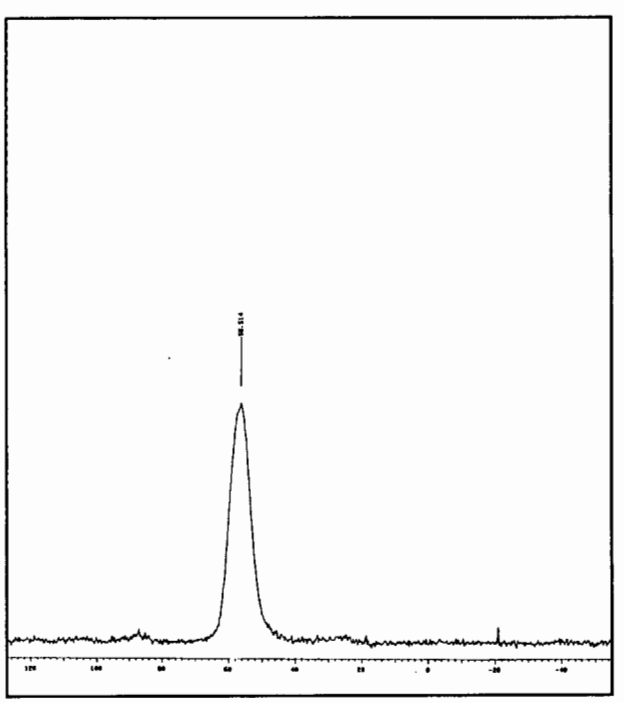

NH_4

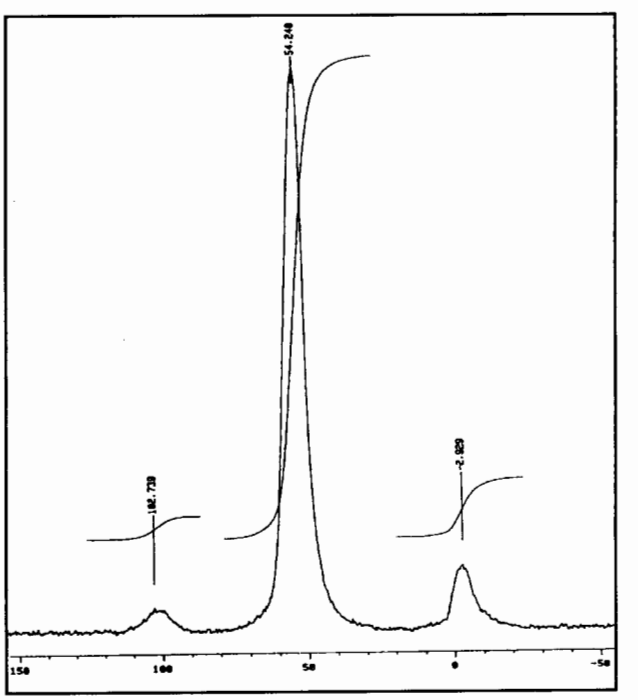

H(400)

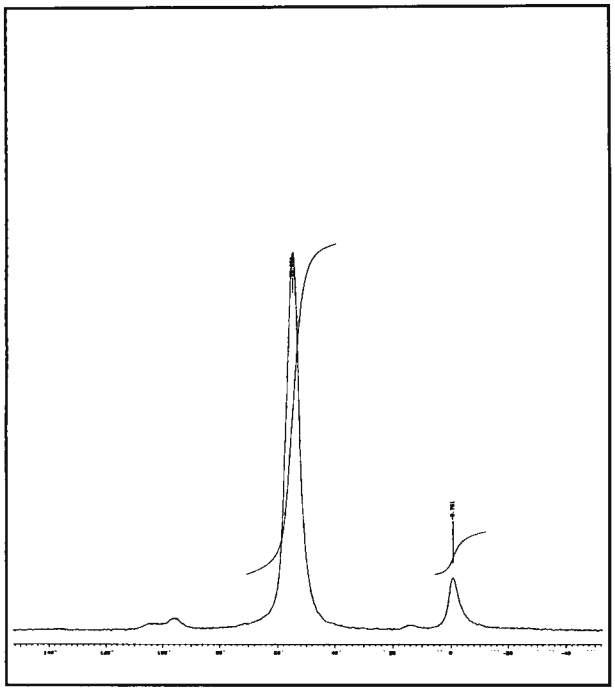

H(550)

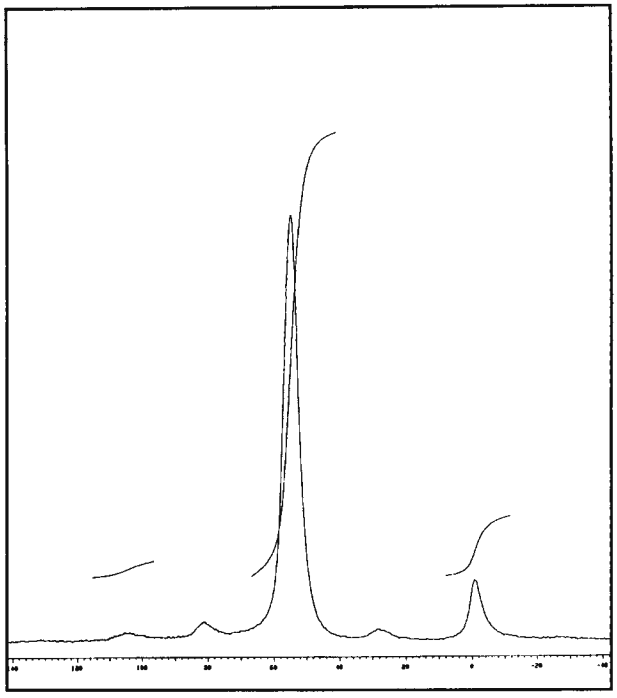

H0

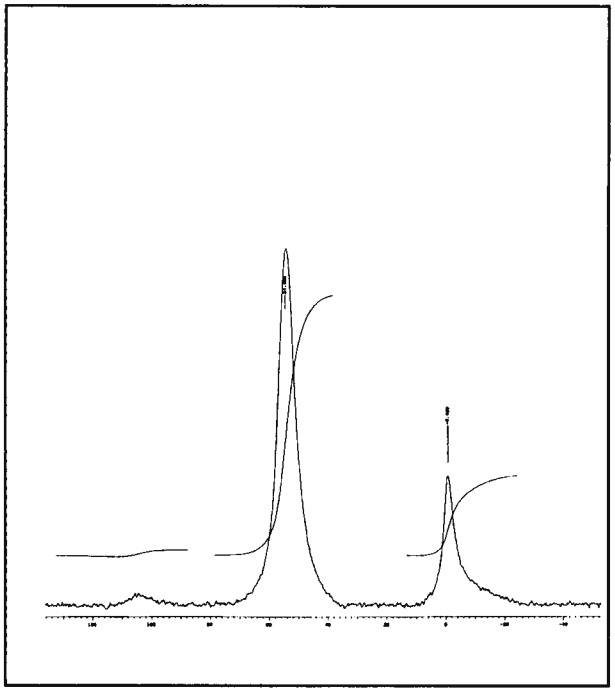

H0.01

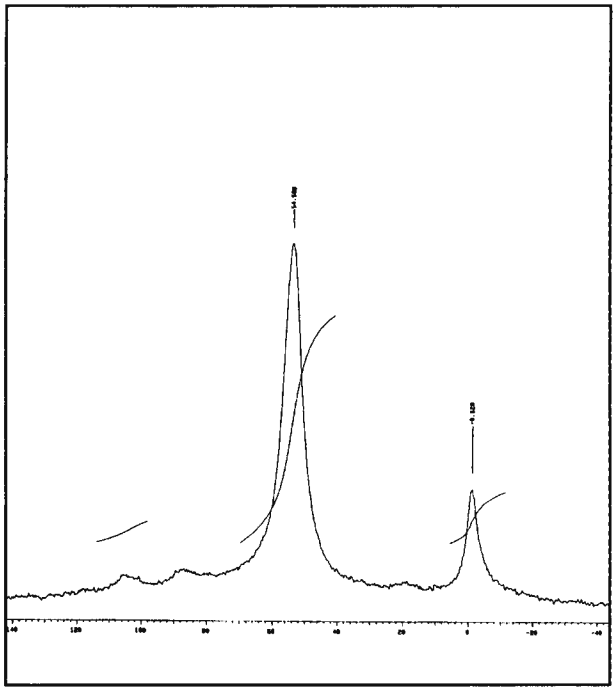

H0.1

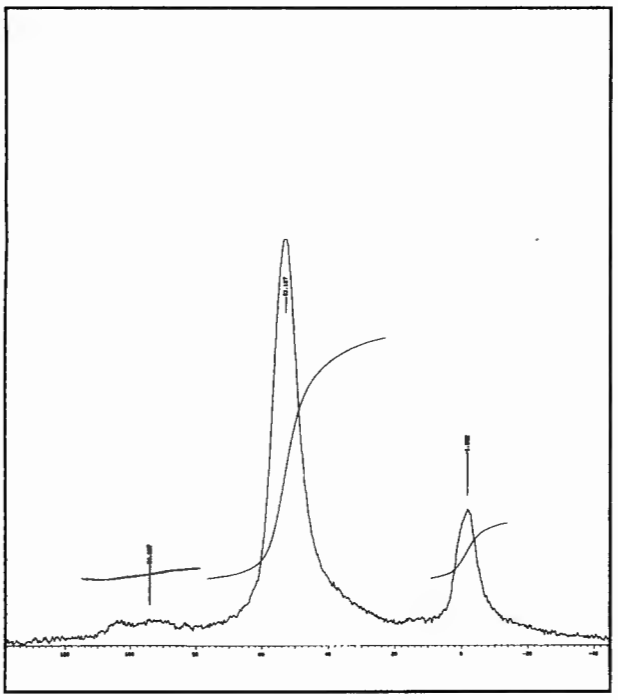

H2

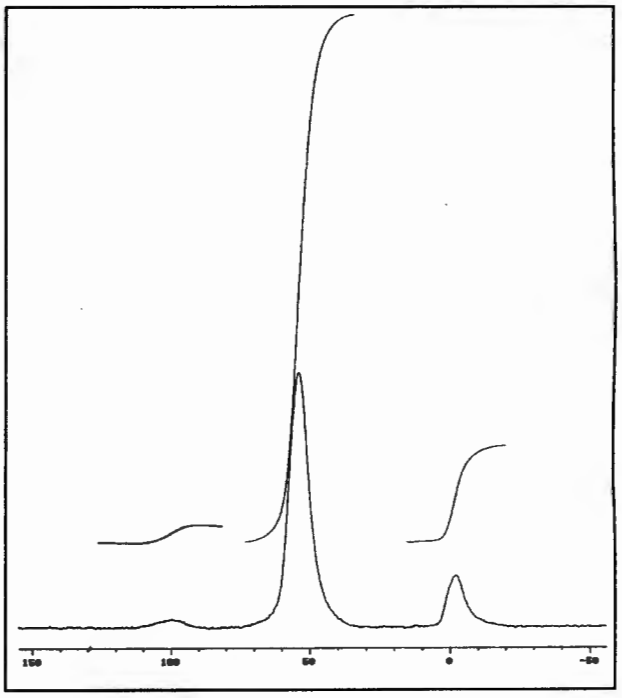

H5

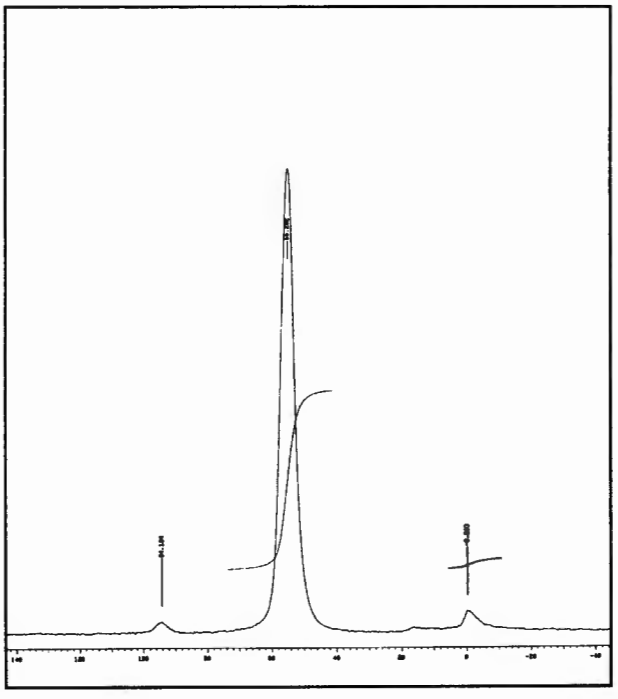

HE

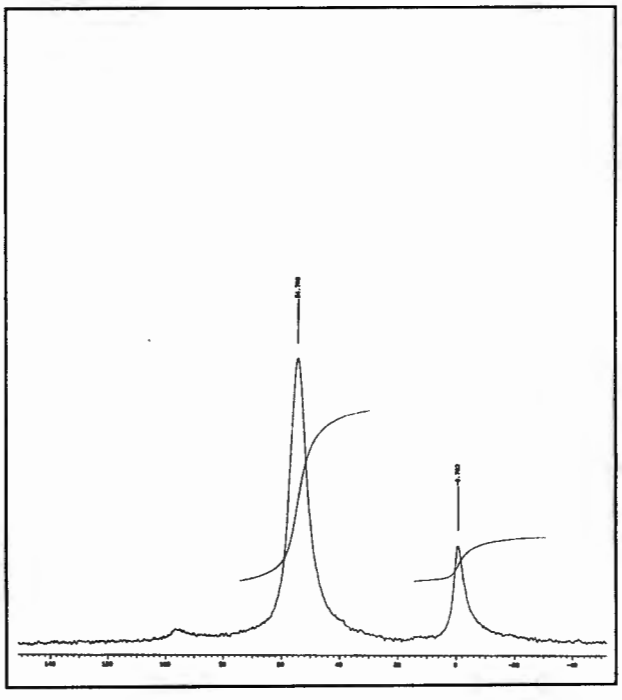

CH

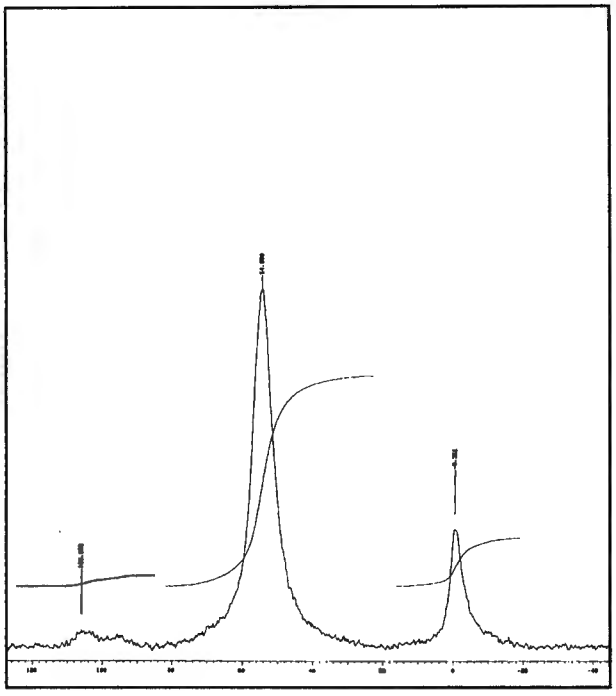

CH0

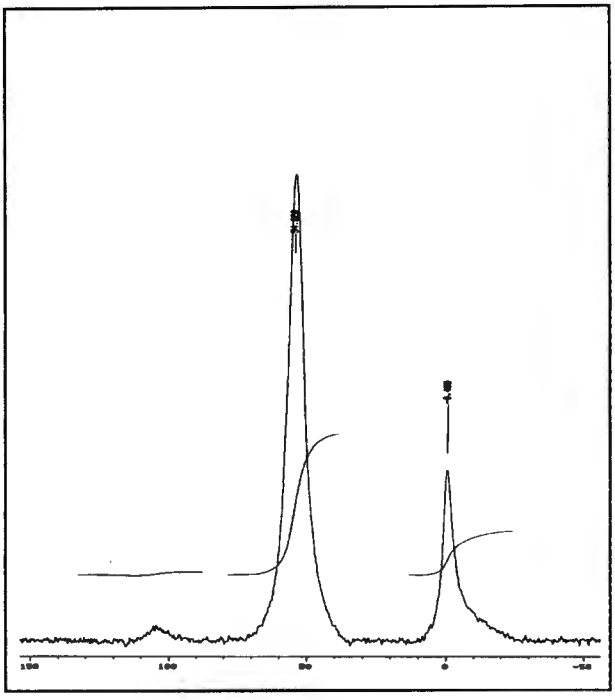

CH0.001

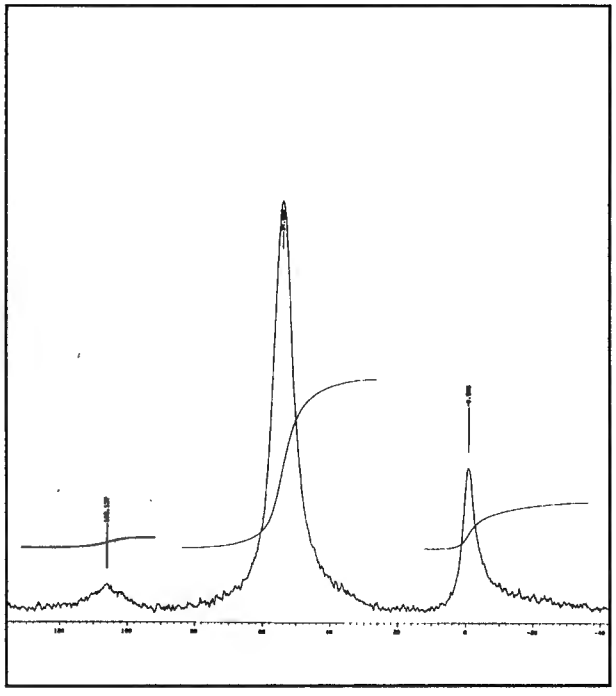

CH0.01

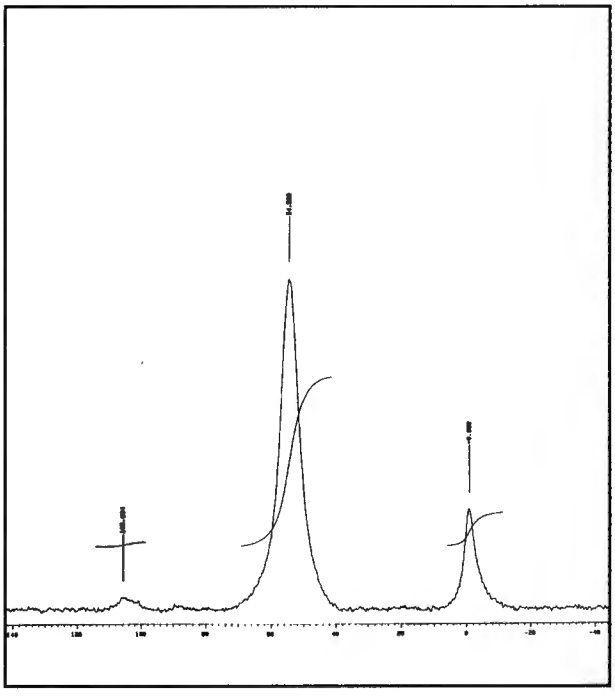

CH0.1

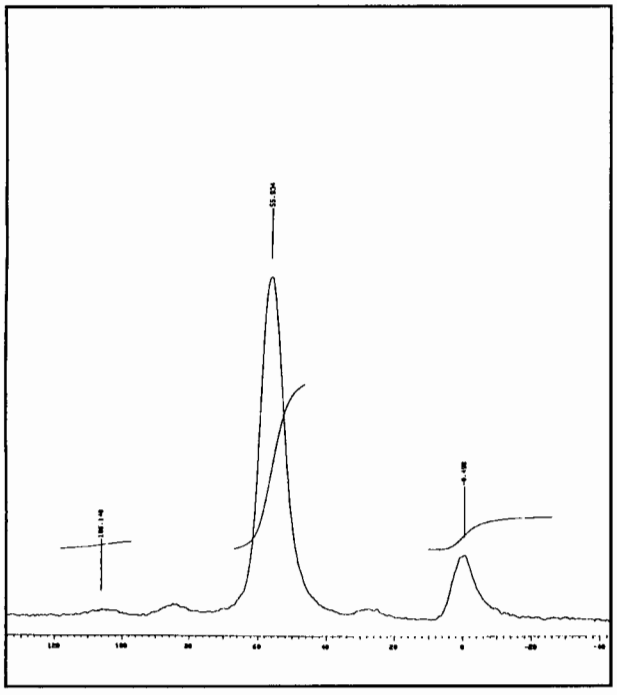

CH1

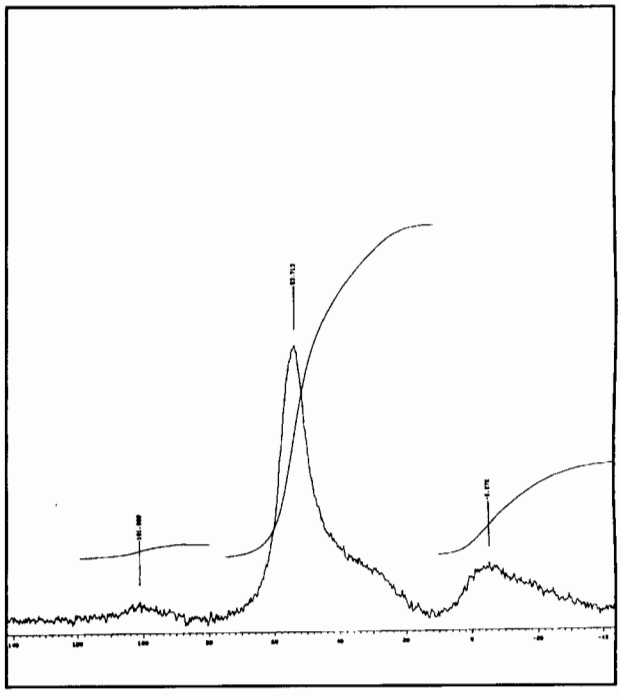

HS

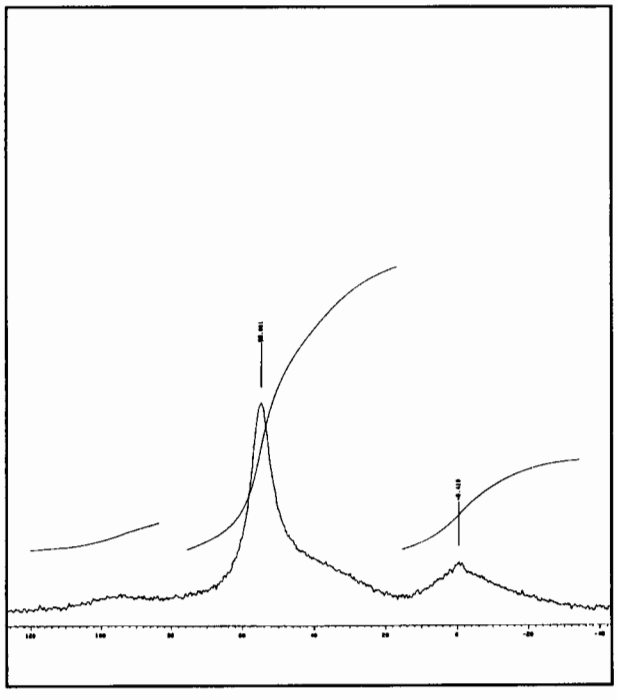

HS0

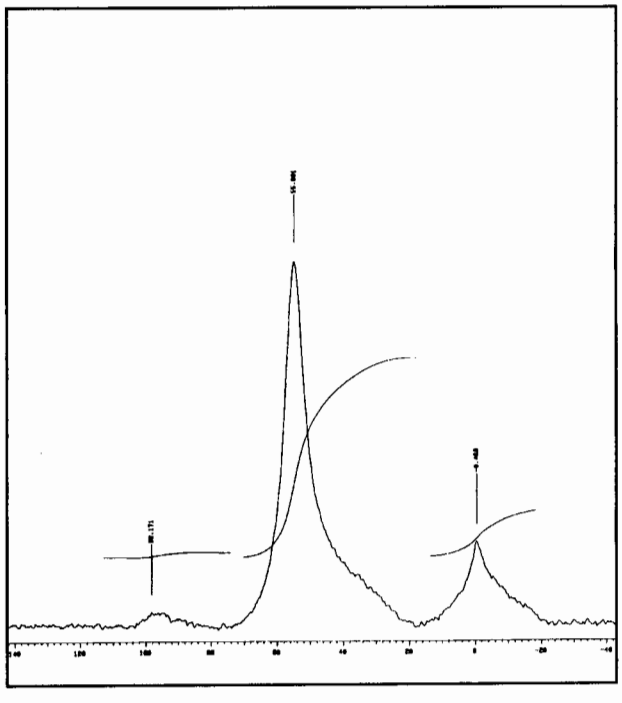

HS0.01

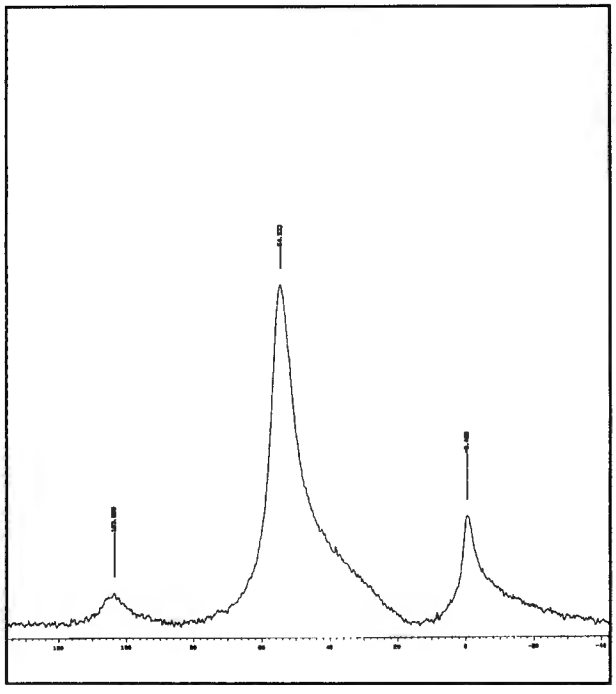

HS0.1

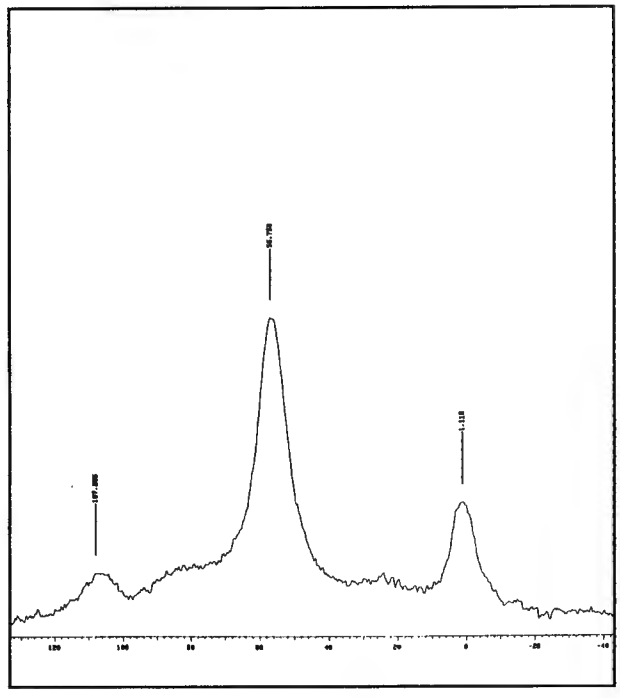

HS1

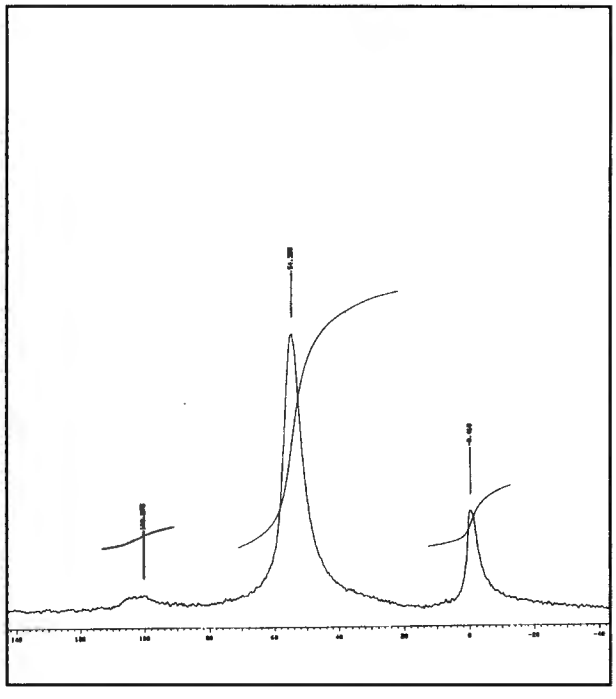

HS2

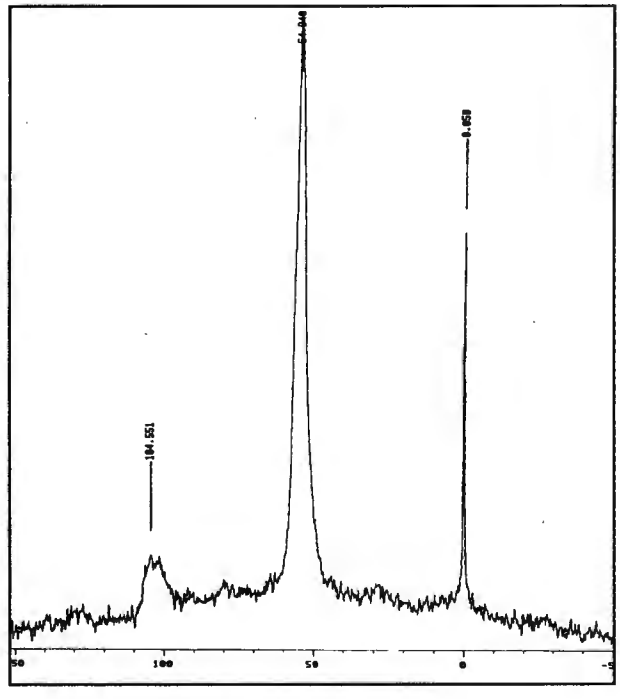

HS10

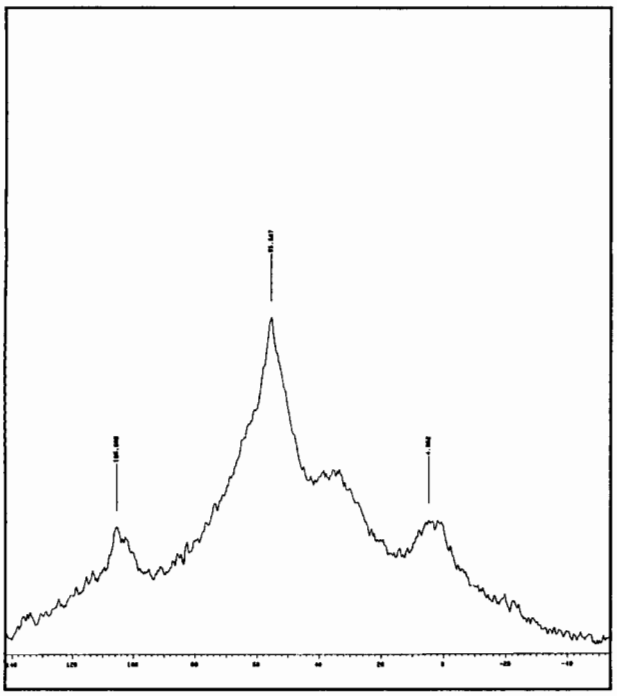

HSS

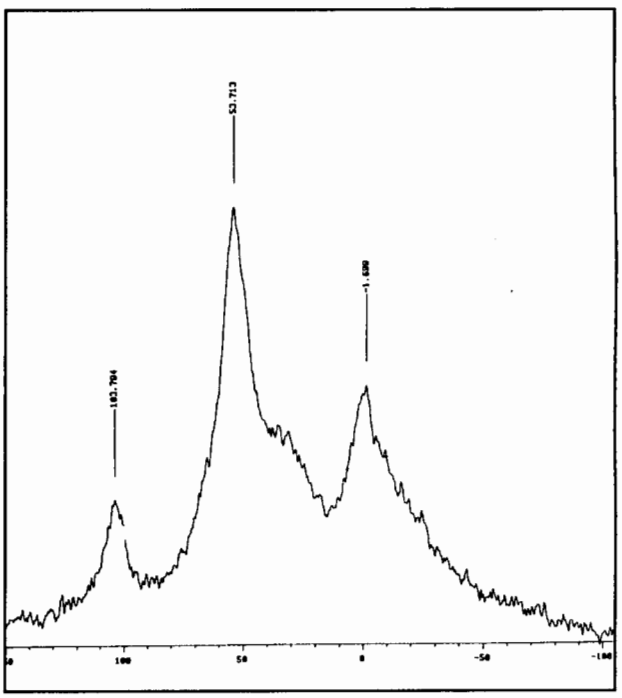

HSS2

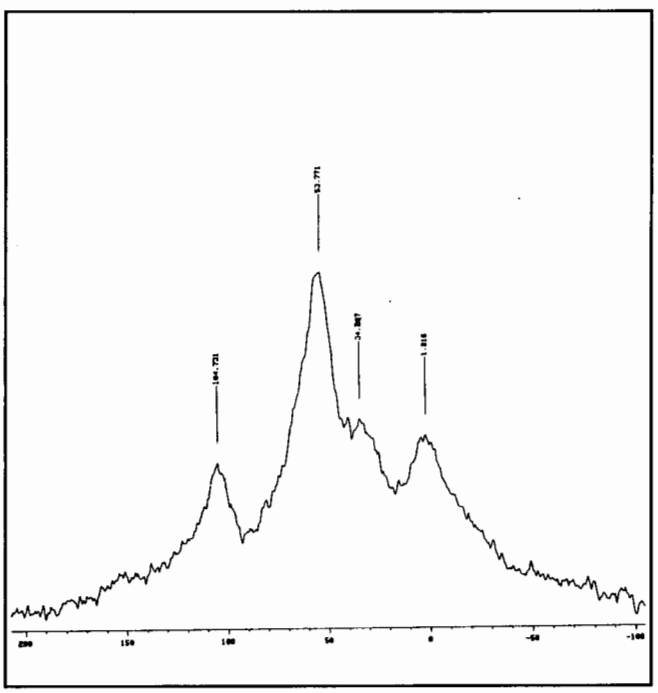

HSS0

APPENDIX IV

Infra-red spectra of catalyst fingerprint region

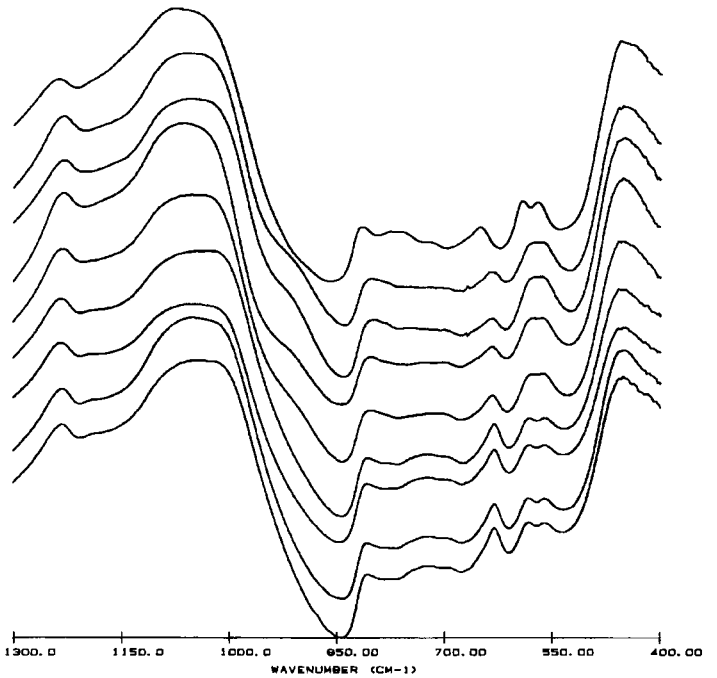

Spectra of acid washed Na-Mordenite: Na (Bottom), Na0, Na0.001, Na0.01, Na0.1, Na1, Na2, Na5 and Na2S (Top)

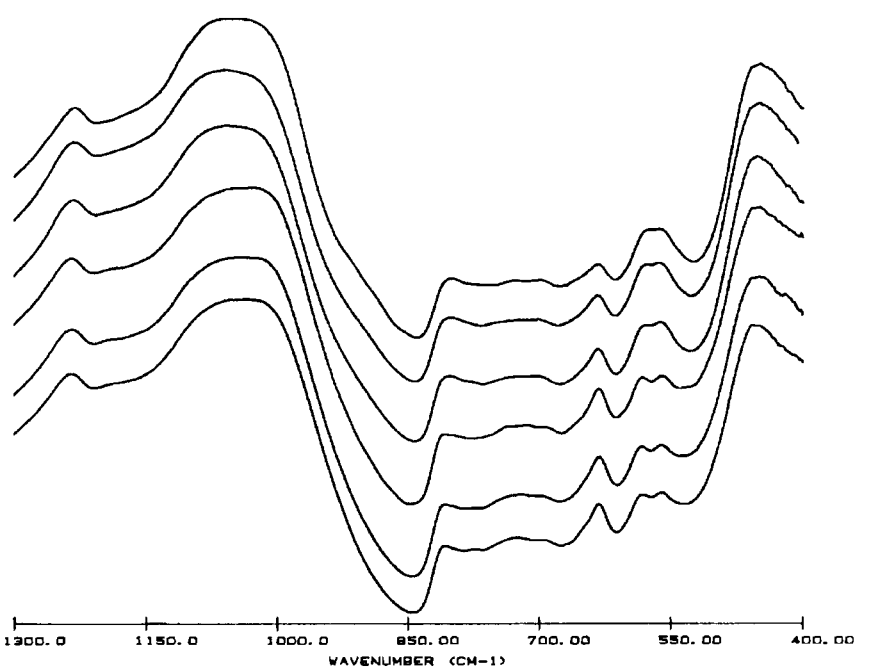

Spectra of steamed and then acid washed Na-Mordenite: NaS (Bottom), NaS0, NaS0.01, NaS0.1, NaS1 and NaS2 (Top)

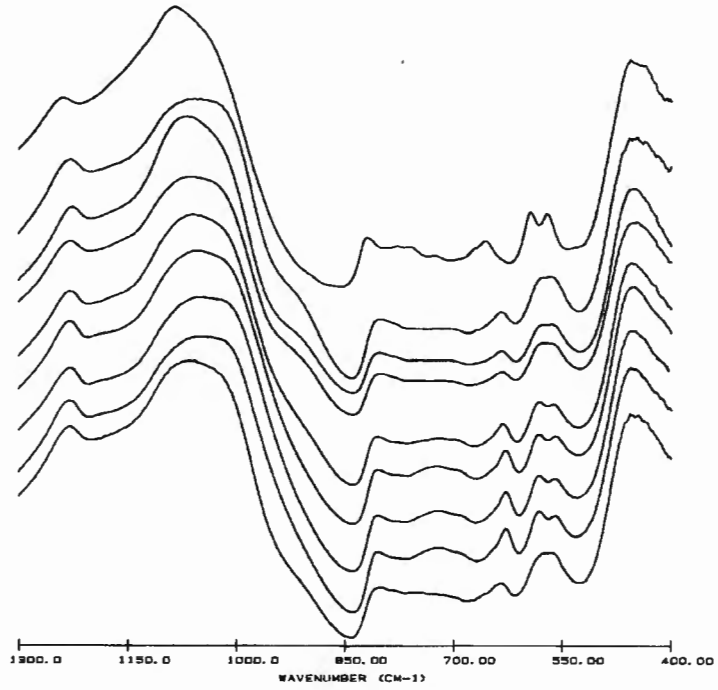

Spectra of acid washed H-Mordenite: H(550) (Bottom), H0, H0.001, H0.01, H0.1, H2, H5, H10 and H2S (Top)

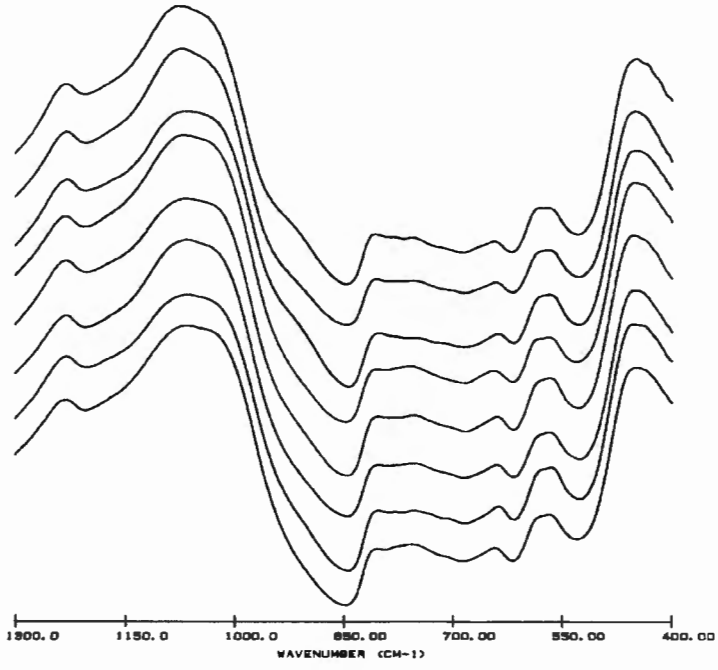

Spectra of deep-bed calcined and then acid washed H-Mordenite: CH (Bottom), CH0, CH0.001, CH0.01, CH0.1, CH1, CH2 and CH5 (Top)

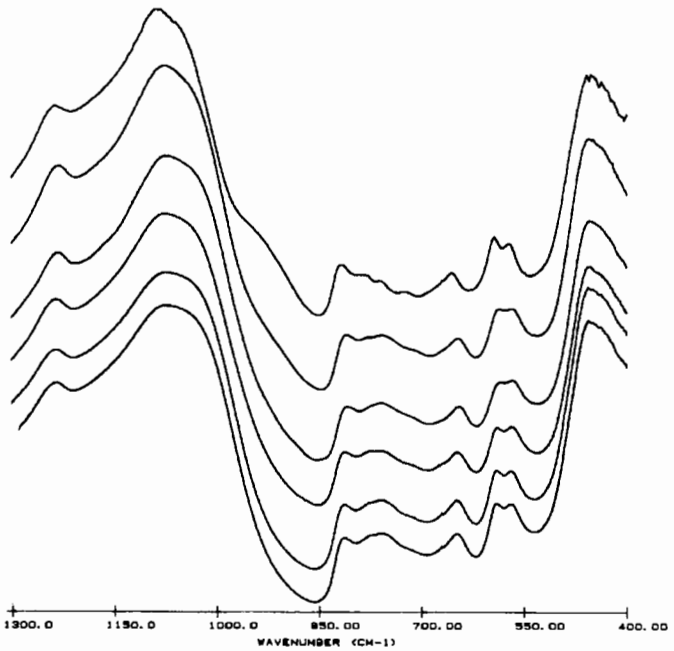

Spectra of mildly steamed and then acid washed H-Mordenite: HS (Bottom), HS0, HS0.01, HS0.1, HS2 and HS5 (Top)

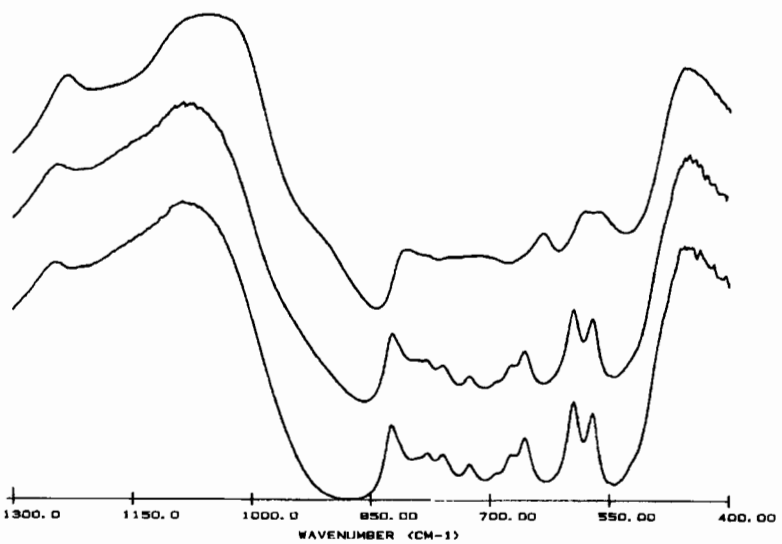

Spectra of severely steamed and EDTA washed H-Mordenite: HSS (Bottom), HSS10 and HE (Top)

APPENDIX V

Response curves of temperature programmed desorption of ammonia

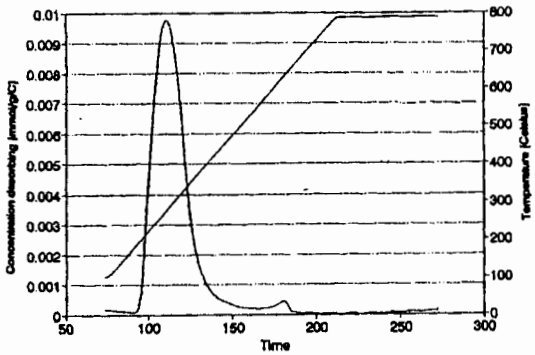

Sample Na

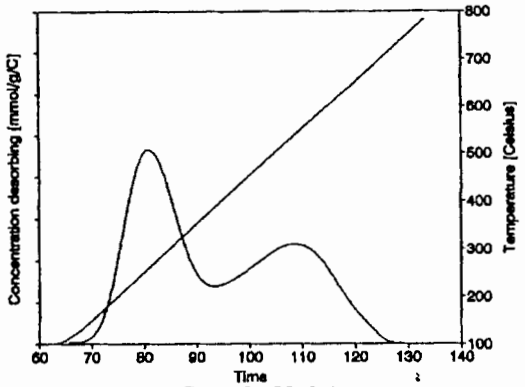

Sample Na0.1

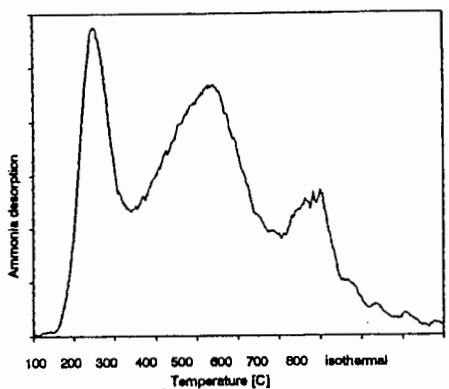

Sample Na1

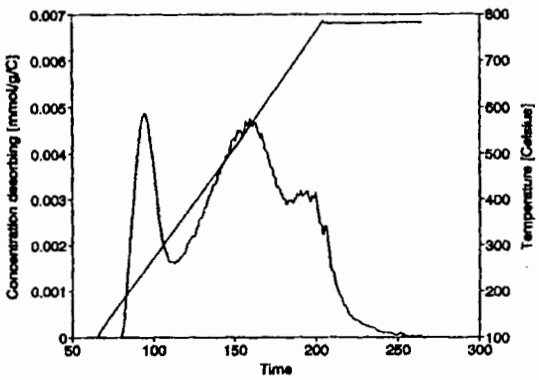

Sample Na5

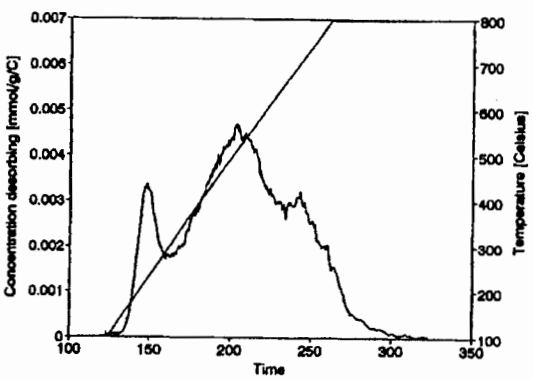

Sample Na10

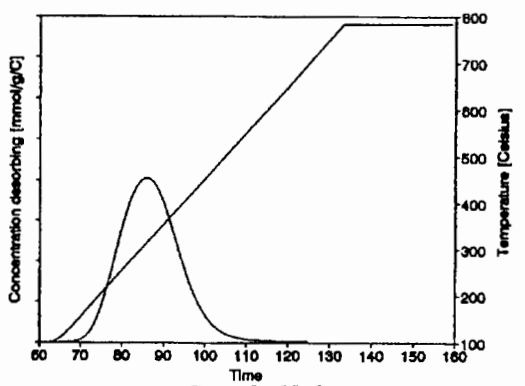

Sample NaS

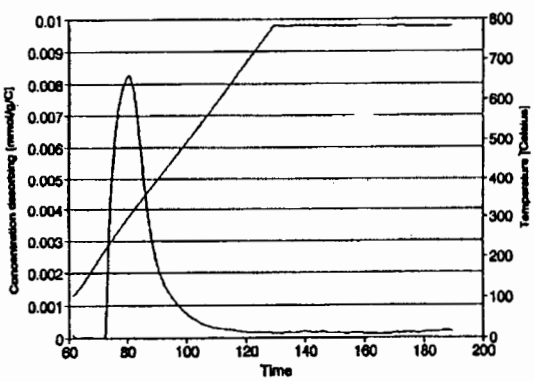

Sample NaS0.01

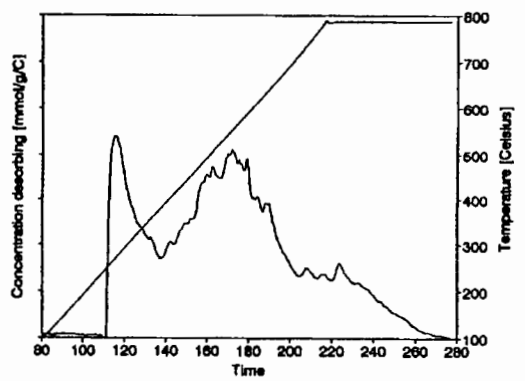

Sample NaS1

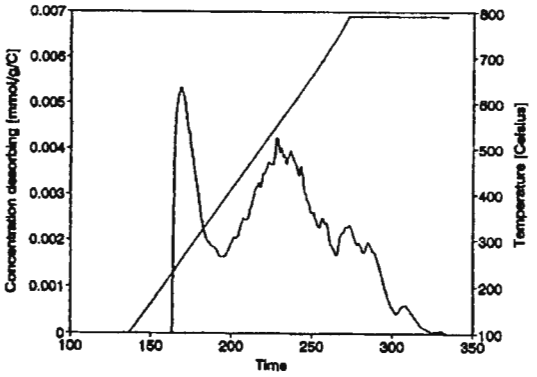

Sample NaS2

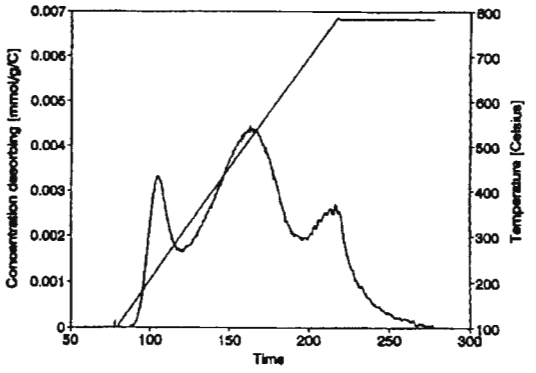

Sample NaS5

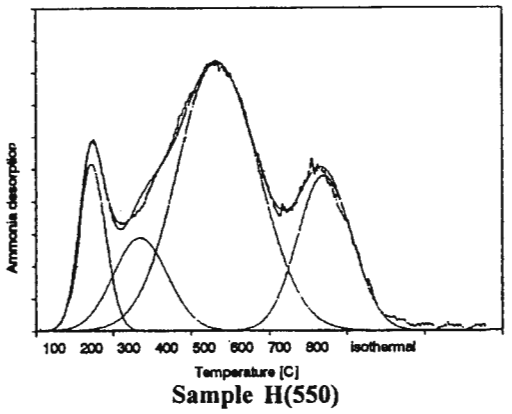

Sample H(550)

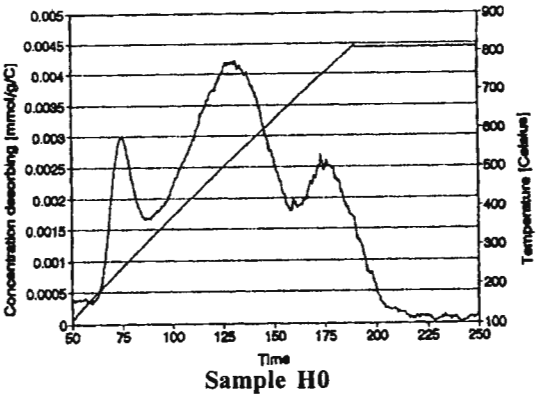

Sample H0

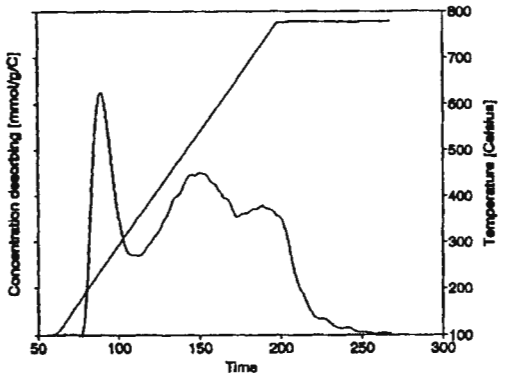

Sample H0.01

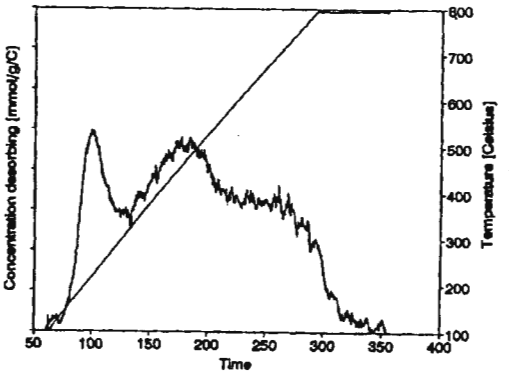

Sample H0.1

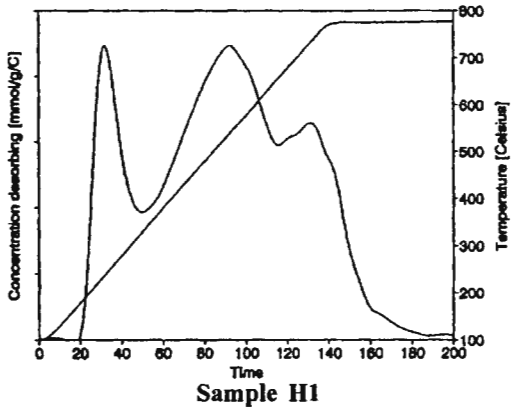

Sample H1

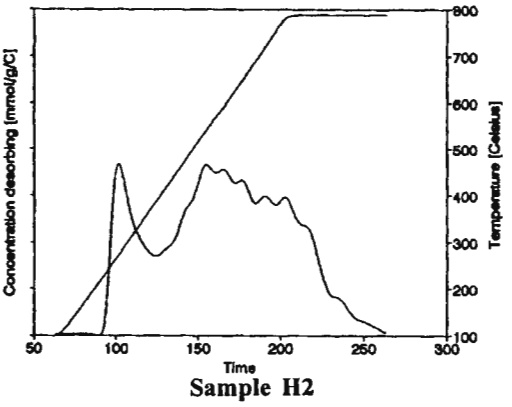

Sample H2

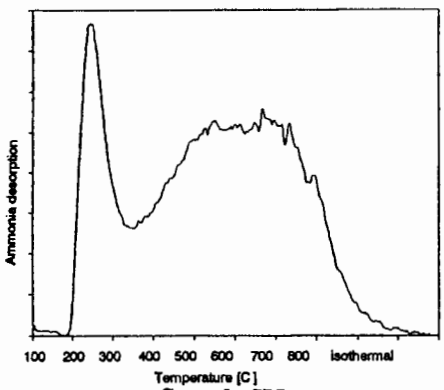

Sample H5

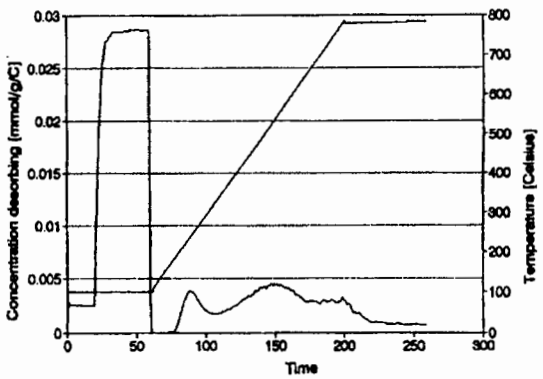

Sample HE

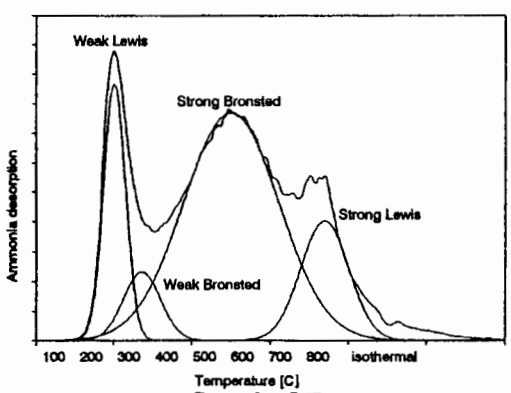

Sample CH

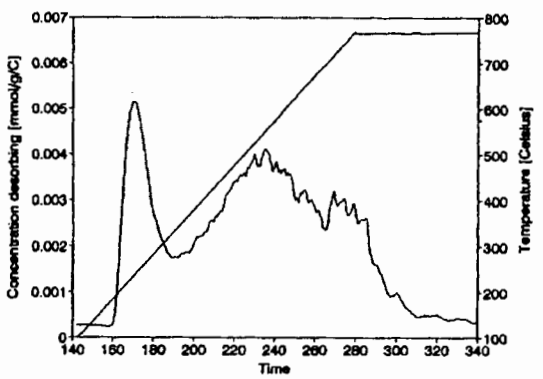

Sample CH0

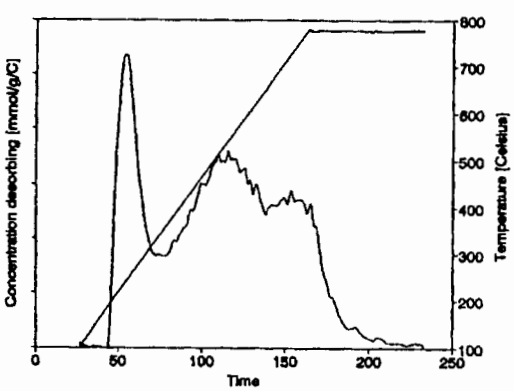

Sample CH0.001

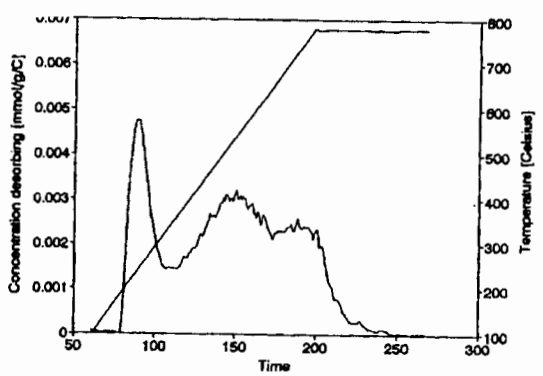

Sample CH0.01

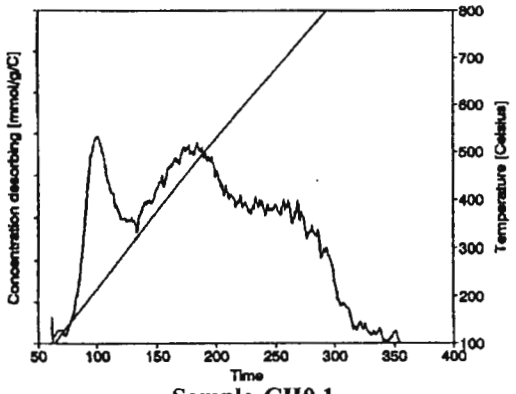

Sample CH0.1

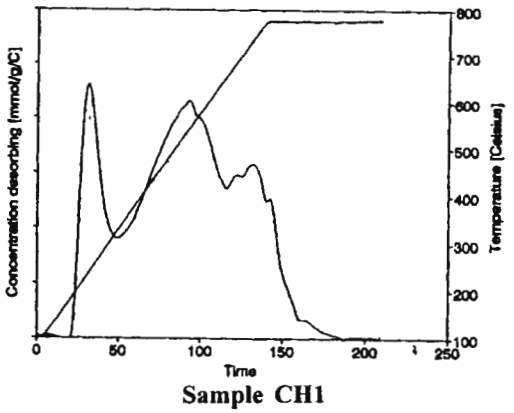

Sample CH1

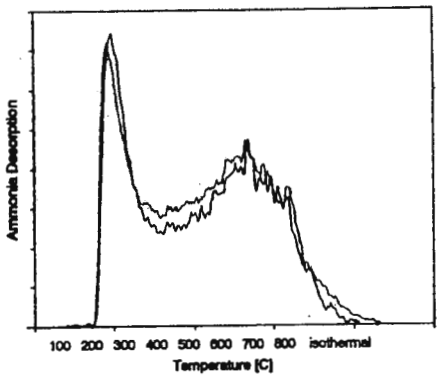

Sample HS

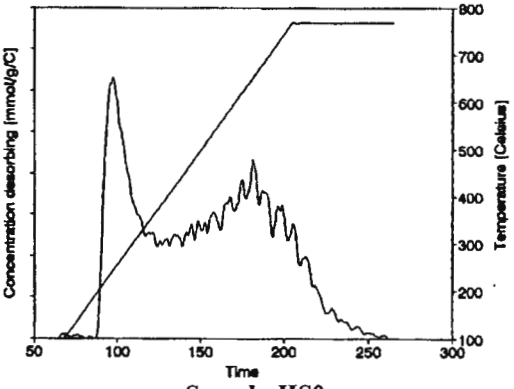

Sample HS0

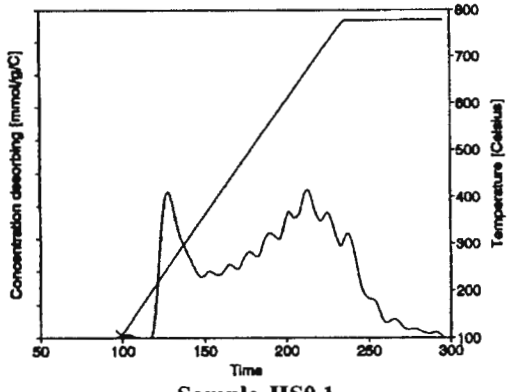

Sample HS0.1

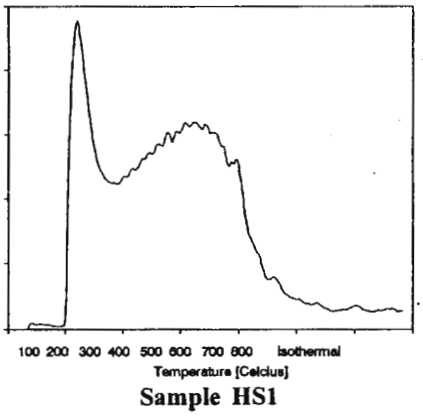

Sample HS1

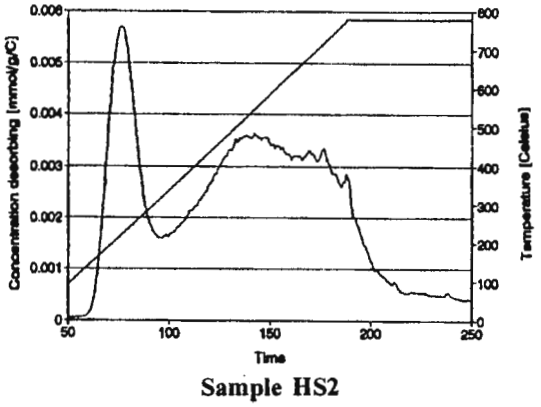

Sample HS2

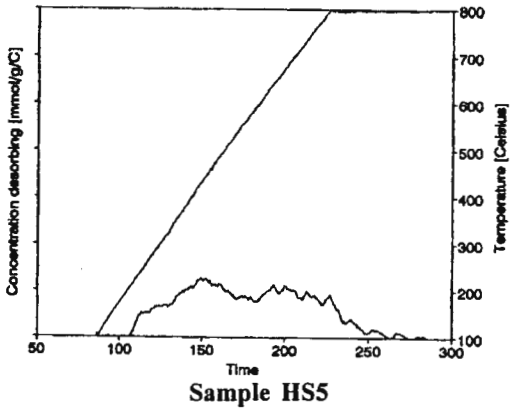

Sample HS5

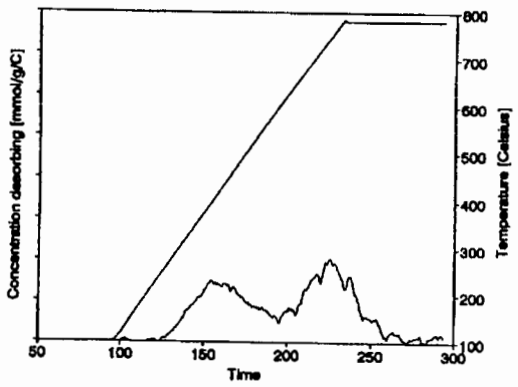

Sample HS10

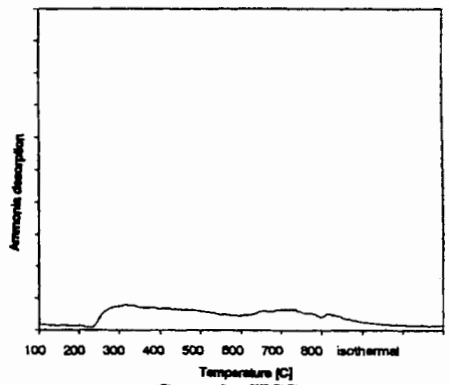

Sample HSS

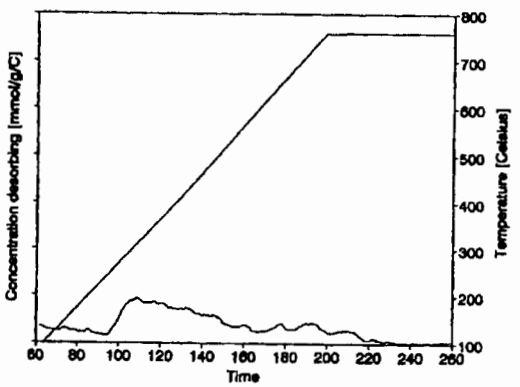

Sample HSS0

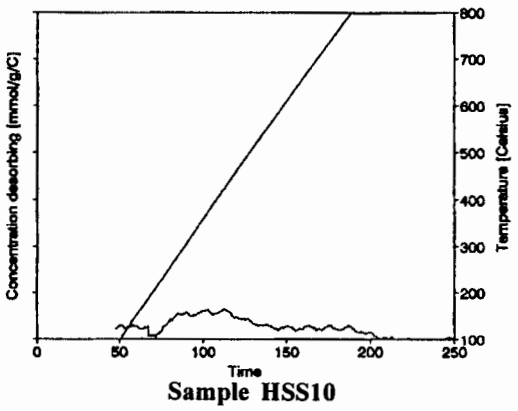

Sample HSS10

APPENDIX VI

Infra-red spectra of pyridine desorption

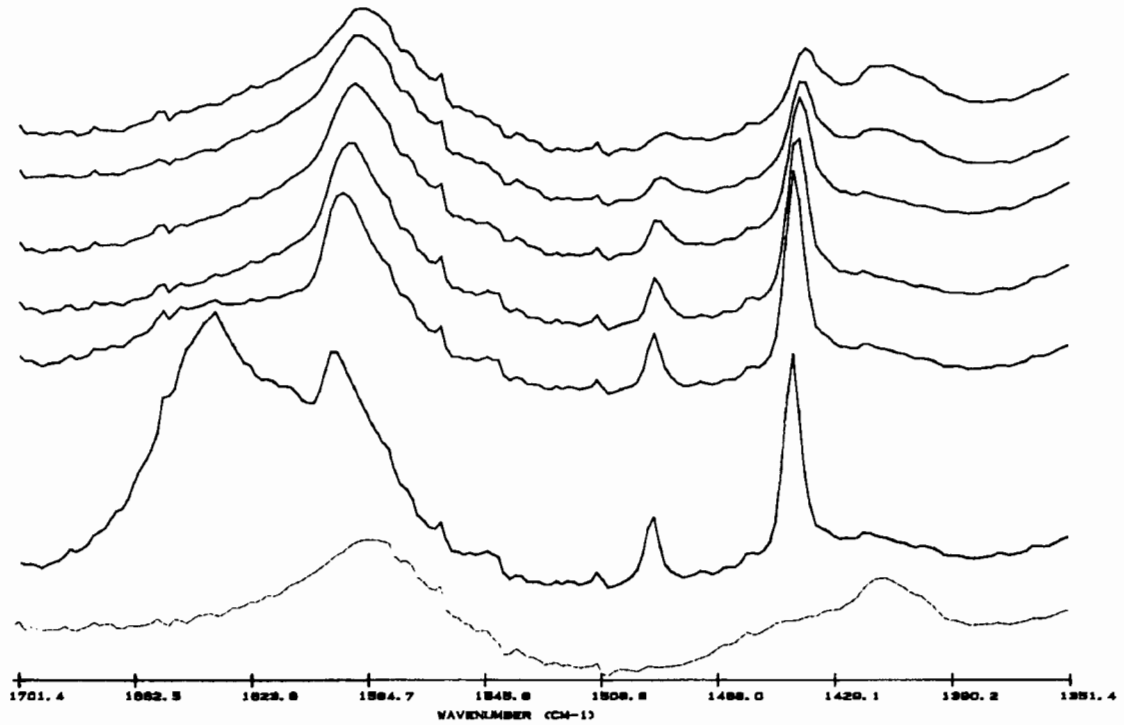

Sample Na: Base (Bottom) and pyridine adsorbed at 100, 200, 300, 400, 500 and 590°C (Top)

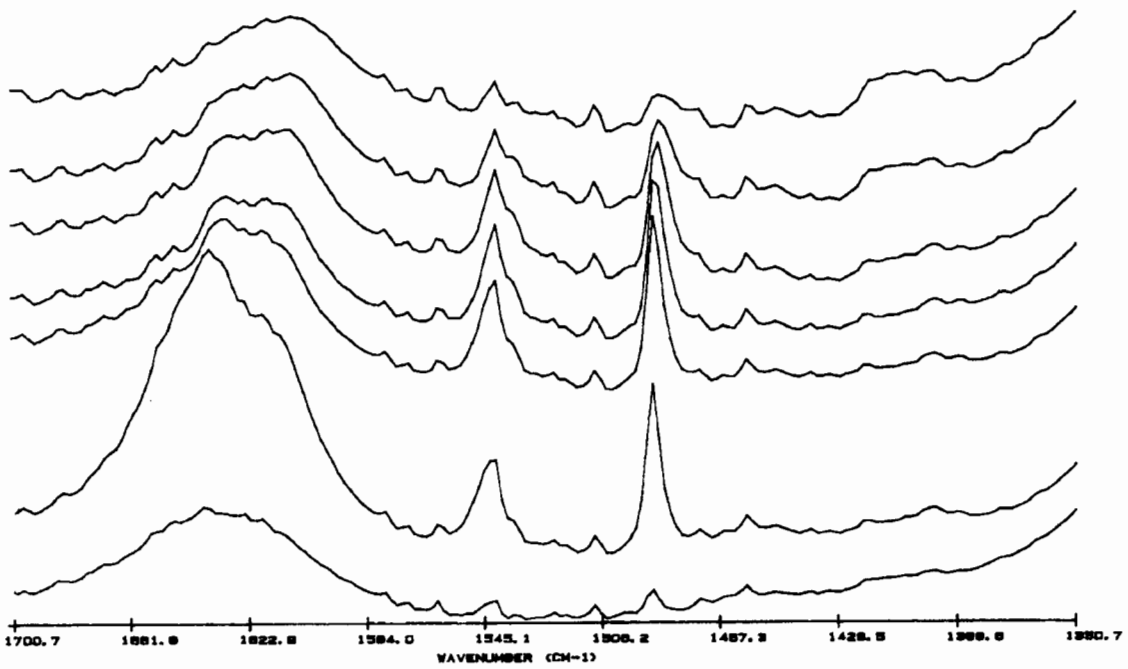

Sample Na0.1: Base (Bottom) and pyridine adsorbed at 100, 200, 300, 400, 500 and 600°C (Top)

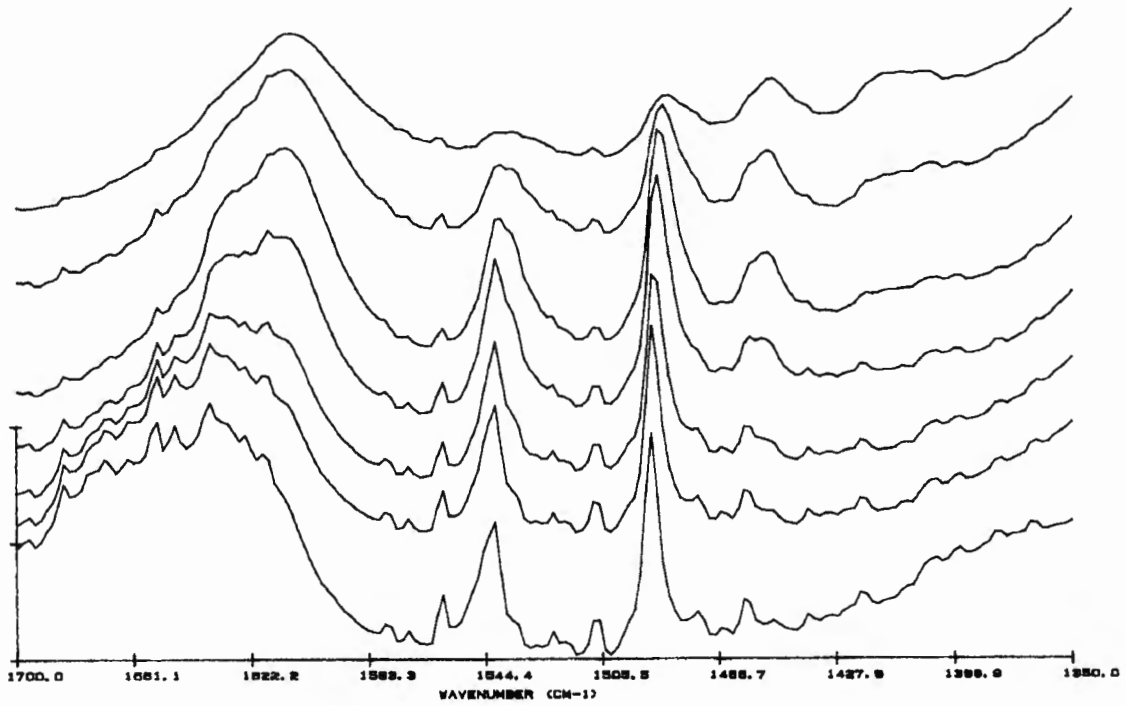

Sample H(550): Pyridine adsorbed at 100 (Bottom), 200, 300, 400, 500, 600 and 650°C (Top)

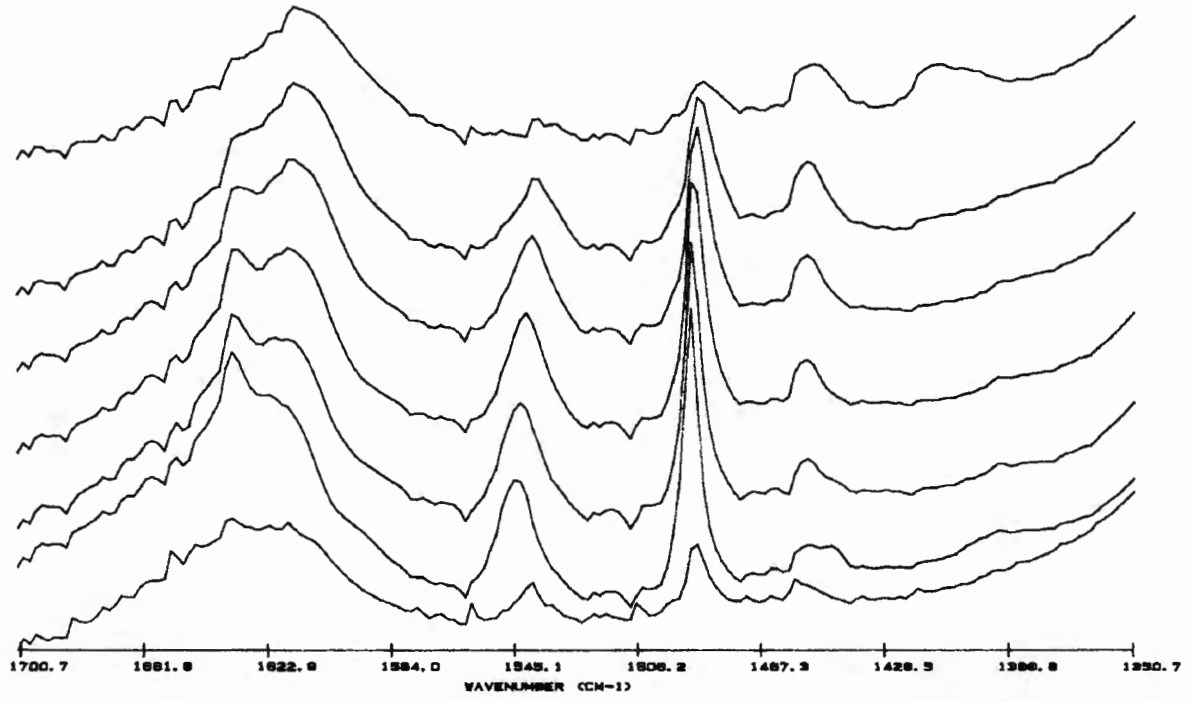

Sample H2: Base (Bottom) and pyridine adsorbed at 100, 200, 300, 400, 500 and 650°C (Top)

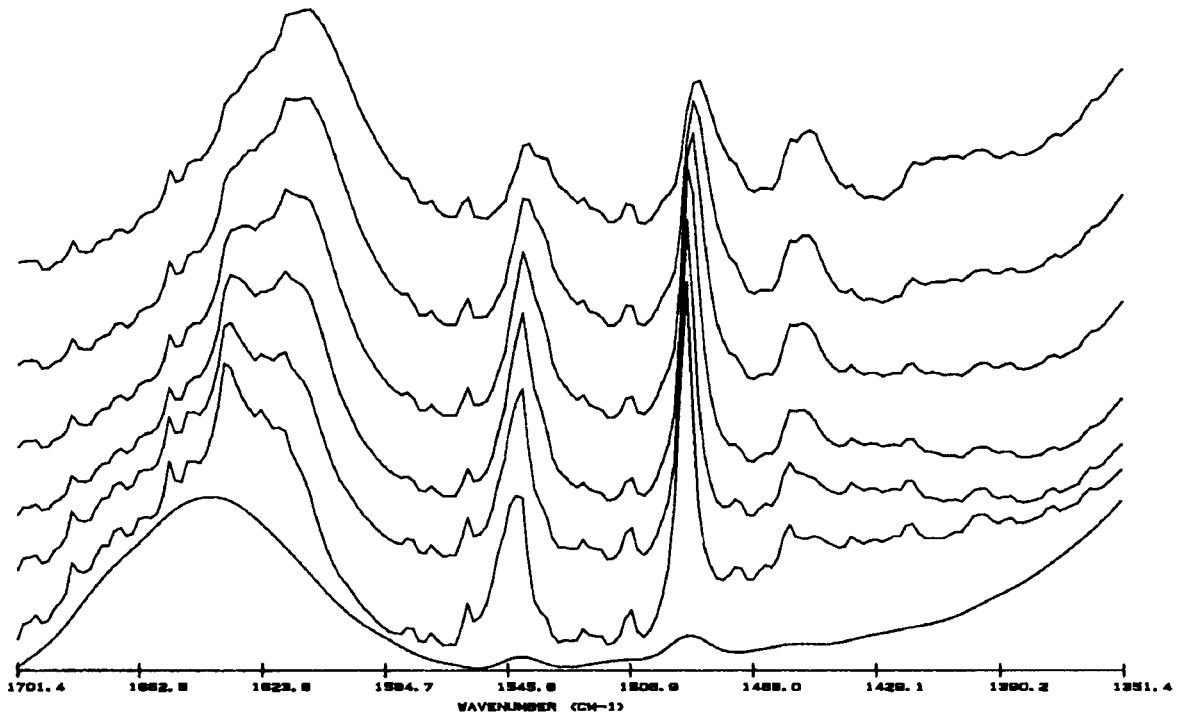

Sample CH: Base (Bottom) and pyridine adsorbed at 100, 200, 300, 400, 500 and 6060°C (Top)

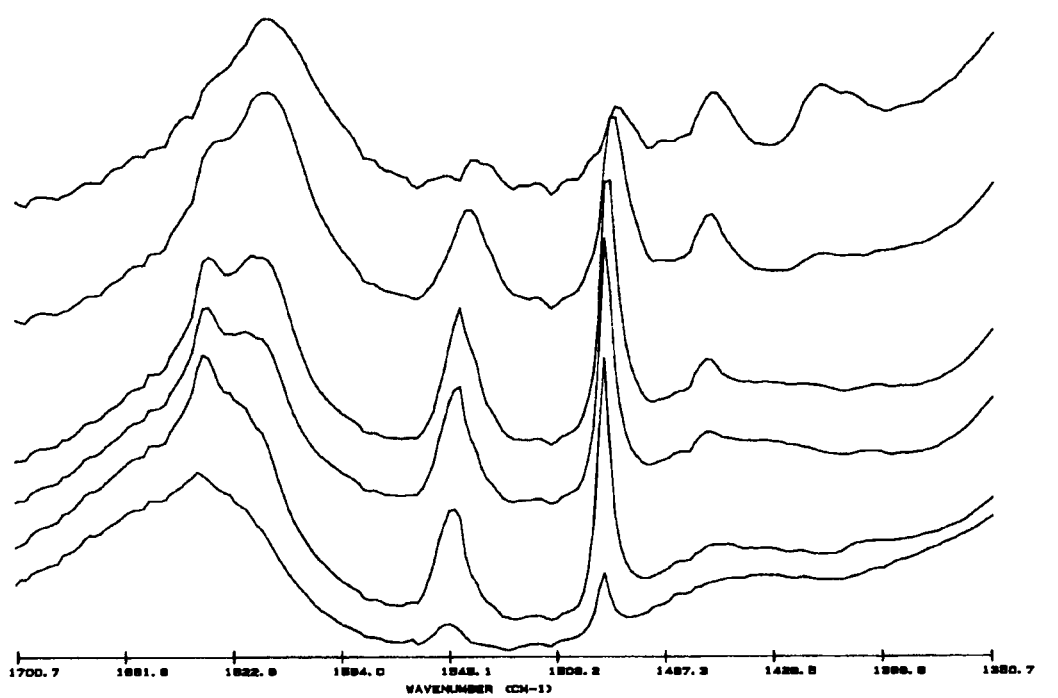

Sample CH0: Base (Bottom) and pyridine adsorbed at 100, 200, 300, 400, 500 and 650°C (Top)

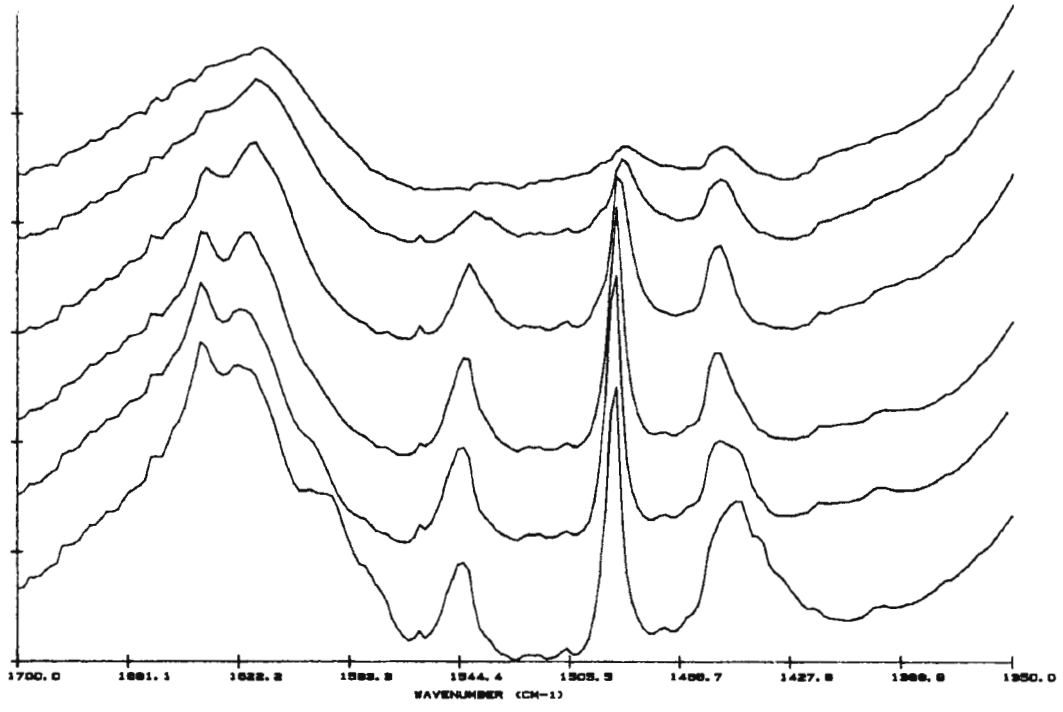

Sample HS: Pyridine adsorbed at 100 (Bottom), 200, 300, 400, 500 and 600°C (Top)

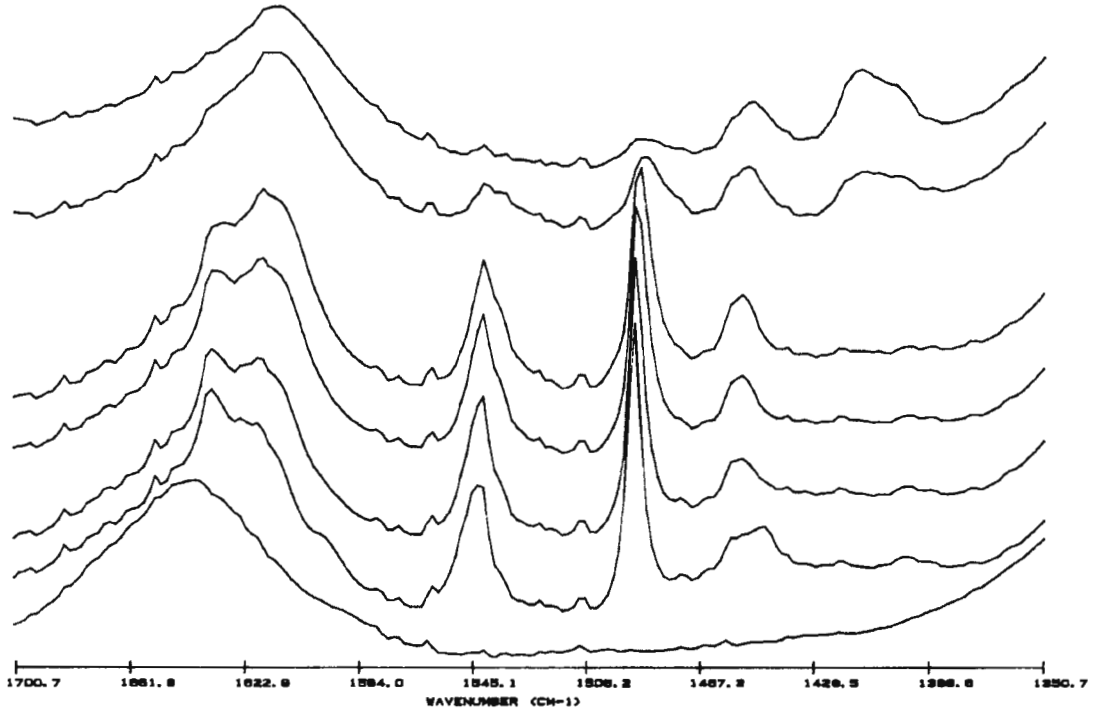

Sample HS1: Base (Bottom) and pyridine adsorbed at 100, 200, 300, 400, 600 and 700°C (Top)

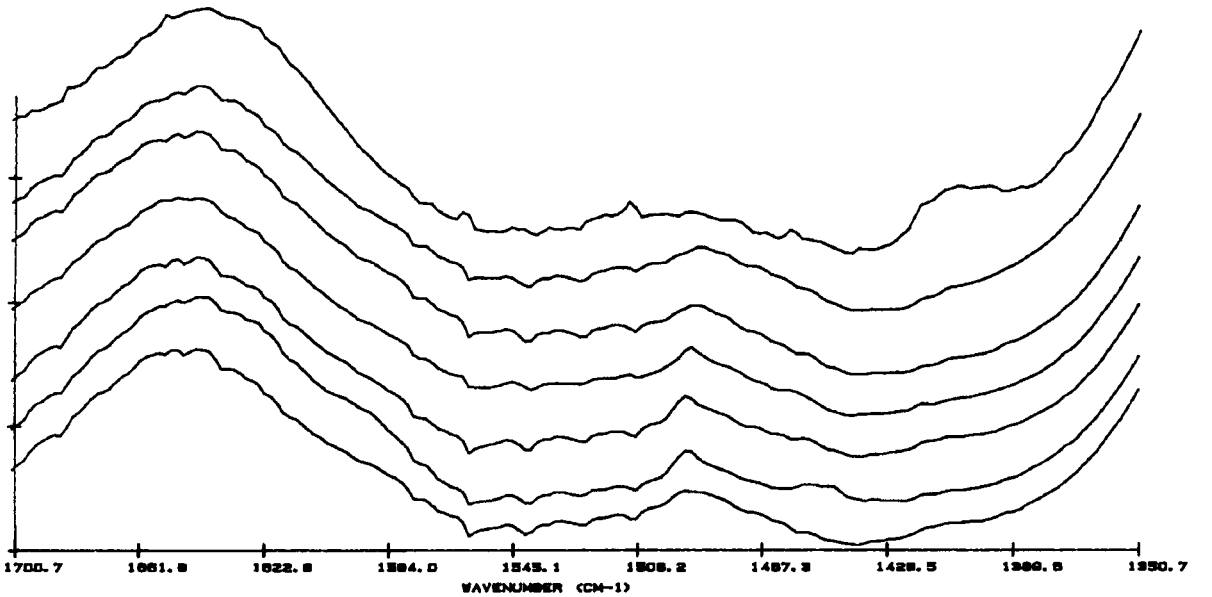

Sample HSS: Base (Bottom) and pyridine adsorbed at 100, 200, 300, 400, 500 and 525°C (Top)

APPENDIX VII

Sample calculation for conversion and selectivity of isobutane cracking

Conversion rates reported refer to the conversion of isobutane based on carbon number. As was specified in Chapter 3, intial conversion rates were determined using an empirical equation with three variables. Product selectivities varied slightly as the catalyst deactivated and the selectivities are reported at initial conditions (i.e. those observed at the first data point), usually after ninety seconds.

A typical product spectrum (that of the isobutane cracking reaction over sample HS after two minutes online) is shown below:

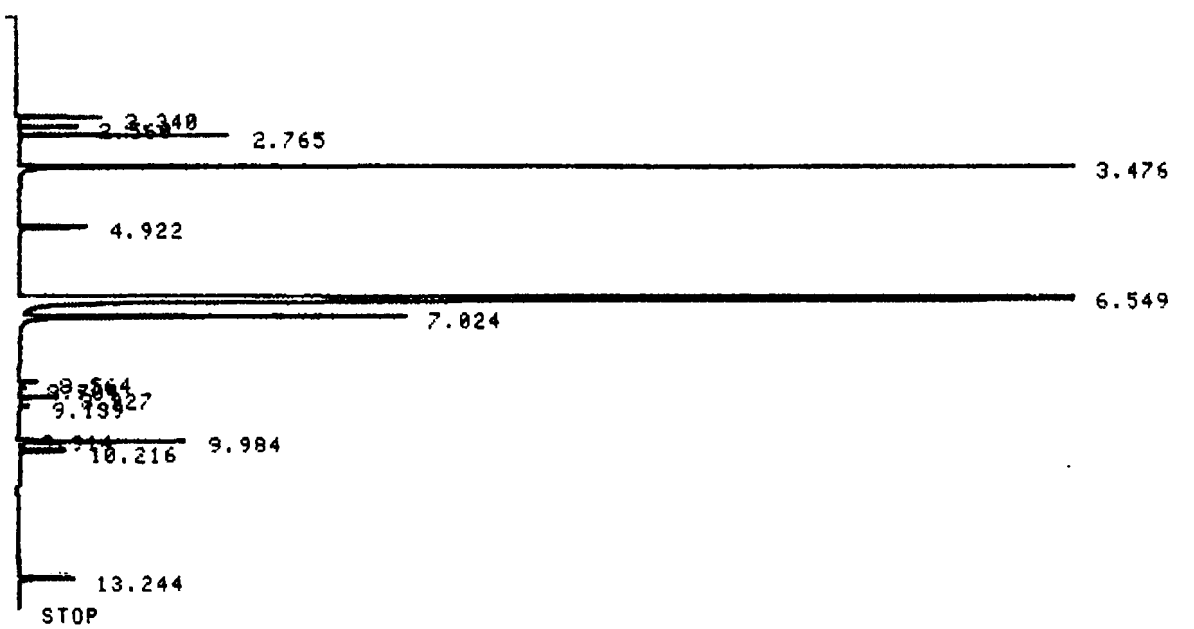

Peak allocations based on observed retention times with corresponding area counts and response factors are shown in Table VII.1

Table VII.1 Example of calculated flowrates of components in product stream

Time [min]	Component	Area	Response Factor [Mass basis]	Carbon Number	Flowrate [mmol.hr^{-1}.g^{-1}]
2.34	Methane	29847	0.9656	1	1.560
2.56	Ethane	10378	0.9915	2	0.279
2.77	Ethene	90565	1.0506	2	2.577
3.48	Propane	730415	1.0030	3	13.223
4.92	Propene	85626	1.0136	3	1.566
6.55	i-Butane	2393241	0.9583	4	31.048
7.02	n-Butane	277931	1.0675	4	4.016
8.56	t-2-Butene	16164	0.9692	4	0.2123
8.70	1-Butene	9918	1.0664	4	0.1430
8.92	Isobutene	34613	0.9877	4	0.4629
9.14	c-2-Butene	26002	1.0597	4	0.373
9.90	Pentanes	136337	0.9954	5	1.470
13.24	n-Hexane	59615	1.0000	6	0.538

n-Hexane was used as an internal standard to perform a mass-balance. No hexane products were observed for the reaction.

The relative product flow rates (F_n) were calculated based on the known flowrate of n-hexane (F_{is}) and their relative response factors (RF_n and RF_{is}). The term M_n refers to the molar mass of the particular molecule *n*.

$$F_n = \frac{F_{is}\ M_{is}\ A_n\ RF_n}{M_n\ A_{is}\ RF_{is}}$$

A carbon mass balance was then performed by comparing the flow of carbon in isobutane fed to the reactor to the carbon in the product stream.

$$F_{i\text{-}C_4\ feed}\ C_{i\text{-}C_4} \approx \sum_{n=C_1}^{C_5} F_{n\ product}\ C_n$$

In the example in Table VII.1, the left side of the equation is known to be 0.070 $C_{atoms}.hr^{-1}$ and the right side calculated to be 0.068 $C_{atoms}.hr^{-1}$, giving an error of 98%. Mass balances of greater than 95% were considered prerequisites for a valid analysis. The conversion rate for each analysis was then determined by:

$$r = \frac{\Delta F_{i-C_4}}{W}$$

Values of r and t were then fitted to the empirical equation

$$r = \frac{r_o}{1 + bt^n}$$

by least squares optimisation taking into account a dead time of 1.5 min between reactor and sample port. The initial conversion rate (r_o) was thus calculated.

Selectivities to each product were calculated on a carbon basis. This was to esure that the selectivity calculated for each product represented the amount of isobutane converted to that product.

$$S_n = \frac{F_n \, C_n}{\sum_{i=CH_4}^{C_5} F_i \, C_i}$$

To calculate Sw, the values of $S_{METHANE}$, $S_{PROPENE}$ and $S_{BUTENES}$ were summed.

APPENDIX VIII

Reaction data for isobutane cracking

Sample	Na					
Time	[min]	1.50	21.40	86.50	103.51	119.88
Rate	[mol/g/hr]	0.0	0.0	0.0	0.0	0.0
Model	[mol/g/hr]	0.0	0.0	0.0	0.0	0.0
Conversion	[%]	0.9	1.1	0.9	1.0	0.6
Selectivity (w)	[%]	8.3	42.1	1.3	8.7	10.7
Product flow	[mmol/g/hr]					
	Methane	0.003	0.002	0.002	0.002	0.004
	Ethane	0.000	0.000	0.000	0.000	0.000
	Ethene	0.000	0.000	0.000	0.000	0.000
	Propane	0.006	0.005	0.014	0.015	0.019
	Propene	0.000	0.000	0.000	0.000	0.000
	Isobutane	44.254	44.135	42.468	44.719	43.811
	n-Butane	0.024	0.016	0.048	0.055	0.069
	t-2-Butene	0.000	0.000	0.000	0.000	0.000
	1-Butene	0.000	0.000	0.000	0.000	0.000
	Isobutene	0.032	0.099	0.003	0.039	0.025
	2-c-Butene	0.000	0.103	0.000	0.000	0.000
	Pentanes	0.357	0.260	0.329	0.355	0.154
	Hexane	0.341	0.341	0.341	0.341	0.341
Carbon Balance	[%]	101.0	100.9	96.9	102.2	99.7

Sample	Na0.001							
Time	[min]	2.00	19.97	52.68	68.28	84.65	100.28	115.90
Rate	[mol/g/hr]	0.0	0.0	0.0	0.0	0.0	0.0	0.0
Model	[mol/g/hr]	0.0	0.0	0.0	0.0	0.0	0.0	0.0
Conversion	[%]	1.2	1.9	1.3	1.5	0.6	0.3	0.2
Selectivity (w)	[%]	0.0	41.9	0.7	8.4	10.7	17.1	19.1
Product flow	[mmol/g/hr]							
	Methane	0.000	0.000	0.000	0.000	0.004	0.000	0.000
	Ethane	0.000	0.000	0.000	0.000	0.000	0.000	0.000
	Ethene	0.000	0.000	0.000	0.000	0.000	0.000	0.000
	Propane	0.000	0.008	0.022	0.023	0.019	0.025	0.017
	Propene	0.000	0.000	0.000	0.000	0.000	0.000	0.000
	Isobutane	41.583	43.591	44.225	45.126	43.811	43.419	42.313
	n-Butane	0.000	0.028	0.073	0.084	0.069	0.058	0.052
	t-2-Butene	0.000	0.000	0.000	0.000	0.000	0.000	0.000
	1-Butene	0.000	0.000	0.000	0.000	0.000	0.000	0.000
	Isobutene	0.000	0.171	0.005	0.059	0.025	0.021	0.016
	2-c-Butene	0.000	0.177	0.000	0.000	0.000	0.000	0.000
	Pentanes	0.466	0.446	0.505	0.543	0.154	0.020	0.000
	Hexane	0.341	0.341	0.341	0.341	0.341	0.341	0.341
Carbon Balance	[%]	100.0	100.0	100.0	100.0	100.0	100.0	100.0

Sample	Na0.01							
Time	[min]	13.95	45.35	63.97	82.23	0.00	0.00	0.00
Rate	[mol/g/hr]	0.2	0.2	0.2	0.2	0.0	0.0	0.0
Model	[mol/g/hr]	0.2	0.2	0.2	0.2	0.0	0.0	0.0
Conversion	[%]	0.4	0.4	0.4	0.4	0.0	0.0	0.0
Selectivity (w)	[%]	63.7	72.1	74.4	77.5	0.0	0.0	0.0
Product flow	[mmol/g/hr]							
	Methane	0.005	0.006	0.007	0.006	0.000	0.000	0.000
	Ethane	0.000	0.000	0.000	0.000	0.000	0.000	0.000
	Ethene	0.000	0.000	0.000	0.000	0.000	0.000	0.000
	Propane	0.024	0.025	0.027	0.028	0.000	0.000	0.000
	Propene	0.024	0.020	0.018	0.021	0.000	0.000	0.000
	Isobutane	66.137	64.340	65.574	68.555	0.000	0.000	0.000
	n-Butane	0.000	0.000	0.000	0.000	0.000	0.000	0.000
	t-2-Butene	0.025	0.026	0.028	0.028	0.000	0.000	0.000
	1-Butene	0.011	0.014	0.014	0.014	0.000	0.000	0.000
	Isobutene	0.102	0.106	0.106	0.109	0.000	0.000	0.000
	2-c-Butene	0.014	0.016	0.018	0.016	0.000	0.000	0.000
	Pentanes	0.079	0.048	0.039	0.028	0.000	0.000	0.000
	Hexane	3.650	3.650	3.650	3.650	0.000	0.000	0.000
Carbon Balance	[%]	99.7	97.0	98.8	103.3	100.0	100.0	100.0

Sample	Na0.1									
Time	[min]	1.50	23.77	49.53	73.52	93.48	118.95	135.28	151.00	166.77
Rate	[mol/g/hr]	9.6	8.9	7.9	7.4	7.0	6.7	6.3	6.2	6.1
Model	[mol/g/hr]	9.6	8.7	8.0	7.4	7.1	6.6	6.4	6.2	6.0
Conversion	[%]	19.0	17.6	15.6	14.7	13.9	13.4	12.6	12.3	12.0
Selectivity (w)	[%]	12.8	12.9	13.4	13.5	13.7	14.2	14.0	14.1	14.1
Product flow	[mmol/g/hr]									
	Methane	0.185	0.170	0.158	0.162	0.158	0.150	0.155	0.151	0.148
	Ethane	0.071	0.062	0.052	0.051	0.046	0.040	0.041	0.039	0.037
	Ethene	0.750	0.666	0.571	0.568	0.540	0.485	0.498	0.467	0.465
	Propane	5.473	4.663	3.838	3.857	3.399	3.043	3.047	2.952	2.832
	Propene	0.801	0.682	0.614	0.610	0.582	0.554	0.554	0.524	0.519
	Isobutane	54.829	52.638	53.592	56.708	58.282	58.153	60.982	60.765	60.809
	n-Butane	3.047	2.875	2.656	2.699	2.637	2.490	2.537	2.506	2.452
	t-2-Butene	0.222	0.203	0.185	0.175	0.173	0.165	0.159	0.164	0.158
	1-Butene	0.080	0.082	0.078	0.078	0.078	0.073	0.075	0.072	0.072
	Isobutene	0.353	0.314	0.294	0.295	0.294	0.288	0.287	0.264	0.277
	2-c-Butene	0.130	0.129	0.122	0.120	0.116	0.112	0.114	0.112	0.111
	Pentanes	1.714	1.430	1.320	1.348	1.349	1.256	1.290	1.227	1.230
	Hexane	3.079	3.079	3.079	3.079	3.079	3.079	3.079	3.079	3.079
Carbon Balance	[%]	101.3	96.0	95.0	99.5	101.3	97.0	104.4	103.7	103.2

Sample	Na1						
Time	[min]	1.50	18.15	40.02	55.53	70.88	433.53
Rate	[mol/g/hr]	14.8	14.0	12.2	11.4	11.0	8.7
Model	[mol/g/hr]	14.8	13.4	12.3	11.7	11.2	6.5
Conversion	[%]	29.2	26.0	24.8	23.0	22.2	13.4
Selectivity (w)	[%]	11.0	11.1	12.1	12.5	12.8	22.2
Product flow	[mmol/g/hr]						
	Methane	0.234	0.256	0.267	0.258	0.249	0.154
	Ethane	0.116	0.118	0.108	0.093	0.085	0.023
	Ethene	0.898	0.936	0.917	0.858	0.822	0.367
	Propane	10.082	8.172	7.145	6.263	5.828	2.249
	Propene	0.887	0.890	0.889	0.813	0.810	0.584
	Isobutane	46.453	46.195	50.545	51.235	52.035	57.670
	n-Butane	4.855	4.315	4.317	4.205	4.130	2.868
	t-2-Butene	0.205	0.229	0.217	0.214	0.214	0.244
	1-Butene	0.086	0.106	0.110	0.110	0.104	0.101
	Isobutene	0.316	0.357	0.373	0.371	0.374	0.572
	2-c-Butene	0.126	0.151	0.152	0.152	0.151	0.320
	Pentanes	2.405	2.454	2.018	1.954	2.050	1.412
	Hexane	3.731	3.731	3.731	3.731	3.731	3.731
Carbon Balance	[%]	102.8	96.3	100.8	99.9	100.3	99.9

Sample	Na2									
Time	[min]	2.50	29.90	49.52	66.80	92.90	108.15	124.75	142.25	167.73
Rate	[mol/g/hr]	17.6	14.9	13.3	12.5	11.3	10.9	10.4	9.9	9.5
Model	[mol/g/hr]	17.7	14.7	13.4	12.5	11.4	10.9	10.4	9.9	9.3
Conversion	[%]	35.6	30.1	26.9	25.2	22.8	22.0	20.9	20.0	19.1
Selectivity (w)	[%]	9.3	10.1	10.8	11.1	11.7	12.8	12.4	12.8	12.8
Product flow	[mmol/g/hr]									
	Methane	0.406	0.341	0.308	0.286	0.260	0.251	0.249	0.236	0.221
	Ethane	0.211	0.160	0.130	0.112	0.091	0.084	0.077	0.072	0.062
	Ethene	1.403	1.149	1.020	0.944	0.834	0.805	0.769	0.730	0.677
	Propane	14.033	10.423	8.497	7.346	6.214	5.766	5.339	4.914	4.531
	Propene	1.123	0.944	0.862	0.811	0.754	0.740	0.724	0.697	0.676
	Isobutane	44.428	47.807	48.647	49.358	50.451	50.960	51.524	52.182	52.000
	n-Butane	4.661	4.719	4.484	4.284	4.048	3.973	3.872	3.798	3.622
	t-2-Butene	0.205	0.207	0.182	0.179	0.180	0.177	0.167	0.159	0.154
	1-Butene	0.072	0.079	0.078	0.076	0.075	0.078	0.071	0.072	0.073
	Isobutene	0.348	0.366	0.352	0.354	0.339	0.445	0.355	0.354	0.326
	2-c-Butene	0.136	0.140	0.131	0.131	0.126	0.158	0.118	0.119	0.118
	Pentanes	1.918	2.089	1.994	2.075	1.943	1.913	1.879	1.864	1.831
	Hexane	2.393	2.393	2.393	2.393	2.393	2.393	2.393	2.393	2.393
Carbon Balance	[%]	103.5	102.7	100.4	99.0	98.0	98.1	97.8	97.8	96.5

Sample	Na10										
Time	[min]	2.33	3.00	4.37	5.00	8.00	20.00	52.50	71.50	84.00	146.00
Rate	[mol/g/hr]	3.8	3.8	3.8	3.8	3.8	3.7	3.5	3.3	3.3	3.1
Model	[mol/g/hr]	3.8	3.8	3.8	3.8	3.8	3.7	3.5	3.4	3.3	3.1
Conversion	[%]	7.7	7.8	7.6	7.8	7.7	7.3	7.1	6.7	6.7	6.2
Selectivity (w)	[%]	11.0	11.1	11.3	11.7	12.9	13.3	14.3	13.7	16.5	13.4
Product flow	[mmol/g/hr]										
	Methane	0.128	0.138	0.125	0.146	0.153	0.124	0.157	0.119	0.157	0.104
	Ethane	0.029	0.041	0.037	0.040	0.034	0.028	0.028	0.018	0.023	0.020
	Ethene	0.275	0.277	0.262	0.285	0.292	0.253	0.267	0.219	0.252	0.183
	Propane	1.587	1.678	1.625	1.744	1.660	1.543	1.447	1.338	1.229	1.209
	Propene	0.214	0.235	0.222	0.240	0.244	0.252	0.251	0.230	0.269	0.206
	Isobutane	59.195	63.195	61.010	64.440	62.501	62.355	63.979	62.307	60.704	63.388
	n-Butane	1.591	1.686	1.619	1.706	1.664	1.609	1.569	1.476	1.374	1.440
	t-2-Butene	0.030	0.032	0.037	0.037	0.049	0.051	0.050	0.049	0.046	0.048
	1-Butene	0.017	0.019	0.018	0.020	0.028	0.030	0.028	0.023	0.028	0.022
	Isobutene	0.132	0.127	0.142	0.150	0.167	0.166	0.173	0.158	0.181	0.146
	2-c-Butene	0.023	0.024	0.023	0.027	0.029	0.032	0.038	0.038	0.034	0.035
	Pentanes	0.898	0.917	0.913	0.923	0.890	0.857	0.848	0.805	0.747	0.768
	Hexane	2.068	2.068	2.068	2.068	2.068	2.068	2.068	2.068	2.068	2.068
Carbon Balance	[%]	96.2	102.6	99.1	104.7	101.8	101.0	103.3	100.2	97.8	101.4

Sample	NaS				
Time	[min]	1.50	19.83	56.60	73.20
Rate	[mol/g/hr]	0.0	0.0	0.0	0.0
Model	[mol/g/hr]	0.0	0.0	0.0	0.0
Conversion	[%]	0.2	0.1	0.1	0.2
Selectivity (w)	[%]	51.6	48.9	14.9	55.0
Product flow	[mmol/g/hr]				
	Methane	0.004	0.002	0.003	0.002
	Ethane	0.000	0.000	0.000	0.000
	Ethene	0.000	0.000	0.000	0.000
	Propane	0.010	0.007	0.014	0.015
	Propene	0.000	0.000	0.000	0.000
	Isobutane	44.254	44.135	42.468	44.719
	n-Butane	0.017	0.008	0.013	0.010
	t-2-Butene	0.000	0.000	0.000	0.000
	1-Butene	0.000	0.000	0.000	0.000
	Isobutene	0.032	0.014	0.003	0.039
	2-c-Butene	0.000	0.000	0.000	0.000
	Pentanes	0.006	0.002	0.007	0.009
	Hexane	0.341	0.341	0.341	0.341
Carbon Balance	[%]	100.2	99.9	96.1	101.3

Sample	NaS0.1						
Time	[min]	1.50	20.13	36.35	63.85	80.05	102.18
Rate	[mol/g/hr]	0.1	0.1	0.1	0.1	0.1	0.1
Model	[mol/g/hr]	0.1	0.1	0.1	0.1	0.1	0.1
Conversion	[%]	0.2	0.2	0.3	0.2	0.2	0.3
Selectivity (w)	[%]	73.5	73.0	82.8	79.6	79.1	83.0
Product flow	[mmol/g/hr]						
	Methane	0.008	0.014	0.017	0.015	0.016	0.014
	Ethane	0.000	0.000	0.000	0.000	0.000	0.000
	Ethene	0.000	0.000	0.000	0.000	0.000	0.000
	Propane	0.038	0.031	0.030	0.029	0.030	0.027
	Propene	0.071	0.042	0.045	0.042	0.045	0.044
	Isobutane	66.129	69.739	67.968	68.035	68.537	63.503
	n-Butane	0.000	0.000	0.000	0.000	0.000	0.000
	t-2-Butene	0.017	0.000	0.014	0.019	0.017	0.014
	1-Butene	0.000	0.000	0.000	0.000	0.000	0.000
	Isobutene	0.009	0.029	0.071	0.038	0.038	0.062
	2-c-Butene	0.000	0.000	0.000	0.000	0.000	0.000
	Pentanes	0.000	0.000	0.000	0.000	0.000	0.000
	Hexane	1.658	1.658	1.658	1.658	1.658	1.658
Carbon Balance	[%]	99.5	104.9	102.3	102.3	103.1	95.6

Sample	NaS1							
Time	[min]	0.50	50.20	68.08	84.67	121.30	151.15	173.88
Rate	[mol/g/hr]	6.8	5.7	5.5	5.2	4.9	4.9	4.8
Model	[mol/g/hr]	6.8	5.8	5.6	5.4	5.1	4.8	4.7
Conversion	[%]	13.6	11.4	11.1	10.5	9.9	9.7	9.6
Selectivity (w)	[%]	11.8	14.3	14.4	14.7	15.1	15.4	15.2
Product flow	[mmol/g/hr]							
	Methane	0.232	0.143	0.155	0.145	0.135	0.131	0.128
	Ethane	0.063	0.039	0.039	0.035	0.029	0.027	0.025
	Ethene	0.633	0.423	0.425	0.385	0.348	0.332	0.323
	Propane	3.979	2.618	2.657	2.374	2.127	2.061	1.985
	Propene	0.533	0.458	0.454	0.428	0.399	0.397	0.378
	Isobutane	57.663	58.585	61.442	60.941	60.080	60.466	59.533
	n-Butane	2.104	2.173	2.313	2.214	2.091	2.088	2.042
	t-2-Butene	0.072	0.126	0.126	0.121	0.117	0.122	0.119
	1-Butene	0.016	0.044	0.048	0.047	0.048	0.048	0.048
	Isobutene	0.170	0.222	0.235	0.229	0.217	0.223	0.209
	2-c-Butene	0.043	0.083	0.088	0.084	0.080	0.083	0.082
	Pentanes	1.213	1.191	1.127	1.089	1.017	1.015	0.996
	Hexane	2.539	2.539	2.539	2.539	2.539	2.539	2.539
Carbon Balance	[%]	100.1	99.2	103.7	102.2	100.1	100.6	98.9

Sample	NaS2									
Time	[min]	1.50	34.13	50.18	69.57	86.63	109.95	155.20	172.97	189.58
Rate	[mol/g/hr]	10.7	9.4	8.5	8.4	8.1	7.7	7.1	6.8	6.5
Model	[mol/g/hr]	10.7	9.3	8.8	8.4	8.0	7.6	7.0	6.8	6.6
Conversion	[%]	21.4	18.7	16.9	16.7	16.1	15.4	14.1	13.8	13.0
Selectivity (w)	[%]	12.0	12.6	13.1	13.2	13.5	13.7	14.4	14.3	14.8
Product flow	[mmol/g/hr]									
	Methane	0.253	0.196	0.184	0.183	0.179	0.168	0.153	0.151	0.150
	Ethane	0.089	0.059	0.051	0.047	0.043	0.037	0.031	0.028	0.027
	Ethene	0.998	0.685	0.823	0.590	0.582	0.515	0.439	0.418	0.403
	Propane	6.014	4.539	3.988	3.779	3.580	3.204	2.774	2.633	2.467
	Propene	0.751	0.686	0.638	0.621	0.607	0.568	0.528	0.503	0.499
	Isobutane	52.354	53.694	55.525	54.885	55.711	54.422	54.792	55.181	55.963
	n-Butane	3.736	3.632	3.451	3.432	3.394	3.180	2.958	2.900	2.834
	t-2-Butene	0.102	0.172	0.167	0.188	0.165	0.146	0.157	0.146	0.141
	1-Butene	0.035	0.065	0.064	0.065	0.066	0.065	0.062	0.062	0.062
	Isobutene	0.256	0.313	0.310	0.311	0.313	0.297	0.288	0.279	0.284
	2-c-Butene	0.066	0.114	0.113	0.110	0.114	0.109	0.106	0.102	0.103
	Pentanes	1.940	1.881	1.724	1.716	1.690	1.603	1.481	1.433	1.401
	Hexane	2.441	2.441	2.441	2.441	2.441	2.441	2.441	2.441	2.441
Carbon Balance	[%]	100.0	99.1	100.3	98.9	99.7	96.5	95.7	95.6	96.6

Sample	NaS5						
Time	[min]	1.50	4.00	25.00	42.00	85.67	149.00
Rate	[mol/g/hr]	2.3	2.0	1.8	1.4	1.1	1.2
Model	[mol/g/hr]	2.2	2.1	1.6	1.4	1.2	1.0
Conversion	[%]	31.8	28.1	23.0	20.1	18.8	17.4
Selectivity (w)	[%]	9.1	9.4	11.2	12.0	12.8	14.9
Product flow	[mmol/g/hr]						
	Methane	0.498	0.384	0.388	0.344	0.325	0.308
	Ethane	0.294	0.145	0.117	0.103	0.093	0.042
	Ethene	0.955	0.919	0.865	0.722	0.580	0.502
	Propane	11.827	9.576	6.913	5.418	4.148	3.519
	Propene	0.864	0.769	0.731	0.652	0.573	0.662
	Isobutane	44.968	47.852	50.617	50.837	54.659	58.253
	n-Butane	4.174	4.441	3.755	3.335	3.200	4.049
	t-2-Butene	0.123	0.140	0.127	0.119	0.115	0.181
	1-Butene	0.051	0.054	0.055	0.052	0.048	0.079
	Isobutene	0.271	0.306	0.295	0.274	0.245	0.415
	2-c-Butene	0.089	0.103	0.098	0.089	0.085	0.131
	Pentanes	1.635	1.864	1.807	1.681	1.637	1.998
	Hexane	2.920	2.920	2.920	2.920	2.920	2.920
Carbon Balance	[%]	98.7	99.9	98.7	95.5	98.6	102.3

Sample	H(550)									
Time	[min]	0.67	1.50	2.00	4.50	23.00	60.00	84.50	135.42	183.00
Rate	[mol/g/hr]	18.8	18.6	18.0	16.0	11.1	7.4	6.1	5.0	4.1
Model	[mol/g/hr]	19.1	18.3	17.9	16.3	11.0	7.4	6.3	4.8	4.1
Conversion	[%]	37.7	37.2	36.1	32.0	22.2	14.9	12.2	10.0	8.2
Selectivity (w)	[%]	8.4	6.2	6.8	7.1	9.5	11.8	11.9	15.0	14.6
Product flow	[mmol/g/hr]									
	Methane	0.565	0.414	0.439	0.347	0.383	0.293	0.242	0.261	0.178
	Ethane	0.350	0.320	0.308	0.215	0.162	0.085	0.080	0.047	0.034
	Ethene	1.619	1.096	1.101	0.827	0.813	0.545	0.402	0.371	0.235
	Propane	16.536	15.994	14.966	11.711	7.364	3.700	2.865	2.023	1.419
	Propene	1.077	0.696	0.716	0.610	0.581	0.444	0.356	0.352	0.254
	Isobutane	43.232	41.492	41.197	44.166	53.305	56.084	59.764	62.441	58.548
	n-Butane	3.878	3.883	3.803	4.713	3.742	3.148	2.720	2.378	1.847
	t-2-Butene	0.136	0.098	0.097	0.115	0.097	0.095	0.082	0.089	0.067
	1-Butene	0.055	0.041	0.043	0.064	0.049	0.048	0.033	0.035	0.033
	Isobutene	0.255	0.204	0.220	0.252	0.264	0.251	0.211	0.226	0.157
	2-c-Butene	0.096	0.070	0.071	0.083	0.074	0.072	0.063	0.074	0.050
	Pentanes	1.544	1.716	1.529	1.901	1.728	1.457	1.220	1.077	0.786
	Hexane	2.312	2.312	2.312	2.312	2.312	2.312	2.312	2.312	2.312
Carbon Balance	[%]	104.1	99.1	98.8	97.8	102.9	102.4	102.1	104.1	92.5

Sample	H0						
Time	[min]	1.25	2.50	8.00	36.50	72.00	87.25
Rate	[mol/g/hr]	19.6	18.6	14.7	8.0	5.8	5.3
Model	[mol/g/hr]	19.7	18.4	14.7	8.3	5.7	5.1
Conversion	[%]	58.8	55.8	44.1	23.9	17.4	15.8
Selectivity (w)	[%]	7.5	7.6	7.7	10.7	12.5	12.2
Product flow	[mmol/g/hr]						
	Methane	0.631	0.608	0.512	0.373	0.283	0.251
	Ethane	0.478	0.393	0.303	0.110	0.073	0.060
	Ethene	1.697	1.760	1.521	0.872	0.602	0.508
	Propane	25.419	23.447	17.167	6.207	3.942	3.356
	Propene	1.205	1.233	1.067	0.670	0.546	0.469
	Isobutane	27.151	29.201	38.208	49.228	54.963	55.271
	n-Butane	6.358	6.332	6.249	4.515	3.729	3.499
	t-2-Butene	0.161	0.173	0.169	0.131	0.139	0.124
	1-Butene	0.067	0.075	0.071	0.056	0.075	0.054
	Isobutene	0.304	0.360	0.374	0.325	0.307	0.271
	2-c-Butene	0.117	0.126	0.128	0.097	0.099	0.090
	Pentanes	2.240	2.336	2.558	2.132	1.793	1.673
	Hexane	2.636	2.636	2.636	2.638	2.638	2.838
Carbon Balance	[%]	98.8	99.1	102.6	97.1	99.9	98.5

Sample	H0.01							
Time	[min]	1.27	2.00	4.50	12.00	34.00	110.50	139.50
Rate	[mol/g/hr]	19.3	18.5	17.3	14.2	9.6	5.8	5.2
Model	[mol/g/hr]	19.4	18.7	17.0	14.0	10.0	5.7	5.0
Conversion	[%]	38.3	36.6	34.4	28.1	19.0	11.5	10.4
Selectivity (w)	[%]	7.5	7.6	7.6	10.2	9.7	13.9	15.8
Product flow	[mmol/g/hr]							
	Methane	0.491	0.475	0.439	0.444	0.302	0.235	0.246
	Ethane	0.319	0.314	0.281	0.199	0.137	0.058	0.040
	Ethene	1.239	1.205	1.123	0.942	0.663	0.409	0.382
	Propane	16.754	16.621	14.780	10.097	5.843	2.522	2.051
	Propene	0.738	0.734	0.762	0.893	0.465	0.388	0.389
	Isobutane	41.164	44.053	45.302	47.039	54.449	60.372	59.081
	n-Butane	3.953	4.001	4.080	3.697	3.399	2.581	2.277
	t-2-Butene	0.113	0.113	0.126	0.114	0.101	0.097	0.089
	1-Butene	0.046	0.046	0.053	0.054	0.041	0.041	0.040
	Isobutene	0.266	0.277	0.320	0.290	0.252	0.257	0.249
	2-c-Butene	0.078	0.082	0.093	0.080	0.073	0.071	0.068
	Pentanes	1.584	1.531	1.656	1.534	1.498	1.181	1.023
	Hexane	2.636	2.636	2.636	2.636	2.638	2.636	2.636
Carbon Balance	[%]	100.2	104.2	103.6	98.1	100.9	102.4	99.0

Sample	H0.1										
Time	[min]	1.00	20.23	37.60	55.47	73.68	91.92	110.30	130.73	147.98	169.82	195.10
Rate	[mol/g/hr]	31.1	20.1	15.4	13.5	12.0	11.0	9.7	8.9	8.2	7.6	6.9
Model	[mol/g/hr]	31.1	19.8	16.0	13.6	11.9	10.7	9.7	8.8	8.3	7.6	7.0
Conversion	[%]	61.9	40.1	30.7	26.9	23.9	21.8	19.4	17.8	16.3	15.1	13.8
Selectivity (w)	[%]	7.7	10.2	10.7	11.4	11.9	12.8	13.2	13.8	14.3	14.9	15.8
Product flow	[mmol/g/hr]											
	Methane	0.465	0.306	0.248	0.228	0.216	0.211	0.194	0.185	0.174	0.162	0.155
	Ethane	0.308	0.158	0.100	0.076	0.062	0.053	0.044	0.037	0.031	0.027	0.022
	Ethene	1.904	1.415	1.066	0.909	0.795	0.737	0.641	0.552	0.516	0.446	0.406
	Propane	24.518	12.191	8.091	6.356	5.312	4.596	3.998	3.512	3.025	2.656	2.365
	Propene	1.556	1.268	0.949	0.832	0.782	0.719	0.680	0.637	0.584	0.540	0.514
	Isobutane	24.722	40.249	45.542	47.314	51.015	51.921	54.222	55.156	55.455	54.755	56.822
	n-Butane	7.469	7.047	5.859	5.400	5.114	4.932	4.471	4.188	3.887	3.539	3.330
	t-2-Butene	0.327	0.333	0.262	0.245	0.240	0.226	0.217	0.212	0.198	0.195	0.199
	1-Butene	0.111	0.122	0.102	0.098	0.095	0.095	0.090	0.088	0.084	0.080	0.079
	Isobutene	0.441	0.489	0.426	0.412	0.411	0.436	0.389	0.375	0.366	0.346	0.345
	2-c-Butene	0.207	0.219	0.178	0.163	0.162	0.167	0.148	0.146	0.139	0.135	0.137
	Pentanes	2.841	3.387	2.874	2.673	2.873	2.324	2.169	1.973	1.817	1.624	1.498
	Hexane	1.979	1.979	1.979	1.979	1.979	1.979	1.979	1.979	1.979	1.979	1.979
Carbon Balance	[%]	97.4	100.8	98.6	97.1	100.7	99.7	101.0	100.7	99.5	96.8	98.6

Sample	H1												
Time	[min]	1.53	18.18	34.22	64.65	89.48	105.48	121.35	160.00	220.00	236.75	252.37	268.00	284.43
Rate	[mol/g/hr]	31.9	21.1	17.0	14.1	12.0	11.0	10.2	7.9	6.5	6.1	5.8	5.8	5.5
Model	[mol/g/hr]	32.0	21.3	17.2	13.1	11.2	10.2	9.5	8.1	6.7	6.4	6.2	6.0	5.7
Conversion	[%]	73.1	48.4	39.0	32.3	27.4	25.1	23.3	18.1	14.9	13.9	13.4	13.2	12.6
Selectivity (w)	[%]	7.4	7.9	8.7	10.0	10.9	11.2	11.5	14.8	16.2	15.5	15.3	17.2	15.7
Product flow	[mmol/g/hr]													
	Methane	0.588	0.382	0.298	0.251	0.220	0.212	0.200	0.156	0.137	0.126	0.133	0.129	0.130
	Ethane	0.495	0.271	0.183	0.122	0.087	0.078	0.068	0.034	0.035	0.029	0.029	0.028	0.030
	Ethene	1.829	1.394	1.219	1.045	0.841	0.813	0.742	0.495	0.368	0.319	0.327	0.299	0.297
	Propane	30.679	17.803	12.477	8.616	6.631	6.009	5.326	3.234	2.390	2.080	2.098	2.002	1.997
	Propene	1.938	1.194	1.031	0.951	0.837	0.796	0.724	0.628	0.533	0.446	0.466	0.442	0.435
	Isobutane	17.276	34.650	40.917	46.073	46.917	52.267	53.450	55.016	57.520	59.246	57.150	56.602	57.919
	n-Butane	7.656	7.413	6.874	6.576	5.998	5.831	5.531	4.421	3.781	3.316	3.435	3.302	3.240
	t-2-Butene	0.237	0.244	0.239	0.252	0.241	0.241	0.237	0.284	0.283	0.205	0.197	0.238	0.190
	1-Butene	0.111	0.117	0.111	0.116	0.115	0.114	0.113	0.127	0.121	0.089	0.088	0.132	0.090
	Isobutene	0.436	0.440	0.429	0.447	0.431	0.430	0.420	0.410	0.382	0.325	0.331	0.371	0.328
	2-c-Butene	0.177	0.172	0.168	0.179	0.172	0.171	0.165	0.184	0.172	0.136	0.135	0.165	0.137
	Pentanes	2.845	3.055	3.150	3.198	2.912	2.841	2.719	2.151	1.880	1.515	1.571	1.502	1.462
	Hexane	1.014	1.014	1.014	1.014	1.014	1.014	1.014	1.014	1.014	1.014	1.014	1.014	1.014
Carbon Balance	[%]	96.5	100.8	100.7	102.1	101.2	104.8	104.6	100.8	101.5	92.8	99.0	97.9	99.4

Sample	H2										
Time	[min]	2.67	24.62	41.05	56.23	77.57	94.90	114.70	135.38	157.25	176.27
Rate	[mol/g/hr]	28.1	19.0	15.3	12.8	11.5	10.4	9.4	8.5	7.9	7.3
Model	[mol/g/hr]	28.1	18.6	15.4	13.3	11.5	10.4	9.4	8.5	7.8	7.3
Conversion	[%]	57.4	39.0	31.3	26.2	23.4	21.4	19.2	17.5	16.3	15.0
Selectivity (w)	[%]	7.5	9.0	10.3	11.2	11.6	12.2	13.3	14.1	14.6	14.9
Product flow	[mmol/g/hr]										
	Methane	0.530	0.348	0.289	0.254	0.236	0.207	0.209	0.190	0.175	0.173
	Ethane	0.373	0.191	0.129	0.093	0.073	0.057	0.052	0.041	0.035	0.030
	Ethene	1.826	1.211	0.994	0.855	0.772	0.847	0.618	0.546	0.476	0.450
	Propane	24.454	11.917	8.418	6.407	5.321	4.326	4.118	3.357	2.973	2.732
	Propene	1.441	1.037	0.901	0.784	0.734	0.681	0.678	0.626	0.584	0.532
	Isobutane	28.965	40.730	45.360	48.140	51.533	50.260	55.081	54.030	53.688	55.824
	n-Butane	6.897	6.474	5.887	5.266	4.973	4.383	4.417	3.976	3.669	3.540
	t-2-Butene	0.261	0.241	0.240	0.221	0.216	0.200	0.213	0.194	0.190	0.190
	1-Butene	0.114	0.111	0.106	0.099	0.100	0.094	0.106	0.091	0.092	0.089
	Isobutene	0.414	0.419	0.418	0.400	0.400	0.389	0.367	0.365	0.351	0.354
	2-c-Butene	0.182	0.172	0.165	0.153	0.152	0.140	0.148	0.148	0.134	0.133
	Pentanes	2.608	3.896	3.097	2.537	2.804	2.577	2.149	1.910	1.748	1.664
	Hexane	2.385	2.385	2.385	2.385	2.385	2.385	2.365	2.365	2.365	2.365
Carbon Balance	[%]	102.2	100.2	99.1	97.9	101.0	95.9	102.3	98.3	96.2	98.6

Sample	H5									
Time	[min]	3.50	21.37	45.45	65.53	89.13	131.77	149.40	192.75	213.25
Rate	[mol/g/hr]	15.9	13.2	11.3	10.0	8.9	7.6	7.0	6.2	8.1
Model	[mol/g/hr]	16.0	13.0	11.0	10.0	9.1	8.0	7.6	6.9	6.6
Conversion	[%]	32.3	26.8	22.9	20.3	18.2	15.4	14.2	12.6	16.5
Selectivity (w)	[%]	7.9	8.9	9.9	10.7	12.1	12.8	12.9	14.1	11.8
Product flow	[mmol/g/hr]									
	Methane	0.420	0.307	0.266	0.223	0.208	0.168	0.165	0.146	0.160
	Ethane	0.277	0.187	0.140	0.106	0.088	0.057	0.051	0.037	0.057
	Ethene	1.137	0.938	0.857	0.756	0.714	0.582	0.556	0.466	0.583
	Propane	13.988	9.855	7.720	6.078	5.213	3.803	3.595	2.832	4.172
	Propene	0.613	0.700	0.665	0.616	0.611	0.548	0.538	0.492	0.560
	Isobutane	45.637	46.810	50.826	50.638	54.827	53.974	57.927	57.350	54.863
	n-Butane	3.330	3.340	3.427	3.185	3.202	2.798	2.809	2.503	3.113
	t-2-Butene	0.124	0.132	0.135	0.135	0.209	0.137	0.129	0.130	0.139
	1-Butene	0.041	0.048	0.052	0.052	0.073	0.051	0.051	0.049	0.054
	Isobutene	0.245	0.258	0.278	0.284	0.280	0.262	0.270	0.280	0.277
	2-c-Butene	0.080	0.086	0.094	0.090	0.093	0.092	0.090	0.086	0.095
	Pentanes	1.276	1.316	1.483	1.382	1.487	1.348	1.350	1.243	1.649
	Hexane	2.393	2.393	2.393	2.393	2.393	2.393	2.393	2.393	2.393
Carbon Balance	[%]	101.1	96.0	99.0	95.3	100.8	95.8	101.4	98.5	98.6

Sample	H10							
Time	[min]	0.00	1.25	4.00	26.50	31.50	35.50	40.00
Rate	[mol/g/hr]	15.0	14.4	14.3	10.0	9.1	8.8	8.4
Model	[mol/g/hr]	14.9	14.7	14.1	10.0	9.3	8.8	8.3
Conversion	[%]	45.2	43.1	42.9	30.1	27.3	26.3	25.3
Selectivity (w)	[%]	6.6	7.1	7.6	9.7	9.8	9.7	10.0
Product flow	[mmol/g/hr]							
	Methane	0.543	0.532	0.538	0.409	0.404	0.332	0.355
	Ethane	0.356	0.352	0.331	0.167	0.162	0.132	0.137
	Ethene	1.478	1.437	1.494	1.083	1.030	0.877	0.902
	Propane	19.928	18.754	18.439	9.546	9.221	6.017	7.770
	Propene	0.967	0.990	1.069	0.829	0.811	0.710	0.728
	Isobutane	37.348	38.551	39.447	45.191	50.843	47.740	49.607
	n-Butane	5.122	4.803	5.203	4.685	4.720	4.353	4.358
	t-2-Butene	0.132	0.130	0.152	0.144	0.145	0.138	0.134
	1-Butene	0.049	0.050	0.062	0.063	0.064	0.061	0.060
	Isobutene	0.242	0.271	0.326	0.336	0.337	0.310	0.314
	2-c-Butene	0.090	0.093	0.108	0.108	0.108	0.100	0.099
	Pentanes	1.844	1.786	1.966	2.058	2.107	2.009	1.977
	Hexane	2.920	2.920	2.920	2.920	2.920	2.920	2.920
Carbon Balance	[%]	102.2	101.7	103.8	97.0	105.0	97.2	99.7

Sample	HE						
Time	[min]	1.50	16.48	31.42	54.55	72.12	106.57
Rate	[mol/g/hr]	20.0	16.7	16.1	15.7	15.5	15.1
Model	[mol/g/hr]	18.6	17.3	16.5	15.8	15.0	14.1
Conversion	[%]	40.5	33.8	32.6	31.7	31.3	30.5
Selectivity (w)	[%]	17.0	16.8	17.2	17.4	17.6	17.7
Product flow	[mmol/g/hr]						
	Methane	0.585	0.484	0.504	0.475	0.499	0.496
	Ethane	0.077	0.063	0.064	0.058	0.056	0.053
	Ethene	2.071	1.691	1.700	1.543	1.580	1.461
	Propane	9.748	7.874	7.822	7.288	7.268	6.962
	Propene	2.457	1.928	2.038	1.938	1.967	1.899
	Isobutane	40.140	42.550	46.150	45.444	46.672	47.282
	n-Butane	7.499	5.912	6.156	5.961	6.023	5.893
	t-2-Butene	0.364	0.282	0.291	0.288	0.292	0.290
	1-Butene	0.237	0.187	0.193	0.192	0.193	0.193
	Isobutene	0.714	0.558	0.579	0.571	0.578	0.579
	2-c-Butene	0.277	0.216	0.225	0.224	0.228	0.225
	Pentanes	3.258	2.538	2.714	2.589	2.618	2.732
	Hexane	1.217	1.217	1.217	1.217	1.217	1.217
Carbon Balance	[%]	101.2	96.5	102.7	99.9	102.0	102.2

Sample	CH											
Time	[min]	0.50	16.00	31.72	53.83	72.73	88.45	104.82	120.62	142.70	167.55	193.72	209.03
Rate	[mol/g/hr]	36.8	18.9	13.7	10.8	9.4	8.4	7.8	7.1	6.4	5.9	5.5	5.4
Model	[mol/g/hr]	36.8	18.6	14.0	10.9	9.4	8.4	7.7	7.1	6.5	5.9	5.4	5.2
Conversion	[%]	78.7	39.3	28.7	22.4	19.5	17.8	16.2	14.8	13.4	12.3	11.4	11.4
Selectivity (w)	[%]	5.8	9.0	10.1	11.3	11.8	12.5	12.8	13.5	14.4	15.0	16.0	17.1
Product flow	[mmol/g/hr]												
	Methane	0.588	0.332	0.263	0.227	0.206	0.192	0.173	0.166	0.157	0.140	0.142	0.148
	Ethane	0.508	0.198	0.114	0.077	0.059	0.048	0.038	0.032	0.028	0.021	0.019	0.019
	Ethene	1.821	1.179	0.870	0.704	0.601	0.537	0.446	0.419	0.359	0.312	0.301	0.286
	Propane	33.430	11.750	7.255	5.070	4.240	3.575	2.990	2.683	2.365	1.995	1.884	1.853
	Propene	1.411	0.968	0.752	0.652	0.580	0.535	0.489	0.459	0.444	0.398	0.404	0.427
	Isobutane	14.670	39.043	46.998	53.032	55.618	57.318	55.947	57.424	58.576	58.658	61.602	62.707
	n-Butane	7.507	6.861	5.887	5.249	4.778	4.446	3.931	3.758	3.471	3.077	3.109	3.134
	t-2-Butene	0.240	0.273	0.240	0.230	0.213	0.205	0.179	0.180	0.179	0.160	0.192	0.214
	1-Butene	0.084	0.099	0.091	0.086	0.080	0.081	0.075	0.069	0.070	0.067	0.080	0.094
	Isobutene	0.335	0.421	0.404	0.392	0.380	0.377	0.345	0.342	0.331	0.312	0.328	0.354
	2-c-Butene	0.149	0.176	0.158	0.150	0.139	0.140	0.125	0.126	0.121	0.118	0.127	0.140
	Pentanes	2.248	3.053	2.849	2.511	2.222	2.074	2.012	1.720	1.537	1.354	1.351	1.370
	Hexane	2.393	2.393	2.393	2.393	2.393	2.393	2.393	2.393	2.393	2.393	2.393	2.393
Carbon Balance	[%]	94.5	96.6	98.9	102.6	103.7	104.4	100.2	101.1	101.5	97.0	104.4	106.2

Sample	CH			
Time	[min]	5.00	26.00	57.00
Rate	[mol/g/hr]	26.1	15.0	10.2
Model	[mol/g/hr]	26.5	15.3	10.6
Conversion	[%]	54.5	31.2	21.4
Selectivity (w)	[%]	6.8	9.8	10.9
Product flow	[mmol/g/hr]			
	Methane	0.443	0.287	0.231
	Ethane	0.349	0.154	0.087
	Ethene	1.576	1.076	0.680
	Propane	22.654	9.402	5.206
	Propene	1.206	0.872	0.648
	Isobutane	31.005	47.947	54.943
	n-Butane	7.401	6.463	4.871
	t-2-Butene	0.249	0.249	0.169
	1-Butene	0.098	0.101	0.093
	Isobutene	0.373	0.407	0.354
	2-c-Butene	0.172	0.177	0.133
	Pentanes	2.637	2.539	2.468
	Hexane	2.393	2.393	2.393
Carbon Balance	[%]	102.3	104.6	104.9

Sample	CH0													
Time	[min]	1.00	19.20	50.82	69.02	89.08	117.17	135.77	152.90	171.58	188.75	236.53	264.50	303.05	264.50
Rate	[mol/g/hr]	23.2	15.2	9.8	8.4	7.7	7.2	6.5	6.0	5.6	5.4	5.0	4.9	4.4	4.9
Model	[mol/g/hr]	23.3	14.5	10.2	9.0	8.0	7.0	6.5	6.1	5.7	5.4	4.8	4.5	4.2	4.5
Conversion	[%]	46.8	30.6	19.8	16.9	15.6	14.5	13.1	12.0	11.3	11.0	10.1	9.9	8.8	9.9
Selectivity (w)	[%]	7.1	9.1	11.1	11.9	12.5	13.1	14.1	14.4	14.6	14.9	16.7	17.2	17.7	17.2
Product flow	[mmol/g/hr]														
	Methane	0.476	0.328	0.224	0.195	0.178	0.159	0.159	0.149	0.140	0.139	0.118	0.117	0.117	0.117
	Ethane	0.358	0.190	0.086	0.064	0.051	0.038	0.035	0.031	0.025	0.025	0.017	0.015	0.014	0.015
	Ethene	1.370	0.990	0.643	0.540	0.485	0.418	0.397	0.352	0.313	0.317	0.246	0.236	0.223	0.236
	Propane	21.382	10.479	5.212	4.053	3.137	2.710	2.546	2.280	2.038	1.956	1.590	1.494	1.410	1.494
	Propene	1.045	0.751	0.560	0.490	0.454	0.423	0.423	0.398	0.370	0.373	0.341	0.343	0.344	0.343
	Isobutane	36.984	46.062	53.627	55.545	54.661	54.264	58.313	59.385	58.689	59.882	57.320	57.346	63.160	57.346
	n-Butane	5.160	4.801	4.020	3.631	3.401	3.104	3.112	2.949	2.746	2.745	2.424	2.387	2.340	2.387
	t-2-Butene	0.188	0.186	0.170	0.159	0.147	0.146	0.157	0.145	0.137	0.136	0.154	0.153	0.154	0.153
	1-Butene	0.094	0.095	0.084	0.079	0.075	0.073	0.078	0.074	0.065	0.070	0.072	0.073	0.074	0.073
	Isobutene	0.332	0.349	0.324	0.308	0.297	0.293	0.307	0.298	0.281	0.282	0.283	0.289	0.287	0.289
	2-c-Butene	0.176	0.133	0.111	0.109	0.105	0.106	0.108	0.103	0.096	0.098	0.108	0.105	0.106	0.105
	Pentanes	1.926	2.038	1.819	1.651	1.737	1.717	1.435	1.344	1.248	1.241	1.103	1.084	1.031	1.084
	Hexane	3.569	3.569	3.569	3.569	3.569	3.569	3.569	3.569	3.569	3.569	3.569	3.569	3.569	3.569
Carbon Balance	[%]	104.3	99.7	100.4	100.3	97.2	95.2	100.7	101.3	99.3	101.0	95.7	95.5	104.0	95.5

Sample	CH0.001									
Time	[min]	2.00	18.20	34.62	50.55	66.58	112.32	127.57	174.77	190.60
Rate	[mol/g/hr]	23.9	17.2	13.1	10.6	9.2	7.1	6.7	5.8	5.3
Model	[mol/g/hr]	24.1	16.6	13.2	11.1	9.6	7.1	6.6	5.3	5.0
Conversion	[%]	47.6	34.2	26.1	21.2	18.4	14.1	13.3	11.1	10.5
Selectivity (w)	[%]	7.3	8.9	10.0	10.8	11.4	13.5	13.6	15.6	15.9
Product flow	[mmol/g/hr]									
	Methane	0.536	0.379	0.313	0.257	0.222	0.166	0.163	0.137	0.136
	Ethane	0.415	0.241	0.156	0.108	0.078	0.041	0.036	0.023	0.021
	Ethene	1.417	0.996	0.834	0.685	0.579	0.411	0.381	0.300	0.286
	Propane	20.835	10.893	7.361	5.364	4.229	2.637	2.460	1.853	1.748
	Propene	1.108	0.808	0.697	0.593	0.526	0.433	0.423	0.377	0.369
	Isobutane	35.820	42.069	50.770	54.667	55.844	56.014	58.947	59.510	61.818
	n-Butane	5.395	5.430	5.317	4.753	4.282	3.384	3.303	2.862	2.821
	t-2-Butene	0.178	0.186	0.180	0.170	0.159	0.155	0.148	0.161	0.160
	1-Butene	0.091	0.089	0.088	0.083	0.078	0.069	0.071	0.072	0.072
	Isobutene	0.354	0.363	0.382	0.366	0.337	0.312	0.318	0.304	0.310
	2-c-Butene	0.124	0.131	0.130	0.118	0.113	0.107	0.107	0.109	0.105
	Pentanes	2.139	2.373	2.440	2.187	1.969	1.508	1.602	1.257	1.223
	Hexane	2.539	2.539	2.539	2.539	2.539	2.539	2.539	2.539	2.539
Carbon Balance	[%]	102.7	96.0	103.1	104.1	102.7	97.9	102.0	100.5	103.7

Sample	CH0.01											
Time	[min]	2.00	22.03	38.08	54.23	74.87	91.50	110.70	128.18	146.18	226.70	315.97
Rate	[mol/g/hr]	19.5	12.0	9.2	7.8	6.7	6.0	5.3	4.9	4.5	3.6	2.9
Model	[mol/g/hr]	19.5	11.7	9.4	7.9	6.7	6.0	5.4	4.9	4.5	3.4	2.7
Conversion	[%]	38.8	24.0	18.3	15.6	13.3	11.9	10.8	9.8	9.0	7.1	5.8
Selectivity (w)	[%]	7.5	10.2	11.0	11.8	12.5	13.3	13.9	14.4	14.9	18.8	21.5
Product flow	[mmol/g/hr]											
	Methane	0.478	0.279	0.202	0.172	0.154	0.140	0.125	0.115	0.111	0.091	0.080
	Ethane	0.398	0.169	0.099	0.070	0.052	0.040	0.030	0.025	0.021	0.011	0.007
	Ethene	1.099	0.744	0.557	0.468	0.396	0.349	0.294	0.262	0.244	0.165	0.115
	Propane	17.668	7.095	4.640	3.605	2.857	2.379	1.874	1.739	1.578	1.028	0.744
	Propene	0.877	0.607	0.481	0.425	0.393	0.366	0.324	0.310	0.292	0.270	0.242
	Isobutane	42.471	48.931	53.082	56.010	56.921	59.140	59.459	59.983	61.960	62.964	64.360
	n-Butane	4.129	4.370	3.670	3.409	3.168	2.868	2.819	2.446	2.343	1.899	1.582
	t-2-Butene	0.156	0.163	0.148	0.145	0.132	0.126	0.120	0.114	0.113	0.141	0.141
	1-Butene	0.073	0.074	0.070	0.074	0.065	0.061	0.058	0.057	0.056	0.060	0.055
	Isobutene	0.341	0.340	0.304	0.299	0.281	0.276	0.266	0.259	0.260	0.254	0.242
	2-c-Butene	0.110	0.117	0.105	0.101	0.102	0.091	0.086	0.082	0.082	0.092	0.088
	Pentanes	1.637	1.497	1.638	1.551	1.439	1.282	1.257	1.092	1.033	0.829	0.650
	Hexane	2.539	2.539	2.539	2.539	2.539	2.539	2.539	2.539	2.539	2.539	2.539
Carbon Balance	[%]	104.2	96.6	97.6	99.6	102.0	100.7	99.8	99.8	102.2	101.8	102.5

Sample	CH1									
Time	[min]	1.00	19.53	41.80	75.37	102.37	121.05	140.72	303.77	319.92
Rate	[mol/g/hr]	32.4	20.7	15.4	11.1	9.8	9.2	8.6	6.1	8.0
Model	[mol/g/hr]	32.4	20.5	15.5	11.9	10.1	9.3	8.5	5.3	5.2
Conversion	[%]	64.3	41.0	30.5	22.1	19.4	18.3	17.0	12.1	11.9
Selectivity (w)	[%]	7.3	9.2	10.5	11.9	12.8	13.5	13.9	18.2	18.2
Product flow	[mmol/g/hr]									
	Methane	0.647	0.378	0.299	0.221	0.198	0.197	0.185	0.144	0.142
	Ethane	0.494	0.220	0.133	0.071	0.054	0.046	0.038	0.017	0.016
	Ethene	1.822	1.259	1.011	0.719	0.591	0.555	0.502	0.295	0.292
	Propane	28.630	13.101	8.314	5.025	3.949	3.664	3.260	1.894	1.839
	Propene	1.552	1.078	0.900	0.698	0.638	0.835	0.587	0.509	0.483
	Isobutane	24.192	38.277	46.374	52.109	53.159	54.434	54.547	58.564	58.852
	n-Butane	6.870	6.556	5.953	4.722	4.232	4.201	3.909	2.975	2.964
	t-2-Butene	0.254	0.259	0.235	0.214	0.200	0.200	0.192	0.228	0.226
	1-Butene	0.124	0.121	0.112	0.100	0.094	0.098	0.094	0.094	0.097
	Isobutene	0.389	0.430	0.422	0.385	0.367	0.372	0.366	0.349	0.350
	2-c-Butene	0.213	0.180	0.165	0.146	0.140	0.139	0.130	0.146	0.144
	Pentanes	2.535	2.975	2.814	2.467	2.304	2.088	1.903	1.436	1.384
	Hexane	2.393	2.393	2.393	2.393	2.393	2.393	2.393	2.393	2.393
Carbon Balance	[%]	101.7	97.3	100.2	100.4	99.0	100.0	98.6	100.0	100.2

Sample	HS								
Time	[min]	0.50	33.40	65.87	100.28	134.50	237.88	268.15	299.20	329.08
Rate	[mol/g/hr]	19.2	16.1	14.1	13.3	12.7	9.5	10.0	9.3	9.6
Model	[mol/g/hr]	19.2	16.0	14.4	13.2	12.2	10.3	9.9	9.5	9.1
Conversion	[%]	39.1	32.8	28.6	27.1	25.9	19.3	20.4	19.0	19.5
Selectivity (w)	[%]	13.8	14.0	15.3	15.9	15.9	16.5	17.2	17.7	17.7
Product flow	[mmol/g/hr]									
	Methane	0.529	0.498	0.467	0.476	0.448	0.296	0.360	0.342	0.360
	Ethane	0.189	0.115	0.092	0.079	0.067	0.041	0.045	0.041	0.042
	Ethene	1.748	1.479	1.364	1.288	1.173	0.735	0.873	0.800	0.827
	Propane	13.456	9.348	7.732	7.110	6.251	4.021	4.496	4.070	4.168
	Propene	1.594	1.448	1.371	1.376	1.307	0.886	1.072	0.993	1.045
	Isobutane	42.126	46.305	49.725	50.727	49.690	51.134	53.947	53.542	53.651
	n-Butane	5.449	5.284	5.068	4.924	4.444	3.569	3.853	3.551	3.623
	t-2-Butene	0.288	0.163	0.238	0.242	0.229	0.206	0.228	0.211	0.211
	1-Butene	0.194	0.143	0.147	0.146	0.143	0.110	0.129	0.118	0.125
	Isobutene	0.628	0.513	0.462	0.500	0.453	0.373	0.422	0.399	0.409
	2-c-Butene	0.506	0.403	0.342	0.265	0.180	0.147	0.164	0.155	0.158
	Pentanes	2.493	3.257	2.637	2.480	2.648	1.839	2.193	1.852	2.042
	Hexane	1.095	1.095	1.095	1.095	1.095	1.095	1.095	1.095	1.095
Carbon Balance	[%]	103.9	103.5	104.6	104.5	100.6	95.1	101.7	99.2	100.1

Sample	HS0											
Time	[min]	1.50	16.88	32.98	48.68	64.62	81.77	107.42	133.72	149.93	166.90	186.82	202.30
Rate	[mol/g/hr]	20.1	14.4	12.2	11.3	10.4	9.8	8.9	8.1	8.1	7.9	7.5	7.4
Model	[mol/g/hr]	19.3	15.1	13.1	11.7	10.7	9.9	8.9	8.1	7.7	7.4	7.0	6.7
Conversion	[%]	40.5	29.1	24.5	22.7	21.0	19.7	18.0	16.4	16.3	16.0	15.2	14.9
Selectivity (w)	[%]	8.7	9.9	10.4	10.7	10.6	10.9	11.4	12.3	12.2	12.1	12.5	12.6
Product flow	[mmol/g/hr]												
	Methane	0.304	0.223	0.202	0.190	0.167	0.168	0.154	0.150	0.156	0.142	0.144	0.147
	Ethane	0.188	0.102	0.074	0.061	0.050	0.047	0.039	0.032	0.034	0.030	0.028	0.027
	Ethene	1.359	0.967	0.785	0.708	0.600	0.586	0.503	0.456	0.474	0.422	0.418	0.416
	Propane	14.422	7.804	6.036	5.032	4.222	4.061	3.464	3.054	3.181	2.818	2.814	2.808
	Propene	1.197	0.650	0.734	0.662	0.564	0.565	0.511	0.483	0.513	0.449	0.461	0.470
	Isobutane	41.157	47.614	51.868	51.797	50.418	53.842	52.701	53.894	58.616	53.376	57.629	59.322
	n-Butane	6.447	5.722	5.401	5.109	4.487	4.555	4.158	4.003	4.256	3.799	3.872	3.957
	t-2-Butene	0.227	0.204	0.194	0.178	0.153	0.155	0.152	0.155	0.169	0.144	0.154	0.158
	1-Butene	0.111	0.100	0.095	0.088	0.080	0.080	0.077	0.078	0.082	0.071	0.079	0.082
	Isobutene	0.436	0.407	0.397	0.382	0.343	0.352	0.320	0.328	0.356	0.316	0.335	0.342
	2-c-Butene	0.152	0.141	0.136	0.123	0.113	0.114	0.105	0.108	0.118	0.101	0.115	0.111
	Pentanes	3.158	2.964	2.801	2.679	2.610	2.526	2.079	1.713	2.104	1.849	1.883	1.892
	Hexane	4.461	4.461	4.461	4.461	4.461	4.461	4.461	4.461	4.461	4.461	4.461	4.461
Carbon Balance	[%]	103.8	100.7	103.2	100.8	95.8	100.8	96.5	96.7	105.2	95.3	102.0	104.7

Sample	HS0.01											
Time	[min]	0.50	36.10	57.45	90.67	117.22	132.77	148.22	175.23	197.73	234.62	329.57
Rate	[mol/g/hr]	17.0	12.1	8.4	7.2	7.6	7.3	7.8	7.6	7.4	6.7	6.9
Model	[mol/g/hr]	17.0	10.3	9.4	8.5	8.0	7.8	7.8	7.3	7.1	6.8	6.2
Conversion	[%]	33.9	24.2	16.8	14.5	15.2	14.6	15.6	15.2	14.9	13.4	13.9
Selectivity (w)	[%]	9.3	11.4	12.9	14.1	13.5	14.1	13.4	13.3	13.9	14.5	15.3
Product flow	[mmol/g/hr]											
	Methane	0.298	0.231	0.185	0.168	0.160	0.158	0.164	0.163	0.164	0.151	0.141
	Ethane	0.191	0.088	0.045	0.032	0.030	0.029	0.034	0.031	0.027	0.024	0.022
	Ethene	1.140	0.767	0.515	0.424	0.389	0.382	0.445	0.423	0.394	0.350	0.342
	Propane	12.015	5.887	3.364	2.663	2.594	2.508	2.951	2.804	2.558	2.328	2.199
	Propene	0.994	0.744	0.537	0.486	0.477	0.466	0.497	0.485	0.466	0.453	0.463
	Isobutane	45.045	50.769	56.323	56.946	55.111	54.485	56.246	55.989	55.560	58.432	56.617
	n-Butane	5.105	5.079	3.982	3.485	3.426	3.391	3.684	3.660	3.616	3.381	3.457
	t-2-Butene	0.220	0.212	0.179	0.173	0.168	0.166	0.177	0.165	0.168	0.175	0.213
	1-Butene	0.094	0.095	0.082	0.080	0.076	0.077	0.091	0.079	0.082	0.080	0.096
	Isobutene	0.394	0.414	0.357	0.337	0.336	0.334	0.343	0.339	0.347	0.334	0.348
	2-c-Butene	0.149	0.147	0.131	0.119	0.116	0.115	0.119	0.113	0.121	0.120	0.129
	Pentanes	2.492	2.575	1.960	1.664	2.115	1.702	1.690	1.804	1.752	1.641	1.702
	Hexane	3.528	3.528	3.528	3.528	3.528	3.528	3.528	3.528	3.528	3.528	3.528
Carbon Balance	[%]	102.3	100.5	101.8	99.9	97.6	95.6	100.0	99.1	97.9	101.3	98.7

Sample	HS0.1					
Time	[min]	1.00	18.75	49.38	88.62	113.65
Rate	[mol/g/hr]	19.8	15.0	10.7	8.0	7.4
Model	[mol/g/hr]	19.8	14.9	10.8	8.2	7.2
Conversion	[%]	40.3	30.5	21.8	16.4	15.0
Selectivity (w)	[%]	7.3	6.5	10.1	11.8	11.6
Product flow	[mmol/g/hr]					
	Methane	0.376	0.302	0.206	0.154	0.141
	Ethane	0.304	0.203	0.104	0.050	0.045
	Ethene	1.199	0.988	0.698	0.498	0.440
	Propane	17.152	10.807	5.710	3.450	3.031
	Propene	0.953	0.766	0.576	0.483	0.415
	Isobutane	41.213	48.472	50.794	52.298	53.322
	n-Butane	4.954	5.236	4.268	3.449	3.268
	t-2-Butene	0.165	0.175	0.156	0.147	0.130
	1-Butene	0.082	0.090	0.075	0.070	0.064
	Isobutene	0.344	0.353	0.318	0.287	0.268
	2-c-Butene	0.105	0.119	0.105	0.094	0.077
	Pentanes	2.147	2.246	1.927	1.591	1.534
	Hexane	2.514	2.514	2.514	2.514	2.514
Carbon Balance	[%]	103.6	104.7	97.5	93.9	94.2

Sample	HS5								
Time	[min]	1.00	4.50	10.50	16.00	44.00	78.67	101.50	183.00	199.50
Rate	[mol/g/hr]	8.5	7.6	7.3	7.0	6.9	7.0	6.8	6.2	6.0
Model	[mol/g/hr]	8.3	7.8	7.4	7.3	6.9	6.7	6.6	6.4	6.3
Conversion	[%]	16.9	15.3	14.7	14.1	13.9	14.0	13.6	12.3	12.0
Selectivity (w)	[%]	10.7	11.7	13.1	12.4	12.0	12.4	12.2	12.8	12.7
Product flow	[mmol/g/hr]									
	Methane	0.208	0.209	0.245	0.199	0.166	0.193	0.198	0.159	0.159
	Ethane	0.064	0.058	0.055	0.048	0.043	0.049	0.052	0.035	0.032
	Ethene	0.655	0.639	0.639	0.558	0.543	0.553	0.522	0.455	0.427
	Propane	4.897	4.510	3.867	3.699	3.728	3.622	3.568	3.064	2.902
	Propene	0.546	0.560	0.556	0.504	0.498	0.524	0.484	0.455	0.430
	Isobutane	52.888	56.765	55.104	55.079	57.288	57.913	58.631	59.239	59.169
	n-Butane	2.655	2.557	2.441	2.368	2.503	2.642	2.576	2.416	2.423
	t-2-Butene	0.089	0.091	0.093	0.088	0.093	0.095	0.092	0.093	0.095
	1-Butene	0.038	0.044	0.046	0.040	0.043	0.045	0.045	0.044	0.044
	Isobutene	0.209	0.229	0.237	0.222	0.238	0.244	0.231	0.243	0.229
	2-c-Butene	0.064	0.067	0.066	0.064	0.070	0.071	0.070	0.074	0.070
	Pentanes	1.354	1.279	1.252	1.228	1.321	1.388	1.357	1.300	1.290
	Hexane	2.271	2.271	2.271	2.271	2.271	2.271	2.271	2.271	2.271
Carbon Balance	[%]	95.6	100.8	97.0	96.2	99.9	101.1	101.8	101.4	101.0

Sample	HS2								
Time	[min]	1.50	21.68	41.22	69.38	95.50	131.95	342.33	406.77
Rate	[mol/g/hr]	27.0	20.8	18.1	15.5	14.0	12.4	8.7	7.8
Model	[mol/g/hr]	27.0	20.7	18.0	15.6	14.1	12.6	8.5	7.8
Conversion	[%]	53.5	41.2	35.8	30.8	27.8	24.6	17.2	15.6
Selectivity (w)	[%]	7.8	9.6	10.1	10.8	11.2	12.2	15.9	15.3
Product flow	[mmol/g/hr]								
	Methane	0.414	0.331	0.301	0.263	0.235	0.206	0.159	0.146
	Ethane	0.291	0.203	0.162	0.120	0.095	0.070	0.030	0.025
	Ethene	1.556	1.411	1.309	1.149	0.999	0.855	0.510	0.447
	Propane	21.018	13.334	11.170	8.829	7.117	5.841	3.181	2.688
	Propene	1.322	1.224	1.142	1.051	0.929	0.853	0.681	0.593
	Isobutane	29.607	38.364	43.797	48.009	48.955	50.046	57.297	55.466
	n-Butane	5.956	6.335	6.288	5.935	5.476	5.018	4.109	3.617
	t-2-Butene	0.253	0.275	0.259	0.241	0.233	0.233	0.304	0.222
	1-Butene	0.112	0.130	0.128	0.126	0.119	0.116	0.143	0.100
	Isobutene	0.382	0.443	0.456	0.453	0.436	0.419	0.427	0.361
	2-c-Butene	0.165	0.179	0.178	0.174	0.163	0.159	0.187	0.146
	Pentanes	2.593	3.035	3.072	2.996	3.064	2.568	2.205	1.873
	Hexane	3.025	3.025	3.025	3.025	3.025	3.025	3.025	3.025
Carbon Balance	[%]	95.6	98.0	102.5	104.1	101.8	99.6	103.9	98.6

Sample	HS1									
Time	[min]	0.50	23.08	44.92	66.00	96.95	118.22	134.73	151.25	186.10	202.22
Rate	[mol/g/hr]	27.4	20.1	16.2	14.3	12.4	11.5	10.4	10.1	9.0	8.1
Model	[mol/g/hr]	27.4	19.9	16.6	14.4	12.3	11.2	10.5	9.9	8.9	8.5
Conversion	[%]	55.0	40.4	32.6	28.8	25.0	23.1	20.9	20.2	18.0	16.3
Selectivity (w)	[%]	8.2	8.3	8.9	9.4	10.1	10.2	10.7	10.3	11.5	11.8
Product flow	[mmol/g/hr]										
	Methane	0.398	0.272	0.223	0.199	0.177	0.163	0.153	0.146	0.139	0.131
	Ethane	0.338	0.189	0.131	0.100	0.074	0.058	0.049	0.043	0.036	0.031
	Ethene	1.394	1.075	0.921	0.816	0.700	0.609	0.560	0.514	0.453	0.417
	Propane	21.975	12.700	8.840	7.378	5.902	4.883	4.288	3.871	3.442	3.058
	Propane	1.197	0.942	0.794	0.735	0.675	0.607	0.585	0.517	0.509	0.465
	Isobutane	28.620	38.775	43.125	46.527	50.268	51.107	52.551	53.514	54.962	55.795
	n-Butane	6.337	6.439	6.039	5.782	5.495	5.076	4.816	4.536	4.362	4.062
	t-2-Butene	0.224	0.201	0.208	0.207	0.207	0.196	0.192	0.174	0.164	0.185
	1-Butene	0.088	0.094	0.087	0.089	0.088	0.082	0.083	0.078	0.080	0.077
	Isobutene	0.401	0.422	0.402	0.395	0.398	0.381	0.369	0.356	0.354	0.331
	2-c-Butene	0.153	0.155	0.146	0.142	0.146	0.140	0.130	0.125	0.124	0.117
	Pentanes	2.459	3.828	3.055	2.947	2.902	3.150	2.700	3.185	2.377	2.037
	Hexane	0.998	0.998	0.998	0.998	0.998	0.998	0.998	0.998	0.998	0.998
Carbon Balance	[%]	95.4	97.7	96.0	98.0	100.6	99.7	99.6	100.7	100.6	100.1

Sample	HS1											
Time	[min]	8.00	26.03	42.60	58.95	93.97	111.97	139.62	155.90	185.28	219.38	235.27
Rate	[mol/g/hr]	23.6	18.6	16.4	14.7	12.9	11.5	10.7	10.1	9.4	9.1	8.7
Model	[mol/g/hr]	23.6	19.3	16.8	15.1	12.5	11.5	10.3	9.7	8.9	8.1	7.8
Conversion	[%]	47.1	37.2	32.8	29.4	25.7	23.1	21.3	20.3	18.8	18.2	17.3
Selectivity (w)	[%]	8.0	8.9	9.4	9.8	10.8	11.0	11.4	11.6	12.1	12.3	12.5
Product flow	[mmol/g/hr]											
	Methane	0.419	0.335	0.303	0.279	0.227	0.227	0.206	0.199	0.075	0.165	0.164
	Ethane	0.278	0.193	0.154	0.127	0.084	0.077	0.062	0.056	0.046	0.039	0.036
	Ethene	1.532	1.325	1.222	1.116	0.892	0.861	0.758	0.707	0.613	0.548	0.530
	Propane	17.426	12.424	10.172	8.610	5.999	5.704	4.827	4.543	3.665	3.463	3.257
	Propene	1.385	1.185	1.071	1.000	0.830	0.822	0.758	0.715	0.661	0.607	0.576
	Isobutane	33.615	42.457	46.226	48.897	47.216	53.228	52.951	54.129	52.950	51.422	52.374
	n-Butane	5.443	5.867	5.801	5.557	4.898	4.920	4.581	4.461	4.125	3.841	3.743
	t-2-Butene	0.292	0.275	0.265	0.247	0.233	0.224	0.218	0.211	0.201	0.198	0.197
	1-Butene	0.120	0.132	0.123	0.122	0.110	0.111	0.105	0.105	0.096	0.095	0.099
	Isobutene	0.437	0.469	0.469	0.458	0.424	0.433	0.408	0.409	0.384	0.368	0.364
	2-c-Butene	0.189	0.191	0.181	0.171	0.162	0.158	0.151	0.151	0.143	0.138	0.133
	Pentanes	2.628	2.780	2.780	2.636	2.497	2.417	2.249	2.194	2.035	1.992	1.854
	Hexane	2.936	2.936	2.936	2.936	2.936	2.936	2.936	2.936	2.936	2.936	2.936
Carbon Balance	[%]	96.0	101.5	103.2	103.9	95.4	103.6	101.0	101.9	97.9	94.4	95.1

Sample	HS10						
Time	[min]	0.50	2.00	7.50	25.00	74.00	146.00
Rate	[mol/g/hr]	1.2	1.1	1.3	1.3	1.3	1.4
Model	[mol/g/hr]	1.3	1.3	1.3	1.3	1.3	1.3
Conversion	[%]	2.5	2.2	2.8	2.7	2.8	2.8
Selectivity (w)	[%]	26.4	30.9	28.6	28.7	27.2	31.0
Product flow	[mmol/g/hr]						
	Methane	0.105	0.080	0.129	0.097	0.084	0.138
	Ethane	0.009	0.007	0.009	0.007	0.004	0.010
	Ethene	0.096	0.041	0.106	0.086	0.064	0.110
	Propane	0.310	0.278	0.332	0.326	0.325	0.363
	Propene	0.150	0.152	0.162	0.159	0.135	0.190
	Isobutane	65.124	66.499	67.088	61.590	62.377	66.502
	n-Butane	0.550	0.461	0.581	0.567	0.572	0.611
	t-2-Butene	0.037	0.041	0.041	0.046	0.047	0.054
	1-Butene	0.014	0.019	0.017	0.020	0.017	0.023
	Isobutene	0.103	0.140	0.133	0.135	0.130	0.158
	2-c-Butene	0.026	0.028	0.032	0.033	0.035	0.038
	Pentanes	0.247	0.241	0.252	0.232	0.232	0.244
	Hexane	2.839	2.839	2.839	2.839	2.839	2.839
Carbon Balance	[%]	100.2	102.0	103.4	95.0	96.1	105.7

APPENDIX IX

Reaction data for cyclohexanol dehydration

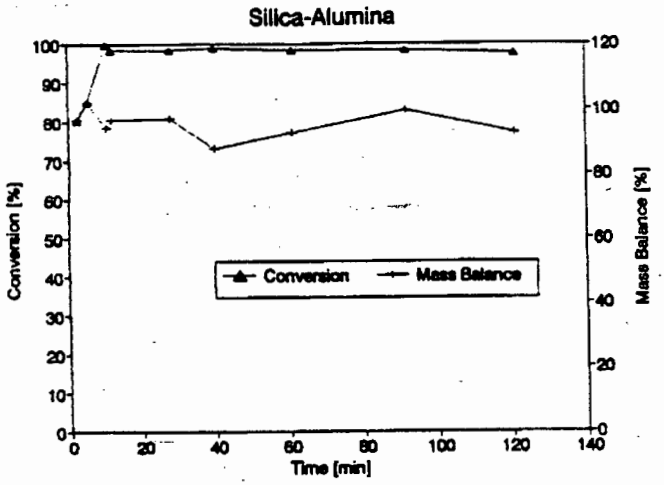
Silica-Alumina
Conversion [%]
Mass Balance [%]
Time [min]
Conversion
Mass Balance

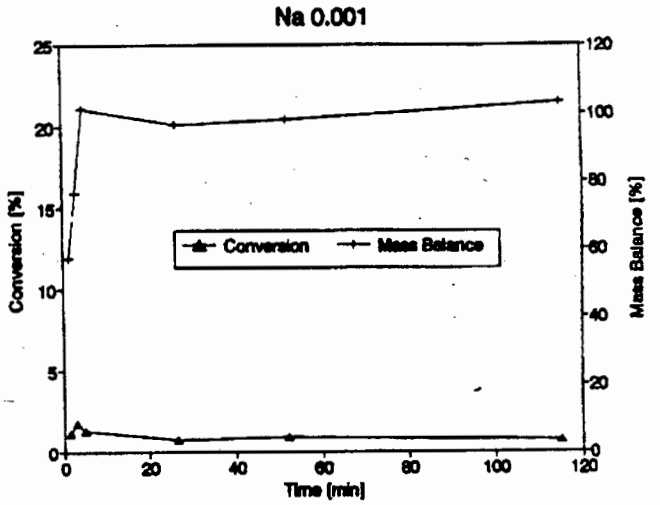
Na 0.001
Conversion [%]
Mass Balance [%]
Time [min]
Conversion
Mass Balance

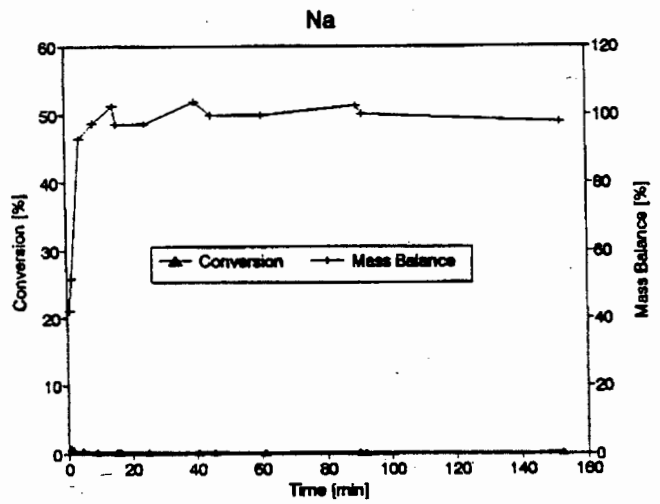
Na
Conversion [%]
Mass Balance [%]
Time [min]
Conversion
Mass Balance

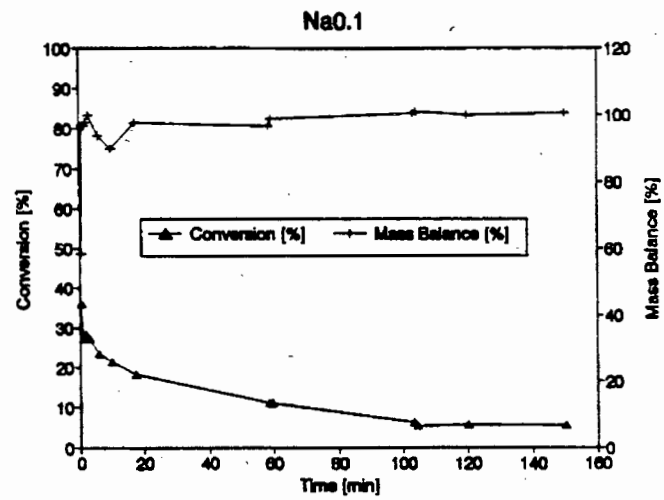
Na0.1
Conversion [%]
Mass Balance [%]
Time [min]
Conversion [%]
Mass Balance [%]

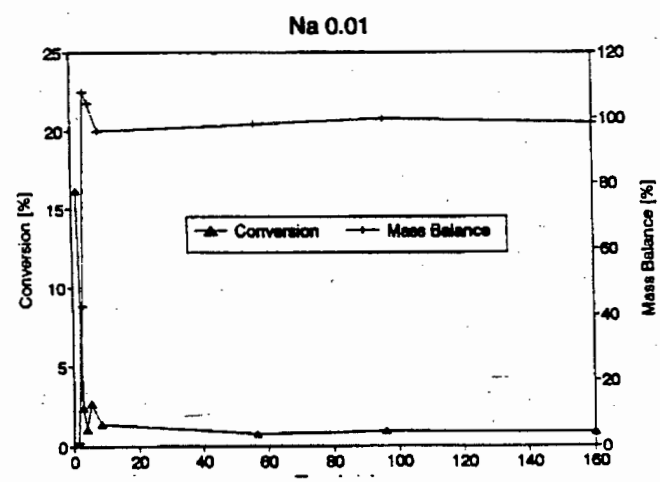
Na 0.01
Conversion [%]
Mass Balance [%]
Time [min]
Conversion
Mass Balance

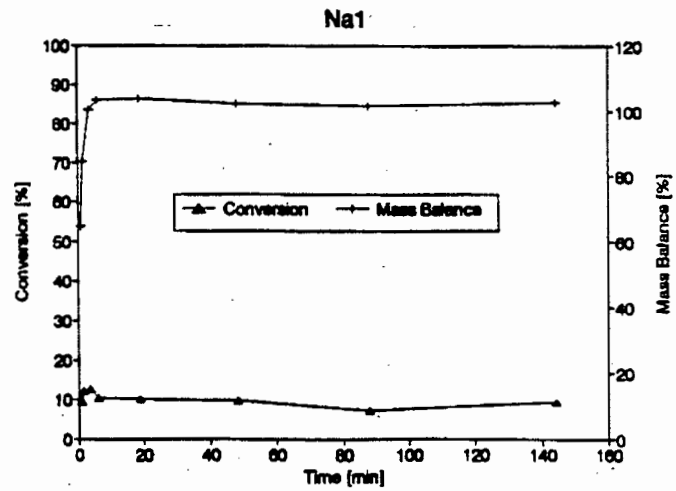
Na1
Conversion [%]
Mass Balance [%]
Time [min]
Conversion
Mass Balance

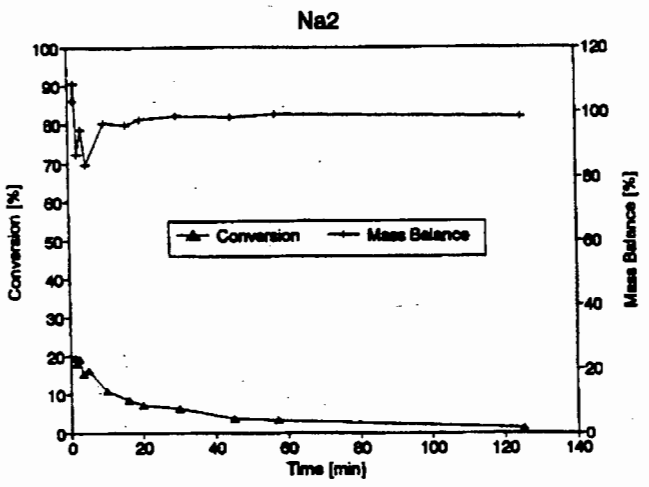
Na2
Conversion [%]
Mass Balance [%]
Time [min]
Conversion
Mass Balance

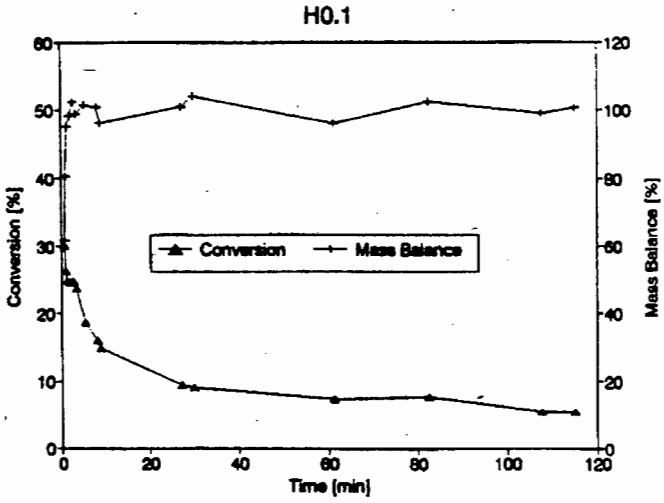
H0.1
Conversion [%]
Mass Balance [%]
Time [min]
Conversion
Mass Balance

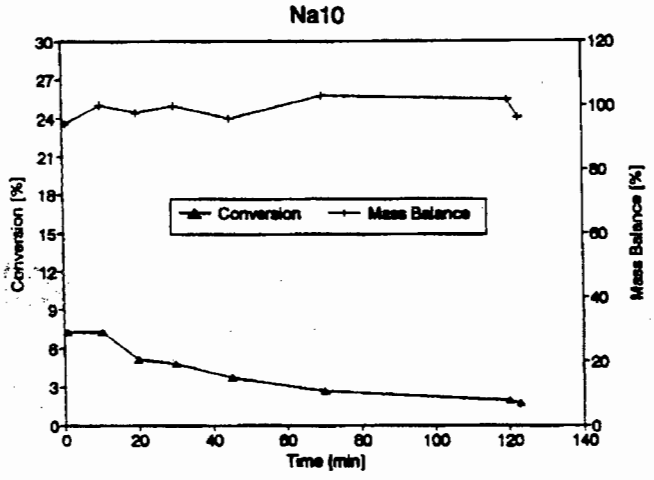
Na10
Conversion [%]
Mass Balance [%]
Time [min]
Conversion
Mass Balance

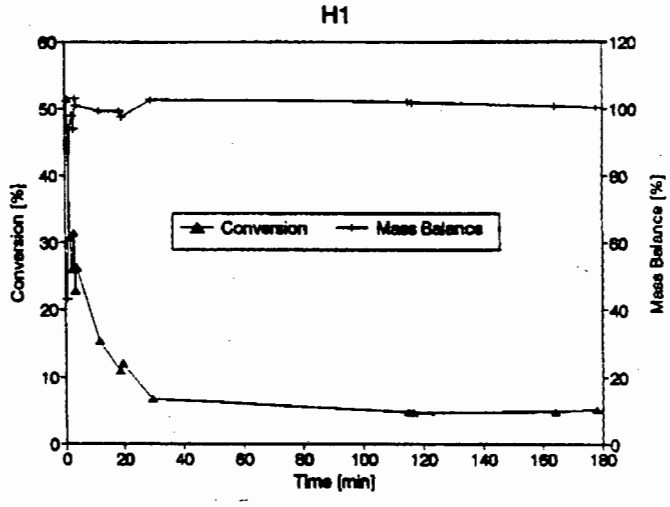
H1
Conversion [%]
Mass Balance [%]
Time [min]
Conversion
Mass Balance

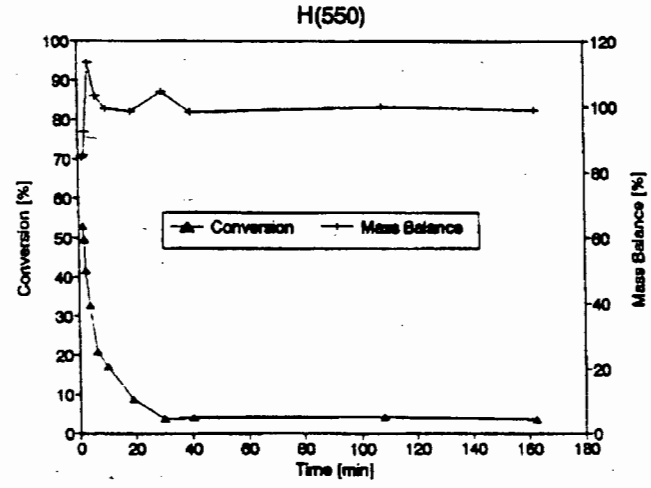
H(550)
Conversion [%]
Mass Balance [%]
Time [min]
Conversion
Mass Balance

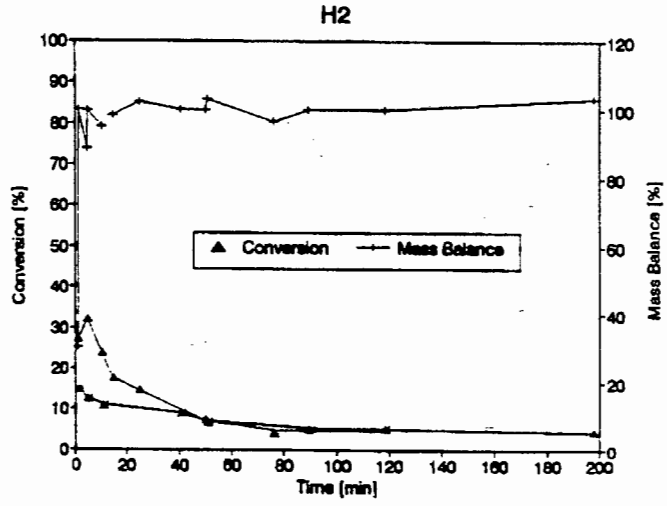
H2
Conversion [%]
Mass Balance [%]
Time [min]
Conversion
Mass Balance

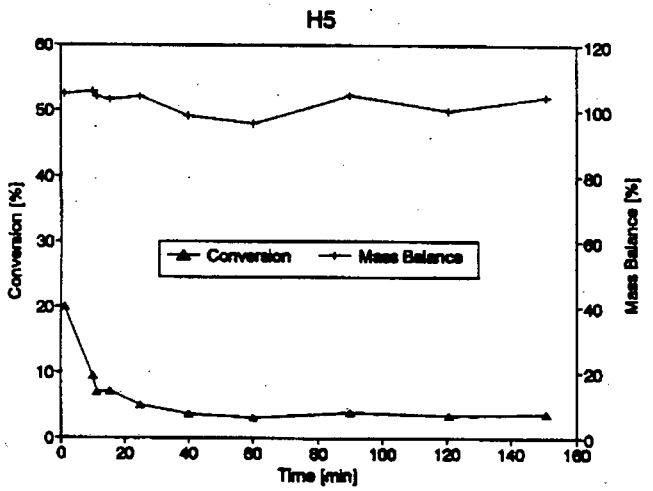
H5
Conversion [%]
Mass Balance [%]
Conversion
Mass Balance
Time [min]

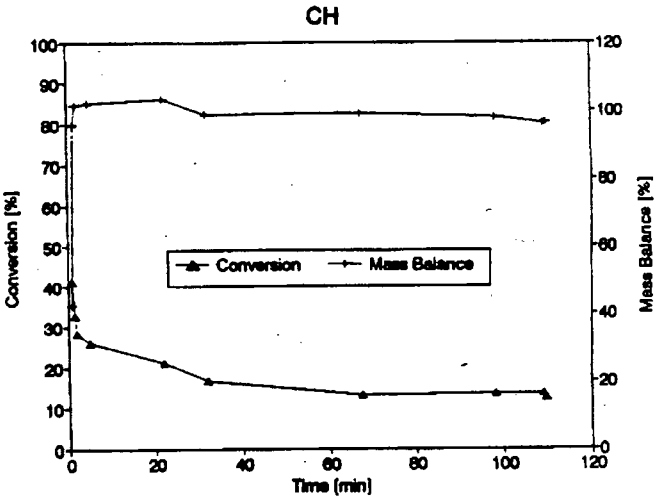
CH
Conversion [%]
Mass Balance [%]
Conversion
Mass Balance
Time (min)

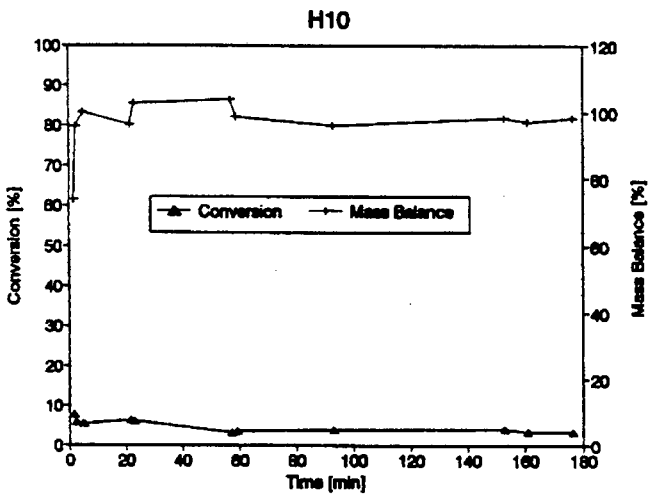
H10
Conversion [%]
Mass Balance [%]
Conversion
Mass Balance
Time [min]

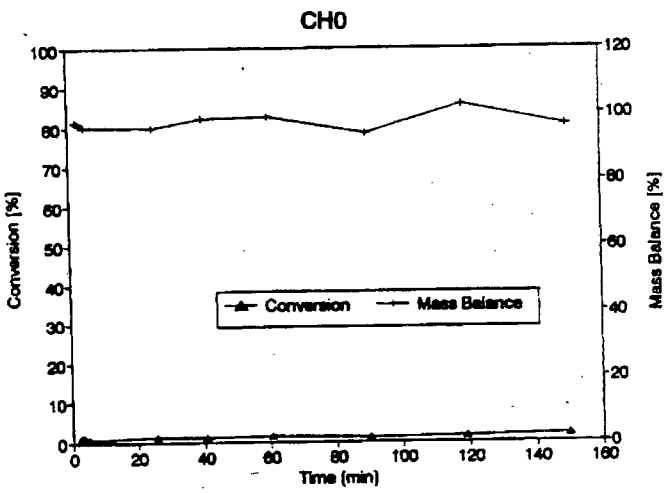
CH0
Conversion [%]
Mass Balance [%]
Conversion
Mass Balance
Time (min)

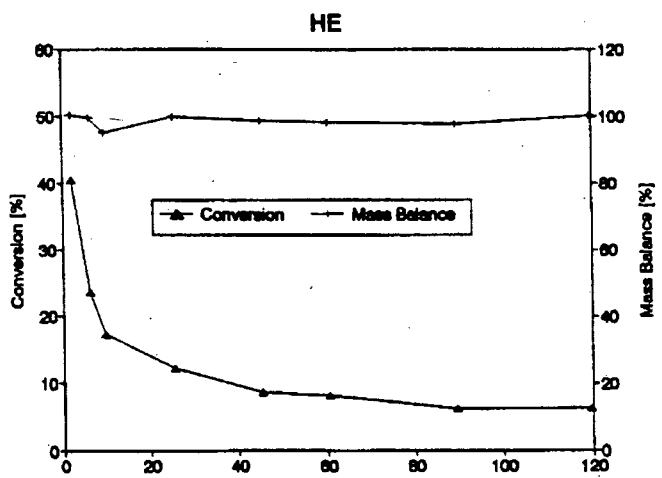
HE
Conversion [%]
Mass Balance [%]
Conversion
Mass Balance

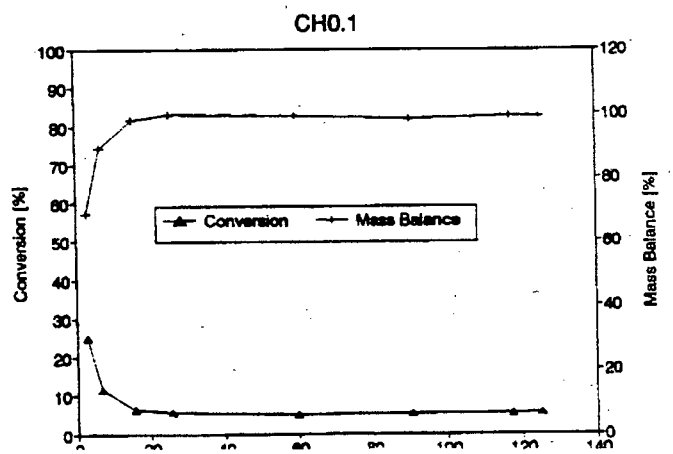
CH0.1
Conversion [%]
Mass Balance [%]
Conversion
Mass Balance

CH1

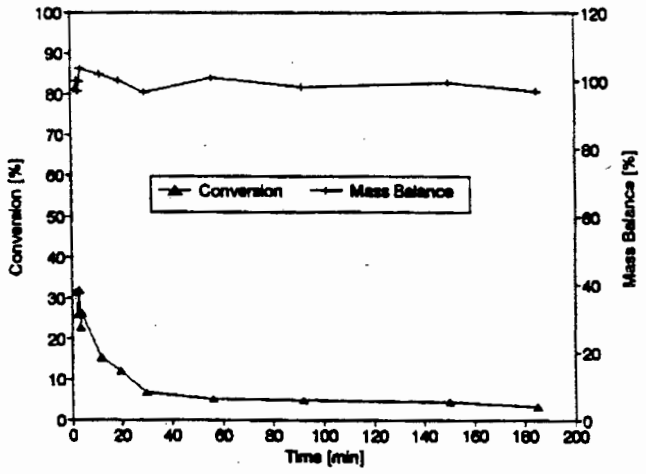

HS1

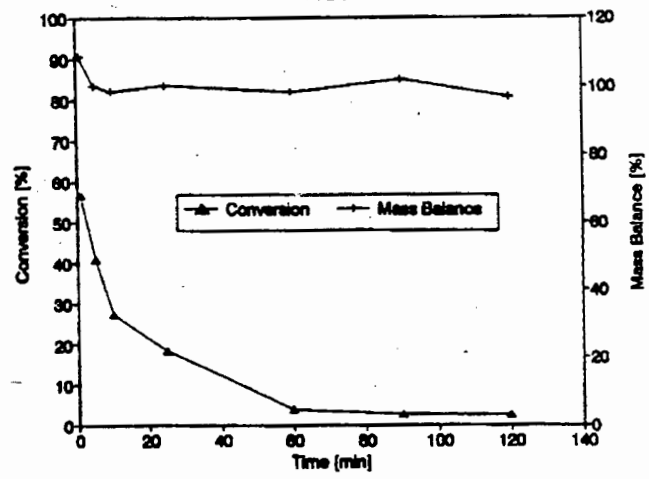

HS

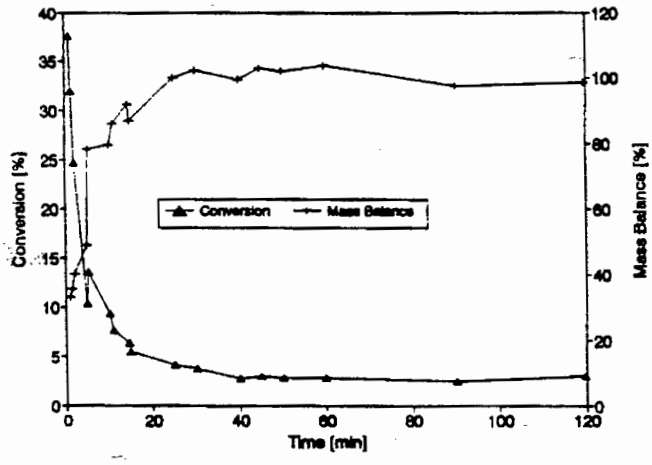

HS2

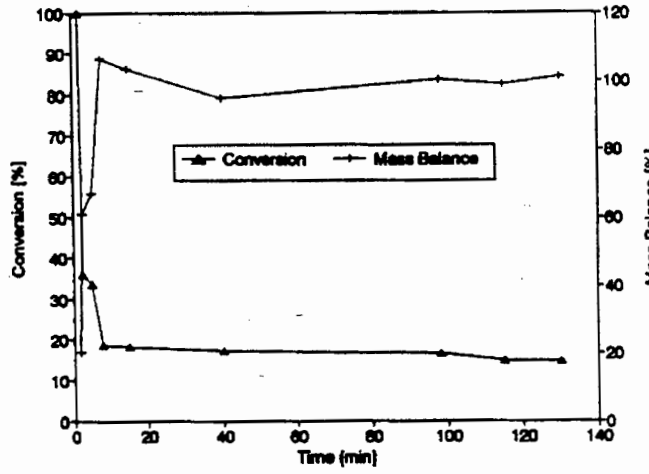

HS0.1

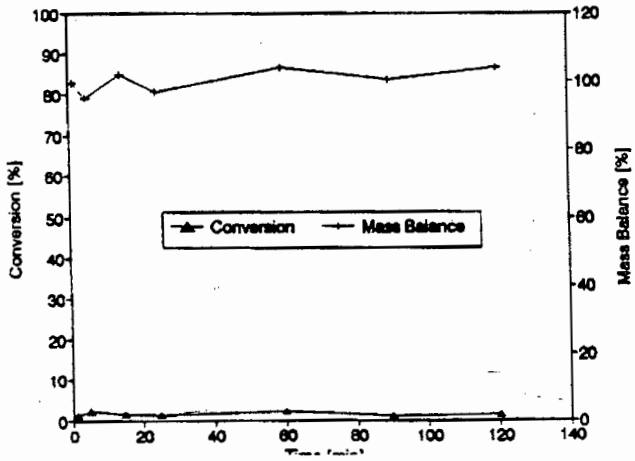

HS5

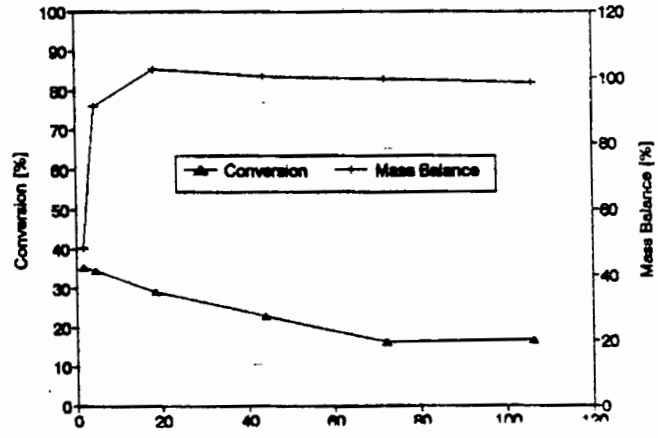

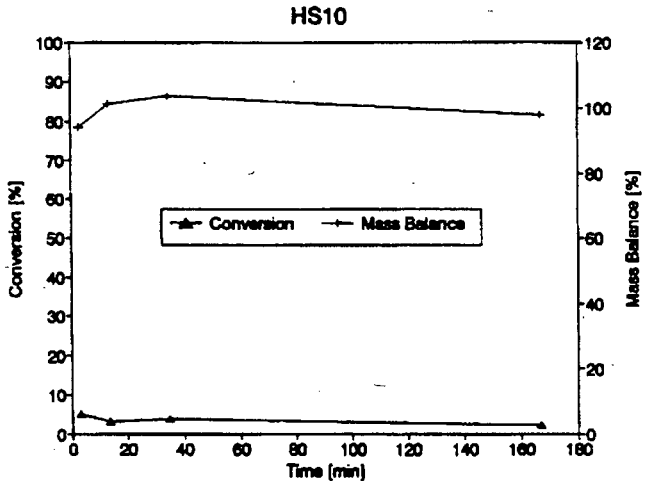
HS10
Conversion [%]
Mass Balance [%]
Conversion
Mass Balance
Time [min]

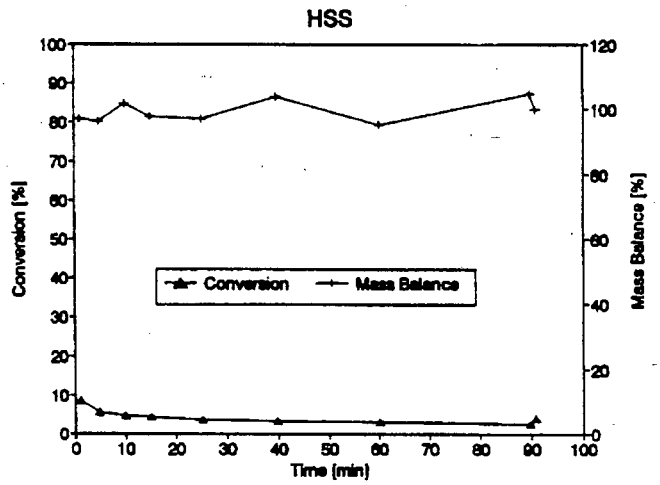
HSS
Conversion [%]
Mass Balance [%]
Conversion
Mass Balance
Time [min]

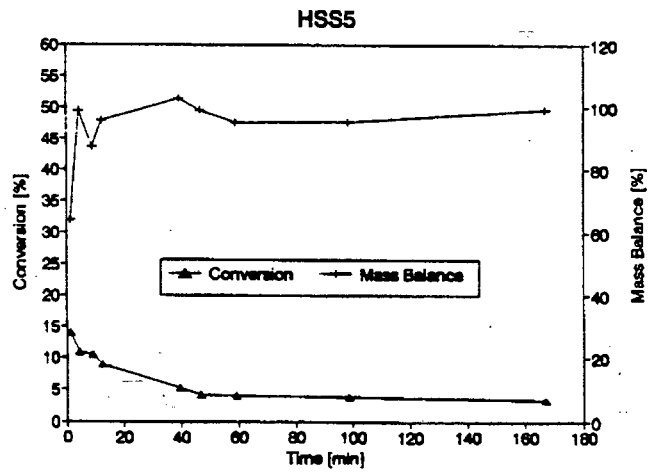
HSS5
Conversion [%]
Mass Balance [%]
Conversion
Mass Balance
Time [min]

APPENDIX X

Reaction data for naphthalene isopropylation

	Aluminium Chloride				
Time [min]	14	138	255	357	600
Conversion of naphthalene	0.88	10.07	12.39	14.16	14.78
2,6-DIPN Selectivity	16.56	30.96	33.81	33.31	32.85
Isopropyl naphthalene Selectivity	53.3	10.3	8.8	10.0	9.6
DIPN Selectivity	45.7	81.4	83.9	82.8	82.7
Tri-isopropyl naphthalene Sel.	1.0	8.4	7.3	7.2	7.6
2,6-DIPN yield	0.15	3.12	4.19	4.72	4.86
Ratio if 2,6-DIPN to 2,7-DIPN	1.58	0.67	0.69	0.69	0.67

	Na	
Time [min]	27	480
Conversion of naphthalene	0.0	0.1
2,6-DIPN Selectivity	21.0	16.0
Isopropyl naphthalene Selecti	52.2	61.4
DIPN Selectivity	47.8	33.2
Tri-isopropyl naphthalene Sel.	0.0	5.4
2,6-DIPN yield	0.01	0.01
Ratio if 2,6-DIPN to 2,7-DIPN	2.46	1.99

	Na1			
Time [min]	30	80	241	480
Conversion of naphthalene	0.4	0.4	0.7	0.7
2,6-DIPN Selectivity	2.4	2.8	2.1	3.2
Isopropyl naphthalene Selecti	31.3	80.8	71.2	64.6
DIPN Selectivity	20.6	14.6	3.0	7.1
Tri-isopropyl naphthalene Sel.	48.0	4.6	0.0	28.3
2,6-DIPN yield	0.01	0.01	0.02	0.02
Ratio if 2,6-DIPN to 2,7-DIPN	7.46	7.43	7.24	6.19

	H(550)				
Time [min]	6	124	250	368	480
Conversion of naphthalene	0.3	1.4	1.9	2.4	2.6
2,6-DIPN Selectivity	2.0	33.3	39.5	40.3	40.0
Isopropyl naphthalene Selecti	87.0	41.9	36.8	34.2	34.0
DIPN Selectivity	11.0	57.1	62.1	64.7	65.0
Tri-isopropyl naphthalene Sel.	2.0	1.0	0.0	1.1	0.9
2,6-DIPN yield	0.01	0.46	0.73	0.95	1.02
Ratio if 2,6-DIPN to 2,7-DIPN	0.68	2.38	2.12	1.97	1.88

	H2				
Time [min]	20	130	260	363	480
Conversion of naphthalene	1.5	1.7	1.6	1.7	1.5
2,6-DIPN Selectivity	0.7	2.0	2.7	3.6	4.0
Isopropyl naphthalene Selecti	91.1	91.2	90.9	87.5	85.4
DIPN Selectivity	8.9	8.1	8.3	9.8	12.4
Tri-isopropyl naphthalene Sel.	-0.0	0.7	0.0	2.7	2.2
2,6-DIPN yield	0.01	0.03	0.04	0.06	0.06
Ratio if 2,6-DIPN to 2,7-DIPN	0.77	2.18	2.27	2.44	2.44

	HE		
Time [min]	1.5	86	480
Conversion of naphthalene	0.8	0.8	1.0
2,6-DIPN Selectivity	13.1	15.1	12.9
Isopropyl naphthalene Selecti	65.3	59.1	68.4
DIPN Selectivity	31.3	40.9	30.2
Tri-isopropyl naphthalene Sel.	3.4	0.0	0.0
2,6-DIPN yield	0.10	0.12	0.13
Ratio if 2,6-DIPN to 2,7-DIPN	7.51	3.79	6.28

	CH					
Time [min]	1.5	7.5	118	242	362	480
Conversion of naphthalene	0.3	0.4	3.6	3.8	4.0	4.3
2,6-DIPN Selectivity	3.0	42.3	50.7	66.0	64.8	64.0
Isopropyl naphthalene Selectivit	90.7	46.1	22.6	12.8	13.3	13.6
DIPN Selectivity	9.3	49.6	67.3	83.1	82.5	82.3
Tri-isopropyl naphthalene Sel.	0.0	4.3	0.0	4.1	4.1	4.1
2,6-DIPN yield	0.01	0.16	1.84	2.51	2.56	2.76
Ratio if 2,6-DIPN to 2,7-DIPN	1.44	7.27	5.09	4.60	4.44	4.28

	HS					
Time [min]	1.5	10	100	130	222	480
Conversion of naphthalene	0.3	0.4	1.0	2.0	2.6	3.8
2,6-DIPN Selectivity	3.0	31.5	62.9	60.9	65.8	60.0
Isopropyl naphthalene Selectivit	90.7	61.4	24.6	22.5	19.8	18.3
DIPN Selectivity	9.3	38.6	75.4	77.5	80.2	81.7
Tri-isopropyl naphthalene Sel.	0.0	0.0	0.0	0.0	0.0	-0.0
2,6-DIPN yield	0.01	0.12	0.61	1.25	1.73	2.31
Ratio if 2,6-DIPN to 2,7-DIPN	1.44	8.06	4.99	5.04	4.58	4.00

	HS0.1				
Time [min]	1.5	113	234	360	480
Conversion of naphthalene	0.9	3.6	4.3	5.2	5.1
2,6-DIPN Selectivity	70.2	73.8	73.2	75.8	73.8
Isopropyl naphthalene Selecti	20.0	8.5	8.3	8.7	9.2
DIPN Selectivity	80.0	86.5	86.7	88.1	85.8
Tri-isopropyl naphthalene Sel.	0.0	5.1	0.0	3.2	5.0
2,6-DIPN yield	0.66	2.63	3.17	3.98	3.73
Ratio if 2,6-DIPN to 2,7-DIPN	8.02	7.26	7.22	7.23	7.26

	HS1				
Time [min]	1.5	112	235	355	480
Conversion of naphthalene	0.6	1.1	2.2	2.8	3.2
2,6-DIPN Selectivity	24.9	47.7	56.3	58.6	64.0
Isopropyl naphthalene Selecti	62.1	38.7	29.4	23.4	21.1
DIPN Selectivity	36.0	60.0	69.2	75.0	77.6
Tri-isopropyl naphthalene Sel.	1.9	1.3	0.0	1.6	1.3
2,6-DIPN yield	0.15	0.51	1.21	1.66	2.07
Ratio if 2,6-DIPN to 2,7-DIPN	6.23	6.98	7.42	5.91	7.75

	HS5				
Time [min]	1.5	68	151	232	480
Conversion of naphthalene	2.7	3.3	3.7	3.9	3.9
2,6-DIPN Selectivity	50.7	50.9	51.3	53.2	59.1
Isopropyl naphthalene Selecti	21.9	20.5	18.3	17.7	17.1
DIPN Selectivity	66.4	67.9	69.4	69.9	69.6
Tri-isopropyl naphthalene Sel.	11.7	11.5	0.0	12.4	13.4
2,6-DIPN yield	1.35	1.69	1.89	2.06	2.32
Ratio if 2,6-DIPN to 2,7-DIPN	5.75	6.81	7.01	7.27	7.56

	HSS			
Time [min]	1.5	120	353	480
Conversion of naphthalene	0.3	0.9	1.1	1.5
2,6-DIPN Selectivity	3.2	5.8	8.2	7.8
Isopropyl naphthalene Selecti	92.3	87.0	81.4	74.3
DIPN Selectivity	7.7	13.0	18.6	25.2
Tri-isopropyl naphthalene Sel.	-0.0	-0.0	0.0	0.6
2,6-DIPN yield	0.01	0.05	0.09	0.12
Ratio if 2,6-DIPN to 2,7-DIPN	0.72	0.81	0.79	0.78

APPENDIX XI

Comparison of the characterisation of sample Na-MOR with that performed at the Fritz-Haber Institute

Elemental analysis performed at Fritz-Haber Institute:

Mass weighed : 201.03 mg dissolved in 500 ml H_2O

Concentrations determined by AAS:

Na : 0.866 μg/ml (Diluted 1:20)
Al : 19.725 μg/ml (Diluted 1:1)
Si : 131.95 μg/ml (Diluted 1:1)

Analysis:

	Mass in weighed sample [mg]	Wt% in true zeolite [%]	Mole% [%]
Na_2O	11.67	6.71	6.92
Al_2O_3	18.64	10.72	6.72
SiO_2	141.12	81.15	86.36
Total	171.43	98.58	100.00

Moisture content by elemental analysis : (201.03-171.43)/201.03 = 14.72%
Moisture content by thermogravimetric analysis: = 13.5 %

Formula: $Na_{6.65}Al_{6.46}Si_{41.5}O_{96}$

Si/Al = 6.42

Elemental analysis in this research:

Mass weighed : 200.6 mg digested aand disolved to make 500 ml solution

Concentrations determined by AAS:

Na : 17.34 μg/ml
Al : 20.04 μg/ml
Si : 133.44 μg/ml

Analysis:

	Mass in weighed sample [mg]	Wt% in true zeolite [%]	Mole% [%]
Na_2O	11.68	6.58	6.86
Al_2O_3	18.94	10.67	6.75
SiO_2	142.72	80.39	86.39
Total	173.34	97.64	100.00

Moisture content by elemental analysis : (200.6-173.3)/200.6 = 13.6%
Moisture content by thermogravimetric analysis: = 11.5 %

Formula: $Na_{6.58}Al_{6.49}Si_{41.5}O_{96}$

Si/Al = 6.4

Both the Si/Al and Na/Al ratios can be seen to be very similar. Although a small change in moisture content was seen, this was probably due to different weather and storage conditions.

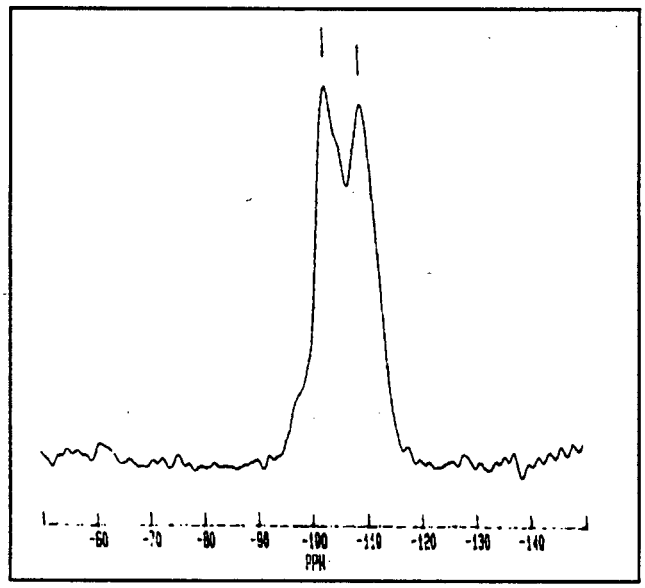

^{29}Si MAS NMR from Fritz-Haber institute

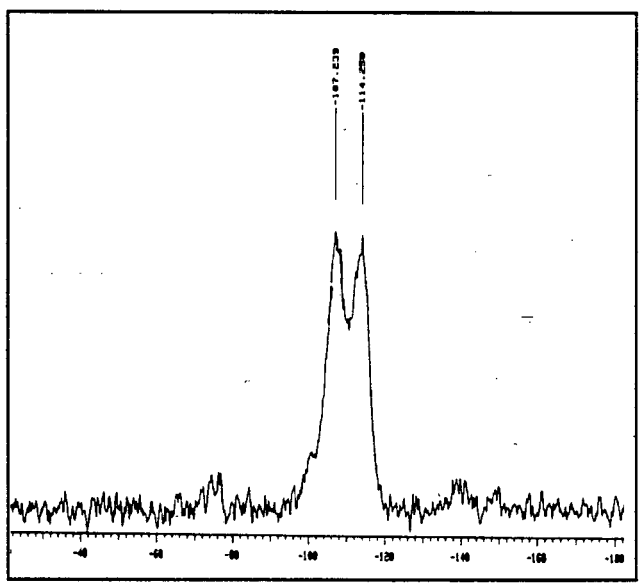

^{29}Si MAS NMR of sample Na

The spectra show similar peak intensities and both gave framework Si/Al ratios of about 6.4

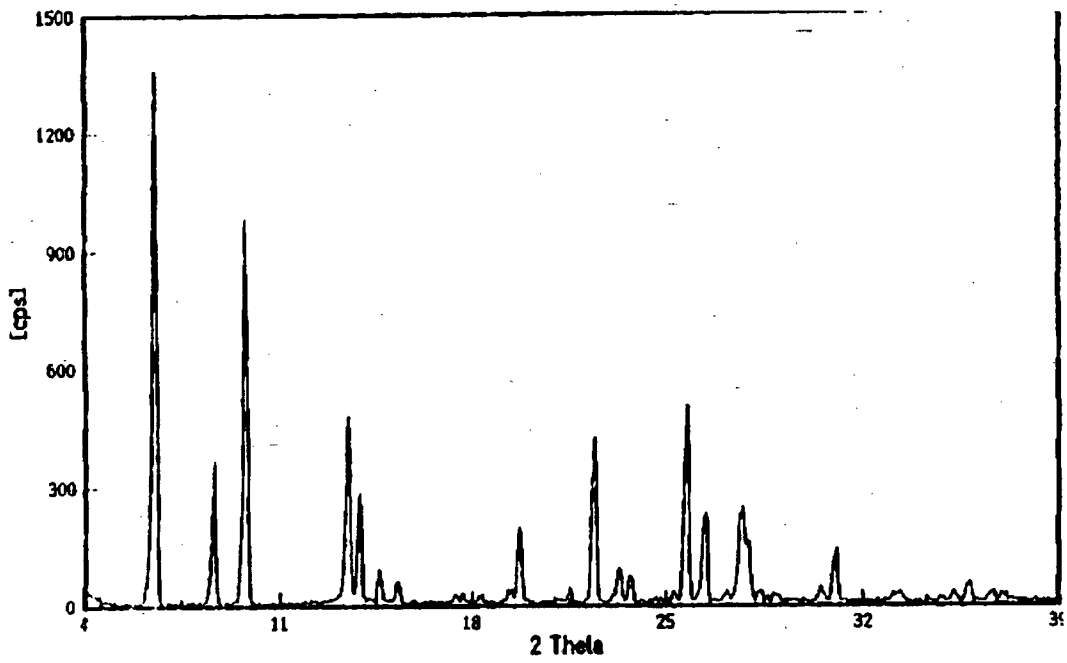

XRD pattern observed at Fritz-Haber Institute

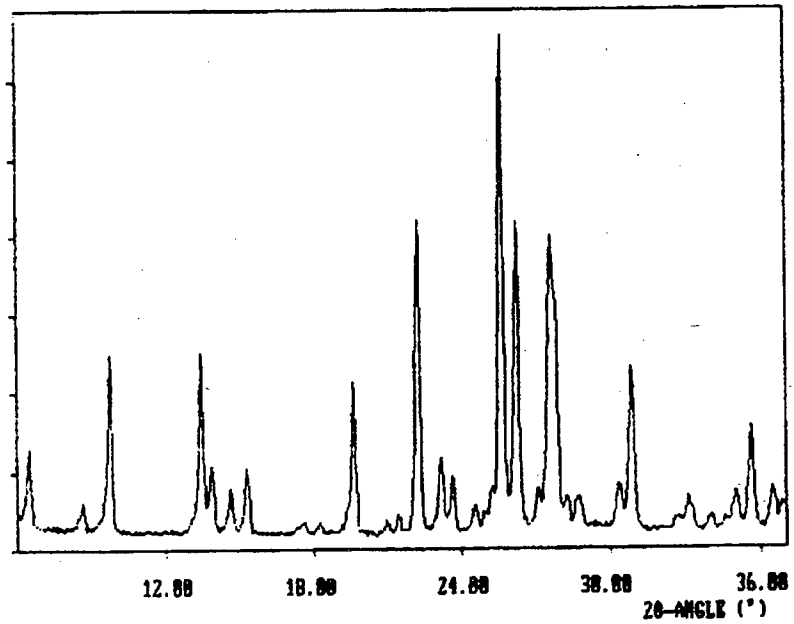

XRD pattern of sample Na

The differences XRD patterns is in the region where 2θ is below 10° and explanation of this is given in Section 3.1.3.

REFERENCES

Abbot, J. and Geurzoni, F.N., *Applied Catalysis*, **85** (1992) 173.

Addison, S.W., Cartlidge, S., Harding, D.A. and McElhiney, G., *Applied Catalysis*, **45** (1988) 307.

Ajot, H., Joly, J.F., Lynch, J., Raatz, F. and Caullet, P., *in* "Characterisation of porous solids II" (F. Rodriguez-Reinoso, J. Rouqueral, K.S.W. Sing and K.K. Unger, Eds.) Studies in Surface Science and Catalysis, Vol.62 , p.583, Elsevier, Amsterdam, 1991.

Akitt, J.W., *Progress in NMR Spectroscopy*, **21** (1989) 1.

Anderson, M.W. and Klinowski, J., *Zeolites*, **6** (1986) 455.

Bajpai, P.K., Rao, M.S. and Gokhale, K.V.G.K., *in* "Thermal analysis, International conference proceedings", **1** (1982) 558.

Bamwenda, G.R., Zhao Y.X. and Wojciechowski, B.W., *J. Catal.*, **250** (1994) 243.

Barras, J. and Klinowski, J., *J Chem. Soc., Faraday Trans. 1*, **90** (1994) 3719.

Barrer, R.M., *J. Chem. Soc.*, (1948) 2158.

Barrer, R.M., *Brit. Chem. Eng.*, **4** (1959) 267.

Barrer, R.M. and Makki, M.B., *Can. J. of Chem.*, **42** (1964) 1481.

Barrer, R.M. and Peterson, D.L., *Proc. R. Soc. London, Ser. A*, **280** (1964) 60.

Beaumont, R., and Barthomeuf, D., *J. Catal.*, **26** (1972) 218.

Beaumont, R., and Barthomeuf, D., *J. Catal.*, **27** (1973) 45.

Beaumont, R., and Barthomeuf, D., *J. Catal.*, **30** (1973) 288.

Belenkaja, I.M., Dubinin, M.M. and Krishtofori, I.I., *Izv. Akad. Nauk SSSR, Ser. Khim.* **7** (1971) 2505.

Beyer, H.K., and Belenykaya, I., *in* "Catalysis by zeolites" (B. Imelik, C. Naccache, Y Ben Taarit, J.C. Vedrine, G. Condurrer and H. Praliand, Eds.) Studies in Surface Science and Catalysis, Vol.5, p.203, Elsevier, Amsterdam, 1980.

Beyer, H.K., Beleykaja, I.M., Mishin, I.W. and Borbely, G., *in* "Structure and reactivity of

modified zeolites" (P.A. Jacobs, N. I. Jaeger, P. Jiru, V.B. Kazansky and G. Scholz-Elkoff, Eds.), Studies in Surface Science and Catalysis, Vol.18, p.133, Elsevier, Amsterdam, 1984.

Beyerlein, R.A., McVicker, G.B., Yacullo, L.N. and Ziemiak, J.J., *J. Phys. Chem.*, **92** (1988) 1967.

Beyerlein, R.A., McVicker, G.B., Yacullo, L.N. and Ziemiak, J.J., *ACS Meeting, Div. Petrol Chem., New York*, **31** (1986) 190.

Bierenbaum, H.S., Subhavadh, C. and Weiss, A.H., *J. Catal.*, **23** (1971) 61.

Bodart, P., Nagy, J.B., Gabelica, Z. and Derouane, E.G., *J. de Chemie Physique*, **83** (1986) 778.

Bosáček, V. and Freude, D., *in* "Innovation in zeolite material science" (P.J. Grobet, W.J. Mortier, E.F. Vansant and G. Schulz-Ekloff, Eds.) Studies in Surface Science and Catalysis, Vol.37, p.231, Elsevier, Amsterdam, 1988.

Breck, D.W., *in* "Zeolite molecular sieves", Wiley, New York, 1974.

Brog, K.C., Jones, W.H. and Verber, C.M., *Phys. Lett.*, **20** (1966) 258.

Brunner, E., Ernst, H., Freude, D., Hunger, M. and Pfeifer, H., *in* "Innovation in zeolite material science" (P.J. Grobet, W.J. Mortier, E.F. Vansant and G. Schulz-Ekloff, Eds.) Studies in Surface Science and Catalysis, Vol.37, p.155, Elsevier, Amsterdam, 1988.

Brunner, E., Ernst, H., Freude, D., Hunger, M., Krause, C.B., Prager, D., Reschetilowski, W., Schwilger, W. and Bergk, K.H., *Zeolites*, **9** (1989) 282.

Brunner, E., Ernst, H., Freude, D., Fröhlich, T., Hunger, M. and Pfeifer, H., *in* "Zeolites, facts, figures, future" (P.A. Jacobs and R.A. van Santen, Eds.) Studies in Surface Science and Catalysis, Vol.49, p.623, Elsevier, Amsterdam, 1989.

Brunner, E., Ernst, H., Freude, D., Fröhlich, T., Hunger, M. and Pfeifer, H., *J. Catal.*, **127** (1991) 34.

Brunner, E., Beck, K., Koch, M., Pfeifer, H., Staudte, B. and Zscherpel, D., *in* "Zeolites and related microporous materials" (J. Weitkamp, H.G. Karge, H. Pfeifer and W.

Hölderich, Eds.) Studies in Surface Science and Catalysis, Vol.84, p.357, Elsevier, Amsterdam, 1994.

Cannings, F.R., *J. Phys. Chem.*, **72** (1968) 350.

Carvajal, R., Chu, P.J. and Lunsford, J.H., *J. Catal.*, **125** (1990) 123.

Chen, N.Y., *J. Phys. Chem.*, **80** (1976) 60.

Chen, N.Y. and Smith, F.A., *Inorganic Chemistry*, **15** (1976) 295.

Chen, F.R., Davis, J.G. and Fripiat, J.J., *J. Catal.*, **133** (1992) 263.

Chumbale, V.R., Chandwadkar, A.J. and Rao, B.S., *Zeolites*, **12** (1992) 63.

Corma, A., Planelles, J., Sanchez-Marin, J. and Tomas, F., *J Catal.*, **93** (1985) 30.

Corma, A., Fornes, V., Perez-Pariente, J., Sastre, E., Martens, J.A. and Jacobs, P.A., *in* "Perspectives in molecular sieve science" (W.H. Flank and T.E. Whyte Jr., Eds.) ACS Symp. Ser., No.368, p.555, Amer. Chem. Soc., Washington, (1988).

Corma, A., *in* "Zeolites, facts, figures, future" (P.A. Jacobs and R.A. van Santen, Eds.) Studies in Surface Science and Catalysis, Vol.49, p.49., Elsevier, Amsterdam, 1989.

Corma, A., Faraldos, M. and Mirsud, A., *Applied Catalysis*, **47** (1989) 125.

Corma, A., Miguel, P. and Orchilles, A.V., *J. Catal.*, **145** (1994) 171.

Crocker, M., Herold, R.H.M., Sonnemans, M.H.W., Emeis, C.A., Wilson, A.E. and van der Moolen, J.N., *J. Phys. Chem.*, **97** (1993) 432.

Csicsery, S., *in* "Catalysis by microporous materials" (H.K. Beyer, H.G. Karge, I. Kiricsi and J.B. Nagy, Eds.) Studies in Surface Science and Catalysis, Vol.94, p.1, Elsevier, Amsterdam, 1995.

Cvetanovic, R.J. and Amenomiya, Y., *Catalysis Reviews*, **6** (1972) 21.

Dashevskii, M.I., Klyachko, A.L., Tsybulevski, A.M. and Rubenshtein, A.M., *Kinet. Katal.*, **19** (1978) 203.

Datka, J., Turek, A.M., Jehng, J.M. and Wachs, I.E., *J. Catal.*, **135** (1992) 186.

Datka, J., Sarbak, Z. and Eischens, R.P., *J. Catal.*, **145** (1994) 544.

Datka, J., Vogt, O., Rakoczy, J. and Kubacka, A., *in* "Catalysis by microporous materials" (H.K. Beyer, H.G. Karge, I. Kiricsi and J.B. Nagy, Eds.) Studies in Surface Science and Catalysis, Vol.94, p.240, Elsevier, Amsterdam, 1995.

Demmin, R.A. and Gorte, R.T., *J. Catal.*, **90** (1984) 32.

Dumisic, J.A., Rudd, D.F., Rekoske, L.M. and Trevino, A.A., *in* "The microkinetics of heterogeneous catalysis" (J.A. Dumisic and D.F. Rudd, Eds.) p.259, Amer. Chem. Soc., 1993.

Dunken and Stephanowitz, R., *Z. Chem.*, **23** (1983) 353.

Dwyer, J., Fitch, F.R., Machado, F., Qin, G., Smyth, S.M. and Vickerman, J., *J. C. S. Chem. Comm.*, (1981) 422.

Dwyer, J., Fitch, F.R., Qin, G. and Vickerman, J.C., *J. Phys. Chem.*, ***86*** *(1982) 4574.*

Dwyer, F.G., in "Structure-activity and selectivity relationships in heterogeneous catalysis" (R.K. Grasselli and A.W. Sleight, Eds.) Studies in Surface Science and Catalysis, Vol.67, p.179. Elsevier, Amsterdam. 1991.

Eberly, P.E., *J. Phys. Chem.*, **67** (1963) 2404.

Eberly, P.E. and Kimberlin, C.N., *Ind. Eng. Chem. Prod. Res, Dev.*, **9** (1970) 335.

Emeis, C.A., *J. Catal.*, **141** (1993) 347.

Engelhaardt, G., Lohse, U., Patzelova, V., Magi, M. and Lippmaa, E., *Zeolites*, **3** (1983) 239.

Engelhardt, G. and Michel, D., "High-resolution solid-state NMR of silicates and zeolites.", John Wiley and Sons, Great Britain, 1987.

Engelhardt, G., Jerschkewitz, H.G. and Lohse, U., *Zeolites*, **7** (1987) 289.

Engelhardt, G., *in* "Introduction to zeolite science and practice" (H. van Bekkum, E.M. Flanigen and J.C. Jansen, Eds.) Studies in Surface Science and Catalysis, Vol.58, p.285, Elsevier, Amsterdam, 1991.

Ernst, H., Ernst, S., Karger, J., Roser, T., Schwarz, H.B., Gnurr, R.Q. and Weitkamp, J., *in* "Catalysis by microporous materials" (H.K. Beyer, H.G. Karge, I. Kiricsi and J. B. Nagy, Eds.) Studies in Surface Science and Catalysis, Vol.94, p.748, Elsevier, Amsterdam, 1995.

Fejes, P., Hannus, I., Kiricsi, I, Pfeifer, H., Freude, D. and Oehme, W., *Zeolites*, **5** (1985) 45.

Fejes, P., Kiricsi, I., Hannus, I. and Schöbel, Gy., *in* "Catalysis on zeolites" (D. Kallo and Kh.M. Minachev, Eds.) p.205, Akademiai Kiado, Budapest, 1988.

Fellman, J.D., Saxton, J., Wentrcek, P.R., Derouane, E.G. and Massiani, P., U.S. Patent 5,026,942 (1991)

Fenske, D., Hunger, M. and Pfeifer, H., *J. of Magn. Res.*, **95** (1991) 477.

Flanigen, E.M., *in* "Introduction to zeolite science and practice" (H. van Bekkum, E.M. Flanigen and J.C. Jansen, Eds.), Studies in Surface Science and Catalysis, Vol.58, p.13. Elsevier, Amsterdam, 1991.

Forni, L. and Magni, E., *J. Catal.*, **112** (1988) 437.

Freude, D., Haase, J., Pfeifer, H. and Prager, D., *Chem. Phys. Lett.*, **114** (1985) 143.

Freude, D., Hunger, M., Pfeifer, H. and Schwieger, W., *Chem. Phys. Lett.*, **128** (1986) 62.

Fritz, P.O. and Lunsford, J. H., *J. Catal.*, **118** (1989) 85.

Garralon, G., Corma, A. and Fornes, V., *Zeolites*, **9** (1989) 84.

Geurts, F.M.M., Kentgens, A.P.M. and Veeman, W.S., *Chem. Phys. Lett.*, **120** (1985) 206.

Ghosh, A.K. and Curthoys, G., *J. Chem. Soc. Chem. Commun.*, (1983_a) 1271.

Ghosh, A.K. and Curthoys, G., *J Chem. Soc., Faraday Trans. 1*, **79** (1983_b) 805.

Ghosh, A.K. and Curthoys, G., *J. Catal.*, **86** (1984) 454.

Gnep, N.S., Martin de Armando, M.L., Marcilly, C. and Guisnet, M., *in* "Catalyst deactivation" (B. Delmon and G.F. Froment, Eds.) Studies in Surface Science and Catalysis, Vol.6, p.79, Elsevier, Amsterdam, 1980.

Goovaerts, F., Vansant, E. F., Philippaerts, J., De Hulsters, P. and Gelan, J., *J. Chem. Soc., Faraday Trans. I*, **85** (1989) 3675.

Gorte, R.J., *J. Catal.*, **75** (1982) 164.

Gruver, V. and Fripiat, J. J., *J. Phys. Chem.*, **98** (1994) 8549.

Ha, B., Guidot, J. and Barthomeuf, D., *J. Chem. Soc., Faraday Trans. I*, **75** (1979) 1245.

Haag, W.O., U.S. Patent 4,374,296 (1983)

Haag, W.O. and Dessau, R.M., *in* "Proceedings, 8th International congress on catalysis" Vol.2, p.305, Frankfurt-am-Main, Berlin, 1984.

Haag, W.O., *in* "Zeolites and related microporous materials" (Weitkamp, J., Karge, H.G., Pfeifer, H. and Hölderich, W., Eds.) Studies in Surface Science and Catalysis, Vol.84, p.1375, Elsevier, Amsterdam, 1994.

Hamdan, H. and Klinowski, J, *J. Chem. Soc, Chem. Commun.*, (1989) 240.

Hannus, I., Fonseca, A., Kiricsi, I., Nagy, J.B. and Fejes, P., *in* "Catalysis by microporous materials" (H. K. Beyer, H.G. Karge, I. Kiricsi and J.B. Nagy, Eds.) Studies in Surface Science and Catalysis, Vol.94, p.155, Elsevier, Amsterdam, 1995.

Hansford, R.C., U.S. Patent 3,354,077 (1967)

Hardenberg, T.A.J., Mertens, L., Mesman, P., Muller, H.C. and Nicolaides, C.P., *Zeolites*, **12** (1992) 685.

Hays, G.R., van Erp, W.A., Alma, N.C.M, Couperus, P.A., Huis, R. and Wilson, A.E., *Zeolites*, **4** (1984) 377.

Hidalgo, C.V., Itoh, H., Hattori, T., Nwa, M. and Murakami, Y., *J. Catal.*, **85** (1984) 362.

Holderich, W.F., and van Bekkum, H., *in* "Introduction to zeolite science and practice" (H. van Bekkum, E.M. Flanigen and J.C. Jansen, Eds.), Studies in Surface Science and Catalysis, Vol.58, p.631, Elsevier, Amsterdam, 1991.

Hong, Y. and Fripiat, J.J, *Microporous Materials*, **4** (1995) 323.

Hopkins, P.D., *J. Catal.*, **12** (1968) 225.

Horsely, J.A., Fellmann, J.D., Derouane, E.G. and Freeman, C.M., *J. Catal.*, **147** (1994) 231.

Hughes, T.R. and White, H.M., *J. Phys. Chem.*, **71** (1967) 2192.

Hunger, M., Freude, D. and Pfeifer, H., *J. Chem. Soc. Faraday Trans.*, **87** (1991) 657.

Hunger, M., Horvath, T., Engelhardt, G. and Karge, H.G., *in* "Catalysis by microporous materials" (H.K. Beyer, H.G. Karge, I. Kiricsi and J.B. Nagy, Eds.) Studies in Surface Science and Catalysis, Vol.94, p.756, Elsevier, Amsterdam, 1995.

Inaoka, W., Kasahara, S., Fukushima, T. and Igawa, K., in "Chemistry of microporous crystals" p.37, Kodansha Ltd., Tokyo, 1991.

Jacobs, P. and Uytterhoeven, J.B., *J. Catal.*, **22** (1971) 193.

Jacobs, P. and Uytterhoeven, J.B., *J. Catal.*, **26** (1973) 175.

Jacobs, P.A. and Beyer, K.H., *J. Phys. Chem.*, **83** (1979) 1174.

Jacobs, W.P.J.H., de Haan, J.W., van de Ven, L.J.M. and van Santen, R.A., *J. Phys. Chem.*, **97** (1993) 10394.

Jacquinot, E., Raatz, F., Macedo, A. and Marcilly, Ch., *in* "Zeolites as catalysts, sorbents and detergent builders" (H.G. Karge and J. Weitkamp, Eds.) Studies in Surface Science and Catalysis, Vol.46, p.115, Elsevier, Amsterdam, 1989.

Janin, A., Lavally, J.C., Macedo, A. and Raatz, F., *in* "Perspectives in molecular sieve science" p.117, Amer. Chem. Soc., 1988.

Janin, A., Maache, M., Lavalley, J.C., Joly, J.F., Raatz, F. and Szydlowski, N., *Zeolites*, **11** (1991) 391.

Jansen, J.C., van der Gaag, F.J. and van Bekkum, H., *Zeolites*, **4** (1984) 369.

Jones, D.M. and Griffin, G.L., *J. Catal.*, **80** (1983) 40.

Jeanjean, J., Aouli, L., Delafosse, D. and Dereigne, A., *Zeolites*, **11** (1991) 360.

Jia, M., Lechert, H. and Forster, H., *Zeolites*, **12** (1992) 32

Karge, H.G., *Surface Science*, **40** (1973) 157.

Karge, H.G., *Z. Phys. Chem. Neue Folge*, **122** (1980) 103.

Karge, H.G., Kosters, H., and Wada, Y., *in* "Proceedings of the sixth international zeolite conference" (D. Olson and A. Bisio, Eds.), p.308, Butterworths, Surrey, UK, 1983.

Karge, H.G. and Weitkamp, J., *Chem.-Ing.-Tech.*, **58** (1986) 946.

Karge, H.G. and Boldingh, E., *Catalysis Today*, **3** (1988) 379.

Karge, H.G. and Dondur, V., *J. Phys. Chem.*, **94** (1990) 765.

Karge, H.G., *in* "Catalysis and adsorption by zeolites" (G. Öhlmann, H. Pfeifer and R. Fricke, Eds.) Studies in Surface Science and Catalysis, Vol.65, p. 133, Elsevier, Amsterdam, 1991.

Karge, H.G., *in* "Proceedings from the ninth international zeolite conference" (R. von Ballmoos, J.B. Higgins and M.M.J. Treacy, Eds.) Vol.II, p.563, Butterworth-Heinemann, USA, 1993.

Karger ,J. and Ruthven, D.M., *in* "Diffusion in zeolites and other microporous solids" John Wiley and Sons, New York, 1992,

Katayama, A., Toba, M., Takeuchi, G., Mizukami, F., Niwa, S. and Mitamura, S., *J. Chem. Soc. Chem. Commun.*, (1991) 39.

Kazansky, V.B., *Acc. Chem. Res.*, **24** (1991) 477.

Kazansky, V.B., *in* "Advanced zeolite science and applications" (J.C. Jansen, M. Stocker, H.G. Karge and J. Weitkamp, Eds.), Studies in Surface Science and Catalysis, Vol.85, p.251, Elsevier, Amsterdam, 1994.

Kerr, G.T., *J. Phys. Chem.*, **17** (1967) 4155.

Kerr, G.T., *J. Phys. Chem.*, **72** (1968) 2594.

Kerr, G.T., *J. Catal.*, **15** (1969) 200.

Kim, J. and Ihm, S.-K., *Feul*, **71** (1992) 815.

Kiovsky, J.R., Goyette, W.J. and Notermann, T.M., *J. Catal.*, **52** (1978) 25.

Klinowski, J., Thomas, J.M., Anderson, M.W., Fyfe, C.A. and Gobbi, G.C., *Zeolites*, **3** (1983) 5.

Klinowski, J., *Progress in NMR Spectroscopy.*, **16** (1984) 237.

Klinowski, J., *Ann. Rev. Mater. Sci.*, **18** (1988) 189.

Klug, H.P. and Alexander, L.E., "X-Ray Diffraction Procedures", John Wiley and Sons, New York, 1974.

Kojima, M., Rautenbach, M.W. and O'Connor, C.T., *J. Catal.*, **112** (1988) 505.

Kokotailo, G.T., Fyfe, C.A., Feng, Y., Grondey, H., Gies, H., Marler, B. and Cox, D. E., *in* "Catalysis by microporous materials" (H.K. Beyer, H.G. Karge, I. Kiricsi and J.B. Nagy, Eds.) Studies in Surface Science and Catalysis, Vol.94, p.78, Elsevier, Amsterdam, 1995.

Kolodziejski, W., Barrie, P.J., He, H. and Klinowski, J., *J. Chem. Soc. Chem. Commun.*, (1991) 961.

Koriada, P.B., Kiovsky, J.R. and Asim, M.Y., *J. Catal.*, **66** (1980) 290.

Kosslick, H., Tuan, V.A., Fricke, R., Martin, A. and Storek, W., *in* "Zeolites and related microporous materials" (Weitkamp, J., Karge, H.G., Pfeifer, H. and Hölderich, W., Eds.) Studies in Surface Science and Catalysis, Vol.84, p.1013, Elsevier, Amsterdam, 1994.

Kubelkova, L., Beran, S., Malecka, A., and Mastikhin, V.M., *Zeolites,* **9** (1989) 12.

Kühl, G.H., Proc. *in* "3rd Int. Conf. on Molecular Sieves, Recent Progress Reports" (J.B. Uytterhoeven, Ed.), Paper 127, p.227, Univ. Leuwen Press, 1973.

Kühl, G.H., *in* "Molecular Sieves II, 4th Int. Conf. on Molecular Sieves" p.96, Amer. Chem. Soc., 1977.

Kühl, G.H., *J. Phys. Chem. Solids*, **38** (1977) 1259.

Kustov, L.M., Borokov, V.Yu., Kazanskii, V.B., *Kinet. Katal.*, **25** (1984) 614.

Lago, R.M., Haag, W.O., Mikovsky, R.J., Olson, D.H., Hellring, S.D., Schmitt, K.D., and Kerr, G.T., *in* "Proceedings of the 7th Int. Zeolite Conf." (Y. Murakami, A. Iijima and J.W. Ward, Eds.), p.677. Kodansha Ltd., Tokyo, 1986.

Lefrancois, M. and Malbois, G., *J. Catal.*, **20** (1971) 350.

Lercher, J.A. and Rumplmayr, G., *Z. Phys. Chem. Neue Folge*, **146** (1985) 113.

Liu, S-B, Personal Communication, 1995.

Loeffler, E., Peuker, Ch. and Jerschkewitz, H.G., *Catalysis Today*, **3** (1988) 415.

Loeffler, E., Lohse, U., Peuker, Ch., Oelhmann, G., Kustov, L.M., Zholobenko, V.L. and Kazansky, V.B., *Zeolites*, **10** (1990) 266.

Löffler, E., Kustov, L.M., Zholobenko, V.L., Peuker, Ch., Lohse, U., Kazansky, V.B. and Öhlmann, *in* "Catalysis and adsorption by zeolites" (G. Öhlmann, H. Pfeifer and R. Fricke, Eds.) Studies in Surface Science and Catalysis, Vol.65, p.425, Elsevier, Amsterdam, 1991.

Lohse, U., Engelhardt, G. and Patzelova, V., *Zeolites*, **4** (1984) 163.

Lohse, U., Löffler, Hunger, M., Stöckner and Patzelova, V., *Zeolites*, **7** (1987) 11.

Lombardo, E.A., Hall, W.K., *J. Catal.*, **112** (1988) 565.

Lombardo, E.A., Sill, G.S. and Hall, W.K., *J. Catal.*, **119** (1989) 426.

Luk'yanov, D.B., *Zeolites*, **11** (1991) 325.

Lunsford, J.H., *J. Phys. Chem.*, **72** (1968) 4163.

Makarova, M.A., Garforth, A., Zholobenko, V.L., Dwyer, J., Earl, G.J. and Rawlence, D., *in* "Zeolites and related microporous materials" (Weitkamp, J., Karge, H. G., Pfeifer, H. and Hölderich, W., Eds.) Studies in Surface Science and Catalysis, Vol.84, p.365, Elsevier, Amsterdam, 1994.

Makarova, M.A., Karim, K. and Dwyer, J., *Microporous Materials*, **4** (1995) 243.

Martin, A., Wolf, U., Nowak, S. and Lucke, B., *Zeolites*, **11** (1991) 85.

Massiot, D., Bessada, C., Coutures, J.P., and Taulelle, F., *J. of Magn. Res.*, **90** (1990) 231.

Mavrodina, V., Penchev, V., Lohse, U. and Gross, T., *Zeolites*, **9** (1989) 203.

McDaniel, C.V. and Maher, P.K., *in* "Proc. 1st International conference on molecular sieves" (R.M. Barrer, Ed.) p.186, London, 1968.

McVicker, G.B., Kramer, G.M. and Ziemiak, J.J., *J. Catal.*, **83** (1983) 286.

Medin, A.S., Borovkov, V.Yu., Kazansky, V.B., Pelmentschikov, A.G. and Zhidomirov, G.M., *Zeolites*, **10** (1990) 668.

Meier, W.M., *Z. Chem.*, **115** (1961) 439.

Meier, W.M. and Olson, D.H., "Atlas of zeolite structure types", Juris Druck und Verlag AG, Zurich, 1978.

Meyers, B.L., Fleisch, T.H., Ray, G.J., Miller, J.T. and Hall, J.B., *J. Catal.*, **110** (1988) 82.

Miller, J.T., Hopkins, P.D., Meyers, B.L., Ray, G.J., Roginski, R.T., Zajac, G.W. and Rosenbaum, N.H., *J. Catal.*, **138** (1992) 115.

Mirodatos, C. and Barthomeuf, D., *J. Chem. Soc., Chem. Commun.*, (1981) 39.

Mishin, I.V., Klyachko, A., and Rubinshtein, A.M., *Izv. Akad. Nauk SSSR, Ser. Khim.*, (1973) 445.

Mishin, I. and Klyachko, A., *Acta Chimica Hungarica*, **126** (1989) 427.

Mishin, I.V., Pal-Borbely, G. and Karge, H.G. *in* "Catalysis by microporous materials" (H. K. Beyer, H.G. Karge, I. Kiricsi and J.B. Nagy, Eds.) Studies in Surface Science and Catalysis, Vol.94, p.294, Elsevier, Amsterdam, 1995.

Mortier, W.J., Pluth, J.J. and Smith, J.V., *Material Research Bulletin*, **10** (1975) 1319.

Moscou, L., *in* "Introduction to zeolite science and practice" (H. van Bekkum, E.M. Flanigen and J.C. Jansen, Eds.) Studies in Surface Science and Catalysiis, Vol.58, p.1. Elsevier, Amsterdam, 1991.

Musa, M., Tarina, V., Stoica, A.D., Ivanov, E., Plostinaru, D., Pop, E., Pop, Gr., Ganea, R., Birjega, R., Musca, G. and Paukshtis, E., *Zeolites*, 7 (1987) 427.

Nieuwenhuys, B.E., Ponec, V., van Koten, G., van Leeuwen, P.W.N.M. and van Santen, R.A., *in* "Catalysis, an integrated appraoch to homogeneous, heterogeneous and industrial catalysis" (J.A. Moulijn, P.W.N.M. van Leeuwen and R.A. van Santen, Eds.), Studies in Surface Science and Catalysis, Vol.79, p.89, Elsevier, Amsterdam, 1993.

Niwa, M., Iwamoto, M. and Segawa, K., *Bull. Chem. Soc. Jpn*, **59** (1986) 3735.

Nock, A. and Rudham, R., *Zeolites*, **7** (1987) 481.

O'Connor, C.T., Dry, M.E. and van Steen E., *in prep.*

Öhlmann, G., Jerschkewitz, H.G., Lischke, G., Eckelt, R., Gross, T., Parlitz, B., Schulz, I., Wehner, K. and Timm, D., *in* "Catalysis and adsorption by zeolites" (G. Öhlmann, H. Pfeifer and R. Fricke, Eds.) Studies in Surface Science and Catalysis, Vol.65, p.415, Elsevier, Amsterdam, 1991.

Olken, M.M. and Garces, J.M., *in* "Proceedings from the ninth international zeolite conference" (R. von Ballmoos, J.B. Higgins and M.M.J. Treacy, Eds.) Vol.II, p.559, Butterworth-Heinemann, USA, 1993.

Olsson, R.W. and Rollmann, L.D., *Inorganic Chemistry*, **16** (1977) 651.

Onyestyak, Gy., Shen, D. and Rees, L.V.C., *in* "Catalysis by microporous materials" (H.K. Beyer, H.G. Karge, I. Kiricsi and J.B. Nagy, Eds.) Studies in Surface Science and Catalysis, Vol.94, p.116, Elsevier, Amsterdam, 1995.

Pardillos, J., Coq, B., and Figueras, F., *Applied Catalysis*, **51** (1989) 285.

Parrillo, D.J., Adamo, A.T., Kokotailo, G.T. and Gorte, R.J., *Applied Catalysis*, **67** (1990) 107.

Parry, E.P., *J. Catal.*, **2** (1963) 371.

Passaglia, E, *Contib. Mineral petrol,* **50** (1975) 65.

Pellet, R.J., Saott Blakewell, C. and Rabo, J.A., *J. Catal.*, **114** (1988) 71.

Pujado, P.R., Rabo, J.A., Antos, G.J., Gembicki, S.A., *Catalysis Today*, **13** (1992) 113.

Raatz, F., Freund, E. and Marcilly, C., *J. Chem. Soc., Faraday Trans. I*, **81** (1985) 299.

Rabo, J.A., Pickert, P.E., Stamires, D.N. and Boyle, J.E, in "Actes Du Deuxieme Congres International De Catalyse" p. 2055, Technip, Paris, 1960.

Rabo, J.A. and Poutsma, M. L., *in* "Proc. 2nd Int. Conf. on Zeolites" (E.M. Flanigen, L.B. Sand, Eds) ACS, No.102, p.284, Amer. Chem. Soc., Washington, D. C., 1971.

Rabo, J.A., *in* "New frontiers in catalysis" (L. Guczi, F. Solymosi and P. Tetenyi, Eds.) Studies in Surface Science and Catalysis, Vol.75, p.1, Elsevier, Amsterdam, 1992.

Ratnasamy, P., Sivasankar, S. and Vishnoi, S., *J. Catal.*, **69** (1981) 428.

Remy, M.J., Genet, M.J., Notte, P.P., Lardinois, P.F. and Poncelet, G., *Microporous Materials*, **2** (1993) 7.

Rhodes, N.P. and Rudham, R., *J. Chem. Soc., Faraday Trans.*, **89** (1993) 2551.

Ribiero, M.F., Lemos, F., Ramôa Ribeiro, F., Marcilly, Ch., Travers, Ch. and Raatz, F., Symposium presented before Division of Petroleum Chemistry, Inc., American Chemical Society, New York City, 1991,

Samoson, A., Kundla, E. and Lippmaa, E., *J. of Magn. Res.*, **49** (1982) 350.

Samoson, A. and Lipmaa, E., *Chem. Phys. Lett.*, **100** (1983) 205.

Samoson, A., Lipmaa, E., Engelhardt, G., Lohse, U. and Jerschkewitz, H.G., *Chem. Phys. Lett.*, **134** (1987) 589.

Sand, L.B., *in* "Molecular sieves", p.71, Soc. Chem. Ind., London, 1968.

Sanders, J.V., *Zeolites*, **5** (1985) 81.

Sano, T., Suzuki, K., Shoji, H., Ikai, S., Okabe, K., Murakami, T., Shin, S., Hagiwara, H and Takaya, H., *Chemistry Letters*, (1987) 1421.

Sauer, J, *J. Molec. Catal.*, **54** (1989) 312.

Sawa, M., Niwa, M. and Murakami, Y., *in* "Proceedings of the 9th International Congress on Catalysis" (M.J. Phillips and M. Ternan, Eds.) Vol.1, p.380, Chemical Institute of Canada, Ottawa, 1988.

Sawa, M., Niwa, M. and Murakami, Y., *Applied Catalysis*, **53** (1989) 169.

Sawa, M., Niwa, M. and Murakami, Y., *Zeolites*, **10** (1990) 307.

Sawa, M., Niwa, M. amd Murakami, Y., *Zeolites*, **12** (1992) 172.

Scherzer, J., and Bass, J.L., *J. Catal.*, **28** (1973) 101.

Scherzer, J., *in* "Catalytic Materials" (T.E. Whyte Jr., R.A. Dalla Betta, E.G. Deroane and R.T.K. Baker, Eds.) p.157, Amer. Chem. Soc., Washington, DC, 1984.

Schulz, H. and Nehren, S., *Erdöl und Kohle - Erdgas -Petrochemie*, **39** (1986) 93.

Schulz, H., Siwei, Z. and Kusterer, H., *in* "Proceedings of the International Symposium on Chemistry of Microporous Crystals" (Kodansha, ed.) p.281, 1991.

Sefik, M.D., Schaefer, J. and Stejskal, E. O., *in* "Molecular Seives II" p. 344, Soc. Chem. Ind., London, 1978.

Sendota, Y. and Ono, Y., *Zeolites*, **8** (1988) 101.

Sharma. S.B., Meyers, B.L., Chen, D.T., Miller, J. and Dumesic, J.A., *Applied Catalysis*, **102** (1993) 253.

Shigeishi, R., Garforth, A., Harris, I. and Dwyer, J., *J. Catal.*, **130** (1991) 423.

Skeels, G.W. and Breck, D.W., *in* "Proc. 6th Int. Conf. on Zeolites" (D. Olson and A. Bisio, Eds.) p.87, Butterworths, London, 1984.

Smith, J.M., in "Chemical engineering kinetics" p.494, McGraw-Hill, Singapore, 1981.

Song, C. and Kirby, S., *ACS Syposium Series, Div. Pet. Chem.*, **38** (1993) 784.

Stach, H. and Jänchen, J., *Zeolites*, **12** (1992) 152.

Stach, H., Jänchen, J. and Lohse, U., *Catalysis Letters*, **13** (1992_a) 389.

Stach, H., Janchen, J., Jerschkewitz, H., Lohse, U., Parlitz, B., Zibrowius, B. and Hunger, M., *J. Phys. Chem.*, **96** (1992_b) 8473.

Stach, H., Janchen, J., Jerschewitz, H-G., Lohse, U., Parlitz, B. and Hunger, M., *J. Phys. Chem.*, **96** (1992_c) 8480.

Stock, T, Dombrowski, D., Hoffman, J. and Fruwert, J., *Z. Phys. Chem. Leipsig*, **265** (1984) 551.

Sugi, Y., Kim, J.-H., Matsuzaki, T., Hanaoka, T., Kubota, Y., Ti, X. and Matsumoto, M., *in* "Zeolites and related microporous materials" (J. Weitkamp, H.G. Karge, H. Pfeifer, and W. Hölderich, Eds.) Studies in Surface Science and Catalysis, Vol.84, p.1837, Elsevier, Amsterdam, 1994_a.

Sugi, Y., Matsuzaki, T., Hanaoka, T, Kubota, Y. and Kim, J.-H., *Catalysis Letters*, **26** (1994_b) 181.

Sugi, Y and Toba, M., *Catalysis Today*, **19** (1994_c) 187.

Sun, Y., Chu, P-J. and Lunsford, J.H., *Langmuir*, **7** (1991) 3027.

Szostak, R., *in* "Introduction to zeolite science and practice" (H. van Bekkum, E.M. Flanigen and J.C. Jansen, Eds.) Studies in Surface Science and Catalysis, Vol.58, p153, Elsevier, Amsterdam, 1991.

Szostak, R., *in* "Handbook of molecular sieves" p.343, Van Nostrand Reinhold, 1992.

Tabak, S.A. and Yurchak, S., *Catalysis Today*, **6** (1990) 307.

Ueda, S., Murata, H. and Koizumi, M., *Am. Mineral.*, **65** (1980) 1012.

Uytterhoeven, J.B., Christner, L.C. and Hall, W.K., *J. Phys. Chem.*, **69** (1965) 2117.

van Broekhoven, E.H., Daamen, S., Smeink, R.G., Wijngaards, H. and Nieman, J., in "Zeolites, facts, figures, future" (P.A. Jacobs and R.A. van Santen, Eds.) Studies in Surface Science and Catalysis, Vol.49, p.1291., Elsevier, Amsterdam, 1989.

van Geem, P.C., Scholl, K. and van der Velden, G., *J. Phys. Chem.*, **92** (1988) 1585.

van Hooff, J.H.C. and Roelofsen, J.W., *in* "Introduction to zeolite science and practice" (H. van Bekkum, E.M. Flanigen and J.C. Jansen, Eds.), Studies in Surface Science and Catalysis, Vol.58, p.241, Elsevier, Amsterdam, 1991.

van Niekerk, M.J., Fletcher, J.C.Q. and O'Connor, C.T., *J. Catal.*, **138** (1992_a) 150.

van Niekerk, M., PhD thesis, University of Cape Town, 1992_b.

van Santen, R.A., *in* "Advanced zeolite science and applications" (J.C. Jansen, M. Stocker, H.G. Karge and J. Weitkamp, Eds.), Studies in Surface Science and Catalysis, Vol.85, p.273, Elsevier, Amsterdam, 1994.

Vasques, M.H., Ribeiro, F.R., Gnep, N. and Guisnet, M., *React. Kinet. Catal. Lett.*, **38** (1989) 301.

von Ballmoos, R., *in* "The ^{18}O-exchange method in zeolite chemistry" p.185, Salle and Sauerlander, Frankfurt am Main, 1981.

von Ballmoos, R., "Collection of simulated XRD powder patterns for zeolites" p.76, Butterworth and Co., Great Britain, 1984.

Wang, Q.L., Giannetto, G., Torrealba, M., Perot, G., Kappenstein, C. and Guisnet, M., *J. Catal.*, **130** (1991_a) 459.

Wang, Q.L., Giannetto, G. and Guisnet, M., *J. Catal.*, **130** (1991_b) 471.

Ward, J.W., *J. Catal.*, **9** (1967) 225.

Ward, J.W. and Hansford, R.C., *J. Catal.*, **13** (1969) 364.

Ward, J.W., *J. Catal.*, **18** (1970) 348.

Ward, J.W., *in* "Zeolite chemistry and catalysis" (J. A. Rabo, Ed.) ACS Monogr.171, p.118, Amer. Chem. Soc., Washington, 1976.

Weilers, A.F.H., Vaarkamp, M. and Post, M.F.M., *J. Catal.*, **127** (1991) 51.

Weisz, P.B. and Frillette, V.J., *J. Phys. Chem.*, **64** (1960) 342.

Weisz, P.B., *Chemtech*, **3** (1973) 498.

Whittemore, O.J., *Amer. Mineral.*, **57** (1972) 1146.

Witzel, F., Karge, H.G. and Gutse, A., *in* "Proceedings from the ninth international zeolite conference" (R. von Ballmoos, J.B. Higgins and M.M.J. Treacy, Eds.) Vol.II, p.559, Butterworth-Heinemann, USA, 1993.

Yaluris, G., Rekoske, J.E., Aparicio, L.M., Madon, R.J. and Dumesic, J.A., *J. Catal.*, **153** (1995) 54.

Zholobenko, V.L., Kustov, L.M., Borovkov, L.M. and Kazansky, V.B., *Zeolites*, **8** (1988) 175.

Zholobenko, V.L., Kustov, L.M., Kazansky, V.B., Loeffler, E., Lohser, U., Peuker, Ch, and Oehlmann, G., *Zeolites*, **10** (1990) 304.

Zholobenko, V.L., Kustov, L.M., Kazansky, V.B., Loeffler, E., Lohser, U, and Oehlmann, G., *Zeolites*, **11** (1991) 132.

Zholobenko, V.L., Makarova, M.A. and Dwyer, J., *J. Phys. Chem.*, **97** (1993) 5962.